

TECHNISCHE UNIVERSITÄT MÜNCHEN

TUM School of Life Sciences

Lehrstuhl für Experimentelle Genetik

**Multi-Omics Analysis Reveals Extensive Lipid and Metabolite
Remodeling During Adipogenesis in Human Adipocytes**

Florian Johannes Miehle

Vollständiger Abdruck der von der Fakultät TUM School of Life Sciences der Technischen
Universität München zur Erlangung des akademischen Grades eines

Doktors der Naturwissenschaften

genehmigten Dissertation.

Vorsitzender: Prof. Dr. Wilfried Schwab

Prüfer der Dissertation: 1. apl. Prof. Dr. Jerzy Adamski

2. Prof. Dr. Michael Rychlik

Die Dissertation wurde am 14.10.2020 bei der Technischen Universität München eingereicht und
durch die Fakultät TUM School of Life Sciences am 09.03.2021 angenommen.

Table of contents

Table of contents.....	I
Summary	IV
Zusammenfassung.....	VI
Abbreviations.....	VIII
1. Introduction	1
1.1. Obesity.....	1
1.2. The three “A’s” in obesity research: adipose tissue, adipocytes, and adipogenesis.....	2
1.3. Cell models for the characterization of adipogenesis	6
1.4. Analyzing biological processes with metabolomics, lipidomics, and transcriptomics	8
1.5. Metabolomics and lipidomics in adipogenesis research.....	11
1.6. Aim of the thesis	11
2. Materials and Methods.....	12
2.1. Chemicals, equipment, and software	12
2.1.1. Chemicals, hormones, enzymes, reagents, and media.....	12
2.1.2. (Internal) standards for the GC-MS assay	13
2.1.3. Consumables.....	14
2.1.4. Human cells and bacteria	14
2.1.5. Kits.....	14
2.1.6. Equipment.....	15
2.1.7. Software and programs.....	16
2.2. Working with human cells.....	17
2.3. Working with <i>Escherichia coli</i> (<i>E. coli</i>)	17
2.4. Working with DNA	18
2.4.1. Isolation of plasmid DNA from <i>E. coli</i>	18
2.4.2. Separation of DNA in agarose gels.....	18
2.4.3. Determination of RNA and DNA concentration and purity.....	18
2.5. Working with RNA.....	19
2.5.1. Isolation of RNA from human cells	19
2.5.2. Reverse transcription into cDNA.....	19

Table of contents

2.6.	Polymerase chain reaction (PCR)	19
2.6.1.	Quantitative real-time PCR (qRT-PCR)	20
2.7.	Cloning of DNA into plasmids	21
2.8.	Sequencing of DNA	21
2.9.	Mass spectrometry approaches	21
2.9.1.	Sample extraction.....	21
2.9.2.	Normalization	22
2.9.3.	Lipidyzer™ method	22
2.9.4.	Absolute/DQ p180 kit.....	23
2.9.5.	Newborn Screening assay	24
2.9.6.	Non-targeted metabolomics using the technology by Metabolon Inc.....	24
2.9.7.	Energy metabolism assay	26
2.10.	Transcriptomics.....	28
2.11.	Statistical analysis.....	29
2.11.1.	Calculation of validation parameters for the GC-MS method.....	29
2.11.2.	Statistical analysis for analysis of metabolomics and lipidomics data	30
2.11.3.	Statistical analysis for transcriptomics.....	32
3.	Results.....	32
3.1.	Validation of the GC-MS based quantification assay for metabolites of the energy metabolism	33
3.2.	Analyzing human adipogenesis with different omics techniques.....	41
3.2.1.	Assessment of adipocyte differentiation	41
3.2.2.	Lipidyzer™ method	43
3.2.3.	Absolute/DQ p180 kit.....	60
3.2.4.	Newborn Screening assay	63
3.2.5.	Non-targeted metabolomics using the technology by Metabolon Inc.....	65
3.2.6.	Energy metabolism assay	71
3.2.7.	Comparison of mass spectrometry-based results.....	72
3.2.8.	Transcriptomics	78
4.	Discussion	91

Table of contents

4.1. Validation of the GC-MS based quantification assay for metabolites of energy metabolism	91
4.2. Analyzing human adipogenesis with different -omics techniques.....	93
4.2.1. Strongly upregulated BCAA degradation during human adipogenesis	94
4.2.2. TCA cycle and oxidative phosphorylation are highly upregulated during human adipogenesis	97
4.2.3. Glycolysis, gluconeogenesis, and glyceroneogenesis are highly upregulated during human adipogenesis.....	100
4.2.4. Lipid remodeling is highly activated during human adipogenesis	102
4.2.5. Polyamine metabolism is highly regulated during human adipogenesis	106
4.2.6. Limitations of the study	110
4.2.7. Proposed model of human adipogenesis using SGBS cells.....	111
Index of figures	113
5. Appendix.....	116
5.1. Significances from analyzing adipogenesis with Lipidizer™ method	116
5.2. Analysis of the fatty acid concentrations during adipogenesis with respect to the lipid classes	117
5.3. Significances of transcriptomics data	123
5.4. Publication and presentations	126
5.4.1. Publication	126
5.4.2. Poster presentations	126
6. Reference list	127
Acknowledgements.....	136

Summary

In the last decades, overweight and obesity have strongly increased to pandemic dimensions. Nowadays in the western world, more than every second adult is overweight and more than every fifth adult is obese. Both disorders share an excessive accumulation of body fat, which presents a high risk to health. Obesity increases the risk for developing diseases like type 2 diabetes, cardiovascular diseases, and many types of cancers, resulting in reduced life expectancy. The main causes of overweight and obesity are nutrition, physical inactivity, and to a minor part also genetics.

Despite decades of research in adipocyte biology, the adipogenic cell differentiation process is still incompletely understood. For this reason, human SGBS cell were differentiated up to 20 days during this PhD work. Samples were collected on every 2nd to 4th day of adipogenesis to study the cellular differentiation process of precursor cells into mature, lipid-laden adipocytes. To unravel fundamental mechanisms of adipogenic differentiation, metabolomic, lipidomic, and transcriptomic approaches were applied. Five analytical approaches based on mass spectrometry were used, one of which, a GC-MS-based method, was specially developed and validated for the quantitative analysis of metabolites of the cellular energy metabolism. For quantitative analysis of amino acids, carnitine, and acylcarnitines, the New Born Screening assay and Biocrates Absolute/DQ p180 kit were used. The latter assay also enabled quantitative analysis of biogenic amines, hexoses, and glycerolipids. Additional metabolites and lipids from several classes were determined using a non-targeted approach. For the quantification of lipid levels and the characterization of bound fatty acids, the Lipidizer™ technology was applied. Besides metabolomics and lipidomics, transcriptomics was used. Total mRNA sequencing enabled pathway analysis of the transcriptome as well as the connection of non-polar lipid species with polar metabolites.

During the first four days of the adipogenic process, the cellular metabolism underwent an energetic switch including a strong upregulation of several amino acid degradation pathways, especially of the branched-chain amino acids (BCAA). Thereby, immense amounts of acetyl-CoA were synthesized, which were putatively used for the synthesis of ATP as tricarboxylic acid (TCA) cycle and oxidative phosphorylation pathways were both transcriptionally upregulated. In addition to amino acids, degradation pathways of redundant (very) long-chain fatty acids (VLCFA) were strongly upregulated on transcript level. In contrast, the biosynthesis pathways of (mono-)unsaturated long-chain fatty acids was strongly upregulated, which continued over the whole observed time period. Starting in this initial phase, the metabolic intermediates were also remodeled into other metabolites and lipids. Metabolites from the TCA cycle, which are derived from BCAA and VLCFA degradation steps, were putatively used in parts for the synthesis of glycerol as glyceroneogenesis was transcriptionally upregulated. The initial phase was additionally characterized by ceramide-mediated signaling leading to cell cycle arrest and inhibition of cell proliferation. Afterwards, the ceramide species were remodeled into glycerophospholipids for the

Summary

plasma membrane, which had increased concentration levels during the whole observed time period. The second phase of adipogenesis was characterized by highly upregulated biosynthesis of triacylglycerols. Thereby, immense amounts of acetyl-CoA and ATP were putatively provided for the elongation of fatty acids, which were then linked to glycerol and stored in lipid droplets of maturing adipocytes. The fatty acids were derived from the *de novo* biosynthesis but also from remodeling of other lipid species.

This work describes an extensive lipid and metabolite remodeling during human adipogenesis. It supports a deeper understanding of the main phenotype of overweight and obesity, namely the immense increase of number and size of adipocytes, forming huge fat depots. The highlighted processes and its metabolites and lipids might help in developing new approaches for prevention and treatment of this pandemic disorder.

Zusammenfassung

Übergewicht und Fettleibigkeit haben in den letzten Jahrzehnten stark zugenommen und erreichen pandemische Ausmaße. Heutzutage ist in der westlichen Welt mehr als jeder zweite Erwachsene übergewichtig und mehr als jeder fünfte Erwachsene adipös. Beiden Erkrankungen ist eine übermäßige Fettansammlung im Körper gemeinsam, die ein hohes Gesundheitsrisiko darstellt. Vor allem erhöht Fettleibigkeit das Risiko, an Krankheiten wie Typ-2-Diabetes, Herz-Kreislauf-Erkrankungen und vielen Krebsarten zu erkranken, was zu einer verkürzten Lebenserwartung führt. Die Hauptursachen für Übergewicht und Fettleibigkeit sind Ernährung, Bewegungsmangel und zu einem geringen Teil auch Genetik.

Trotz jahrzehntelanger Forschung auf dem Gebiet der Adipozytenbiologie ist der adipogene Zelldifferenzierungsprozess immer noch nicht vollständig aufgeklärt. Aus diesem Grund wurden für diese Doktorarbeit menschliche SGBS-Zellen bis zu 20 Tage lang differenziert. An jedem 2. bis 4. Tag der Adipogenese wurden Proben genommen, um den zellulären Differenzierungsprozess aus Fibroblasten-ähnlichen Vorläuferzellen zu reifen, lipidbeladenen Adipozyten zu untersuchen. Um grundlegende Mechanismen der adipogenen Differenzierung zu entschlüsseln, wurden metabolomische, lipidomische und transkriptomische Ansätze angewandt. Es wurden fünf auf Massenspektrometrie-basierende analytische Ansätze verwendet, von denen einer, eine GC-MS-basierte Methode, speziell für die quantitative Analyse von Metaboliten des zellulären Energiestoffwechsels entwickelt und validiert wurde. Für die quantitative Analyse von Aminosäuren, Carnitin und Acylcarnitinen wurden der New Born Screening Assay und das Biocrates Absolute/DQ p180 Kit verwendet. Letzterer Assay ermöglichte auch die quantitative Analyse von biogenen Aminen, Hexosen und Glycerolipiden. Zusätzliche Metaboliten und Lipide aus mehreren Klassen wurden mit Hilfe eines nicht zielgerichteten metabolomischen Ansatzes bestimmt. Für die Charakterisierung der Lipide sowie ihrer gebundenen Fettsäuren wurde die Lipidyzer™ Technologie angewandt. Neben Metabolomik und Lipidomik wurde auch Transkriptomik verwendet. Die Sequenzierung der gesamten mRNA ermöglichte die Analyse des Transkriptoms sowie die Verknüpfung der Daten der nichtpolaren Lipidspezies mit den polaren Metaboliten.

Während der ersten vier Tage des adipogenen Prozesses durchlief der zelluläre Stoffwechsel eine energetische Umstellung, die eine starke Hochregulation mehrerer Aminosäuren-Abbauege, insbesondere der verzweigt-kettigen Aminosäuren (BCAA), beinhaltete. Dabei wurden große Mengen Acetyl-CoA synthetisiert, die mutmaßlich für die Synthese von ATP verwendet wurden, da der Tricarbonsäure-(TCA)-Zyklus und die oxidativen Phosphorylierungswege beide transkriptionell hochreguliert waren. Zusätzlich zu den Aminosäuren wiesen auch redundante (sehr) langkettige Fettsäuren (VLCFA) einen stark hochregulierten Abbau-Signalweg auf Transkriptionsebene auf. Im Gegensatz dazu zeigten (mono-)ungesättigte langkettige Fettsäuren einen stark hochregulierten Biosyntheseweg, der sich über den gesamten beobachteten Zeitraum fortsetzte. Ab dieser Anfangsphase wurden die Stoffwechselzwischenprodukte auch in andere

Zusammenfassung

Metaboliten und Lipide umgewandelt. Metabolite aus dem TCA-Zyklus, die aus dem Abbau der BCAA und VLCFA stammen, wurden vermutlich teilweise für die Synthese von Glycerin verwendet, da die Glyceroneogenese transkriptionell hochreguliert war. Die Anfangsphase war zusätzlich durch Ceramid-vermittelte Signalisierung gekennzeichnet, die zum Stillstand des Zellzyklus und zur Hemmung der Zellproliferation führte. Danach wurden die Ceramidspezies in Glycerophospholipide für die Plasmamembran umgewandelt, die während des gesamten beobachteten Zeitraums erhöhte Konzentrationen aufwies. Die zweite Phase dieses Zelldifferenzierungsprozesses kennzeichnete sich durch eine stark hochregulierte Biosynthese von Triacylglyceriden. Dabei wurden mutmaßlich große Mengen Acetyl-CoA und ATP zur Verlängerung von Fettsäuren verwendet, die dann an Glycerin gebunden und in Lipidtröpfchen reifender Adipozyten gespeichert wurden. Die Fettsäuren stammten aus der *de novo* Biosynthese, aber auch aus dem Umbau anderer Lipidspezies.

Diese Arbeit beschreibt einen umfassenden Lipid- und Metabolitenumbau während der menschlichen Adipogenese. Sie unterstützt ein tieferes Verständnis des Hauptphänotyps von Übergewicht und Adipositas, nämlich der immensen Zunahme von Anzahl und Größe der Adipozyten, die dabei große Fettdepots bilden. Die hervorgehobenen Prozesse und ihre Metaboliten und Lipide könnten dazu beitragen, neue Ansätze zur Prävention und Behandlung dieser pandemischen Gesundheitsstörung zu entwickeln.

Abbreviations

13C3-Pyr	13C3-pyruvic acid
13C4-3HB	13C4-3-hydroxybutyric acid
13C4-Rib	13C4-ribose
D3-2-HG	D3-2-hydroxyglutaric acid
D3-Mal	D3-malic acid
D4-Cit	D4-citric acid
α-KG	α-ketoglutaric acid
2-HB	2-Hydroxybutyric acid
QTRAP	triple quadrupole linear ion trap
MeOH	methanol
ACER	alkaline ceramidase
ACO	aconitase
ADIPOR	adiponectin receptor
ADSCs	adipose derived stem cells
Ala	alanine
ALDO	fructose-bisphosphate aldolase
AMP	adenosine monophosphate
AP-1	activator protein 1
Arg	arginine
ASAH	N-acylsphingosine amidohydrolase
ATP	adenosine triphosphate
B4GALT6	β-1,4-galactosyltransferase 6
BAT	brown adipose tissue
BCAA	branched-chain amino acid
BMI	body mass index
BPGM	bisphosphoglycerate mutase
C/EBPs	CCAAT-enhancer-binding proteins
Cal	calibrator
CDP	cytidine diphosphate
CDIPT	CDP-diacylglycerol-inositol 3-phosphatidyltransferase
CDS2	CDP-Diacylglycerol Synthase 2
CE	cholesteryl ester
CEPT1	choline/ethanolamine phosphotransferase 1
CER	ceramide
CERK	ceramide kinase
CERS	ceramide synthase
CHPT1	choline phosphotransferase 1
Cit	citrate

Abbreviations

CoA	coenzyme A
CRLS1	cardiolipin synthase 1
CV	coefficient of variation
DAG	diacylglycerol
DCER	dihydro ceramide
DEGS1	sphingolipid δ -(4)-desaturase 1
DGK	diacylglycerol kinase
DHA	docosahexaenoic acid
DHAP	dihydroxyacetone phosphate
DNA	deoxyribonucleic acid
ELOVL	elongation of very long chain fatty acid
EM	energy metabolism
ENO	enolase
EPA	eicosapentaenoic acid
ESI	electro spray ionization
FA	fatty acid
FATP	long-chain fatty acid protein
FBP1	fructose-bisphosphatase 1
FBS	fetal bovine serum
FDA	food and drug association
FFA	free fatty acid
FPKM	fragments per kilobase of exon model per million reads mapped
Fum	fumarate
G3P	glyceraldehyde 3-phosphate
G6PC	glucose-6-phosphatase catalytic subunit
GALC	galactosylceramidase
GalCER	galactosylceramide
GALM	galactose mutarotase
GAPDH	glyceraldehyde-3-phosphate dehydrogenase
GBA	glucosylceramidase β
GCK	glucokinase
GC-MS	gas chromatography-mass spectrometry
GLB1	galactosidase β 1
Glc	glucose
GlcCER	glucosylceramide
Gly	glycine
GPC	glycerophosphocholine
GPE	glycerophosphoethanolamine
GPG	glycerophosphoglycerol
GPI	glycerophosphoinositol
GR	glucocorticoid receptor

Abbreviations

GTP	guanosin triphosphate
HCER	hexosylceramide
HeLa	human cervix adenocarcinoma cell line
HESI-II	heated electrospray ionization
HILIC	hydrophilic interaction liquid chromatography
His	histidine
HK	hexokinase
HMGU	Helmholtz Zentrum München GmbH
IBMX	3-isobutyl-1-methylxanthine
Ile	isoleucine
Isocit	isocitrate
ISTD	internal standard
KDSR	3-ketodihydrosphingosine reductase
KEGG	Kyoto Encyclopedia of Genes and Genomes
KLF	Krüppel-like transcription factor
Lac	lactate
LCER	lactosylceramide
LCFA	long-chain fatty acid
LC-MS	liquid chromatography – mass spectrometry
LDH	lactate dehydrogenase
Leu	leucine
LLOQ	lower limit of quantification
LOD	limit of detection
LPC	lysophosphatidylcholine
LPE	lysophosphatidylethanolamine
LPG	lysophosphatidylglycerol
LPI	lysophosphatidylinositol
LPIN	lipin
LPS	lysophosphatidylserine
MARK	microtubule affinity regulating kinase
MCFA	medium-chain fatty acid
MECR	mitochondrial trans-2-enoyl-CoA reductase
MEFs	mouse embryonic fibroblasts
Met	methionine
MINPP1	multiple inositol-polyphosphate phosphatase 1
MR	mineralcorticoid receptor
mRNA	messenger ribonucleic acid
MSI	metabolomics standards initiative
MS/MS	tandem mass spectrometry
MTAP	methylthioadenosine phosphorylase
MTBE	methyl-tert-butylether

Abbreviations

NA	not applicable
NADH	nicotinamide adenine dinucleotide
NBS	Newborn screening assay
NMR	nuclear magnetic resonance
ODC1	ornithine decarboxylase 1
Orn	ornithine
PA	phosphatidic acid
PAOX	polyamine oxidase
PC	phosphatidylcholine
PC	principal component
PCA	principal component analysis
PCK	phosphoenolpyruvate carboxykinase
PCR	polymerase chain reaction
PE	phosphatidylethanolamine
PEMT	phosphatidylethanolamine N-methyltransferas
PEP	phosphoenolpyruvate
PFKL	phosphofructokinase liver type
PFKM	phosphofructokinase muscle type
PFKP	phosphofructokinase platelet type
PFPA	perfluoropentanoic acid
PG	phosphatidylglycerol
PGAM	phosphoglycerate mutase
PGK1	phosphoglycerate kinase
PGM1	phosphoglucomutase 1
PGP	phosphatidylglycerol phosphate
PGS	phosphatidylglycerophosphate synthase 1
Phe	phenylalanine
PI	phosphatidylinositol
PKM	pyruvate kinase muscle isozyme
PLS-DA	partial least-square discriminant analysis
PPARG	peroxisome proliferator activated receptor gamma
Pro	proline
PS	phosphatidylserine
PTDSS	phosphatidylserine synthase
PTPMT1	protein tyrosine phosphatase mitochondrial
Pyr	pyruvate
QC	quality control
qRT-PCR	real-time quantitative PCR
RBP-4	retinol binding protein 4
Rib	ribose
RIN	RNA integrity number

Abbreviations

RNA	ribonucleic acid
RSD	relative standard deviation
RXR	retinoid X receptor
SAT1	spermidine/spermine N1-acetyltransferase
SDH	succinate dehydrogenase complex flavoprotein
Ser	serine
SGBS	Simpson Golabi Behmel Syndrome
SGMS1	sphingomyelin synthase
Shn-2	schnurri-2
SIM	single ion monitoring
SIRT-1	sirtuin-1
SM	sphingomyelin
SMPD	sphingomyelin phosphodiesterase
SMS	spermine synthase
SPTLC	serine palmitoyltransferase long-chain base
SPTSSA	serine palmitoyltransferase small subunit A
SREP	sterol regulatory element-binding protein
SRM	spermidine synthase
Suc	succinate
SVF	stromal vascular fraction
T2D	type 2 diabetes
T3	triiodothyronine
TAG	triacylglycerol
TBP	TATA-binding protein
TCA	tricarboxylic acid
Thr	threonine
TPI1	triosephosphate isomerase
Trp	tryptophan
Tyr	tyrosine
UGCG	UDP-glucose ceramide glucosyltransferase
UPLC	ultra performance liquid chromatography
Val	valine
VIP	variable of the important features
VLCFA	very long-chain fatty acid
WAT	white adipose tissue
WHO	world health organization
ZFP	zinc finger protein

1. Introduction

1.1. Obesity

The worldwide prevalence of overweight and obesity has increased to pandemic dimensions in recent decades (1). Nowadays, about one-third of the world population is classified as overweight or obese (2). In numbers, over 1.9 billion adults (39% of all grown-ups) were overweight in 2016, of whom more than 650 million were obese in the world (13 % of all grown-ups) (3). In addition, 340 million children and adolescents were overweight or obese in 2016. Overweight and obesity are defined by the World Health Organization (WHO) to be abnormal or excessive fat accumulation, which presents a risk to health (3). A measure of obesity is the body mass index (BMI), which is defined by dividing the body weight in kilograms by the square of height in meters. For adults, the guidelines from the US Centers of Disease Control and Prevention and the WHO uses five BMI ranges to classify the weight status of human beings. Underweight is defined for BMI <18.5 kg/m², normal weight when BMI is 18.5 - <25 kg/m², overweight people have an BMI between 25.0 and <30 kg/m², obese people have a BMI ≥30 kg/m², and severe obesity is defined as a BMI ≥40 kg/m². Worldwide, the prevalence of overweight and obesity has increased strongly since the last century (see Figure 1). American, European, and Eastern Mediterranean people had the highest prevalence in 2015, in descending order (2, 4). Around 64.2% of all American were overweight and 28.3% were obese at the same time. In Europe, the prevalence of overweight also increased from the 1980s to 2015 to 59.6% and the prevalence of obesity increased to 22.9%. In contrast, the regions South East Asia and West Pacific had the lowest prevalence in 2015. But also in these regions, the prevalence of overweight increased to 24.3% in South East Asia and to 28.2% in the West Pacific region. Similar to overweight, obesity also increased during these 35 years to 6.2% (South East Asia) and 4.9% (West Pacific).

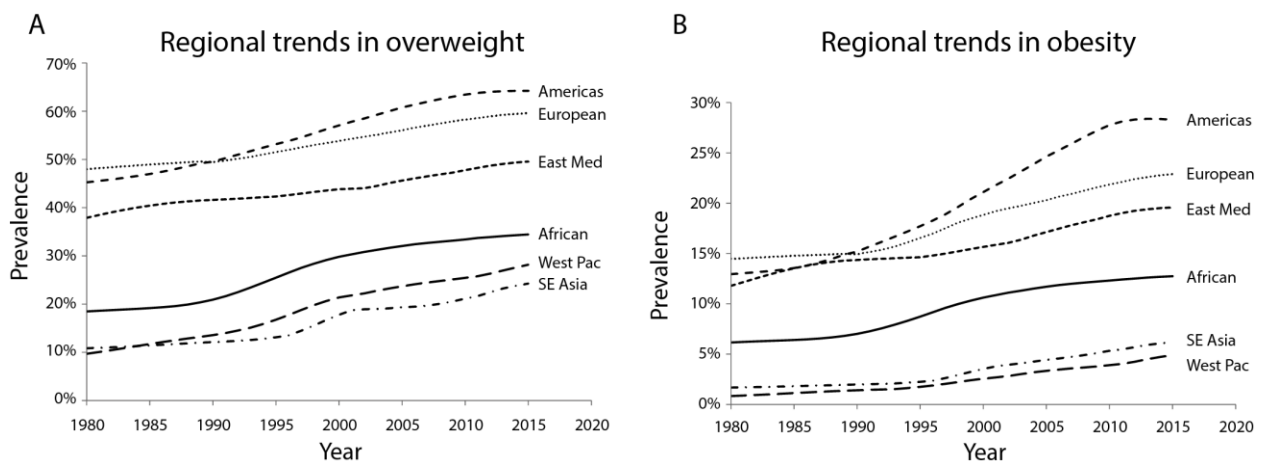


Figure 1: Prevalence of overweight (panel A) and obesity (panel B) strongly increased worldwide from 1980 until 2015. However, there are great differences in adults between cluster of geographical regions. American, European and Eastern Mediterranean (East Med) had the highest prevalence. People from the West Pacific (West Pac) and South East Asia (SE

Introduction

Asia) region had the lowest prevalence. Reprinted from "The epidemiology of obesity" by Chung Chooi and coworkers in the journal Metabolism Clinical and Experimental (Vol. 92, 2019), with permission from Elsevier (2).

Obesity has an adverse impact on a huge range of physiological processes of the body, thereby increasing the risk for developing multiple diseases like type 2 diabetes (T2D) (5), cardiovascular diseases (5, 6), several types of cancer (7, 8), musculoskeletal diseases (9), and diseases affecting mental health (10). Obesity as the major risk factor for these diseases might decrease life expectancy up to 5-20 years depending on the severity of the disorders (11-13). In addition, obesity and its associated diseases have strong negative effects on social and economic aspects. There are major impacts on the quality of life of each individual as well as its family, on the work productivity, on the healthcare system, and thereby on the national economy. Overweight and obesity conditions are considered to cost of 0.47-0.6% of the gross domestic product in Europe (14). In the US, the health costs of obese patients were estimated to be US\$ 149.4 billion in 2014 (15).

Overweight and obesity are complex, multifactorial health issues. Both can be seen as the result of a combination of causes and contributing factors with individual factors like genetics and behavior (2, 16). The contributing behavior is characterized by e.g. physical (in)activity, sedentary lifestyle, education, diet, or medication (16). Our food system changed during the last decades as it is producing more cheap and processed food, promoting high overconsumption of nutrient-poor but energy-rich food and beverages (17). Therefore, the food system itself has a strong contribution in the development of overweight and obesity in humans (2, 17).

Overweight and obesity result in a chronic positive energy balance. When dietary energy intake exceeds the energy expenditure, it leads to storage of energy in triacylglycerols in the adipose tissue. These fat depots expand in size and number resulting in increased body fat and weight gain.

1.2. The three "A's" in obesity research: adipose tissue, adipocytes, and adipogenesis

Research on adipocyte biology became an important exploration field since the pandemic increase of overweight and obesity, as both are characterized by an excess of white adipose tissue (WAT). This type of tissue accounts for up to 25% of the body weight in healthy, normal weight humans (18). In addition, it is widely dispersed in the body, however, major depots can be found in subcutaneous (deep and superficial abdominal as well as gluteal-femoral) and visceral (omental, mesenteric, mediastinal, and epicardial) regions (19). Adipose tissue consists of several types of cells such as adipocytes, adipose precursor cells, fibroblasts, blood cells, mesenchymal stem cells (MSCs), endothelial cells macrophages, and muscle cells (20). The main constituents of white adipose tissue are adipocytes, which are derived from MSCs. These special stem cells first differentiate into lipoblasts, followed by preadipocytes, and finally into adipocytes (21).

Introduction

Adipocytes control the energy balance of the body by storing triacylglycerols in periods of energy excess and breaking down these lipids during energy deprivation (22). However, the physiological role of adipocytes is much more complex than only acting in energy storage. These cells secrete numerous distinct lipids and proteins, known as adipokines, which are transported through circulation, controlling, and regulating various body functions like appetite, immunological and inflammatory responses, glucose metabolism, and blood pressure and thereby act as an endocrine organ (22-24). Obesity is characterized by dysregulated adipokine expression and disturbed disposal of glucose and lipids. This has in turn a strong contribution to chronic inflammation, hyperglycemia, hyperlipidemia, and insulin resistance and thereby also contributes to the development of type 2 diabetes and other metabolic diseases (25).

Another important fat type in mammals is the brown adipose tissue (BAT), which generates heat via mitochondrial uncoupling of lipid oxidation (26). Until the first years of this millennium, it was a generally accepted dogma that BAT cannot be found in adults, because it was exclusively found in newborns for non-shivering thermogenesis. However, since 2003, PET-scan identified small amounts of BAT depots (27-29) in narrow fascial layers among organs and bones in the upper thorax (30). In addition to visceral locations, brown fat can be also found subcutaneous, e.g. between anterior neck muscles (30).

In addition to the white and brown adipocytes, a third cell type was identified during the last decade. These cells are called beige adipocytes, and have similar morphological features to brown adipocytes. Both brown and beige cell types have central nuclei, multilocular lipid droplets, and high numbers of mitochondria in common (31). In contrast, white adipocytes have large lipid droplets and the nucleus is flattened and located closely to the plasma membrane (32). Beige adipocytes appear upon external stimuli such as activity during chronic cold exposure, exercise, as well as administration of β 3-adrenergic receptor agonists (33). In contrast to brown adipocytes, beige cells reside within a WAT depot. However, the origin, development, and function of beige adipocyte is not yet incompletely understood.

Adipogenesis is the cell differentiation process of fibroblast-like preadipocytes into lipid-laden and insulin-responsive adipocytes. (23) Therefore, it is the major pathway of adipose tissue development. It can be separated into two main phases: commitment of preadipocytes to differentiation and their terminal differentiation into mature adipocytes. The second phase is often divided into two separate subphases, namely differentiation and maturation. This adipogenic process requires a cascade of transcription factors, of which peroxisome proliferator-activated receptor gamma (PPAR γ) and CCAAT/enhancer-binding proteins (C/EBPs) are the most important ones (34, 35). The PPAR γ protein has two isoforms, PPAR γ 1 and PPAR γ 2, produced by alternative and differential promoter usage (36). Isoform 1 is expressed in low levels in several tissues, whereas isoform 2 is highly abundant in adipose tissue (37). Although there are many distinct factors involved in the transcriptional activation of adipogenesis, none are as essential and critical as PPAR γ . There are several studies, which could demonstrate its fundamental role in adipogenesis (34, 37, 38). PPAR γ induces cell differentiation and if PPAR γ is lacking, this cellular process, is

Introduction

inhibited which cannot be rescued by other factors (40, 41). Knockout experiments of PPAR γ in mice showed placental dysfunction and lethality during embryogenesis (42). Other transcription factors involved in adipogenesis, such as C/EBP β , C/EBP δ , or EBF1 (see Figure 2), induce PPAR γ 's expression. PPAR γ has several synthetic and endogenous lipophilic ligands derived from fatty acid metabolism pathways. Endogenous ligands are for example essential omega-3 fatty acids like docosahexaenoic acid (DHA), eicosapentaenoic acid (EPA), and eicosanoids (43-45). Thus, dietary lipids have a fundamental influence on adipogenesis. Synthetic ligands belong to the thiazolidinediones (e.g. rosiglitazone and pioglitazone) which are used in the therapy of type 2 diabetes (46-48). The mechanism of action of PPAR γ is dependent on ligand binding, followed by translocation of the complex to the nucleus, where PPAR γ interacts with retinoid X receptor (RXR) to form a heterodimer. Afterwards, PPAR γ binds to several PPAR responsive genes, such as fatty acid transport protein (FATP), fatty acid translocase (FAT/CD36), and fatty acid-binding protein (aP2) and is thereby initiating differentiation (49). Because activation of PPAR γ has massive consequences on the function of cells, protein action can also be inhibited by a variety of covalent modifications like phosphorylation by mitogen activated kinase (MAPK) (50), ubiquitinylation (51), SUMOylation (52), or acetylation (53).

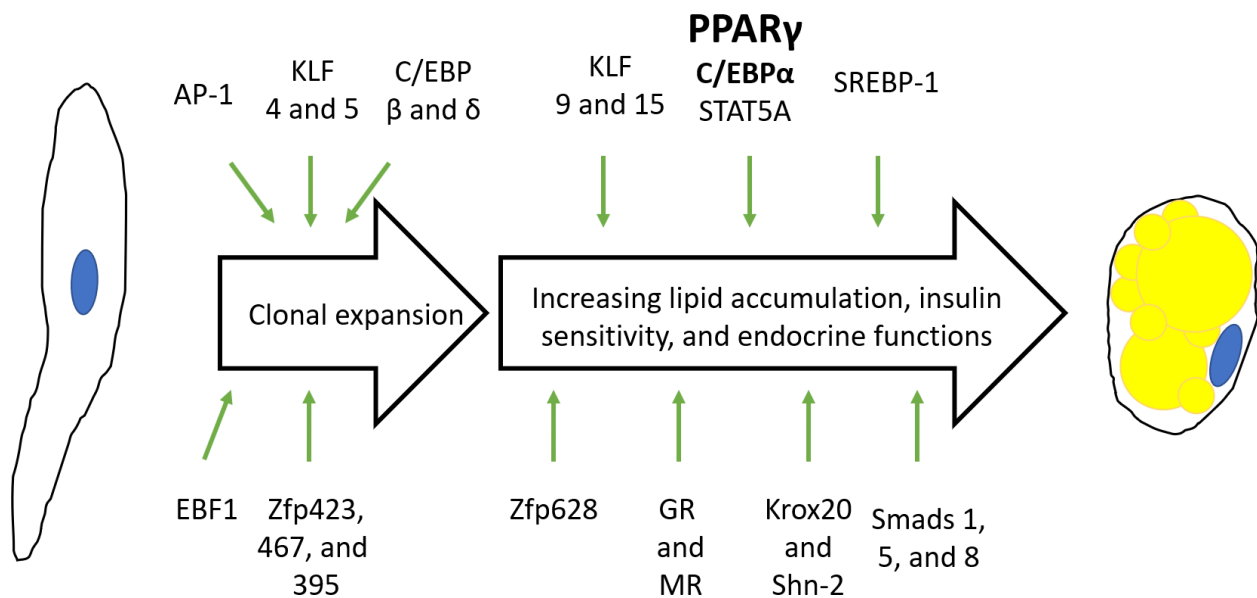


Figure 2: Transcriptional activation of adipogenesis requires a large number of different factors with a precise timing. Members of the activator protein 1 (AP-1) family, Zinc finger proteins (Zfp), Krüppel-like transcription factors (KLF), and others are essential for the induction of clonal expansion. Later, PPAR γ , C/EBP α , other members of KLF and Zfp family as well as other factors activate cell differentiation. The figure indicates the relative timing of activation of each transcription factor. The figure was modified based on (54).

Some of the oldest known transcription factors of adipogenesis are C/EBP α , - β , and - δ (55). They belong to a family consisting of six members, which are also involved in cell proliferation and differentiation in other cell types (56, 57). Mice carrying C/EBP α -knockout show severe abnormalities in their body fat metabolism like impairment of lipid accumulation in WAT and BAT

(58). The mice carrying these deletions have strong physiological and metabolic anomalies like hyperlipidemia, hyperinsulinemia, and hepatosteatosis (59). Not only neonatal mice have severe problems when one of these C/EBP proteins is missing, but ablation of C/EBP α in adults also leads to impairments. Yang and coworkers showed that these adult mice have a strong reduction of WAT mass, which indicates that C/EBP α is also important in mature adipocytes (60). Others showed that knockouts of either C/EBP β or δ result in impairments of adipogenesis and WAT growth (61). However, Tanaka and coworkers identified potential compensatory mechanisms for initiation of adipogenic gene expression by showing that a double knockout of C/EBP β or δ lead to survival of about 20% of the neonates. Adult mice have normal levels of PPAR γ , C/EBP α and aP2 with reduced overall body fat mass. Interestingly, the C/EBP transcription factors are expressed at different stages of adipogenesis. C/EBP β has its maximal expression during early adipogenesis (62, 63) where it regulates C/EBP α expression. In detail, C/EBP β and δ together induce low levels of C/EBP α and PPAR γ (62). These two induced transcription factors in turn induce each other's expression in a positive feedback loop which promotes and maintains the ongoing differentiation (see Figure 3). Thereby, C/EBP α is necessary for maintaining the expression of PPAR γ as well as promoting insulin sensitivity. However, PPAR γ is the major and direct regulator of adipogenesis (64). C/EBP α is most abundant during the maturing phase and in mature adipocytes (65). Wu and coworkers showed that C/EBP α is crucial for insulin-responsive glucose uptake. Others confirmed this model as they showed that ectopic PPAR γ expression is able to rescue the adipogenic process in mouse embryonic fibroblast cells (MEFs), which do not express C/EBP α (64). However, the rescuing process by PPAR γ has not yet been conclusively clarified. Other C/EBP transcription factors might also have compensatory mechanisms.

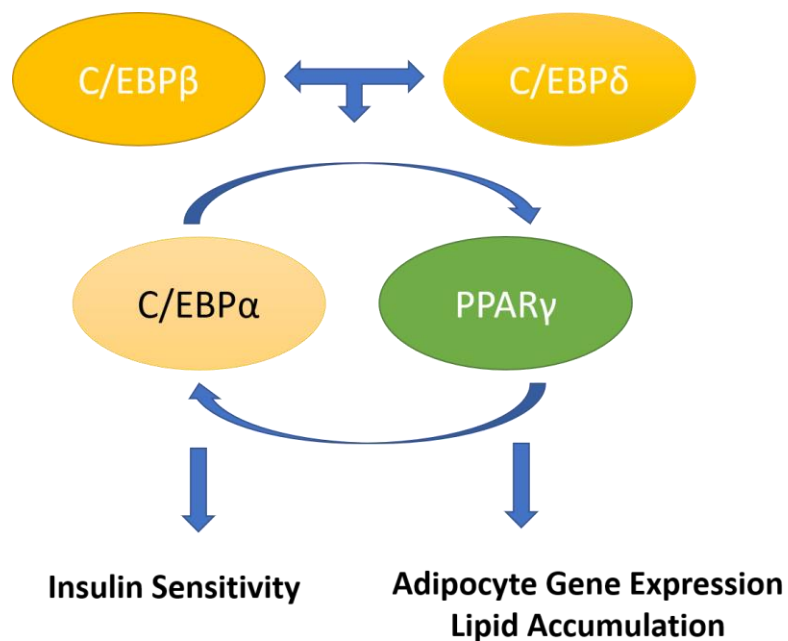


Figure 3: Transcriptional regulation of adipogenesis is highly dependent on PPAR γ and members of the C/EBP protein family.

Introduction

C/EBP β and δ jointly induce the expression of C/EBP α and PPAR γ . These two transcription factors induce each other's expression in a positive feedback loop, which promotes and maintains the ongoing differentiation. PPAR γ is responsible for adipocyte gene expression and lipid accumulation, whereas C/EBP α is responsible for maintaining the adipocyte's insulin sensitivity for glucose uptake. Figure was modified based on (64) and (54).

Other important regulators, modulators, and distributors of adipogenesis are steroid hormones and their receptors. Estrogen receptors ER α and ER β are expressed in preadipocytes, adipocytes, and other cells that can be found in adipose tissue (66, 67). Results from *in vitro* and *in vivo* studies showed an inhibitory influence of estrogens on cell differentiation by decreasing gene expression of adipogenic genes and inhibition of PPAR γ coactivator recruitment (68, 69).

Furthermore, two research groups recently identified polyamines as additional important adipogenic factors (70, 71). Polyamines like putrescine, spermidine, and spermine are involved in several fundamental cellular processes including proliferation, cell growth and survival, stabilization of chromatin structure, protection from oxidative damage, and maintenance of protein and nucleic acid synthesis (72-77). Brenner and coworkers showed that depletion of these metabolites in murine cells results in inhibition of PPAR γ and C/EBP α expression (70, 71). In addition, they also identified that this depletion inhibits the second division of mitotic clonal expansion (70, 71).

1.3. Cell models for the characterization of adipogenesis

Most of the knowledge about adipogenesis and adipocyte biology was gained by using *in vitro* cell models of murine, human, and rat origin. In the last century, murine cells were used for most of the findings. In the 1960s, methods were developed that enabled the separation of adipocytes from the stromal and vascular cells of surgically removed adipose tissue (78). Interestingly, these methods are still used today. About 10 years later, Green and coworkers established one of the first preadipocyte cell lines, namely 3T3-L1 (79, 80). Therefore, they isolated cells from disaggregated 17 to 19 days old mouse embryos (79, 80). Clonal expansion was applied to immortalize Swiss 3T3 mouse embryonic fibroblasts that are morphologically indistinguishable from nonadipogenic fibroblasts with high differentiation potential. For differentiation, a hormonal cocktail consisting of dexamethasone, 3-isobutyl-1-methylxanthine (IBMX), and insulin was supplemented into the media (79, 80). Despite immortalization of the cells, the capacity to differentiate decreases with increasing subcultivation events (20). Nevertheless, this cell line was and still is very useful for the identification of key transcription factors and molecular markers to characterize adipogenesis. Some years later, Kuri-Harcuch and Green generated a second adipocyte cell line, named 3T3-F442A, with similar capabilities (81).

Both cell lines have major advantages compared to primary murine cells as they are much easier to handle, less costly, easy to obtain from commercial vendors, and have a homogenous cell population (82). Thereby, these cells enable homogeneous experimental conditions. However, immortalized cell lines in general come with some limitations. The morphological difference is the

Introduction

most obvious one. 3T3-L1 adipocytes are multilocular, which distinguishes them largely different from the unilocular phenotype of mature adipocytes *in vivo* (79). In addition, most of the cell lines are aneuploid and therefore differ significantly from white primary adipocytes (83, 84), which are diploid (85). Furthermore, the cells express much lower amounts of leptin than adipocytes *in vivo* (86).

Another murine cell model, C3H10T1/2 which was established in 1973 (87), is derived from mouse embryonic stem cell precursors. C3H10T1/2 cells have the capability to differentiate into mesodermal cell types like adipocytes, but also into chondrocytes, osteoblasts, and myotubes, depending on the applied differentiation cocktail (88).

The OP9 mouse stromal cell line is a more recent addition to the adipocyte cell models (89). The cells are also widely accepted for studying adipogenesis, because they differentiate fast within two days, enabling high-throughput screening (89). In addition, these cells can be cultivated for long periods (89).

OP9, C3H10T1/2, and 3T3 cell lines have one major limitation in common, they are all derived from mouse (embryos) and their physiological characteristics differ strongly from human adipocytes (20). Therefore, results obtained by studying murine cell models cannot be directly compared to humans.

Porcine primary preadipocytes can bridge this major limitation, because these cells have a much higher similarity to human cells (90). Thus, these cells are a better cell model for research of adipogenesis, obesity, T2D, and other obesity-related diseases in human. Porcine cultures were used for studying several additional promoting and inhibiting adipogenic-factors like retinol binding protein 4 (RBP-4), Akt2, sirtuin 1 (SIRT-1), and several miRNAs (91-94). Nevertheless, porcine cell models also differ from human cells in terms of physiological properties, but to a lesser extent than murine models (90). Therefore, human cell models were developed to enable a higher comparability to the *in vivo* situation.

For generating human models, stromal vascular fractions (SVF) are commonly used consisting of several cell types like stem cells, preadipocytes, endothelial, and immunological cells (95). Adipose-derived stem cells (ADSCs) are putatively the most important human cells used to study human adipogenesis. Interestingly, these cells were first observed and described in rabbits in 1940 (96). In the following decades, immense effort was undertaken to analyze the characteristics and potential of human ADSCs. It was discovered that these cells are multipotent stem cells, which can be differentiated into several different cell types similar to the murine C3H10T1/2 cell line (97). In addition to their multipotency, the cells have following advantages. ADSCs show a high expansion capacity and have the ability to be cultivated for several generations (98). Furthermore, the differentiated cells show the same morphological characteristics as freshly isolated adipocytes (20). Lastly, the cells respond to hormones used in physiological concentrations (99).

In addition to ADSCs, primary human preadipocytes derived from adipose tissue are a suitable model of adipogenesis, because they also show an excellent ability to differentiate. As their

characteristics are highly dependent on the donor and the collection site (subcutaneous or visceral adipose tissue), these cells are also an ideal model for examinations of differences between individuals. For instance, differences between diseased patients and healthy control patients can be studied (100, 101). On the downside, primary human preadipocytes and ADSCs do not proliferate well in culture and not every laboratory has easy access to these cells.

Until this date, only two stable human cell lines derived from white adipose tissue have been established. Both originate from a working group of the University of Ulm (102, 103). Results from first investigations of the first cell line, LiSa-2, were published in 2000. The cells are derived from a poorly differentiated, pleomorphic liposarcoma and showed potential for cell differentiation with multiple small lipid droplets (104). Only a few studies used this cell line, possibly due to its differences in gene expression profiles especially of genes of the fatty acid metabolism compared to freshly isolated adipocytes (104-106). In addition, the establishment of the second cell line from the same working group with a higher capacity for differentiation might have hindered the further use of LiSa-2 cells. This second cell line became well accepted and is highly used by the scientific community. The human cells are derived from a male infant patient with Simpson-Golabi-Behmel syndrome (SGBS). This rare X-linked disorder is characterized by pre- and postnatal overgrowth (107-110). The preadipocytes were isolated from a stromal cell fraction of subcutaneous adipose tissue. These cells still are the only fully inducible preadipocyte cell line of human origin using a well-defined differentiation cocktail (103). The cells provide an almost unlimited source of human preadipocytes, because after stimulation with differentiation medium, up to 95% of all SGBS cells until generation 30 differentiate into mature adipocytes. These fully differentiated cells show a similar gene expression profile compared to mature human fat cells (111). Moreover, the cells cannot be distinguished from *in vitro* differentiated adipocytes from healthy subjects based on their morphology, biochemical, and functional properties (111). Others also confirmed these initial findings from Wabitsch and coworkers (111, 112). However, recent studies showed a potential of SGBS cells to a beige phenotype upon stimulation with PPAR γ -agonists and irisin (113, 114). A very recently published study demonstrated that ADSCs cells also showed this propensity when stimulated with these factors under equal conditions (112). Nevertheless, SGBS cells are a good cell model for studying human adipogenesis because the advantages of this model markedly outweigh the disadvantages.

1.4. Analyzing biological processes with metabolomics, lipidomics, and transcriptomics

Metabolomics is a research field which uses distinct strategies for the identification or quantification of small molecular substrates, intermediates, or end products of the metabolism (115). Analytical technologies are combined with statistical methods for data analysis and interpretation. The information is used for a comprehensive analysis of metabolites in biological systems for the understanding of the complexity of biological processes (115). In the late 1940s

and early 1950s, Williams and coworkers published results of “metabolic patterns” in urine and saliva using paper chromatography for the first time (116). Technological improvements in the following decades enabled quantitative analyses of metabolite profiles. Therefore, the emergence of metabolomics is closely linked with the development of gas chromatography systems, which were later coupled to mass spectrometers as detectors (117). In the 1970s the terminus “metabolic profile” became more prominent when Horning, Mamer and others analyzed metabolite profiles with GC-MS systems in human urine and tissue extracts (117, 118). From that time onward, this research field gained more and more importance (119-121). In addition, the development of nuclear magnetic resonance spectroscopy (NMR) and especially liquid chromatography coupled to mass spectrometry have pushed metabolomics from a niche to an important tool in science. In the last 20-30 years, mass spectrometers were greatly improved regarding sensitivity, resolution, dynamic range, and other features, which enabled their use in a wide range of applications (122-124). In addition, recent commercial applications of ion mobility coupled to mass spectrometers have driven metabolomics towards much higher separation powers, especially for lipids. These analytical improvements in turn drove research on lipids and the understanding of their role in cells, tissues, and whole bodies, named lipidomics. In addition to the development of high resolution mass spectrometers, the introduction of more ¹³C- and deuterium-labeled internal standards (ISTD) for lipids has further increased the importance of lipidomics for biomedical research in basic research, drug, and biomarker development (125).

As mentioned before, there are various approaches for metabolomics and lipidomics (126). On the one hand, non-targeted approaches are used for qualitative profiling of the metabolome and lipidome, delivering information on the presence of many hundreds up to thousands features (127, 128). For peak or ion trace analysis, reference databases are required for the annotation of signals to specific metabolites. On the other hand, targeted methods are applied for quantitative determination of a defined set and number of metabolites and lipids (128). The number of measured species in targeted approaches can be up to several hundreds. To determine the exact concentrations, stable isotope labeled standards and calibration curves are commonly used. By using the targeted approach, a very high throughput is possible, because many methods use fast liquid chromatographic conditions (126). Non-targeted approaches are characterized by complex peak or ion trace analyses, which require reference databases for the annotation of signals to specific metabolites.

Analytical methods must deliver reliable and reproducible results. Therefore, the development and validation of methods fulfilling these requirements are indispensable. The European Medicines Agency (EMA) and the American Food and Drug Administration (FDA) give detailed instructions for bioanalytical method development and validation (129, 130). In addition, the metabolomics standards initiative (MSI) provides information on the minimal reporting standards when applying metabolomics (131). In the last years, the strongly emerging field of lipidomics provided recommendations for an appropriate nomenclature and reporting of lipid data (132, 133). Furthermore, standardized workflows and data evaluation approaches are necessary to ensure high quality of the measurements and to enable comparisons between different studies.

Introduction

Cell culture metabolomics and cell culture lipidomics can be regarded as a subdiscipline, because both require special attention to sample preparation and analytics (134, 135). Harvesting of the cells is highly dependent on the cultivation conditions. For suspension cultures, cells can be isolated from medium by filtration or centrifugation followed by washing steps to remove the medium (135, 136). For adherent cell cultivation, the cells are usually detached from the surface by scraping in ice-cold methanol or other organic solvents allowing immediate quenching of cellular metabolism (135, 137). Formerly, trypsinization was also used, which enabled cell counting (138). However, this harvesting procedure has a strong impact on the metabolome and therefore should be avoided (135).

Cell culture samples usually have cases low concentrations of the metabolites and lipids of interest. Therefore, it is crucial to develop and apply analytical methods that can detect or quantify metabolites in these low concentrations.

In contrast to the analysis of blood samples, the used volume of cell samples can be very heterogeneous in terms of cell number. In every well of a cell culture plate, different numbers of cells are growing (137). In addition, the harvesting error can vary between the wells. Thus, cell numbers will inevitably vary between samples. These variations have a strong influence on analytical data. Therefore, a normalization approach is required to account for these variations. The most promising approaches are the use of proteins or DNA for normalization (135, 137, 139). However, findings from Silva and coworkers demonstrated the usage of DNA as the most applicable marker for normalization regarding feasibility and accuracy. In addition, my former colleagues developed and validated a DNA-based normalization approach for adipocytes (135).

Metabolomics and lipidomics have shed light on cellular processes at the time of cell harvest. However, sample storage can have a significant influence on the metabolome as recently shown (140). Haid and coworkers showed that in human plasma samples the concentration levels of amino acids and lipids like acylcarnitines and phosphatidylcholines changed up to 18% during five years of storage at -80 °C (140). Therefore, long-term storage should be avoided, or the storage conditions should be highly stable and always below -80 °C.

Transcriptomics allows the analysis of actively expressed genes at the time when the cells are harvested. This omics technique has been routinely used since the 1990s for the identification of gene functions or pathways (141-143). In the past, it was also applied for the characterization of the adipogenic differentiation process (144-146). However, mRNA, which is the most important analyzed product in transcriptomics studies, is not the final molecule that is translated into proteins (147, 148). Post-transcriptional modifications, alternative splicings, but also degradation of mRNA are common mechanisms leading to variable proteins and their expression levels. Therefore, transcriptomics studies alone can only give a hint about active biological processes whereas metabolomics is able to identify ongoing and past processes. Thus, the combination of transcriptomics, metabolomics, and lipidomics enables a comprehensive analysis of biological processes

1.5. Metabolomics and lipidomics in adipogenesis research

In the last two decades, metabolomics and lipidomics approaches were also applied for the elucidation of the adipogenic process. Roberts and coworkers were one of the firsts to publish a study about the analysis of the cell differentiation process using murine 3T3-L1 cells and a broad analytical setup (149). They identified metabolites with significantly changed concentration levels during adipogenesis which are involved in the TCA cycle, glycolysis, fatty acid synthesis and degradation as well as polyamine biosynthesis (149). Later, Kirkwood and coworkers identified strongly changed levels of phosphatidylcholines during murine differentiation (150). Halama and coworkers analyzed at the same time the 3T3-L1 differentiation process (146). They identified strong regulation of pathways like the synthesis of phosphatidylcholine, the metabolism of even and odd chain fatty acids, and the catabolism of the three branched-chain amino acids (146).

More recent studies showed that part of the energy for adipocyte differentiation and lipogenesis is derived from degradation of branched-chain amino acids (BCAA) (151). Green and coworkers showed that proliferating, undifferentiated murine preadipocytes use glucose and glutamine for acetyl-coenzyme A (CoA) generation (151). Differentiated murine adipocytes catabolize leucine (Leu) and isoleucine (Ile) from the medium or protein degradation to such an extent that both are responsible for about 30% of the lipogenic CoA pool (151). Collins and coworkers analyzed the pathway of *de novo* lipogenesis in human cells in greater detail (152). Glucose provided around 45% and glutamine around 10% of the carbon used for lipogenesis (152). However, for TAG-glycerol synthesis, glucose is the most important supplier as it provided about 72% (152).

All in all, most of the studies, which analyzed the metabolome and lipidome of the adipogenic process on, were performed with murine cells. There is less knowledge about the adipogenic processes in human cells. Furthermore, the published results did not resolve the lipid isobars due to a lack of appropriate instruments.

1.6. Aim of the thesis

The overall aim of this PhD thesis was to increase the knowledge in obesity research by characterizing human adipogenesis with a strong focus on the lipidome. During the past decades, several hundreds of research papers were published, elucidating the highly complex process of adipogenic cell differentiation. Nonetheless, the process is still not fully understood, evidenced by the fact that only in the last decade another fat cell type (beige adipocytes) was identified (153). To this date, several important transcription factors have been identified during *in vivo* and *in vitro* studies. Knockdown and overexpression studies have been invaluable for elucidating adipogenic mechanisms. Most studies on transcripts, metabolites, and lipids during adipogenesis used murine cells (146, 149, 150). In addition, several studies only compared the levels in fully differentiated adipocytes with undifferentiated cells missing changes during the process (151, 154). There are only a few studies published which used cells of human origin. These studies (151, 152) have in

Materials and Methods

common that they only analyzed metabolites and lipids of a small number of different classes. In addition, most of them were unable to resolve the lipids on their isobar level. Moreover, only a few studies (146, 155) combined data of the metabolome and the transcriptome, and none included data of the lipidome for a deeper understanding.

Therefore, lipidomics, metabolomics, and transcriptomics approaches were combined with several independent methods to identify changes in metabolites, lipids, and transcripts as well as regulated metabolic pathways during adipogenesis using human cells. In addition, a GC-MS based method was developed and validated for the measurement of metabolites from energy metabolism.

This broad and unique analysis of cell culture samples intended to shed light onto the cellular processes during adipogenesis and obesity development. A better understanding of obesity-related processes is necessary, to be able to counteract the pandemic dimensions it reached in the last decades with no hope for recovery. This PhD thesis can help in developing new approaches for the prevention or treatment of this disorder several hundreds of million affecting.

2. Materials and Methods

2.1. Chemicals, equipment, and software

2.1.1. Chemicals, hormones, enzymes, reagents, and media

Ampicillin sodium salt	Merck (Darmstadt, Germany)
0.05% Trypsin (0.53 mM EDTA)	Life Technologies (Darmstadt, Germany)
3-isobutyl-1-methylxanthine	Merck (Darmstadt, Germany)
Biotin	Merck (Darmstadt, Germany)
Dexamethasone	Merck (Darmstadt, Germany)
Dichloromethane	Merck (Darmstadt, Germany)
Dimethylsulfoxid	Carl Roth GmbH & Co. KG (Karlsruhe, Germany)
DNA agarose	Biozym Scientific GmbH (Hessisch Oldendorf, Germany)
DMEM / F-12	Life Technologies (Darmstadt, Germany)
Ethanol	Merck (Darmstadt, Germany)
FBS Superior	Biochrom GmbH (Berlin, Germany)
Hoechst 33342	Life Technologies (Darmstadt, Germany)
Hydrocortisone	Merck (Darmstadt, Germany)
Insulin solution human	Merck (Darmstadt, Germany)
LB-agar	Carl Roth GmbH & Co. KG (Karlsruhe, Germany)
LB-medium	Carl Roth GmbH & Co. KG (Karlsruhe, Germany)
Metformin hydrochloride	Merck (Darmstadt, Germany)

Materials and Methods

Methanol	AppliChem (Darmstadt, Germany)
Methoxyamine hydrochlorid	Merck (Darmstadt, Germany)
Methyl tert-butyl ether (MTBE)	Merck (Darmstadt, Germany)
N-Methyl-N-(trimethylsilyl)-trifluoroacetamid (MSTFA)	Merck (Darmstadt, Germany)
Panthothenate	Merck (Darmstadt, Germany)
Phenformin hydrochloride	Merck (Darmstadt, Germany)
Phenylisothiocyanate	Merck (Darmstadt, Germany)
Pyridine	Merck (Darmstadt, Germany)
Rosiglitazone	Merck (Darmstadt, Germany)
Taq polymerase	In-house (produced and provided by G. Zieglermaier)
Transferrin	Merck (Darmstadt, Germany)
Triiodothyronine (T3)	Merck (Darmstadt, Germany)
TRIzol Reagent	Invitrogen (Carlsbad, USA)

2.1.2. (Internal) standards for the GC-MS assay

DL-13C4-3-hydroxybutyric acid	Euriso-top (Saarbrücken, Germany)
13C4- α -ketoglutaric acid	Euriso-top (Saarbrücken, Germany)
13C4-fumaric acid	Merck (Darmstadt, Germany)
13C3-lactic acid	Merck (Darmstadt, Germany)
13C3-pyruvic acid	Merck (Darmstadt, Germany)
13C4-ribose	Campro Scientific (Berlin, Germany)
13C6-glucose	Euriso-top (Saarbrücken, Germany)
D3-2-hydroxyglutaric acid	Euriso-top (Saarbrücken, Germany)
DL-D3-malic acid	Merck (Darmstadt, Germany)
D4-citric acid	Euriso-top (Saarbrücken, Germany)
2-hydroxyglutaric acid	Merck (Darmstadt, Germany)
2-hydroxybutyric acid	Merck (Darmstadt, Germany)
3-hydroxybutyric acid	Merck (Darmstadt, Germany)
α -ketoglutaric acid	Merck (Darmstadt, Germany)
citric acid	Schubert und Weiss (Bremen, Germany)
fumaric acid	Merck (Darmstadt, Germany)
glucose	Schubert und Weiss (Bremen, Germany)
isocitric acid	Merck (Darmstadt, Germany)
L-(+)-lactic acid	Merck (Darmstadt, Germany)
L-(-)-malic acid	Schubert und Weiss (Bremen, Germany)
pyruvic acid	Merck (Darmstadt, Germany)
ribose	Merck (Darmstadt, Germany)
succinic acid	Merck (Darmstadt, Germany)

Materials and Methods

2.1.3. Consumables

6-well plate Cell+	Sarstedt AG & Co. KG (Nümbrecht, Germany)
96 well plate (F96, black, flat bottom)	Nunc, Thermo Fisher Scientific (Schwerte, Germany)
96-well plate 350 μ L PCR plate	Sarstedt (Nümbrecht, Germany)
Cell culture flasks T75 cm ³	Greiner Bio-One GmbH (Frickenhausen, Germany)
Cell culture flasks T175 cm ³	Greiner Bio-One GmbH (Frickenhausen, Germany)
Cell scraper 25 cm	Sarstedt (Nümbrecht, Germany)
CryoTube Vials	Thermo Fisher Scientific (Roskilde, Germany)
Micro tubes 0.5 mL PP	Sarstedt (Nümbrecht, Germany)
Micro tubes 2 mL PP	Sarstedt (Nümbrecht, Germany)
Eppendorf tubes 1.5 mL DNA LoBind	Eppendorf AG (Hamburg, Germany)
Eppendorf tubes 2 mL DNA LoBind	Eppendorf AG (Hamburg, Germany)
Precellys Glass Beads (0.5 mm)	peqlab Biotechnologie GmbH (Erlangen, Germany)
Pre-slit silicon mat	Fisher Scientific (Rochester, USA)

2.1.4. Human cells and bacteria

SGBS (human)	kindly provided by Prof. Dr. med Martin Wabitsch (103)
<i>E. coli</i> DH5 α	Life Technologies (Darmstadt, Germany)

Genotype *E. coli* DH5 α : F- Φ 80*lacZ* Δ M15 Δ (*lacZYA-argF*) U169 *recA1 endA1 hsdR17* (rk-, mk+) *phoA supE44 thi-1 gyrA96 relA1* λ -

2.1.5. Kits

Absolute/DQ p180 kit	Biocrates Life Sciences AG (Innsbruck, Austria)
Agilent RNA 6000 Pico	Agilent Technologies Deutschland GmbH & Co. KG (Böblingen, Germany)
BigDye3.1 Terminator c3.1 Cycle Sequencing Kit	Applied Biosystems (Darmstadt, Germany)
Lipidizer™ kit	Sciex Germany GmbH (Darmstadt, Germany)
MassChrom® Newborn Screening Assay	ChromSystems (Gräfelfing, Germany)
MycAlert™ Mycoplasma Detection Kit	Lonza (Basel, Switzerland)
NucleoSpin Plasmid kit	Macherey-Nagel GmbH & Co. KG (Düren, Germany)
RevertAid First Strand cDNA Synthesis Kit	Thermo Fisher Scientific (Schwerte, Germany)

Materials and Methods

Absorbance and fluorescence reader

2100 Bioanalyzer kit	Agilent Technologies Deutschland GmbH & Co. KG (Böblingen, Germany)
GloMax Multi Detection System	Promega (Mannheim, Germany)
Safire ²	Tecan (Männerdorf, Switzerland)
NanoDrop 1000 Spectrophotometer	Thermo Fisher Scientific (Wilmington, USA)
Qubit 2.0 Fluorometer	Thermo Fisher Scientific (Schwerte, Germany)

Evaporation systems

Barkey Evaporator 60 samples	Barkey GmbH & Co. KG (Leopoldshöhe, Germany)
TurboVap 96	Biotage (Uppsala, Sweden)

More laboratory equipment

AxioVert 40 CFL inverse microscope	Carl Zeiss AG (Jena, Germany)
Cellometer [®] Auto T4 Plus	peqlab Biotechnologie GmbH (Erlangen, Germany)
Hamilton Microlab STAR [™] workstation	Hamilton Bonaduz AG (Bonaduz, Switzerland)
Precellys 24 homogenizer	peqlab Biotechnologie GmbH (Erlangen, Germany)
ThermoALPS Sealer	ThermoFisher Scientific (Dreieich, Germany)
QuantStudio 7 Flex Real-Time PCR system	ThermoFisher Scientific (Dreieich, Germany)

2.1.7. Software and programs

Agilent MassHunter Workstation	Agilent Technologies Deutschland GmbH & Co. KG (Böblingen, Germany)
Analyst [®] version 1.6	Sciex Germany GmbH (Darmstadt, Germany)
AxioVision LE	Carl Zeiss Microscopy GmbH (Jena, Germany)
GraphPd Prism 8.1.1	GraphPad Software (San Diego, USA)
Lipidyzer [™] Workflow Manager	Sciex Germany GmbH (Darmstadt, Germany)
MetaboAnalyst 4.0	http://www.metaboanalyst.ca/ (156)
Met/DQ [™]	Biocrates Life Sciences AG (Innsbruck, Austria)
R Version 3.5.1	http://www.R-project.org/ (157)
RStudio Version 1.0.136	RStudio Inc. (Boston, USA)
Primer-Blast	http://www.ncbi.nlm.nih.gov/tools/primer-blast/ (158)

2.2. Working with human cells

The Simpson-Golabi-Behmel-Syndrome (SGBS) preadipocyte cell strain was cultured and differentiated up to 20 days as described before (22, 159, 160). In brief, cryo-conserved cells were thawed in a water bath at 37 °C and transferred into 10 – 15 mL pre-warmed DMEM/F12 medium, supplemented with 10% FBS, 3.3 mM biotin, and 1.7 mM pantothenate, referred as cultivation medium. Cells were centrifuged for 5 min at 1000 x g, the supernatant was discarded, the cells were resuspended in 40 mL cultivation medium, transferred to a T175 cultivation flask, and cultivated at 37 °C and 5 % CO₂ in a humidified atmosphere. For passaging, medium was aspirated and cells were washed with 30 mL pre-warmed PBS. Then, the cells were detached using 5 mL of 0.05% Trypsin (0.53 mM EDTA) and the trypsinization reaction was stopped by the addition of 15 mL cultivation medium. The cell suspension was transferred to a 50 mL falcon tube, pelleted at 5,000 x g for 5 min, resuspended in 15 mL cultivation medium, subsequently the cells were counted.

For experiments, 50,000 preadipocyte cells were seeded in each well of a 6-well plate in cultivation medium. Cell differentiation was initiated when cells reached approximately 90% confluence. For this purpose, medium was exchanged by serum-free medium, supplemented with 10 µg/mL transferrin, 0.2 nM triiodothyronine (T3), 250 nM hydrocortisone, 20 nM human insulin, 25 nM dexamethasone, 250 µM 3-isobutyl-1-methylxanthine (IBMX), and 2 µM rosiglitazone. After in a 4-day rhythm, medium was replaced with serum-free medium containing 10 µg/mL transferrin, 0.2 nM T3, 250 nM hydrocortisone, and 20 nM human insulin (maturation medium). For cryo-conservation, cells were washed with PBS, detached with trypsin-EDTA and resuspended in 15 mL cultivation medium (160). Afterwards, cells were pelleted by centrifugation for 5 min at 1000 x g, the supernatant was discarded, and the cells resuspended in cultivation medium supplemented with 10 % glycerol. 5-10 x 10⁵ cells were transferred into cryo-tubes and placed in a freezing container at -80 °C for controlled freezing at -1 °C/min. Afterwards, the cells were stored in liquid nitrogen.

2.3. Working with *Escherichia coli* (*E. coli*)

E. coli cells were cultured in liquid LB-medium and on LB-agar plates both containing ampicillin with a final concentration of 100 µg/mL. *E. coli* cells were cultivated on LB-agar plates for the selection of transformed cells. For colony screens, *E. coli* cells were cultured in liquid medium at 37 °C with gentle agitation (200 rpm). For long-term storage, 1000 µL *E. coli* cells from an overnight culture were mixed with 500 µL sterile 80% glycerol and transferred to -80 °C.

For transformation of chemically competent *E. coli* cells, 50 µL of the DH5α strain was thawed on ice and 1 – 10 µL of plasmid solution or ligation reaction were added. The mixture was incubated on ice for 30 min before a heat shock at 42 °C for 1 min was induced. After that, the cells were immediately placed back on ice. Into each reaction tube with transformation reactions, 400 µL

Materials and Methods

LB-medium was added and the tubes were incubated with gentle agitation (200 rpm) at 37 °C for 60-90 min. Afterwards, 50-300 µL of the transformation reactions were plated on LB-agar plates and incubated at 37 °C overnight.

2.4. Working with DNA

2.4.1. Isolation of plasmid DNA from *E. coli*

Plasmids were isolated from *E. coli* cultures (up to 4 mL) with the NucleoSpin Plasmid kit according to the manufacturer's instructions for high-copy plasmids. After eluting with 50 µL Buffer AE, the plasmid DNA was stored at 4 °C for up to a few days and at -20 °C for long-term.

2.4.2. Separation of DNA in agarose gels

DNA fragments were separated using agarose gel electrophoresis for monitoring PCR amplifications and DNA purity. Different agarose gels were prepared depending on the size of fragments to be analyzed (1 % (w/v) agarose in 1x TBE for fragments > 2 kb, 2 % (w/v) agarose in 1x TBE for fragments < 2 kb). Before starting the gel electrophoresis, DNA was mixed with loading dye and subsequently loaded on a gel containing 0.025 % (v/v) Midori Green Advance DNA stain. Gel electrophoresis was performed for 30 – 60 min depending on the size of DNA fragments.

10x TBE	108 g Tris	
	55 g boric acid	
	9.3 g EDTA	ad. 1 L H ₂ O
6x Loading Dye	15 % Ficoll 400	
	0.25 % bromophenol blue	
	0.25 % xylene cyanol FF	

2.4.3. Determination of RNA and DNA concentration and purity

To determine the concentration and purity of isolated RNA and DNA, three different approaches were used depending on downstream experiments. For standard downstream applications such as polymerase chain reactions (PCR), optical density was determined using a NanoDrop ND-1000 spectrophotometer at $\lambda = 260$ nm for quantity and the ratio of 260 / 280 nm for purity. DNA samples with 260 / 280 ratios ~ 1.8 were considered to be of high purity. RNA samples with 260 / 280 ratios ~ 2.0 were considered to be of high purity.

Materials and Methods

For RNA sequencing (see section 2.10), Qubit 2.0 fluorometer was used for a more precise measurement of the RNA concentration. The determination was performed according to the manufacturer's instructions. In addition, the quality of RNA for sequencing was assessed by using the 2100 Bioanalyzer and the corresponding Agilent RNA 6000 Pico kit. The measurements were also performed according to the manufacturer's instructions. RNA samples with RIN-values ≥ 9.0 were used for sequencing.

2.5. Working with RNA

2.5.1. Isolation of RNA from human cells

Total RNA was extracted from cells using miRNAeasy mini kit according to the manufacturer's protocol. In brief, the cells were scraped off the wells using rubber tipped cell scrapers and disrupted in 500 μ L QIAzol Lysis Reagent. Harvested cell-solvent suspension of four wells was pooled into 5 mL tubes. The samples were stored at $-80\text{ }^{\circ}\text{C}$ until further use. Then the RNA was extracted according to the protocol including the optional DNase digestion step.

2.5.2. Reverse transcription into cDNA

Total RNA was reverse transcribed into cDNA using the RevertAid First Strand cDNA Synthesis Kit according to the manufacturer's instructions. The reverse transcription was performed using an anchored oligo(dT)₁₈ primer (5'-TTTTTTTTTTTTTTTTTVN-3') in a final concentration of 0.5 μ M for priming cDNA synthesis.

2.6. Polymerase chain reaction (PCR)

Standard DNA amplifications via PCR from different templates (bacterial cultures, plasmid DNA, and cDNA) were conducted in 20 μ L reactions containing 0.2 mM dNTP mixture, 0.5 μ M forward and reverse primer each, and 0.5 – 2.5 U lab-made *Taq* polymerase in 1x PCR buffer (160). The amplification program was run on a Robocycler PCR machine with an initial denaturation step for 5 min (10 min for bacterial cultures) at $95\text{ }^{\circ}\text{C}$ followed by 35 cycles with 30 sec at $95\text{ }^{\circ}\text{C}$, 30 sec at $55\text{ }^{\circ}\text{C}$, and elongation for 1 min at $72\text{ }^{\circ}\text{C}$.

10x PCR buffer	100 mM Tris-HCl, pH 9.0
	500 mM KCL
	15 mM MgCl ₂

2.6.1. Quantitative real-time PCR (qRT-PCR)

Primers for qRT-PCR were designed using the Primer3 web-tool to span at least one exon-intron boundary to avoid falsified amplification results (161). Applied parameters for primer design are summarized in Table 1.

Table 1: Parameters for primer design using Primer3.

* X denotes the position of the target exon-intron-boundary. 20 base pairs around this position have to be included into the amplification product.

Parameter	Chosen range / value
Target	X, 20 *
Product size	120-220
Max 3' stability	7
Max mispriming	10
Pair max mispriming	20
Length of primer	18-22 bp
Melting temperature (T_M) of primer	58-61 °C
Max T_M difference	1.5
GC content	45-65%
Max self complementarity	6
Max 3' self complementarity	2

Primers were purchased from Metabion and are listed in Table 2.

Table 2: Primers for PCR experiments.

Gene	Sequence (5' → 3')
PPARG_463_for	GACCACTCCCACTCCTTTGA
PPARG_463_rev	GAGATGCAGGCTCCACTTTG
CEBPA_1136_for	AACAGCTGAGCCGCGAACTG
CEBPA_1136_rev	CGGAATCTCCTAGTCCTGGCT
TBP_578_for	CAGCCGTTCCAGCAGTCAA
TBP_578_rev	CTGCGGTACAATCCCAGAAC

Amplification of freshly prepared or stored cDNA as well as data analysis were performed as recently published (22). In detail, amplification was conducted in triplicates using Power SYBR Green PCR Mastermix with ROX as passive reference and a QuantStudio Flex 7 real-time PCR system as follows: denaturation at 95 °C for 10 min, 39 amplifications and quantification cycles with 95 °C for 15 sec and 60 °C for 1 min, and finally a melting curve program (95 °C for 15 sec, followed by 60-95 °C with a heating rate of 0.1 °C/sec) and continuous fluorescence measurement. The qRT-PCR device software was also used for the determination of the cycle threshold (CT) values. These values were used for the calculation of the relative gene expression based on the comparative $2^{-\Delta\Delta CT}$ method (162). To evaluate and correct for the performance of the qRT-PCR measurements, amplification efficiencies were determined based on the slope of the calibration

curve consisting of five different cDNA concentrations each amplified in triplicates. The calculated efficiencies were as follows: *PPARG* (106.3%), *CEBPA* (96.3%), and *TBP* (88.7%). The respective efficiencies were used to normalize the fold-change values for gene expression using a published procedure (162). Relative gene expression data for *PPARG* and *CEBPA* was subsequently normalized to the reference gene tata-box binding protein (*TBP*; in pre-experiments tested to be suited) and the expression of genes at day 0 of adipogenesis.

2.7. Cloning of DNA into plasmids

DNA fragments were cloned into plasmid with the TOPO-TA cloning strategy according to the manufacturer's instructions. Thereby, the vector pCR 2.1 TOPO was used. The *Taq* polymerase used for amplification synthesizes an A-overhang at the DNA fragment during the PCR, which can be ligated to the corresponding T-overhang in the respective vector. To increase the yield of the ligated products, the topoisomerase is attached to the vectors' cloning sites.

2.8. Sequencing of DNA

The accuracy of freshly amplified PCR products for the gene of interests was verified using the Sanger dideoxy method and the BigDye3.1 Terminator cycle sequencing kit as published (160). For this, 50 – 150 ng DNA were mixed with 1 μ L of the respective primers (forward / reverse, 10 μ M), 1 μ L 5x buffer, 1 μ L BigDye 3.1, and ddH₂O for a final volume of 5 μ L. Next, the DNA was amplified, after an initial denaturation step for 5 min at 95 °C, in 36 cycles with 30 sec at 95 °C, 45 sec at 53 °C, and 4 min at 60 °C. Afterwards, products were purified using the Montage Seq₉₆ sequencing reaction clean-up kit according to the manufacturer's instructions. Finally, purified sequencing reactions were analyzed on an ABI 3730 DNA analyzer.

2.9. Mass spectrometry approaches

2.9.1. Sample extraction

Cell samples for mass spectrometry analyses were harvested, homogenized, and the obtained values were normalized to cell number as recently published (22, 135). Shortly, after one washing step with 6 mL warm PBS per 6-well the cells were scraped off the wells using rubber tipped cell scrapers. The cells were collected in 500 μ L extraction solvent of ice-cold 80 % methanol per well. To increase the amount, harvested cell-solvent suspensions of four wells were pooled into pre-cooled 2 mL micro tubes containing 400 mg glass beads. Then, the samples were stored at -80 °C until further use. Cells were homogenized immediately before analysis at 4 – 10 °C for two times 25 s at 5500 rpm using a Precellys24. The resulting homogenates were used for lipidomics and

metabolomics measurement. In addition, the homogenates were also used for DNA quantification, as DNA content reflects indirectly the cell number of the sample, it was determined for normalization (135).

2.9.2. Normalization

For normalization of the mass spectrometry results (concentrations and signal intensity values) to the cell number, Hoechst assay was applied as recently published (22, 135). In detail, the fluorochrome Hoechst 33342 was diluted in PBS to the final concentration of 20 µg/mL. Of this solution, each 80 µL was pipetted into the wells of a black 96-well plate. 20 µL of vortexed cell homogenates or plain solvent (80 % MeOH; blanks) were added to the Hoechst solution and mixed by pipetting. Samples and blanks were applied in triplicates. The plate was incubated in the dark for 30 min at room temperature. Fluorescence signals were read using a GloMax multi detection system, equipped with an UV filter ($\lambda_{\text{ex.}} = 365 \text{ nms}$, $\lambda_{\text{em.}} = 410 -460 \text{ nm}$, Promega).

2.9.3. Lipidizer™ method

The Lipidizer™ method was used to analyze the cellular lipid levels of the SGBS cells as recently published (22). Fatty acid side chains of medium-chain (MCFA; C12), long-chain (LCFA; C13 - C21), and very long-chain (VLCFA; C22 - C26) lengths from 13 classes can be detected using this system. In detail, these are the following lipid classes: cholesterol esters (CE), ceramides (CER), dihydroceramides (DCER), diacylglycerols (DAG), free fatty acids (FFA), hexosylceramides (HCER), lactosylceramides (LCER), lysophosphatidylcholines (LPC), lysophosphatidylethanolamines (LPE), phosphatidylcholines (PC), phosphatidylethanolamines (PE), sphingomyelins (SM), and triacylglycerols (TAG). Since the notation rules from Liebisch and coworkers only know the case that either no fatty acid is known (e.g., TAG 52:2) or all three (e.g., TAG 16:0_18:1_18:1) [56], the nomenclature for TAG species in our study was adopted to these recommendations. The internal standard (ISTD) mix was prepared in accordance to the Lipidizer™ manual. The ISTD mix consisted of up to 10 ISTD per lipid class. For quality control (QC) samples, 250 µL of pooled cell homogenates were used, consisting in equal parts of undifferentiated, differentiating (day 8 of differentiation), and maturely differentiated cells (day 16). Three reference plasma samples of 100 µL in volume were spiked each with 50 µL of the QC spike mix, consisting of unlabeled lipid species at known concentrations. The use of reference plasma allows the investigation of inter-run and inter-project effects. For lipid extraction, a two-phase separation using methanol (MeOH), methyl tert-butyl ether (MTBE), and water (163) was used. Shortly, 250 µL of cell homogenates for the key experiments or 10-300 µL for method evaluation experiments, QC samples, or QC spiked plasma samples were transferred to 1.5 mL safe-lock reaction tubes. Afterwards, 160 µL of MeOH, then 900 µL of MTBE were added to each tube and incubated for 30 min at 900 rpm and room temperature in a shaker. Phase separation was conducted by the addition of 500 µL H₂O to each

Materials and Methods

tube, followed by vortexing. Then, the tubes were centrifuged at $15,000 \times g$ for 4 min at RT. The upper organic phases were transferred into chromatographic glass vials. This extraction step was repeated once, and organic phases were combined in the same glass vials. Afterward, organic solvents were evaporated to complete dryness under a stream of gaseous nitrogen. Finally, residuals were reconstituted in 250 μL of sample running buffer [10 mM ammonium acetate in dichloromethane:methanol (50:50 v/v)]. Samples were then directly flow injected with a UHPLC system and analyzed with the Lipidyzer™ method, consisting of a Sciex 5500 MS/MS QTRAP system equipped with a Selexion ion source for differential mobility spectrometry (DMS), in accordance with the manufacturer's instructions (164). Data were acquired automatically with the Lipidyzer™ Workflow Manager software. The obtained concentration values in nmol/g supplied by the software were converted to $\mu\text{mol/L}$, assuming that 1 mL of cell culture sample was equal to 1 mL of human plasma which is equal to 1 g (165).

Data quality control was conducted as recently published (22). Metabolites were excluded from the data set when concentration values were missing (NA) in more than 33.3 % of the samples within a time point. Missing values were replaced with the respective minimal lipid species concentration measured divided by $\sqrt{2}$ and multiplied by a randomly chosen factor between 0.75 and 1.25. Lastly, the obtained concentration values were normalized to cell number as described in sections 2.9.2 and 2.11.2.

2.9.4. Absolute/IDQ p180 kit

The Biocrates Absolute/IDQp180 kit was used for the quantitative analysis of metabolites and lipids of seven different classes, namely, amino acids, biogenic amines, sum of hexoses, acylcarnitines, lysophosphatidylcholines, phosphatidylcholines, and sphingolipids. However, this assay cannot resolve lipid species at the fatty acyl/alkyl level as the Lipidyzer™ method allows (see section 2.9.3). The assay was performed as published in detail earlier (166, 167). Additionally, the assay was validated according to the EMA's "Guideline on bioanalytical method validation" (130). Samples were handled with a Hamilton Microlab STAR™ robot. For the analysis, 10 μL of cell homogenates was used. Data evaluation and quality assessment of the measurements were done with the software MultiQuant 3.0.2 and Met/IDQ™. Measurements on a LC-ESI-MS/MS and FIA-ESI-MS/MS system, data evaluation, and quality assessment were performed by Silke Becker.

Data quality control was conducted as recently published (22). Metabolites were completely excluded from the data set if concentration values were missing (NA) in more than 33.3 % of the samples within a time point. Missing values were replaced by the LOD or, if not available, with the respective minimal metabolite concentrations measured divided by $\sqrt{2}$ and multiplied by a randomly chosen factor between 0.75 and 1.25. The obtained concentration values were afterwards normalized to cell number as described in sections 2.9.2 and 2.11.2.

2.9.5. Newborn Screening assay

The adapted MassChrom® Newborn Screening assay was applied for the measurements of 43 amino acids and acylcarnitines as previously published (168, 169). For the assay, 17.5 μL of the cell homogenates were pipetted into single wells of a 96-well plate. Subsequently, 200 μL extraction buffer containing internal standards was added to each well and mixed by shaking for 20 min at 600 rpm. Then, liquid mixture was evaporated using a speed-vac centrifuge at 60 °C. For derivatization, 60 μL of derivatization reagent was added to the dried sample extract followed by an incubation step for 18 min at 72 °C. The liquid was evaporated at 72 °C to complete dryness under a stream of gaseous nitrogen. Afterwards, samples were reconstituted in 100 μL reconstitution buffer. Finally, the plate was shaken for 10 min at 600 rpm. For analysis, 20 μL of the reconstituted sample was flow injected into a mass spectrometry system consisting of a 4000 QTrap triple quadrupole coupled with a Shimadzu prominence liquid chromatography system. The system was controlled by Analyst 1.7. Data evaluation for calculation of metabolite concentrations was performed with the software ChemoView 2.0.4. Metabolite concentrations were reported in $\mu\text{mol/L}$.

Data quality control was conducted as recently published (22). Metabolites were completely excluded from the data set if concentration values were missing (NA) in more than 33.3 % of the samples within a time point. Missing values were replaced with the respective minimal metabolite concentrations measured divided by $\sqrt{2}$ and multiplied by a randomly chosen factor between 0.75 and 1.25. The obtained concentration values were afterwards normalized to cell number as described in sections 2.9.2 and 2.11.2.

2.9.6. Non-targeted metabolomics using the technology by Metabolon Inc.

Non-targeted metabolomics was applied for the analysis of polar metabolites as well as lipids from several different classes and pathways. For the analysis of differentiating SGBS samples, Metabolon's technology was used which has a much higher pathway coverage than the methods described in section 2.9.4, 2.9.5, and 2.9.7. Cell sample harvesting and homogenization were described in section 2.9.1. All following sample preparation steps as well as the measurements itself were performed by Simone Huber and Dr. Anna Artati as published (170). For the assay, 50 μL of the cell homogenates were transferred into single wells of a 96-well plate. In addition, for later QA and QC analyses, three types of control samples were also transferred into the plate: human plasma for platform evaluation, control matrix samples containing aliquots from all SGBS samples served as technical replicates throughout the data set, and water samples as process blanks. For protein removal and quality assessment, extraction buffer containing methanol and several internal standards in a total volume of 500 μL were added to each well. The resulting extract was divided into five parts of 100 μL each: One part for HILIC/UPLC-MS/MS analysis in negative ion mode electrospray ionization (ESI), one for RP/UPLC-MS/MS analysis with negative

Materials and Methods

ion mode ESI, two parts for RP/UPLC-MS/MS analysis in positive ion mode ESI, and one part was reserved for backup. Samples were evaporated under a nitrogen stream using a TurboVap and reconstituted with 40 μL of reconstitution buffer containing ISTD compatible to each of the four analysis methods. For analysis, 5 μL of the reconstituted samples were injected into the mass spectrometry system consisting of a Waters Acquity UPLC and a Thermo Scientific Q-Exactive high resolution/accurate MS interfaced with a heated electrospray ionization (HESI-II) source and Orbitrap mass analyzer operated at 35,000 mass resolution for all measurements. The first aliquot of the processed samples was separated with a HILIC column (Waters UPLC BEH Amide 2.1x150 mm, 1.7 μM) and a gradient consisting of water and acetonitrile with 10 mM ammonium formate, pH 10.8 followed by analysis in negative ionization mode. The second aliquot was measured under conditions which were optimized for basic negative ions. Therefore, a C18 column (Waters UPLC BEH C18 2.1x100 mm, 1.7 μM) was used for the gradient elution of the analytes using methanol and water with 6.5 mM ammonium bicarbonate pH 8.0 followed by analysis in negative ionization mode. The aliquots three and four were analyzed in positive ionization mode. The third aliquot was chromatographically separated using the mentioned C18 column using water and methanol with 0.05% perfluoropentanoic acid (PFPA) and 0.1% formic acid (FA) to enable the measurement of more hydrophilic compounds. The fourth aliquot was also analyzed using acidic positive ion conditions; however, the chromatographic separation was used for more hydrophobic compounds. Therefore, the mentioned C18 column was used for the separation again, but with slightly different mobile phases: methanol, acetonitrile, water, 0.05% PFPA and 0.01% FA were used at an overall higher organic content. For the MS analysis, alternated MS and data dependent MS² scans using dynamic exclusion were applied. The scan range was 70-1000 m/z with slight variations between the four methods. Data extraction, peak identification, and QC evaluation were conducted by Metabolon. In brief, compounds were identified by automated comparison of the ion feature in the experimental samples to the library of standards based on retention time/index (RI), mass to charge ratio (m/z), and chromatographic data (including MS/MS spectral data). Peaks were quantified based on the area-under-the-curve and were reported as signal intensity values.

Afterwards, I performed additional data quality control as recently published (22). Metabolites were completely excluded from the data set if signal intensity values were missing (NA) in more than 33.3 % of the samples within a time point. Missing values were replaced with the respective minimal metabolite species concentration measured divided by $\sqrt{2}$ and multiplied by a randomly chosen factor between 0.75 and 1.25. The obtained concentration values were afterwards normalized to cell number as described in sections 2.9.2 and 2.11.2.

In addition, six lipid species had to be renamed because Metabolon used an incorrect notation. In detail, the lipid species 1-palmitoyl-GPC (16:0), 2-palmitoyl-GPC (16:0), 1-palmitoleoyl-GPC (16:1), 2-palmitoleoyl-GPC (16:1), 1-stearoyl-GPE (18:0), and 2-stearoyl-GPE (18:0) were named according their prevalence in mammalian systems. However, with the used instrumental system it is not possible to determine the correct *sn*-position of the fatty acid bound to their respective headgroup. Therefore, the signal intensity values of each lipid species pair were summarized (LPC 16:0, LPC 16:1, and LPE 18:0).

2.9.7. Energy metabolism assay

In course of this PhD study, a method for the quantification of metabolites of energy metabolism of human SGBS cells was developed. The analyzed metabolites are shown in Table 3 that also includes the concentrations of all seven calibrators for the standard curve. The cell samples were harvested and homogenized as described in section 2.9.1.

Table 3: Concentration of the calibrators and the ISTD used for the standard curve for the quantification of the metabolites of the energy metabolism.

The concentrations are shown as the concentrations on the column after sample preparation.

	Cal1 [μ M]	Cal2 [μ M]	Cal3 [μ M]	Cal4 [μ M]	Cal5 [μ M]	Cal6 [μ M]	Cal7 [μ M]		ISTD [μ M]
Pyruvate (Pyr)	0.10	0.50	1.00	2.50	5.00	10.00	20.00	13C3-Pyr	2.50
Lactate (Lac)	5.00	10.00	25.00	50.00	75.00	150.00	225.00	13C3-Lac	25.00
2-Hydroxybutyrate (2-HB)	0.25	0.50	1.00	2.50	5.00	10.00	20.00	13C4-3-HB	2.5
3-Hydroxybutyrate (3-HB)	0.30	0.60	1.20	1.80	2.40	3.60	7.20		
Succinate (Suc)	0.60	0.90	1.20	2.40	4.80	7.20	10.80		
Fumarate (Fum)	0.25	0.50	1.00	2.50	5.00	10.00	20.00	13C4-Fum	1.25
Malate (Mal)	0.50	1.00	1.25	2.50	5.00	10.00	20.00	D3-Mal	5.00
2-Hydroxyglutarate (2-HG)	0.20	0.50	1.00	2.00	4.00	8.00	10.00	D3-2-HG	1.00
Isocitrate (Isocit)	0.20	0.40	0.80	1.60	3.20	4.80	6.40		
α-Ketoglutarate (α-KG)	0.25	0.50	1.00	1.25	2.50	7.50	15.00	13C4- α -KG	2.50
Ribose (Rib)	0.30	0.60	1.20	1.80	2.40	3.60	7.20	13C4-Rib	1.00
Citrate (Cit)	0.75	1.50	3.00	6.00	9.00	12.00	24.00	D4-Cit	10.00
Glucose (Glc)	40.00	80.00	160.00	240.00	320.00	480.00	720.00	13C6-Glc	200.00

Based on sample volume titration experiments, 400 μ L of the homogenized sample were transferred to a 1.5 mL chromatographic glass vial without insert. For QC samples, 400 μ L pooled cell homogenates were used, consisting in equal parts of undifferentiated, differentiating (day 8 of differentiation), and maturely differentiated cells (day 16) (22). Subsequently, 10 μ L of the ISTD

Materials and Methods

solution was also added to the vial containing samples, QC sample or blank (80% MeOH). The solutions were dried under a stream of dry air to complete dryness. Afterwards, 50 μ L of 20 mg/mL methoxyamine hydrochloride in pyridine were added into each vial, properly closed with a cap, and derivatized for 60 min at 60 °C in the evaporation and heating system. Next, the vials were left to cool down to room temperature to avoid unnecessary evaporation before 50 μ L of MSTFA were added. The vials were closed with new caps, then transferred to the heating unit again for 60 min at 60 °C for the second derivatization step. After cooling down to room temperature, derivatized samples were transferred into vial inserts. Then, the freshly capped vials were transferred into the tempered auto-sampler tray at 10 °C and afterwards analyzed.

After analysis, data quality control was conducted as recently published (22). Missing values were replaced with the respective minimal lipid species concentration measured divided by $\sqrt{2}$ and multiplied by a randomly chosen factor between 0.75 and 1.25. The obtained concentration values were afterwards normalized to cell number as described in sections 2.9.2 and 2.11.2.

The analysis system consisted of a 6890 Series gas chromatograph coupled with a 5973N mass selective detector. The GC-MS system was operating in the single ion monitoring (SIM) mode with an HP5-MS column (30 m x 0.25 mm, 0.25 μ M). The corresponding SIM values are illustrated in Table 4 and were determined by total ion scans.

Table 4: Retention times, time segment, and m/z values for all analytes and their ISTD.

Analyte / ISTD	Time segment	Retention time [min]	Type	m/z
Pyruvate	1	8.41	Target	174.1
ISTD Pyr (= 13C3-Pyr)	1	8.41	ISTD	177.1
Lactate	1	8.62	Target	219.1
ISTD Lac (= 13C3-Lac)	1	8.62	ISTD	222.1
2-Hydroxybutyrate	2	9.85	Target	205.1
3-Hydroxybutyrate	2	10.42	Target	233.2
ISTD 3-HB / 2-HB / Suc (= 13C4-3HB)	2	10.42	ISTD	237.1
Succinate	3	13.07	Target	247.1
Fumarate	3	13.61	Target	245.1
ISTD Fumarate (= 13C4-Fum)	3	13.61	ISTD	249.1
Malate	4	16.02	Target	233.1
ISTD Mal (= D3-Mal)	4	16.02	ISTD	236.1
α-Ketoglutarate	5	17.36	Target	198.1
ISTD α-KG (= 13C4-α-KG)	5	17.36	ISTD	308.1
2-Hydroxyglutarate	5	17.33	Target	247.1
ISTD 2-HG / Isocit (= D3-2-HG)	5	17.33	ISTD	250.2
Ribose	6	19.72	Target	307.1
ISTD Rib (= 13C4-Rib)	6	19.72	ISTD	310.2
Citrate	7	23.40	Target	273.1

Materials and Methods

ISTD Cit (= D4-Cit)	7	23.40	ISTD	276.1
Isocitrate	7	23.51	Target	245.1
Glucose	7	25.25	Target	319.1
ISTD Glc (= 13C6-glucose)	7	25.25	ISTD	323.2

The temperature settings are shown in Table 5. The injection volume was set to 1.5 μ L. The GC-MS system was controlled by the MassHunter data acquisition software from Agilent Technologies.

Table 5: GC-MS parameter settings for the EM quantification assay.

GC settings	Injection volume	1.5 μL
	Inlet temperature	280 °C
	Split ratio	8:1
	Flow	1.0 mL/min
	Transfer line temperature	310 °C
Temperature gradient	50 °C	1 min hold time
	Rate: 8 °C/min to 175 °C	
	175 °C	5 min hold time
	Rate: 8 °C/min to 200 °C	
	Rate: 50 °C/min to 300 °C	
	Post run: 300 °C	5 min hold time
MS settings	Ionization mode	Electron impact (EI)
	Detection mode	Single ion monitoring (SIM)
	Ion source temperature	240 °C
	MS Quadrupole temperature	150 °C

2.10. Transcriptomics

For total RNA sequencing, RNA from SGBS samples was isolated according to section 2.5.1. The samples were from the same passage number as used for lipidomics and metabolomics studies. Only RNA, which had highest quality, represented as RIN > 9.0, was used, measured with Agilent's 2100 Bioanalyzer (RNA 6000 Nano Kit). Concentration was determined with the Quant-iT PicoGreen dsDNA Assay kit. Library preparation, sequencing, and differential expression analysis were performed by the sequencing unit of the HMGU (Head: Dr. Tim Strom) as recently published (169). In detail, library preparation was performed using the TruSeq Stranded Total RNA Library Prep Kit with Ribo-Zero. For library preparation, 1 μ g of RNA was depleted for cytoplasmatic rRNAs, then fragmented, and reverse transcribed using the "elute, prime, fragment mix". Afterwards, A-tailing, adaptor ligation, and library enrichment were performed according to the manufacturer's protocol of TruSeq RNA sample prep guide. Then, RNA libraries were analyzed as

Materials and Methods

150 bp paired-end runs using an Illumina HiSeq4000 platform. For split-read alignment against the human genome assembly hg19 (GRCh37) and UCSC known Gene annotation, the STAR aligner (v2.4.2a) with modified parameter settings (-twopassMode=Basic) was used (171). HTseq-count (v0.6.0) was used for the quantification of the number of reads mapping to annotated genes (172). FPKM (fragments per kilobase of transcript per million fragments) values were calculated using scripts of the core facility. For differential expression analysis, the R Bioconductor package DESeq2 was applied (173). All downstream data analyses were carried out by me. To evaluate the changes in transcription levels, ratios were calculated in relation to the transcription level at day 0. Therefore, the individual values of each transcript were converted to four different ratios, namely day 2 vs. day 0, abbreviated as "day 2", day 4 vs. day 0 (abbreviated "day 4"), day 8 vs. day 0 (abbreviated "day 8"), and day 12 vs. day 0 (abbreviated "day 12").

2.11. Statistical analysis

2.11.1. Calculation of validation parameters for the GC-MS method

For the validation of the GC-MS based energy metabolism assay, several validation parameters were chosen and calculated (160) according to the "Guidance for Industry: Bioanalytical Method Validation" by the FDA (129) and the "Guideline on bioanalytical method validation" by the EMA (130).

Accuracy:

The accuracy, expressed in percentage, is defined as the closeness of the determined concentration to the nominal (true) concentration and is calculated according to Equation 1.

Equation 1, Accuracy

$$accuracy [\%] = \frac{\text{determined value}}{\text{true value}} * 100 \%$$

Precision:

The precision represents the closeness of repeated individual measurements of an analyte. It is expressed as coefficient of variation (CV) in percentage and calculated according to Equation 2.

Equation 2, Precision

$$precision [\%] = \frac{\text{standard deviation}}{\text{average value}} * 100 \%$$

LOD:

The limit of detection (LOD) is the lowest concentration at which the analytes can be detected with an acceptable signal intensity. It is defined as the analyte signal which is at least three times

higher than the baseline analyte signal of the according blank sample. The LOD is calculated according to Equation 3.

Equation 3, Limit of detection

$$LOD = 3 * signal_{blank} + mean_{blank}$$

LLOQ:

The lower limit of quantification (LLOQ) is the lowest concentration at which the analytes can be quantified with an acceptable signal intensity. It is defined as the analyte signal with a minimum of ten times higher than the baseline analyte signal of the according blank sample. The LLOQ is calculated according to Equation 4.

Equation 4, Lower limit of quantification

$$LLOQ = 10 * signal_{blank} + mean_{blank}$$

Matrix effects:

The matrix effect is defined as the suppression or enhancement of analyte ionization by the presence of matrix components in biological samples. It can be quantitatively measured with the matrix factor. Because there is no appropriate biological matrix available, which is free of the endogenous metabolites, matrix effects were analyzed with blank and SGBS samples from six different time points of cell differentiation. The effects were calculated according to Equation 5.

Equation 5, Matrix factor

$$matrix\ factor\ [\%] = \frac{peak\ area\ analyte_{sample} - peak\ area\ analyte_{blank}}{peak\ area\ ISTD_{sample} - peak\ area\ ISTD_{blank}} * 100\ \%$$

2.11.2. Statistical analysis for analysis of metabolomics and lipidomics data

Statistical analyses and graphical illustrations of metabolomics and lipidomics data were performed as recently published (22). The R-based web-tool MetaboAnalyst 4.0 (156) as well as the software GraphPad Prism 8.1.1 and R 3.5.1 (157) were used.

Univariate statistical analyses were performed using the Mann-Whitney U test and Kruskal-Wallis test with Dunn's post-hoc test. The Spearman's rank correlation analysis was used to test putative correlations between metabolites and lipids, respectively. Prior to PCA and other multivariate statistical analysis, concentrations and in case of non-targeted metabolomics results, signal intensity values, were log-normalized and auto-scaled (mean-centered and divided by the standard deviation of each variable, see Equation 6) to achieve a normal distribution of the data set. Averaged concentrations as well as signal intensity values, are shown with standard deviations.

Materials and Methods

Normalization of concentrations and signal intensity values for direct comparison:

During metabolomic and lipidomic measurements, several analytes were measured in several assays. This allows the comparison of the results for single analytes obtained with the different assays (see section 3.2.7). However, for direct comparison studies, the different datasets had to be normalized because the non-targeted approach did only report signal intensity values, whereas the other approaches reported absolute concentrations. Therefore, the results were auto-scaled according to Equation 6. $x_{auto-scaled}$ represents the auto-scaled concentration or signal intensity value, x_{mean} is the calculated mean, x represents the single concentration or signal intensity value to be scaled, and SD represents the standard deviation of the averaged values.

Equation 6, Auto-scaled concentration or signal intensity value

$$x_{auto-scaled} = \frac{x - x_{mean}}{SD}$$

Normalization of plate effects:

The normalization of plate effects was done using QC samples [pooled cell samples for all metabolomics approaches with the exception of Biocrates Absolute/DQ p180 kit (reference plasma)] according to Equation 7. For each plate and each single metabolite or lipid, a unique plate normalization factor had to be calculated.

Equation 7, Plate normalization factor

$$\text{Plate normalization factor } x = \frac{\text{averaged QC metabolite concentration}_{all\ plates}}{\text{averaged QC metabolite concentration}_{single\ plate\ x}}$$

Normalization to cell number:

The normalization was done according to Muschet *et al.* (135). Normalization of measured analyte concentration to cell number was performed using Equation 8. For calculation, the fluorescence value of each sample was calculated in relation to the fluorescence signal of one fixed sample (fluorescence signal_{normalized to}).

Equation 8, Normalization to cell number

$$\text{analyte conc}_{normalized} = \frac{\text{analyte conc}_{measured} * \text{fluorescence signal}_{normalized\ to}}{\text{fluorescence signal}_{measured}}$$

2.11.3. Statistical analysis for transcriptomics

Split-read alignments to annotated human genes and differential expression analysis after total RNA sequencing was kindly performed from Dr. Thomas Schwarzmayr of the HMGU core facility (Head: Dr. Tim Strom) as described in chapter 2.10.

All other statistical analyses and graphical illustrations of transcriptomics data were done by me using the R-based web-tool MetaboAnalyst 4.0 (156) as well as the software GraphPad Prism 8.1.1 and R 3.5.1 (157).

Univariate statistical analyses were performed using the Mann-Whitney U test and Kruskal-Wallis test with Dunn's post-hoc test. Prior to PCA and other multivariate statistical analysis, log₂ fold-change values were auto-scaled (mean-centered and divided by the standard deviation of each variable) to achieve a normal distribution of the data set. Averaged log₂ fold-change values are shown with standard deviations.

3. Results

The aim of this PhD thesis was to unravel human adipogenesis on the level of lipids, metabolites, and transcripts, as the adipogenic processes are incompletely understood in humans. In addition, until recently there was a lack of "high-resolution" mass spectrometry combined with a lack of internal standards which did not allow the identification of lipid species at the fatty acyl/alkyl level. Therefore, lipidomics, metabolomics, and transcriptomics were applied to human SGBS cell samples that were differentiated into adipocytes for up to 20 days. Lipidomics was used for the quantitative measurement of lipid species of 11 lipid classes. Non-targeted metabolomics was applied for the analysis of polar analytes from several classes, as well as lipids from additional lipid classes than already measured with the lipidomics method. Two quantitative metabolomics approaches analyzed the concentration levels of polar metabolites from several classes like amino acids and acylcarnitines as well as some glycerophospholipids. However, a quantitative assay for polar metabolites of the energy metabolism was not established in the lab yet. Therefore, a quantitative GC-MS based assay for this kind of analytes was developed and validated. In the first chapter, I am presenting the results of the validation of the GC-MS based quantification assay of the energy metabolism analytes (section 3.1). The second chapter is dedicated to the assessment of successful differentiation of SGBS cells (section 3.2.1), which are used for adipogenesis characterization. In the next chapter (section 3.2.2), the analysis of the lipids with the Lipidizer™ method during cell differentiation is presented. These results are the core of this PhD thesis and were recently published (22). In the following chapters, I am showing the results for the polar metabolites by using several metabolomics assays: Biocrates Absolute/DQ p180 (section 3.2.3), Newborn Screening Assay (NBS assay, section 3.2.4), non-targeted metabolomics using Metabolon's technology (section 3.2.5), and the self-developed energy metabolism assay (section

3.2.6). During the different measurements, several assays and methods were used to analyze the same metabolites and lipids. Thus, the lipidomics and metabolomics chapters will be closed with the comparison of the results for selected analytes (section 3.2.7). The last chapter of the results section will present the results from the transcriptomics analyses (section 3.2.8). The results from the different omics-approaches are combined in the discussion section (section 4.2) to shed light on the cellular processes during the different stages of adipogenesis.

3.1. Validation of the GC-MS based quantification assay for metabolites of the energy metabolism

In course of this PhD study, a method had to be developed for the quantification of metabolites of energy metabolism like the TCA cycle of human SGBS cells. Due to the low concentration of all metabolites in cell culture derived samples, cell culture metabolomics always requires special attention. Therefore, it was crucial to develop a method which uses calibrators near to the limit of detection (LOD). In addition to the low analyte concentrations, SGBS cells dramatically change their cellular composition during adipogenesis and therefore different matrix effects could be expected. For example, undifferentiated cells have low levels of interfering lipids; however, during adipogenesis the lipid content increases strongly and becomes dominant. Only proteins are precipitated during the harvesting step with 80% methanol prior to the analysis. However, lipids and other metabolites were not removed, and these substances might interfere with quantification.

The validation of the energy metabolism assay was based on the "Guideline on bioanalytical method validation" by the EMA (130) and the "Guidance for Industry: Bioanalytical Method Validation" by the FDA (129). The most important criteria for the method development and validation were robustness, linear range, specificity, accuracy, precision, LOD, lower limit of quantification (LLOQ), and acceptable high-throughput suitability.

The LOD was defined as the concentration of the metabolite in the calibration curve, which was at least three times higher than the baseline value of the respective blank sample (80% methanol in water, without ISTD; Equation 3) (160). The LLOQ was defined as the concentration with a minimum of ten times higher than the baseline value of the respective blank sample (80% methanol in water, without ISTD; Equation 4) (160). Table 6 summarizes the results for the LOD and LLOQ calculations. Nearly all analytes had LOD and LLOQ values below calibration level 1 except pyruvate whose values were between Cal 1 and Cal 2.

Results

Table 6: LOD and LLOQ of the GC-MS based EM quantification method.

A standard curve consisting of seven calibrators was prepared thrice ($n = 3$). All analytes had LOD and LLOQ below calibration level 1 except for pyruvate. Its LOD and LLOQ values were between calibrator 1 and 2.

	LOD	LLOQ
Pyruvate (Pyr)	0.17	0.42
Lactate (Lac)	1.75	4.94
2-Hydroxybutyrate (2-OHb)	0.23	0.24
3-Hydroxybutyrate (3-OHb)	0.01	0.02
Succinate (Suc)	0.65	0.89
Fumarate (Fum)	0.00	0.00
Malate (Mal)	0.26	0.32
2-Hydroxyglutarate (2-HG)	0.17	0.18
α-ketoglutarate (α-KG)	0.00	0.00
Ribose (Rib)	0.00	0.00
Citrate (Cit)	0.00	0.01
Isocitrate (Isocit)	0.07	0.09
Glucose (Glu)	10.40	11.61

For determination of the linear range (Table 7) and the accuracy (Table 8), a standard curve with seven calibration levels was prepared thrice and measured. The analyte concentrations were calculated using a linear regression analysis of the analyte peak areas which were normalized to the corresponding IS peak areas. Only for glucose, a quadratic regression analysis was performed, because this metabolite showed a trend of non-linear performance at higher concentrations.

Table 7: Calculated analyte concentrations based on the standard curve.

A standard curve consisting of seven calibrators was prepared thrice ($n = 3$).

	Calculated concentrations of the standard curve						
	Cal1	Cal2	Cal3	Cal4	Cal5	Cal6	Cal7
Pyr	0.11 ± 0.01	0.49 ± 0.06	0.99 ± 0.05	2.52 ± 0.08	5.03 ± 0.08	10.12 ± 0.11	20.00 ± 0.13
Lac	5.32 ± 1.85	10.12 ± 0.52	24.25 ± 1.44	50.91 ± 2.41	74.56 ± 3.02	150.39 ± 8.94	224.73 ± 2.82
2-OHb	0.30 ± 0.12	0.55 ± 0.07	0.98 ± 0.04	2.45 ± 0.09	5.01 ± 0.12	10.02 ± 0.44	19.99 ± 0.22
3-OHb	0.40 ± 0.08	0.63 ± 0.06	1.16 ± 0.10	1.78 ± 0.01	2.44 ± 0.09	3.50 ± 0.25	7.25 ± 0.07
Suc	1.05 ± 0.14	1.28 ± 0.16	1.42 ± 0.12	2.23 ± 0.12	4.37 ± 0.23	6.71 ± 0.50	11.31 ± 0.66
Fum	0.20 ± 0.04	0.45 ± 0.05	0.94 ± 0.04	2.50 ± 0.07	5.06 ± 0.10	10.21 ± 0.56	19.88 ± 0.19
Mal	0.69 ± 0.08	1.09 ± 0.07	1.32 ± 0.05	2.45 ± 0.06	4.73 ± 0.07	9.84 ± 0.68	20.14 ± 0.25

Results

2-HG	0.23 ± 0.07	0.58 ± 0.04	1.02 ± 0.01	1.97 ± 0.06	3.85 ± 0.12	7.97 ± 0.44	10.08 ± 0.23
α-KG	0.18 ± 0.07	0.46 ± 0.04	0.99 ± 0.02	1.28 ± 0.05	2.50 ± 0.10	7.66 ± 0.55	14.92 ± 0.22
Rib	0.17 ± 0.02	0.51 ± 0.02	1.20 ± 0.02	1.89 ± 0.03	2.48 ± 0.06	3.79 ± 0.24	7.07 ± 0.08
Cit	0.97 ± 0.11	1.63 ± 0.07	2.99 ± 0.06	5.94 ± 0.21	8.86 ± 0.35	12.12 ± 0.63	23.99 ± 0.20
Isocit	0.17 ± 0.05	0.37 ± 0.03	0.79 ± 0.02	1.71 ± 0.07	3.29 ± 0.20	4.56 ± 0.30	6.51 ± 0.06
Glu	39.95 ± 2.38	81.16 ± 3.30	158.61 ± 9.96	230.73 ± 7.75	316.53 ± 6.83	478.92 ± 10.86	717.67 ± 3.88

The accuracy values of Cal 1 of the standard curve were impaired for most of the analytes due to the demand of very low concentrations within calibration level 1. Eight of 13 analytes had values outside the accepted range of 80 – 120% for the validation of bioanalytical methods (129, 130). In detail, 2-hydroxybutyrate (121.68 ± 38.56%), 3-hydroxybutyrate (133.73 ± 21.06%), succinate (174.43 ± 12.93%), fumarate (78.40 ± 16.13%), malate (137.30 ± 12.17%), α-ketoglutarate (73.41 ± 29.30%), ribose (56.62 ± 8.19%), and citrate (129.43 ± 11.28%) had accuracy values outside the accepted range on their first calibration level. Additionally, succinate (142.09 ± 12.41%) had also an accuracy value outside the accepted range on its second calibration level.

Table 8: Determination of the accuracy of the standard curves of the GC-MS based quantification assay for the metabolites of the energy metabolism.

A standard curve was prepared thrice (n = 3). The standard deviations represent the variations of the multiple preparations.

	Accuracy ± SD [%]						
	Cal1	Cal2	Cal3	Cal4	Cal5	Cal6	Cal7
Pyr	105.14 ± 9.95	98.31 ± 12.64	99.26 ± 5.34	105.42 ± 5.98	101.22 ± 3.04	102.35 ± 2.15	99.97 ± 1.30
Lac	106.37 ± 34.81	101.18 ± 5.10	97.01 ± 5.91	101.81 ± 4.73	99.41 ± 4.05	100.26 ± 5.94	99.88 ± 1.26
2-OHb	121.68 ± 38.56	109.58 ± 13.3	97.83 ± 4.42	98.13 ± 3.83	100.15 ± 2.34	100.16 ± 4.39	99.97 ± 1.10
3-OHb	133.73 ± 21.06	104.71 ± 9.73	96.45 ± 8.98	99.02 ± 0.80	101.62 ± 3.69	97.10 ± 7.06	100.64 ± 0.94
Suc	174.43 ± 12.93	142.09 ± 12.41	118.24 ± 8.12	92.73 ± 5.59	90.94 ± 5.26	93.15 ± 7.39	104.68 ± 5.82
Fum	78.40 ± 16.13	90.50 ± 9.98	94.11 ± 4.25	100.09 ± 2.77	101.29 ± 2.09	102.10 ± 5.58	99.42 ± 0.93
Mal	137.30 ± 12.17	108.82 ± 6.20	105.53 ± 3.80	97.88 ± 2.65	94.53 ± 1.48	98.42 ± 6.94	100.70 ± 1.25
2-HG	116.87 ± 31.31	115.07 ± 7.68	102.22 ± 0.93	98.29 ± 2.99	96.16 ± 3.11	99.69 ± 5.53	100.82 ± 2.32

Results

α-KG	73.41 ± 29.30	92.79 ± 8.88	99.13 ± 2.31	102.34 ± 3.68	100.11 ± 4.06	102.11 ± 7.40	99.47 ± 1.45
Rib	56.62 ± 8.19	84.38 ± 3.87	99.68 ± 1.42	105.00 ± 1.85	103.27 ± 2.68	105.22 ± 6.56	98.21 ± 1.18
Cit	129.43 ± 11.28	108.63 ± 4.51	99.83 ± 2.05	98.96 ± 3.47	98.50 ± 3.90	101.00 ± 5.20	99.96 ± 0.83
Isocit	84.78 ± 25.18	92.73 ± 8.28	98.30 ± 3.02	106.79 ± 4.48	102.88 ± 6.15	95.09 ± 6.17	101.69 ± 0.93
Glu	99.87 ± 5.97	101.45 ± 4.06	99.13 ± 6.28	96.14 ± 3.38	104.06 ± 8.68	99.77 ± 2.68	99.68 ± 0.54

Furthermore, precision for the standard curve was checked. Ideally, the coefficient of variation (CV) should be below 15% according to the guidelines (129, 130). Table 9 shows the results for the analysis of inter-run precision, Table 10 for the injection precision. In all cases, the standard curves showed good values <15%.

Table 9: Inter-run precision of the standard curve of the GC-MS based quantification assay for the metabolites of the energy metabolism.

A standard curve was prepared and measured thrice (n = 3). The values represent the coefficient of variations for multiple preparations.

	Precision (CV) of the standard curve [%]						
	Cal1	Cal2	Cal3	Cal4	Cal5	Cal6	Cal7
Pyr	11.22	4.21	1.46	3.41	3.48	2.96	0.69
Lac	2.36	3.99	3.61	0.30	3.26	2.61	0.23
2-OHb	6.57	6.39	2.38	0.60	3.89	5.27	1.21
3-OHb	13.59	13.84	4.92	1.39	3.42	7.46	0.19
Suc	6.89	8.10	1.94	6.85	4.61	5.52	1.33
Fum	3.68	2.85	2.80	0.23	3.60	0.59	1.02
Mal	0.59	2.14	2.17	0.24	2.94	0.27	1.16
2-HG	3.32	2.74	2.22	0.68	2.14	0.43	1.20
α-KG	10.50	7.05	2.70	2.05	4.20	1.06	0.71
Rib	1.13	2.78	2.58	0.15	3.29	0.39	0.64
Cit	1.32	5.01	2.24	0.57	1.65	1.66	1.26
Isocit	3.66	4.85	2.30	1.92	1.86	3.36	1.02
Glu	0.29	3.98	4.48	4.08	2.56	5.73	2.17

Table 10: Injection precision of the GC-MS based quantification assay for the metabolites of the energy metabolism.

A calibration sample was injected thrice (n = 3). The values represent the coefficient of variations for multiple injections.

Injection precision CV [%]							
	Cal1	Cal2	Cal3	Cal4	Cal5	Cal6	Cal7
Pyr	3.90	1.25	1.29	3.41	2.37	0.29	3.17
Lac	1.49	0.54	0.22	0.30	0.27	0.12	0.45

Results

2-OHb	7.12	4.50	2.38	0.60	0.16	0.40	2.16
3-OHb	4.58	2.60	2.04	0.62	0.95	0.41	0.19
Suc	1.15	6.28	1.73	5.81	1.47	5.22	0.60
Fum	0.64	1.29	1.52	0.23	1.29	0.67	0.48
Mal	0.28	0.22	0.36	0.24	0.16	0.22	0.12
2-HG	4.83	0.43	0.52	0.68	0.59	0.09	1.08
α-KG	8.18	3.42	1.11	2.05	0.63	1.50	2.39
Rib	0.51	0.14	0.13	0.15	0.28	0.20	0.06
Cit	0.71	1.01	0.46	0.57	0.49	0.70	0.47
Isocit	0.02	2.56	1.24	1.92	2.33	0.57	1.93
Glu	0.30	3.93	4.09	4.17	2.77	5.21	2.21

Additionally, the long-term stability was checked for the calibrators since it was not feasible to prepare new calibrators for each routine measurement. Therefore, the diluted calibrators were stored for 6 months at $-80\text{ }^{\circ}\text{C}$. Then, they were thawed, derivatized, and measured together with freshly prepared standards. Overall, the calibrators showed good stability under the tested conditions. However, the first calibrator of lactate, 2-hydroxyglutarate, ribose, isocitrate, and 2-hydroxybutyrate (calibration level Cal 1 and Cal 2) as well as the Cal 2 and Cal 3 level of glucose showed higher deviations of the stored standards compared to the freshly prepared ones.

Table 11: Long term stability of prepared calibrators of the GC-MS based quantification assay.

A standard curve was prepared and stored for 6 months at $-80\text{ }^{\circ}\text{C}$. Then the samples were thawed, derivatized, and measured together with freshly prepared standards. The values of the new standards were set as 100%.

Stability: long term storage (6 months) [%]							
	Cal1	Cal2	Cal3	Cal4	Cal5	Cal6	Cal7
Pyr	97.43	109.32	102.81	87.56	105.64	94.87	100.95
Lac	75.93	89.80	102.53	98.46	101.52	94.88	101.40
2-OHb	58.11	78.74	96.29	99.56	108.16	97.35	100.16
3-OHb	89.26	92.89	112.71	95.22	107.77	93.56	100.83
Suc	91.97	89.92	104.66	93.96	107.65	91.89	102.34
Fum	129.35	108.13	106.64	99.00	102.83	95.54	100.99
Mal	99.89	98.87	100.49	97.68	107.13	93.78	101.20
2-HG	76.16	94.44	101.53	99.11	108.48	95.84	101.51
α-KG	149.51	111.13	101.06	99.24	105.15	93.80	101.50
Rib	128.57	105.87	103.57	98.50	107.94	94.22	100.69
Cit	80.97	88.17	100.49	99.74	109.90	94.13	100.25
Isocit	74.78	87.80	99.22	98.47	113.59	96.02	98.97
Glu	96.87	122.61	128.58	111.81	96.59	115.63	112.88

In the next step, the influence of the changing cellular compositions of differentiation adipocytes on the analysis of the analytes as well as their corresponding ISTDs was checked (see Figure 4). For this, the peak areas of the 10 ISTDs in blank and SGBS samples of six different time points (day

Results

0, 2, 4, 8, 12, and 16 of cell differentiation) were used to calculate the matrix effects according to Equation 5. $^{13}\text{C}_3$ -pyruvate, D3-2-hydroxyglutarate, $^{13}\text{C}_4$ -3-hydroxybutyrate, $^{13}\text{C}_4$ - α -ketoglutarate, and D3-malate showed no ion-suppression and no significant change in their peak areas during adipogenesis. $^{13}\text{C}_4$ -ribose, $^{13}\text{C}_3$ -lactate, and especially $^{13}\text{C}_6$ -glucose showed strongly increased peak areas compared to the other analytes. However, the matrix effect of these three metabolites was stable throughout adipogenesis. In contrast, $^{13}\text{C}_4$ -fumarate revealed strong ion-suppression effects at day 2 and 4 of adipogenesis. No matrix effects for $^{13}\text{C}_4$ -fumarate were observed with samples collected at other time points during adipogenesis.

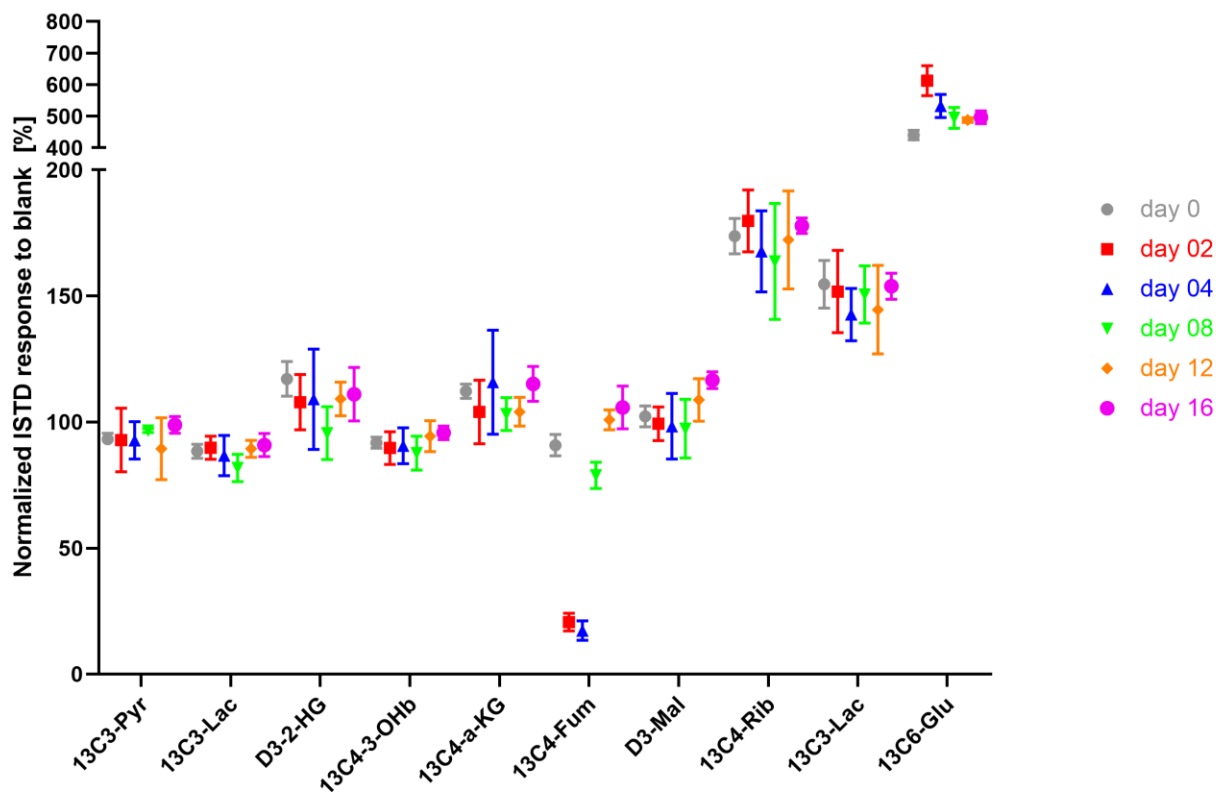


Figure 4: Matrix effects were similar in all matrices obtained during adipogenesis of SGBS cells with the EM assay. $^{13}\text{C}_3$ -Pyr, $^{13}\text{C}_3$ -Lac, D3-2-HG, $^{13}\text{C}_4$ -3-OHb, $^{13}\text{C}_4$ - α -KG, and D3-Mal did not show strongly changing ISTD responses during adipogenesis when normalized to blank samples. $^{13}\text{C}_4$ -Rib, $^{13}\text{C}_3$ -Lac, and especially $^{13}\text{C}_6$ -Glu showed strongly increased but stable responses during adipogenesis. The analysis of $^{13}\text{C}_4$ -Fum revealed ion suppression effects at day 2 and 4, whereas the ISTD in samples from other days were not disturbed by matrix effects. Peak areas of ISTD of samples were divided by peak areas of ISTD of blanks multiplied with 100 to obtain percent values.

To show the gas chromatographic separation of the analytes, total ion chromatograms of Cal 5 (Figure 5) and of a representative sample (Figure 6) were illustrated. With the exception of 2-hydroxyglutarate and α -ketoglutarate, all other analytes can be separated by their retention time. For the separation of the two named analytes, different SIM values were sufficient for a selective separation (Table 4).

Results

An exemplary total ion chromatogram of a maturing SGBS sample (day 8) is shown in Figure 6. It can be easily seen that the glucose concentration is much higher than in Cal 5 (Figure 5). Moreover, isocitrate and ribose cannot be quantified due concentrations below LOD. Panel B shows a magnification of the total ion chromatogram of the retention time between 8.0 and 17.5 min for a better peak identification.

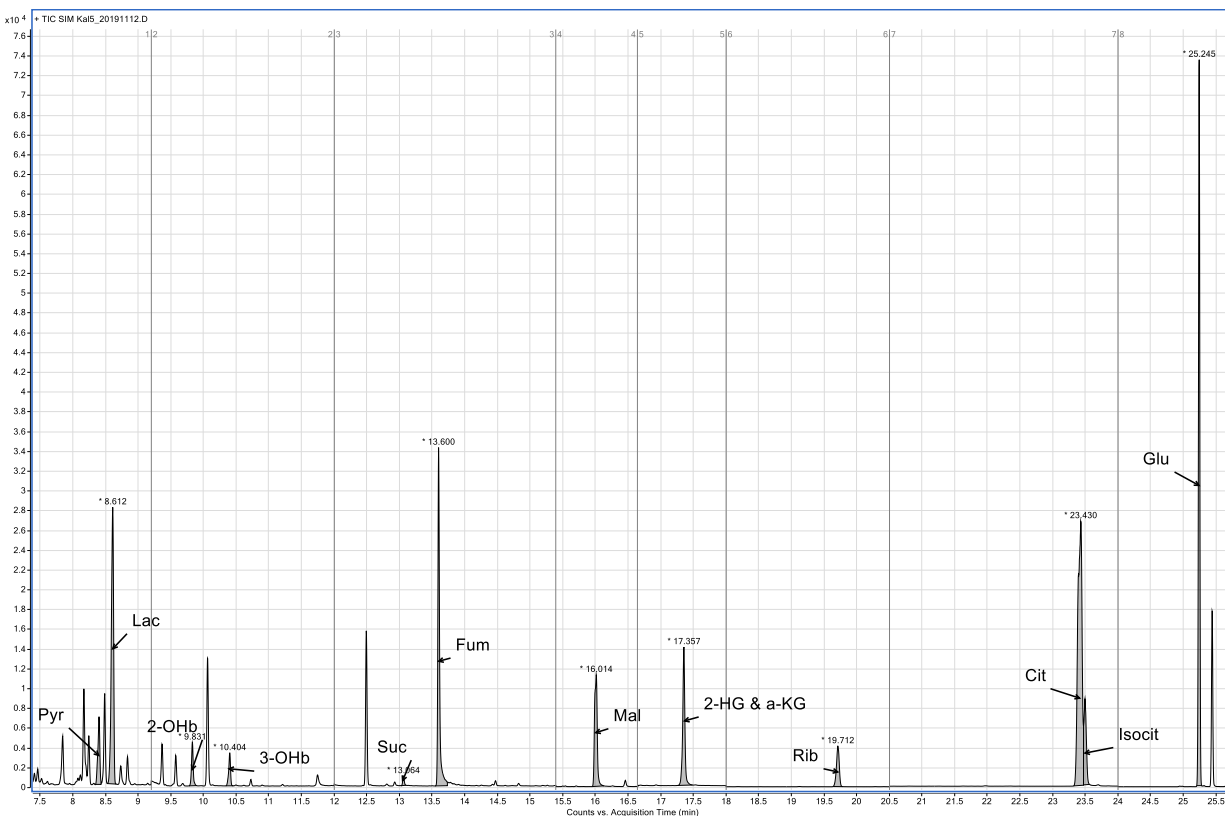


Figure 5: Total ion chromatogram of Cal 5 revealed a good separation of the analytes. However, 2-HG and α -KG could be only separated by the subsequent separation with different SIM values.

Results

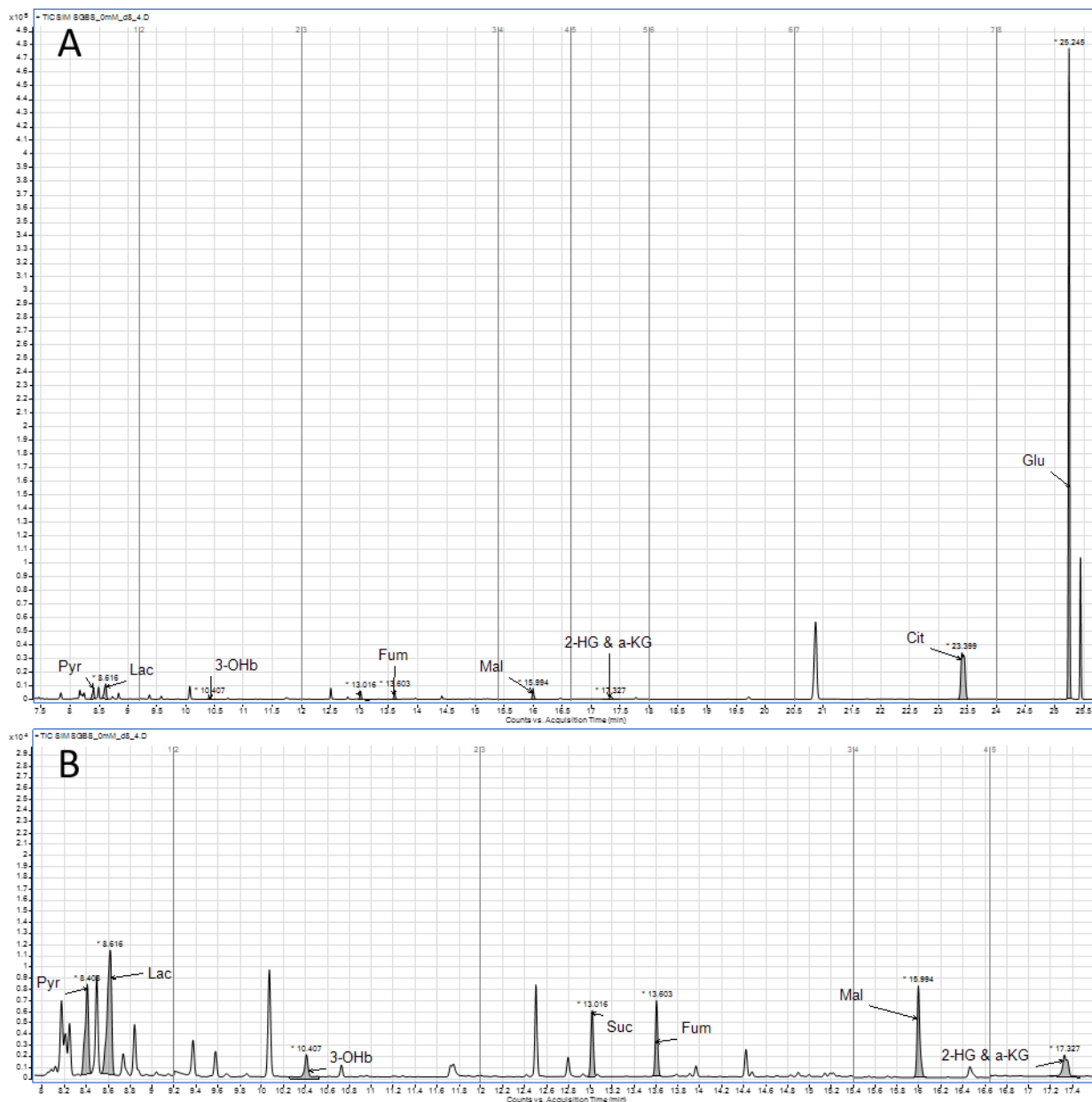


Figure 6: Total ion chromatogram of a maturing SGBS sample (day 8) revealed clear detection of eight analytes (panel A).

For the separation of 2-HG and α -KG different SIM values were used. Panel B shows a magnification of the analytes with a retention time between 8.0 and 17.5 min.

The separation of analytes is ideally determined with an orthogonal method for a successful analytical method development and validation. Therefore, the results from the GC-MS based quantification assay were additionally checked with Metabolon's non-targeted approach, which is based on liquid chromatography separation. For the comparison of both methods, the resulting concentration time courses of the measurement with the EM assay and the resulting signal intensity time courses of the Metabolon assay were auto-scaled (see Equation 6) and log-normalized. All detectable EM assay analytes showed the same auto-scaled time courses in both

Results

approaches (see section 3.2.7). Thus, the non-targeted approach could confirm the obtained results gained with the newly developed GC-MS method.

In summary, the developed and validated GC-MS based method enables the quantification of metabolites of the energy metabolism. It is an accurate, precise, and robust assay for the analysis of (un)differentiated SGBS cell samples. It can be easily integrated into existing metabolomics portfolios and the validated cell normalization assay. In future, it should be tested for other cell lines and for cell culture supernatants.

3.2. Analyzing human adipogenesis with different omics techniques

The aim of this PhD thesis was to unravel adipogenesis on the level of lipids, metabolites, and transcripts and combine the results of all three approaches. Therefore, human SGBS cells were differentiated until day 20 and samples were collected every second day during the differentiation phase and every fourth day during the maturation phase (day 0, day 2, day 4, day 8, day 12, day 16, and day 20) for the three omics techniques. However, sample collection and measurement could not be performed for each day and every approach at the same time due to technical, financial, and logistic reasons. Measurements with Metabolon's non-targeted approach as well as the GC-MS based quantification assay were performed with the same samples of one experimental batch that were collected on day 0, 2, 4, 8, 12, and 16. All other measurements were performed with samples from separate experiments, respectively. Day 2 samples were not collected for Lipidizer™ technique, Newborn Screening Assay, and Biocrates Absolute/DQ p180 kit. However, with the latter targeted approach, samples from day 20 of differentiation were not measured. Samples for transcriptomics were only collected until day 12.

3.2.1. Assessment of adipocyte differentiation

To assess the successful differentiation of preadipocytes into mature, lipid-laden adipocytes, microscopic analyses were performed (Figure 7) and the relative mRNA levels of the most important adipogenic transcription factors *PPARG* and *CEBPA* (Figure 8) were determined. These results were previously published (22). During cell differentiation, the cells changed their morphology from long and flat fibroblast-like cells (day 0) to a more oval shape with increasing amounts and diameters of lipid-laden droplets. This could be easily observed in the microscopic assessment of adipogenesis (Figure 7).

Results

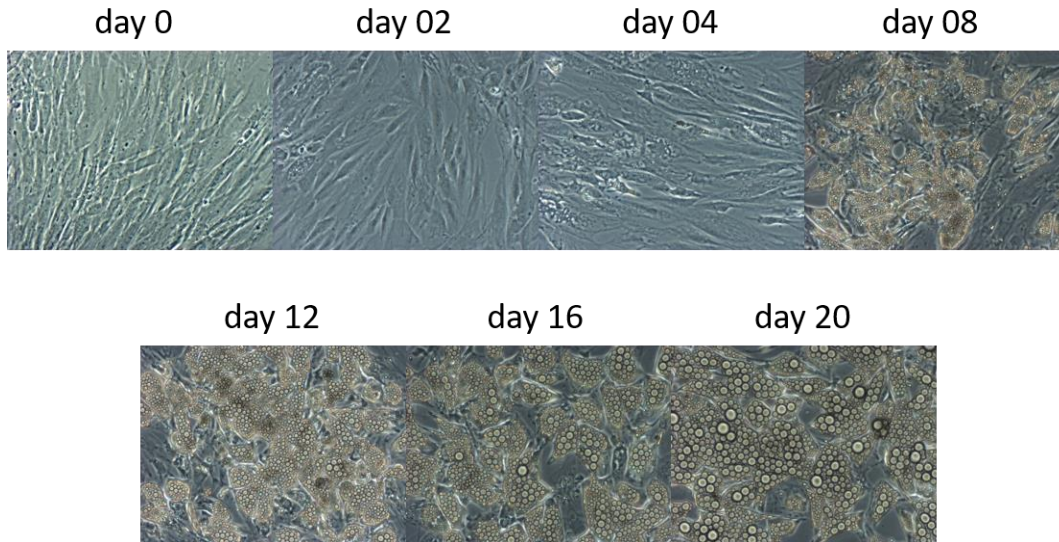


Figure 7: SGBS cells were successfully differentiated based on the microscopic analysis. Undifferentiated cells had a long and flat fibroblast-like morphology. During cell differentiation, the cells contracted and turned into more oval shaped cells with increasing storage of lipids into lipid droplets. Magnification in all images was 100-fold.

The relative mRNA expression levels were analyzed using qRT-PCR. Thereby, a strong upregulation of *PPARG* (40.7 ± 9.5 fold change at day 12 normalized to day 0) and *CEBPA* (52.0 ± 8.8 fold change at day 12 normalized to day 0) during cell differentiation were detected.

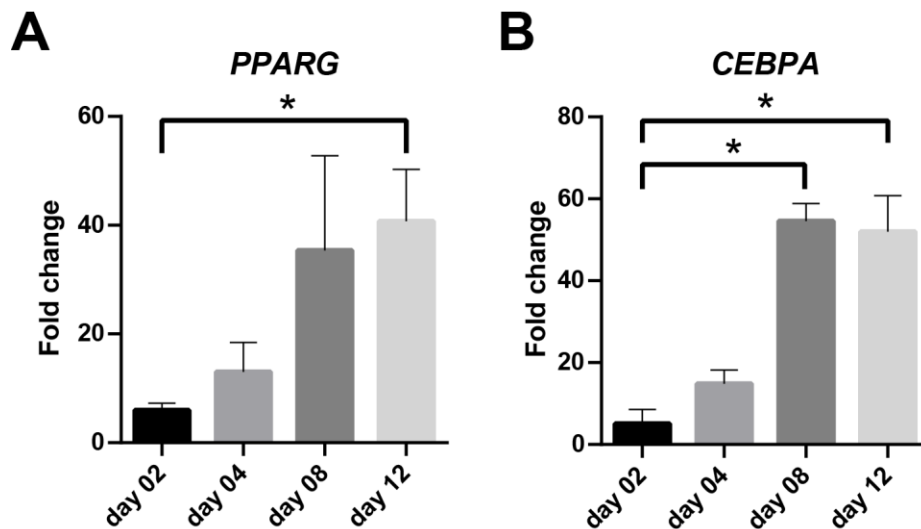


Figure 8: Transcript levels of the key adipogenic transcription factors *PPAR γ* (*PPARG*) and *C/EBP α* (*CEBPA*) were highly upregulated during adipogenic cell differentiation. Relative mRNA expression determined by qRT-PCR is shown as fold change with standard deviations. For each time point, the mean of four samples was normalized to expression of *TBP* and day 0 of differentiation. Univariate statistical analyses were performed using the Kruskal-Wallis test with Dunn's post-hoc test. * $p < 0.01$.

These results demonstrated successful SGBS cell differentiation into mature, lipid-laden adipocytes.

3.2.2. Lipidyzer™ method

The novel Lipidyzer™ technology was used for the analysis of the lipid levels during differentiation of SGBS cells to characterize the human adipogenesis. Results from this section were recently published (22). Because this analytical method originally was developed and validated for the analysis of human plasma (174), it had to be validated prior to the application to cell culture samples. Therefore, the analytical performance regarding repeatability and linearity of the assay were analyzed by the measurements of undifferentiated and differentiated (day 15) SGBS cells, pooled QC, and blank samples, respectively. For evaluation of the linearity, nine different volumes of undifferentiated and differentiated cell samples (10, 20, 40, 50, 60, 80, 100, 200, and 300 μ L) were measured. The mean concentrations of the single lipid classes were calculated and plotted against the used sample volumes.

Figure 9 and Figure 10 illustrate the linearity examination of all 13 lipid classes. The linearity, reflected by determination of the coefficients of determination (R^2) of the linear regression, were in most cases higher than 0.9 for both sample types (Table 12). This demonstrates that the analytical method had good linearity for the used samples. However, the analyses of dihydroceramides (DCER) and free fatty acids (FFA) showed lower linearity for both sample types. Moreover, lactosylceramides (LCER) had lower linearity using differentiated cells ($R^2 = 0.0479$). The relative standard deviations (CV) of the QC samples were calculated for repeatability evaluations. All lipid classes, except DCER, had CV values $< 15\%$ (Table 12). For background signal evaluation of the lipid classes, a lower cut-off value was fixed at a value of 1.5 x the value measured in the blank samples. All lipid classes, except free fatty acids (FFA), had higher concentrations in the pooled QC samples than the corresponding lower cut-off value. To conclude, the Lipidyzer™ method had good linearity and repeatability for 11 analyzed lipid classes using SGBS cells. Based on this method validation, the lipid classes FFA and DCER were removed from the data set. LCER was not removed, because the pronounced concentration decrease from undifferentiated to differentiated cells might be a notable result of the study.

Results

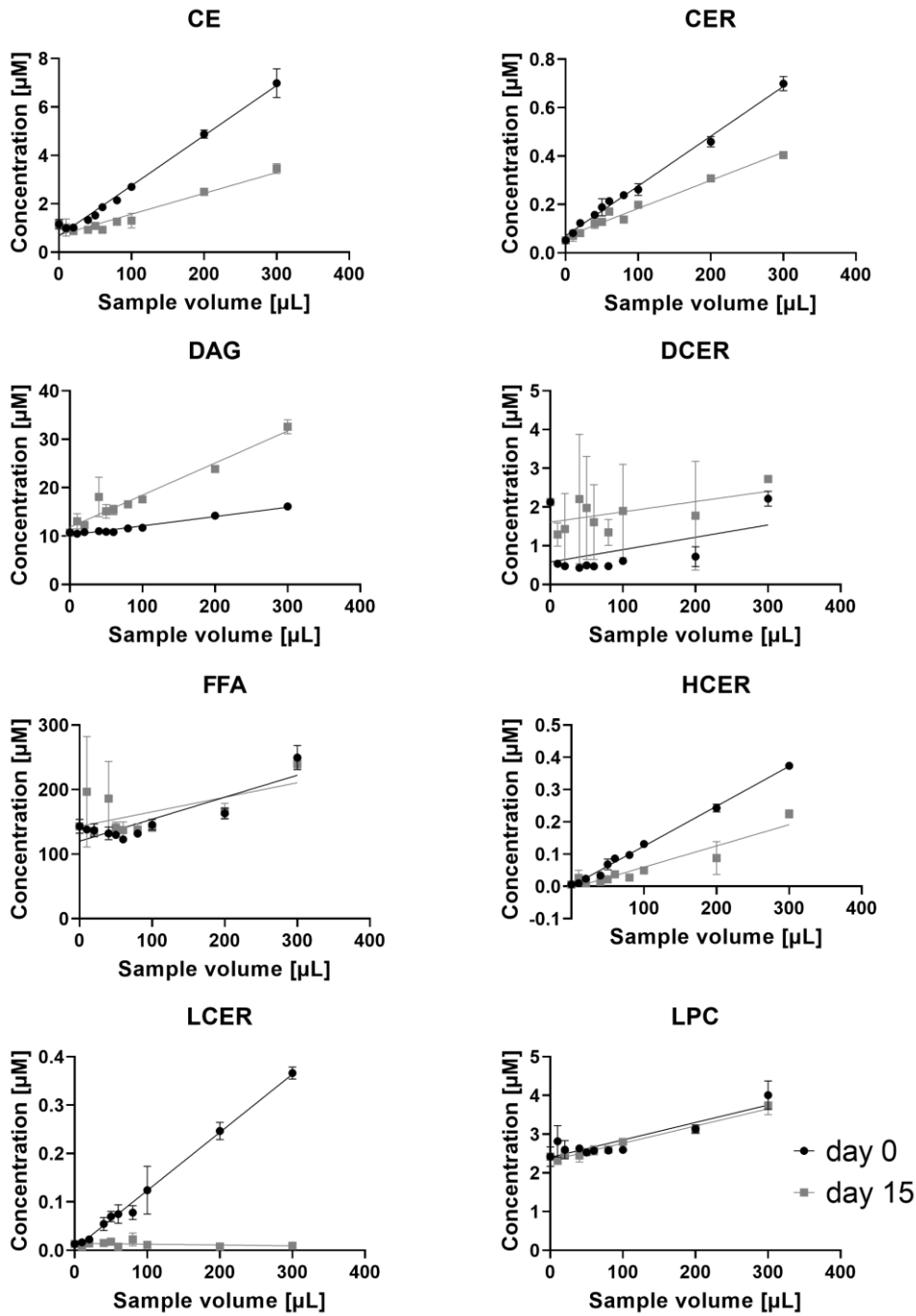


Figure 9: Analysis of the analytical performance of the Lipidyzer™ method revealed high linearity for most lipid classes using undifferentiated and differentiated cells.

Nine different sample volumes of cell homogenates from day 0 (preadipocytes) or day 15 (lipid-laden adipocytes) of differentiation, namely, 10, 20, 40, 50, 60, 80, 100, 200, and 300 µL were analyzed in triplicates each. For most of the lipid classes, satisfying linearity for both sample types (coefficient of determination of the linear regression > 0.9) were achieved. Only dihydroceramides (DCER) and free fatty acids (FFA) showed low linearity for both sample types. Therefore, both lipid classes were excluded from further evaluation.

Results

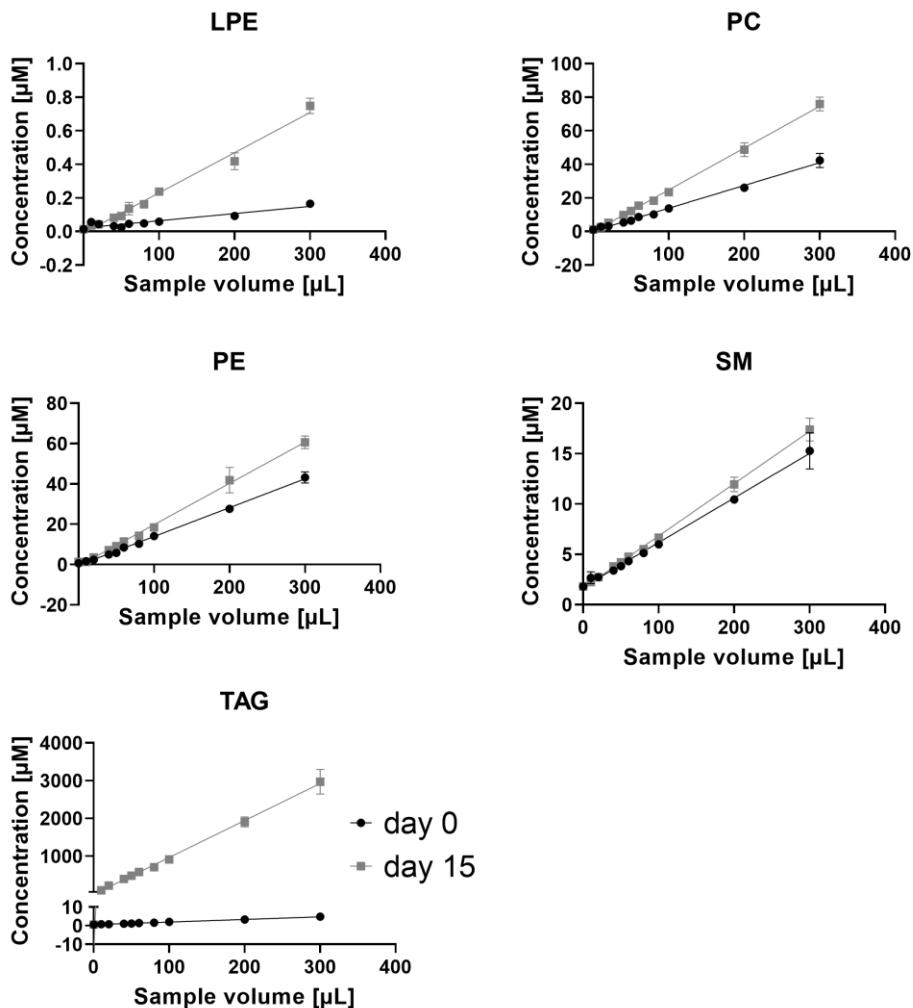


Figure 10: Analysis of the analytical performance of the Lipidzyzer™ method revealed high linearity for the lipid classes LPE, PC, PE, SM, and TAG using undifferentiated and differentiated cells.

Nine different sample volumes of cell homogenates from day 0 (preadipocytes) or day 15 (lipid-laden adipocytes) of differentiation, namely, 10, 20, 40, 50, 60, 80, 100, 200, and 300 µL, were analyzed in triplicates each. For most of the lipid classes we achieved satisfying linearity for both sample types (coefficient of determination of the linear regression > 0.9).

Table 12: Results of Lipidzyzer™ validation experiments.

	Coeff. of determination day 0	Coeff. of determination day 15	CV [%]	Mean QC [µM]	Mean Blank [µM]	1.5 x Mean Blank [µM]
CE	0.9798	0.8913	8.42	5.02	0.55	0.83
CER	0.9869	0.9665	2.85	1.15	0.11	0.17
DAG	0.9392	0.9077	3.04	17.27	1.69	2.54
DCE R	0.1833	0.0673	28.77	0.67	0.65	0.98
FFA	0.7292	0.2199	4.26	44.37	54.18	81.27
HCE R	0.9922	0.8490	11.56	0.36	0.02	0.03

Results

LCER	0.9734	0.0479	5.01	0.26	0.04	0.05
LPC	0.7112	0.9029	1.40	3.83	4.36	6.55
LPE	0.8572	0.9782	5.72	1.81	0.06	0.09
PC	0.9846	0.9931	1.31	195.54	0.64	0.97
PE	0.9929	0.9863	6.00	91.36	0.68	1.01
SM	0.9810	0.9926	3.73	18.17	0.42	0.62
TAG	0.9804	0.9874	4.67	2579.03	0.65	0.98

For the characterization of human adipogenesis on the lipid level, cells were differentiated until day 20 and samples were collected every fourth day of differentiation starting directly before induction of differentiation (day 0, 4, 8, 12, 16, and 20). In general, the analytical method simultaneously quantified 743 lipid species of 11 lipid classes by accurate identification of lipid isobars.

Principal component analysis (PCA, Figure 11 A) and partial least squares-discriminant analysis (PLS-DA, Figure 11 B) were conducted for the identification of putative differences between the concentrations of lipid species at the different time points of cell differentiation. Both score plots showed a strong separation of the samples from the different adipogenic time points using the first two principal components with 68.7% and 12.7% (PCA) as well as 68.5% and 12.7% (PLS-DA) of explained variance. The early phase of cell differentiation (day 0, 4, and 8) was mostly separated by the (principal) component 1. However, the second component was required for the separation of the time points days 12, 16, and 20 of adipogenesis. The model was predictive and not overfitted as the results from cross-validation and permutation test showed (R^2 : 0.97, Q^2 : 0.97; $p < 5e-4$ (0/2000 permutation numbers), test statistics selected by separation distance (B/W)).

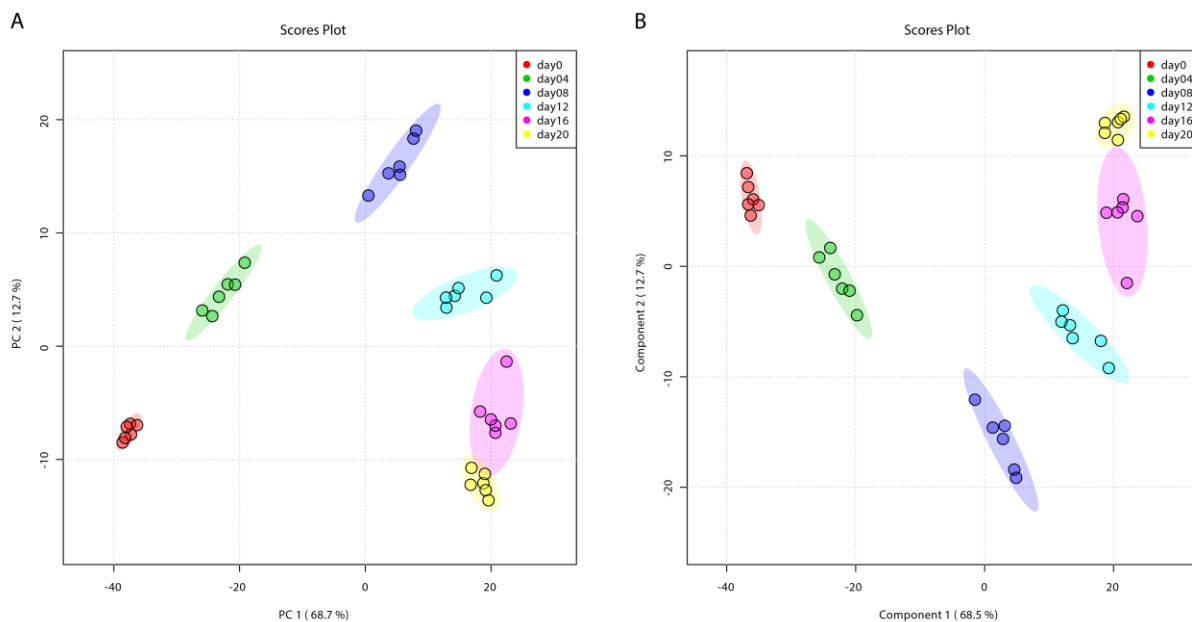


Figure 11: PCA (A) and PLS-DA (B) score plots showed clear separation of the different adipogenic time points and a clear clustering of individual samples of each time point.

Results

The (principal) components 1 (A: PCA, 68.7%; B: PLS-DA, 68.5% variance) separated the early adipogenic phase (days 0, 4, and 8) and the second (principal) component separated the later stages of differentiation (days 12, 16, and 20, both 12.7 % variance). The box inside the figure illustrates the used color code for the different days of adipogenesis. Shown are also the 95 % confidence intervals for each group. Each group consisted of six samples.

TAG species had a strong influence on the separation during PLS-DA. Component 1 of the PLS-DA was markedly influenced by different TAG species, whereas the TAG influence on component 2 was lower (see Table 13).

Table 13: Top 30 variable importance in projection (VIP) of PLS-DA for component 1 and 2. Each column was sorted from the largest VIP values to the smallest ones. Component 1 was most influenced by TAG species (25 out of 30), component 2 to a lesser extend (17 out of 30).

Lipid	Component 1	Lipid	Component 2
TAG56:2-FA18:0	1.2756	PE(P-16:0_22:5)	1.2681
TAG56:3-FA20:2	1.2749	PE(P-16:0_22:6)	1.2578
TAG54:2-FA18:1	1.2729	PE(16:0_22:5)	1.2471
TAG56:2-FA20:1	1.2719	PE(P-18:0_22:6)	1.2423
TAG56:2-FA20:0	1.2693	TAG54:0-FA18:0	1.2398
TAG54:2-FA18:0	1.2680	TAG54:1-FA18:1	1.2398
TAG50:0-FA14:0	1.2677	PE(18:1_22:5)	1.2396
TAG48:1-FA12:0	1.2670	PE(P-18:1_22:5)	1.2393
PE(P-18:0_18:1)	1.2664	TAG56:2-FA18:0	1.2384
TAG54:3-FA18:2	1.2659	TAG54:1-FA18:0	1.2377
PE(18:1_22:5)	1.2654	TAG56:4-FA20:3	1.2374
TAG54:1-FA18:1	1.2633	TAG56:3-FA20:2	1.2368
TAG56:5-FA20:3	1.2632	TAG54:2-FA18:0	1.2363
TAG54:3-FA18:1	1.2629	PE(P-18:0_18:1)	1.2349
TAG56:3-FA18:0	1.2626	TAG54:2-FA18:1	1.2328
TAG56:1-FA18:1	1.2625	PE(P-18:1_22:6)	1.2322
TAG47:2-FA18:1	1.2623	TAG56:3-FA18:0	1.2316
TAG53:2-FA17:0	1.2623	PE(P-18:0_22:4)	1.2310
TAG55:2-FA18:1	1.2620	PC(16:0_16:0)	1.2296
PE(P-18:0_22:5)	1.2595	TAG56:2-FA20:1	1.2293
TAG55:3-FA18:1	1.2591	TAG56:2-FA20:0	1.2291
TAG53:1-FA17:0	1.2583	TAG54:2-FA18:2	1.2267
LPE(18:1)	1.2580	TAG56:1-FA18:1	1.2249
TAG53:2-FA18:1	1.2579	PC(16:0_20:4)	1.2243
TAG55:1-FA18:1	1.2569	PE(P-18:0_22:5)	1.2230
TAG56:8-FA18:1	1.2566	TAG54:3-FA18:2	1.2218
TAG56:4-FA20:3	1.2562	TAG53:1-FA17:0	1.2206
PE(P-18:0_20:2)	1.2561	PE(18:1_22:4)	1.2203
TAG44:0-FA18:0	1.2560	TAG50:0-FA14:0	1.2202
TAG52:1-FA18:0	1.2558	TAG56:5-FA20:3	1.2195

Results

Lipid class concentrations and compositions can be calculated by summation of the corresponding lipid species concentrations. Figure 12 A illustrates the lipid class composition from day 0 to day 20. In general, preadipocytes (day 0) had a very heterogeneous lipid composition. The most abundant classes were PE (32.1% \pm 0.9%), PC (26.3% \pm 0.4%), SM (19.7% \pm 0.6%), and TAG (10.3% \pm 0.5%). On the one hand, the relative proportions of PE, PC, and SM dropped during adipogenesis. But on the other hand, the proportion of TAG in lipid class composition increased massively from 10.3 \pm 0.5% at day 0 to 96.9 \pm 0.4% at day 20. At the same time, the relative fractions of all other classes decreased to 1.2% and lower. In summary, the different days of adipogenesis could be clearly separated based on their relative lipid compositions (Figure 12 A), resembled by PCA (Figure 11 A), and PLS-DA (Figure 11 B). The relative lipid class compositions were not markedly changed after day 8 of SGBS cell differentiation.

Results

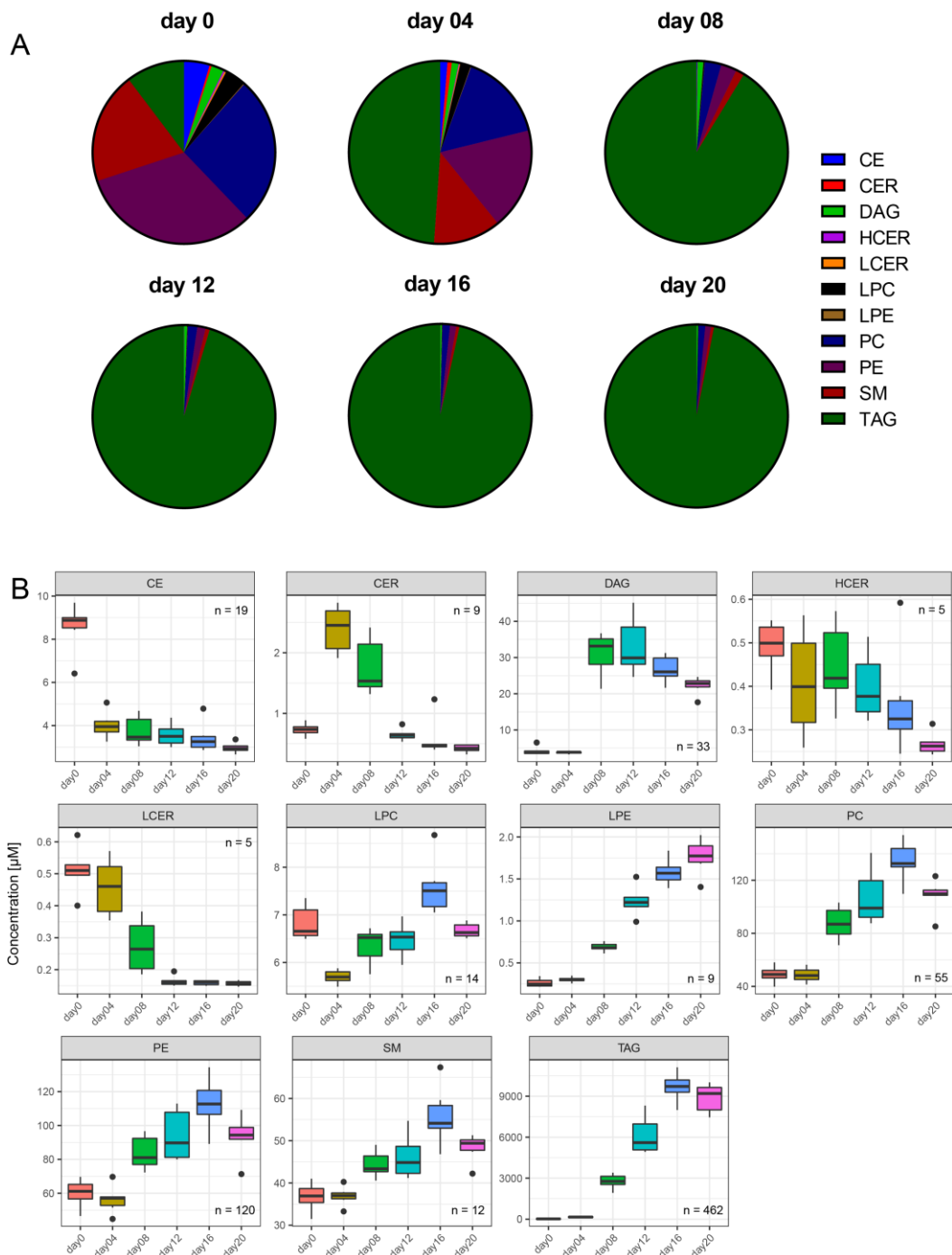


Figure 12: Lipid class compositions and concentrations were highly changed during adipogenesis.

Panel A shows a very heterogeneous lipid class composition (shown in in molarity %) before differentiation start. This became very homogeneous as the amount of TAG strongly increased during adipogenesis from 10.3 ± 0.5 molarity % at day 0 to 96.9 ± 0.4 molarity % at day 20.

Panel B illustrates lipid classes which had distinct concentration patterns during cell differentiation. On the one hand, CE, HCER, and LCER concentrations strongly decreased during adipogenesis. But on the other hand, LPE, PC, PE, and TAG concentrations strongly increased during adipogenesis. The concentrations of CER species increased only from day 0 to day 4, and finally decreased below the values measured in preadipocytes. The concentration profile of DAG species had a concentration maximum from days 8 to 12. The profile of LPC species differed from the other lipid classes as it fluctuated during adipogenesis.

Results

Figure 12 B illustrates the analysis of the lipid class concentrations over time. This revealed an interesting alternative perspective on the adipogenic process compared to the time courses of the lipid class compositions in Figure 12 A. Only three of them, namely, cholesteryl esters (CE; $p = 4.52e-4$, appendix 5.1), hexosylceramides (HCER; $p = 5.23e-3$), and lactosylceramides (LCER; $p = 2.80e-5$), had continuous and significant concentration decreases during the whole observed time period. Ceramide (CER) species had a slightly different profile as their concentrations initially increased significantly until day 4 ($p = 1.51e-5$) and then decreased significantly below LOD. TAG concentrations levels had an opposed profile over time because the TAG concentration levels increased continuously ($p = 4.01e-6$). Moreover, the TAG concentration level was the highest among all lipid classes. The concentration values were $19.2 \pm 2.0 \mu\text{M}$ on day 0 and increased to $8874.3 \pm 1072.1 \mu\text{M}$ on day 20. In addition, the concentrations of lysophosphatidylethanolamine (LPE), PC, and PE increased markedly during cell differentiation, whereas SM concentrations only slightly increased during the whole observed time period ($p = 5.04e-5$). In contrast, diacylglycerol (DAG) had a concentration profile over time which initially increased from day 4 to day 8 and subsequently remained at high level ($p = 3.40e-5$). Lysophosphatidylcholine (LPC) concentrations fluctuated around the value from day 0 during the whole analyzed time period ($p = 1.50e-4$).

By analyzing the lipid species concentrations, significant changes of 725 out of 743 lipids could be observed, this equals to 97.7% of all detected lipid species. With the Lipidizer™ method it is also possible to identify up to two fatty acids bound to the headgroup. Therefore, all fatty acids can be determined during the analysis, except for TAG species (132). For TAG, the method elucidates only the numbers of double bonds (DB) and number of C-atoms for one fatty acid side chain as well as the total number of the C-atoms and DB of all three side chains. Nevertheless, with this method the concentration changes were analyzed for the single FA species during SGBS differentiation. Figure 13 shows the individual concentration time courses of side chains which were summarized over all 11 analyzed lipid classes. Except C20:4, the medium-chain FA lauric acid (C12:0) and all LCFA had marked concentration increases during cell differentiation. The most abundant fatty acids were C18:1, C16:0 (palmitic acid), C16:1, and C18:0 (stearic acid) in descending order. Most of the VLCFA had a strongly decreasing concentration profile during adipogenesis, except three FA with 22 C-atoms, namely C22:0, C22:1, and C22:2, as these FA had fluctuating concentration patterns (Figure 13)

Next, FA were more deeply analyzed. Therefore, the single FA side chains were separately illustrated for each lipid class allowing a more detailed study of human adipogenic cell differentiation (Figure 14). Enlarged illustrations can be found in the appendix 5.2. The changes in FA concentration over time were highly individual in each lipid class. The FA species of the three ceramide classes (CER, HCER, and LCER) showed similar concentration profiles. In detail, the concentrations of LCFA and VLCFA decreased during cell differentiation. In contrary, the concentrations of LCFA in five lipid classes, namely DAG, LPE, PC, PE, and TAG, markedly increased. FA C18:1 and C16:0 showed a strong concentration increase during cell differentiation; for example, TAG-C16:0 increased from $2.5 \mu\text{M}$ on day 0 to $1515.1 \mu\text{M}$ on day 20. On the contrary, only low levels of VLCFA were present in the classes of DAG, LPE, PC, PE, and TAG. The class of SM

Results

differed markedly regarding FA compositions of the other analyzed classes. The SM species comprised the highest absolute amounts of VLCFA. In particular, the concentration levels of C22:0 (behenic acid) and C24:0 (lignoceric acid) were in SM 320 times higher at day 20 compared with all other classes. The analysis of the fatty acid concentrations of the LPC species revealed another picture, without marked changes during cell differentiation. In contrary, LCFA decreased to half the maximal concentrations and the VLCFA of LPC decreased even stronger during adipogenesis. To sum up, nearly all LCFA showed strongly increased concentration levels during adipogenesis, whereas most VLCFA had a strongly decreased concentration profile in common.

Results

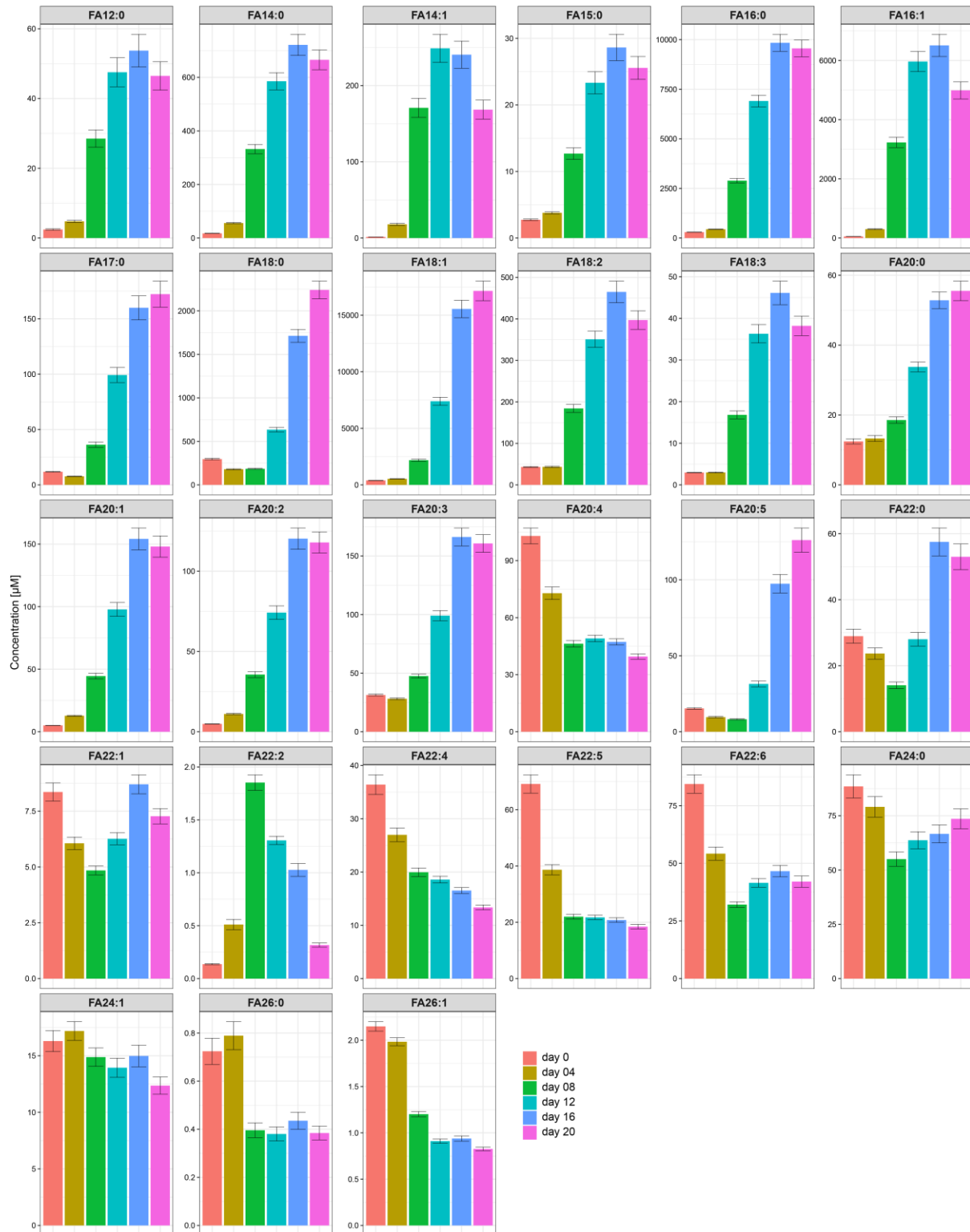


Figure 13: Individual concentration time courses of each FA side chains bound in the lipids were summarized and showed consistent patterns.

Four dominant fatty acids could be identified, namely FA 18:1, FA 16:0, FA16:1, and F18:0. Their concentrations increased markedly during cell differentiation. In addition, the other long-chain fatty acids (LCFA, except FA 20:4) and the medium-

Results

chain FA (MCFA) 12:0, had also increasing concentration profiles. In contrast, the very long-chain fatty acids (VLCFA) mostly decreased during cell differentiation.



Figure 14: Analyses of concentrations and compositions of FA identified marked changes during adipogenesis. Before differentiation start, all analyzed lipids had a very heterogeneous side chain composition with high concentration levels of LCFA and VLCFA. The VLCFA concentrations markedly decreased in all lipid classes, except SM. The concentration profiles of LCFA were more heterogeneous as the levels markedly decreased in CE species, but markedly increased within the classes DAG, LPE, PC, PE, and TAG. The FA concentration profiles of the SM differed strongly from the other classes as the concentrations of VLCFA did not show strong changes during cell differentiation.

Results

Since there were strong opposing trends in the lipid class and lipid species concentrations, Spearman's rank correlations of the lipid species concentration trajectories were computed to analyze possible associations between the lipid species (Figure 15). Overall, lipids could be dedicated to six clusters (Figure 15 A). For each cluster, the averaged concentration profiles were calculated and are shown in Figure 15 B. Species of different lipid classes were found to be widely distributed between the six clusters (Figure 16 A and Figure 17).

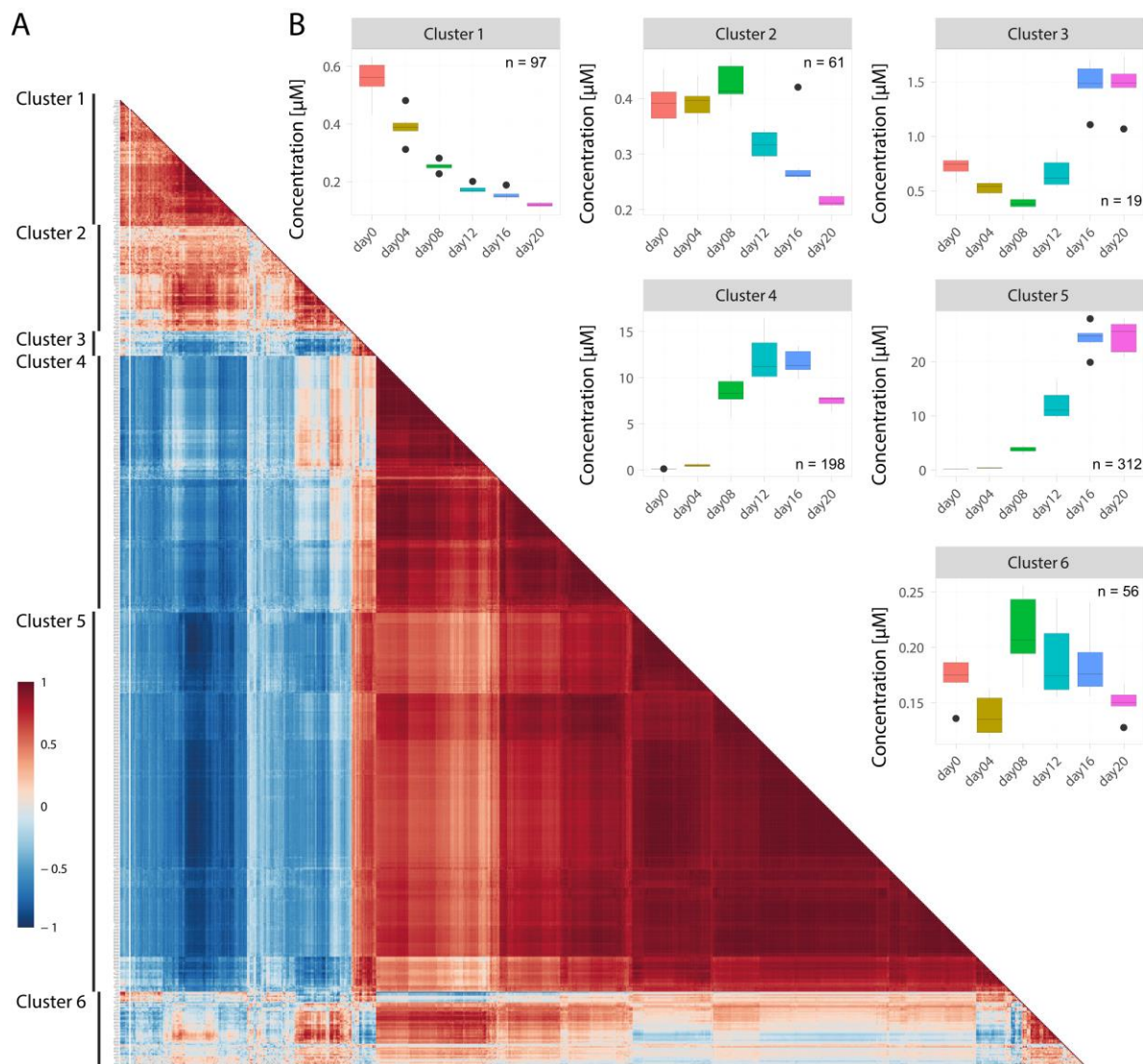


Figure 15: Spearman's rank correlation analysis of lipid concentration trajectories identified marked correlations and clustering of the lipid species.

Panel A shows the matrix of this analysis where each square indicates the Spearman's rank correlation coefficient. Positive correlations between each lipid species are shown in red, while negative correlations are illustrated in blue. Based on the correlation matrix, six lipid clusters were assigned. Clustering was performed Ward's clustering algorithm. Panel B illustrates the average lipid concentration profiles in the six clusters.

In the following, the different clusters are described in more detail: Cluster 1 (n = 97 lipid species) contained lipid species which had decreasing concentrations over the whole observed time in

Results

common (Figure 15 B). Lipid species from all classes, except SM, and with the highest averaged fatty acid (FA) side chain lengths (expressed as average total number of C-atoms) as well as number of DB can be found in cluster 1 (Figure 16 A–D). This cluster contained high amounts of PE (37.6%) and PC (20.8%) species. In addition, 80% of all LCER species of the dataset could be found in this cluster (Figure 17 A). Moreover, about 74.3% of the lipid species of this cluster had at least one FA side chain with at least 20 C-atoms and a low number of DB. To conclude, this cluster can be considered as the “PUFA cluster”.

Cluster 2 (n = 61) contained lipid species with decreasing concentration profiles after day 8 of differentiation. The species of this could be assigned to all classes except LPE. The species had the third highest number of C-atoms and DB (Figure 16 B–D). In addition, this cluster had many sphingolipid species: 56.6% of all CER, 40.0% of all HCER, and 41.7% of all SM species of the dataset (Figure 17 B) could be identified in this cluster. To conclude, this cluster can be characterized as the “sphingolipid and PUFA cluster.”

Lipid species of cluster 3 (n = 19) had fluctuating concentrations over time in common. Initially, the concentrations decreased until day 8, followed by an increase to concentrations higher than in preadipocytes (day 0). Only four lipid classes were found in this cluster: TAG (42.1%), DAG (10.5%), PC (15.8%), and PE (31.6%). Interestingly, 79% of these lipids had at least one FA with 18 carbon atoms.

Lipid species of clusters 4 and 5 (n = 198 and 312, respectively) had in general a strong concentration increase in common. However, species of cluster 4 strongly increased only until days 12–16. Afterwards, these species decreased to half their maximum concentrations. Species from cluster 5 had a concentration plateau at day 16. TAG species were clearly the most abundant ones (75.8%) in cluster 4, followed by PE species (13.1%), and DAG species (6.1%). In contrast, ceramide species (CER, HCER, and LCER) cannot be assigned to this cluster. The species of this cluster had a characteristic in common as these species had the lowest number of C-atoms and DB within the dataset (Figure 16 B–C). In cluster 5, the relative amount of TAG species was markedly higher (88%) than in cluster 4 (Figure 16 A). Since to the highest number of TAG species, clusters 4 and 5 also had the highest lipid concentrations in total (Figure 16 B). To conclude, both clusters can be characterized as “TAG clusters.”

Cluster 6 contained lipid species (n = 56) with a different concentration profile compared to the other clusters. In detail, they had a fluctuating concentration profile during adipogenesis. The cluster comprises species from all lipid classes with the exception of LCER (Figure 16 A).

The results from the Spearman’s correlation analysis between the clusters might provide new insights into lipid remodeling during cell differentiation of human pre-adipocytes in mature adipocytes. This hypothesis is supported by markedly negatively correlated lipid species of clusters 1 and 2 with lipids of clusters 4 and 5. In particular, several TAG species from cluster 5 showed strong negative correlations with PE species of cluster 1 (between -0.7 and -0.96). Both correlation groups had characteristics in common as the PE species had mostly polyunsaturated

Results

and VLCFA bound to their headgroup, whereas the TAG species had at least one LCFA at their glycerol headgroup.

In addition to PE and TAG species, sphingomyelins, especially SM 20:0 (cluster 4), SM 22:0 (cluster 5), and SM 24:0 (cluster 5), had high negative Spearman's correlation coefficients (down to -0.84) with ceramide species of clusters 1 and 2. These results point to regulatory interactions between lipid species over several lipid classes during human adipogenesis (22).

In addition, DAG and TAG species had very high positive correlation coefficients. These values were between 0.85 and 0.98. Those DAG and TAG species had mostly one or two of the most abundant FA (C16:0, 16:1, 18:0, and 18:1) as side chains. Furthermore, these TAG species had C-atom numbers between 42 and 54, which points to LCFA as the main bound FA side chains.

Results

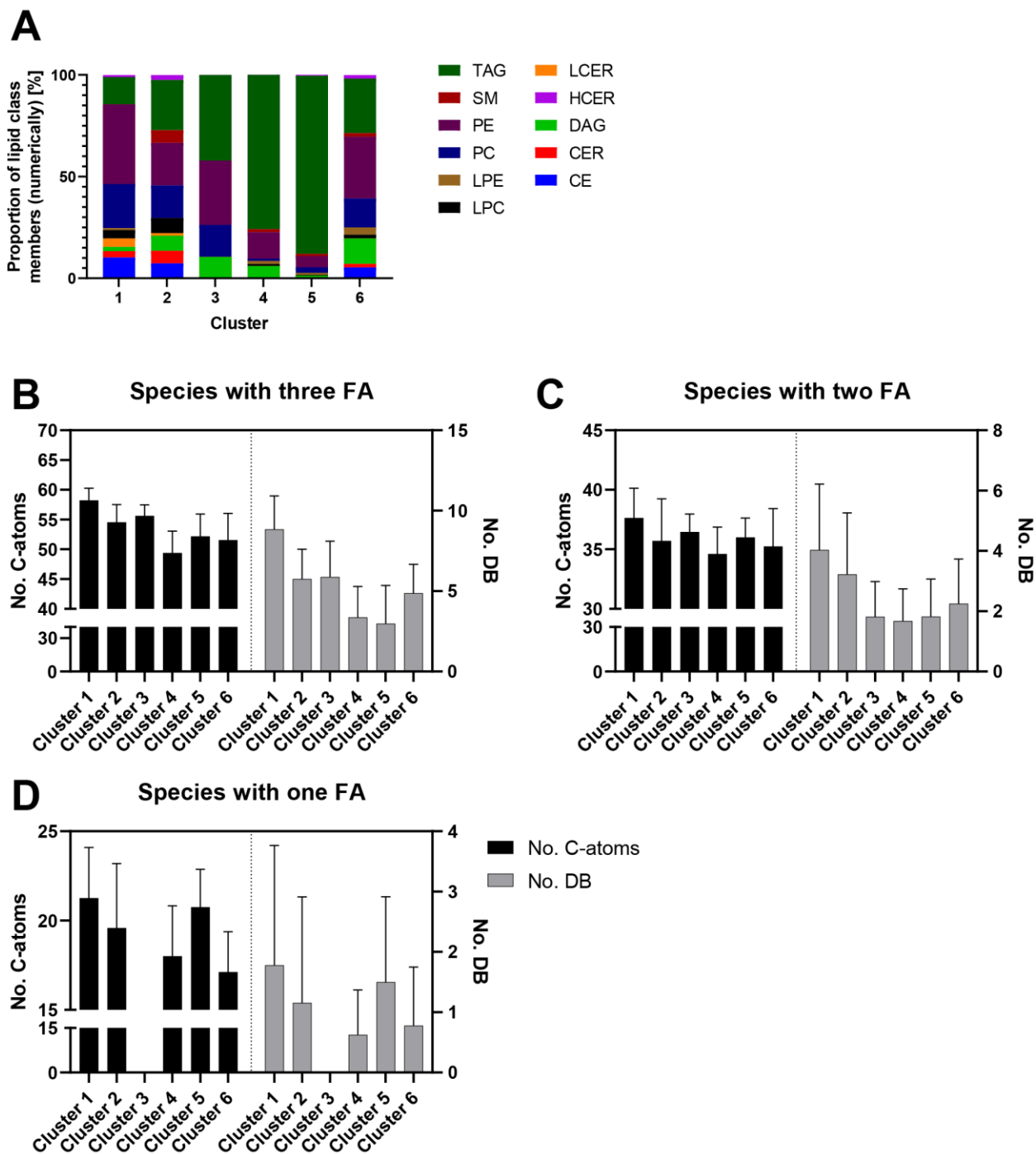


Figure 16: Clusters from Spearman's rank correlation analysis differed markedly regarding lipid species and lipid class composition.

Panel A shows the cluster compositions by illustrating the relative numerical proportions of the lipid class members. Panel B illustrates the analysis of side chain length and number of DB with the lipid class which have three bound FA (TAG). Panel C illustrates the analysis of lipid classes with two bound FA, and panel D with only one bound FA. In general, lipid species with decreasing concentration profiles throughout adipogenesis had the highest numbers of DB and the longest side chain lengths, independent of their number of side chains.

Results

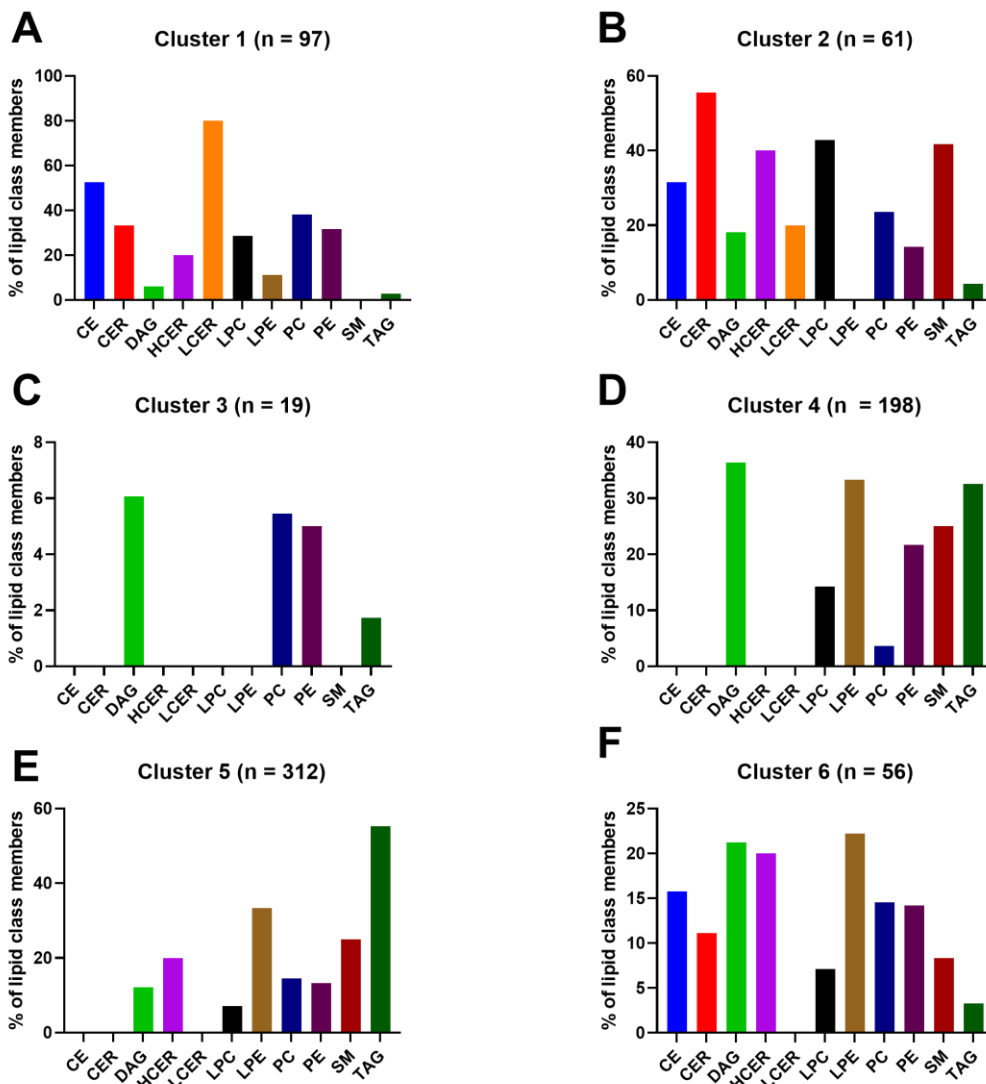


Figure 17: Analysis of the cluster showed distinct relative lipid class compositions.

Panels A-F show the lipid class compositions for each cluster normalized to the species' total number per class over all clusters.

To avoid misinterpretation of the results from the lipid analyses, the used cultivation and differentiation media were also analyzed with the Lipidizer™ method. Therefore, 300 μ L of each medium was analyzed in six replicates. Figure 18 illustrates the summations of the FA concentrations over all lipid classes derived from this analysis. In general, all FA were very high concentrated in the FBS-containing medium used for cell cultivation before initiation of differentiation. The overall highest concentration was found for palmitic acid (FA C16:0) with more than 1000 μ M. The lipids with very long-chain PUFAs were also highly concentrated in the FBS-containing medium. The medium without FBS, which is supplemented with factors inducing and promoting adipogenesis as well as with 1.5 μ M linoleic acid (C18:2) as the only fatty acid source, had quite low FA concentration levels.

Results

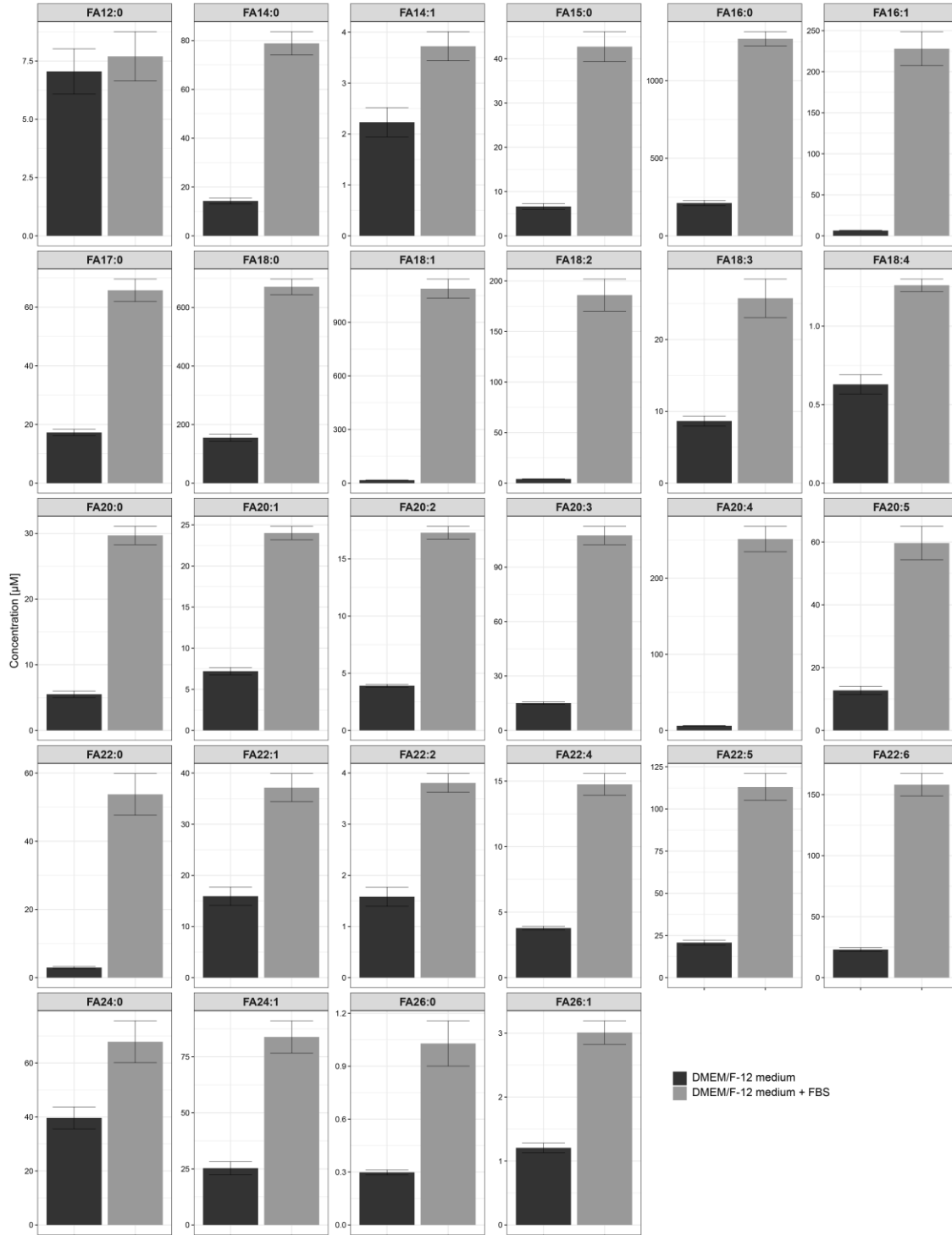


Figure 18: All fatty acids in FBS-containing medium were highly concentrated. For analysis, 300 µL medium was used. Shown are the concentration levels of the fatty acids summarized over all lipid classes. n = 6 per group.

Results

3.2.3. Absolute/DQ p180 kit

Additional to the characterization of the human adipogenesis with lipidomics, metabolomics measurements were also performed to increase the knowledge on concentration levels of polar analytes. Therefore, Biocrates Absolute/DQ p180 kit was used, which enabled the quantification of analytes from seven different classes, namely amino acids, biogenic amines, carnitine and acylcarnitines, hexoses, spingomyelins, and (lyso-)phosphatidylcholines. However, a resolution on isomer and isobar level of the PC is not possible. Therefore, detailed data analysis of changing concentration levels during adipogenesis was only performed with the polar metabolites.

Figure 19 illustrates the PLS-DA and VIP scores plot of the whole data set. A very clear clustering of the metabolites regarding the different time points of adipogenesis could be monitored. Component 1 was mostly sufficient to separate the different time points of the cell differentiation process. Three amino acids, namely glutamate (Glu), proline (Pro), and glycine (Gly), as well as the polyamine putrescine had a very strong influence on the separation. Moreover, some PC and lyso-PC as well as SM OH C16:1 strongly contributed to the separation.

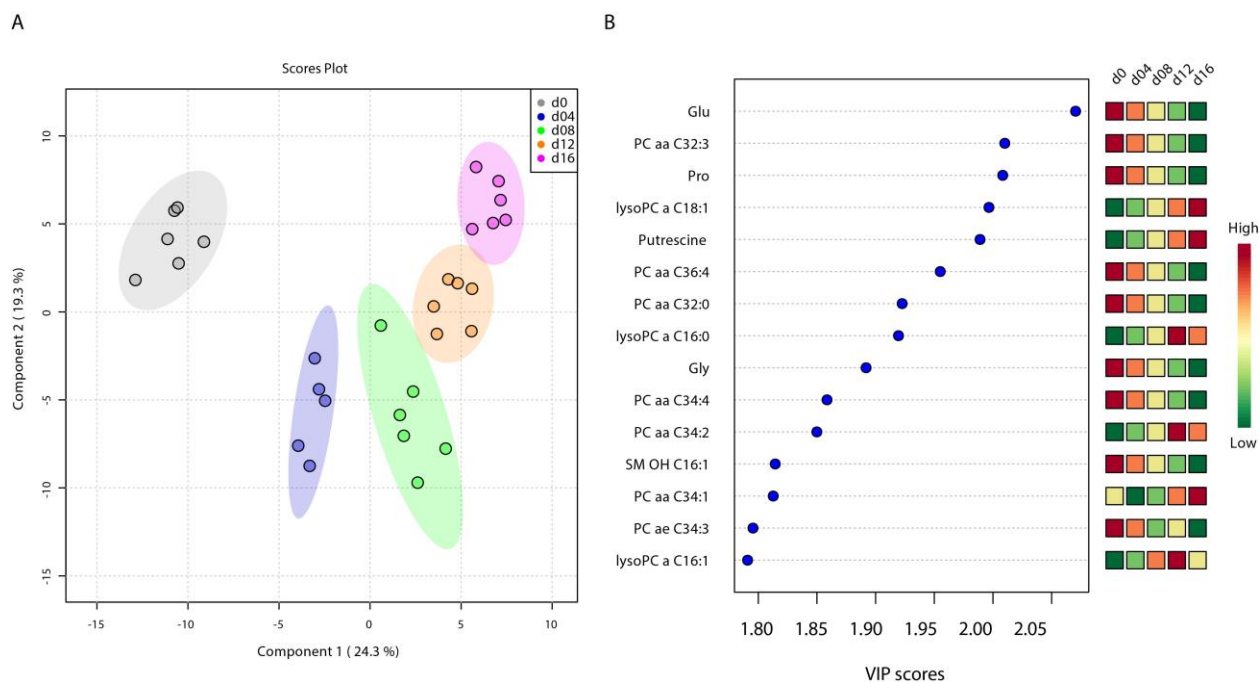


Figure 19: PLS-DA scores plot (Panel A) showing very clear clustering of the analytes regarding the different time points of adipogenesis.

VIP scores plot (panel B) revealed strong influence of some amino acids (Glu, Pro, and Gly), putrescine and some phosphatidylcholines as well as SM OH C16:1 on the separation. The model was predictive and not overfitted as the results from cross-validation and permutation test showed (R^2 : 0.97, Q^2 : 0.99; $p = 0.0075$ (15/2000 permutation numbers), test statistics selected by separation distance (B/W)). Each group consisted of six samples with the exception of day 4 samples which consisted of only five samples.

Figure 20 illustrates the heatmap of the top 80 metabolites of the complete data set. Like in the PLS-DA score plot, a good clustering of the five time points could be achieved. In general, three

Results

metabolite clusters could be identified based on their changing concentration profiles during adipogenesis. The first cluster is characterized by species that have a strong relative decreasing concentration profile. This cluster contained most of the amino acids, some biogenic amines, and several PC species. The second cluster contained many acylcarnitines and spermine. All concentrations of metabolites increase until day 4 followed by a decrease. The third cluster is characterized by species with a concentration increase throughout adipogenesis. Members of this cluster are (lyso-)PC, putrescine, and alanine (Ala).

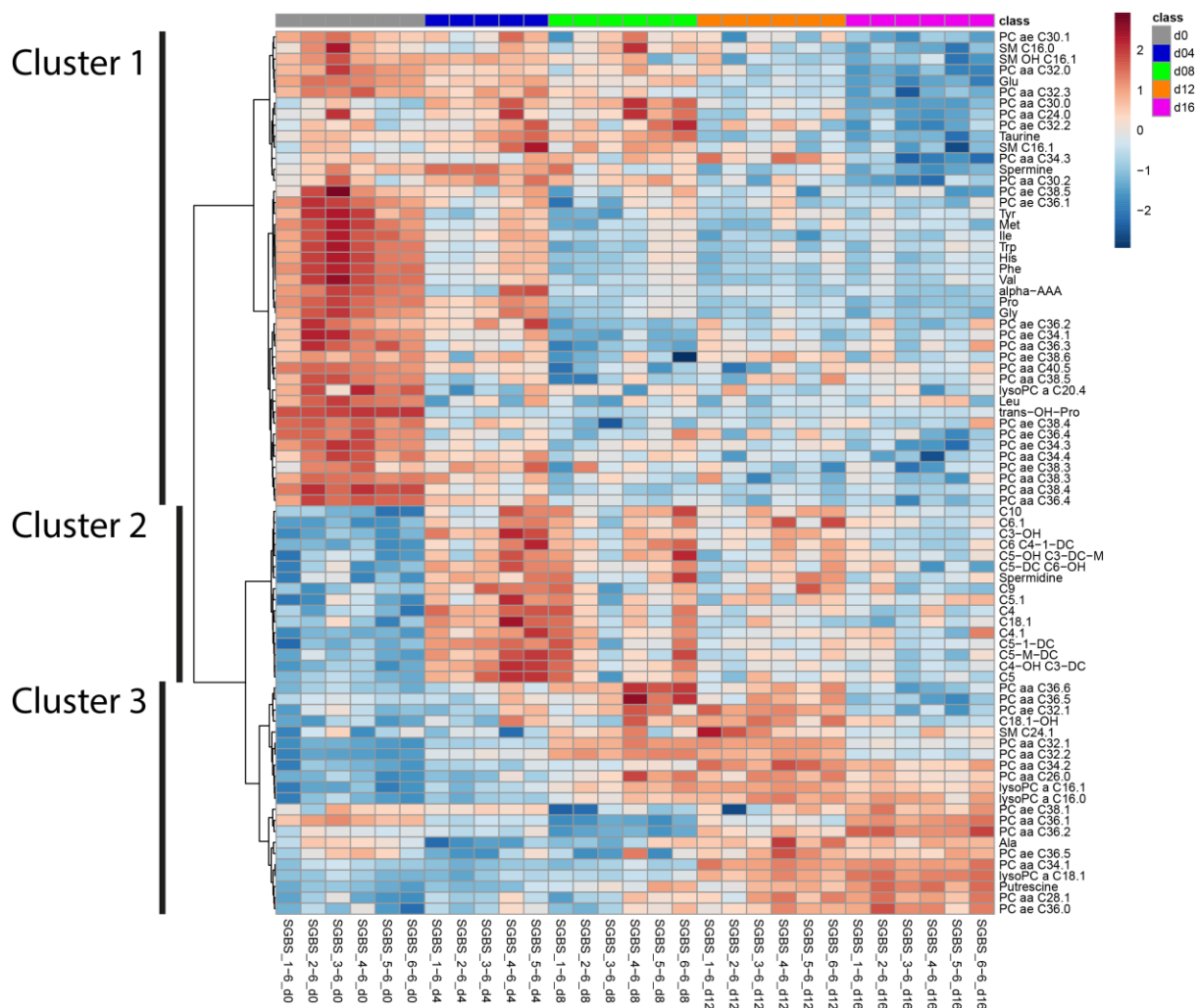


Figure 20: Heatmap of the top 80 metabolites revealed a strong clustering of metabolites and samples. The metabolites could be assigned into three cluster based on their concentration time course. The first cluster contained metabolites with a decreasing concentration during the analyzed time. The second cluster grouped metabolites, mostly acylcarnitines, with a concentration peak at day 4, followed by a concentration decrease. Cluster three summarized species with an overall increasing concentration time course. For clustering, the Ward method was used with euclidean distance measurement. Data were log-normalized and auto-scaled, but not clustered based on sampling time points.

Figure 21 illustrates a detailed data analysis of the changing concentration levels of the amino acids and biogenic amines during human adipogenesis. Glu, Gly, histidine (His), methionine (Met), the branched-chain amino acids isoleucine (Ile), leucine (Leu), and valine (Val) as well as the

Results

aromatic amino acids phenylalanine (Phe), tryptophan (Trp), and tyrosine (Tyr) showed strongly decreasing concentration levels. In addition, the levels of α -amino adipic acid and trans-OH-proline decreased strongly from day 0 to day 4 and stayed at levels below LOD afterwards. In contrast, putrescine had a strongly increasing concentration profile during the whole observed time. Spermidine and spermine, which are downstream metabolic products of putrescine, had their concentration peaks between day 4 – 8 followed by a concentration decrease. In addition, several acylcarnitines had a similar concentration profile during adipogenesis.

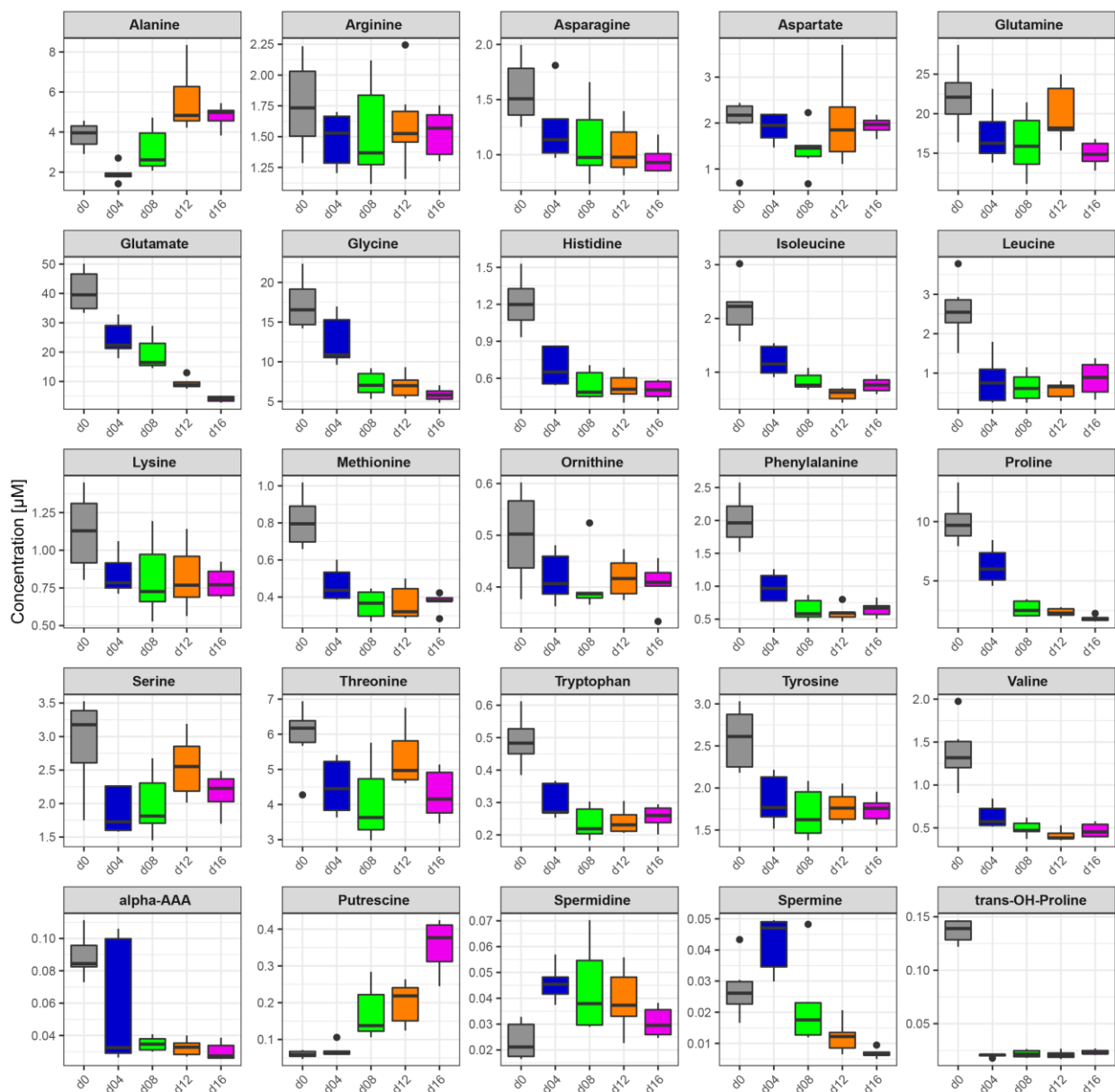


Figure 21: Analysis of amino acids and biogenic amines revealed markedly changed concentration time courses (Biocrates AbsoluteDQ p180 kit).

Results

Most of the amino acids had strongly decreasing concentration levels throughout adipogenesis. Spermidine and spermine had a concentration peak between day 4 and 8, while putrescine had strongly increasing concentration levels throughout cell differentiation.

3.2.4. Newborn Screening assay

In addition to the Absolute/IDQ p180 kit, the Newborn Screening assay was used for the analysis of amino acids, free carnitine, and acylcarnitines to verify and confirm the obtained metabolomics results. For this analysis, SGBS cells from a separate experiment were used to increase the validity of the analysis. A clear clustering of the metabolites regarding the different time points of adipogenesis was obtained (Figure 22 A). Component 1 had an essential influence on the separation of the time points with 27.4% of explained variance. However, between day 12 and 20, the separation power was reduced. This can be explained with the variables of the important features (VIP) plot in Figure 22 B and the heatmap in Figure 23, because the changes of concentration levels were generally less pronounced at these later stages of adipogenesis compared to the earlier ones. It should be also noted that with this measurement more species with a decreasing concentration profile than species with an increasing concentration profile were quantified. Consequently, the measured concentration changes of these metabolites did not change markedly at the later stages. Therefore, a separation of the clusters of these stages was no longer possible.

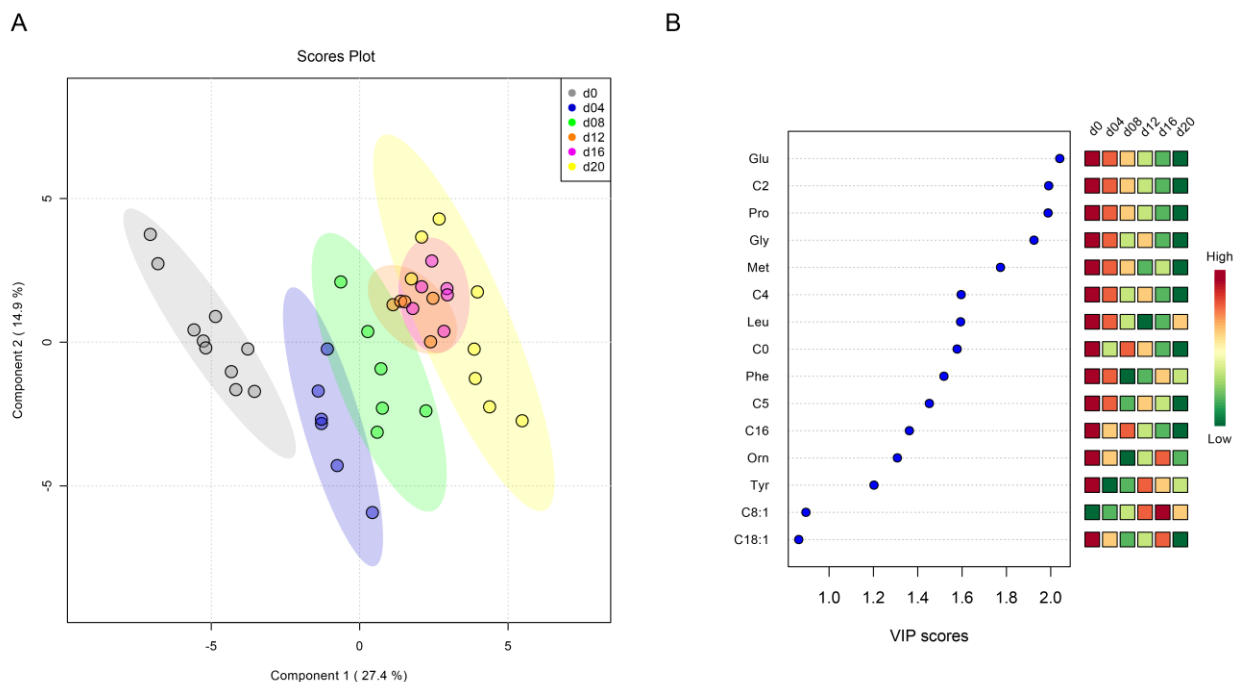


Figure 22: PLS-DA analysis revealed clustering of the samples into separate time points based on the metabolites of the Newborn Screening assay.

Panel A illustrates scores plot while panel B shows plot from analysis of variation of importance. The box inside the figure illustrates the used color code for the different days of adipogenesis. Shown are also the 95 % confidence intervals for each

Results

group. The model was predictive and not overfitted as the results from cross-validation and permutation test showed (R^2 : 0.98, Q^2 : 0.91, $p < 5e-4$ (0/2000 permutation numbers), test statistics selected by separation distance (B/W)).

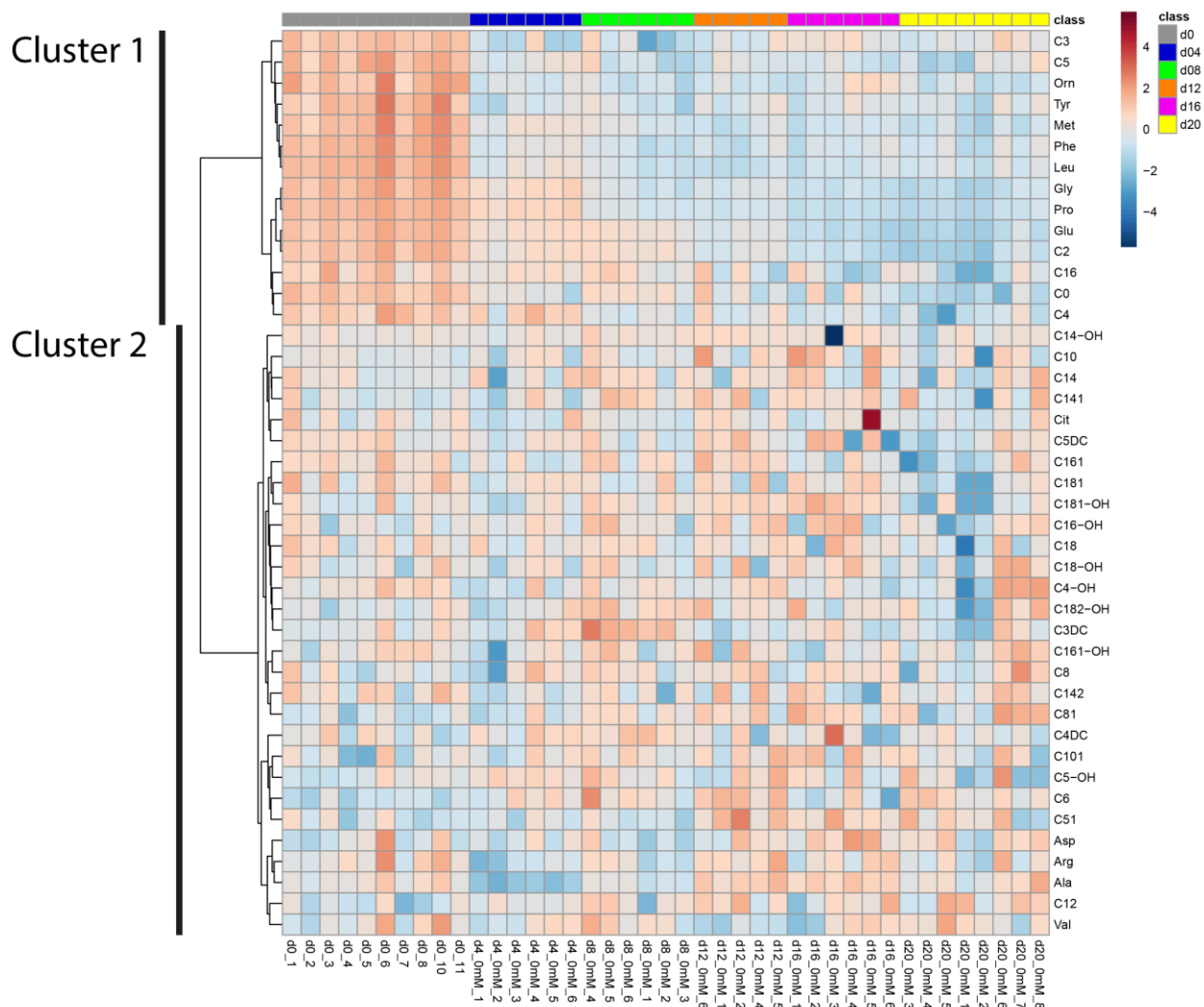


Figure 23: Heatmap of the metabolites from the analysis with the NBS assay revealed two clusters.

The first cluster contained most amino acids, acylcarnitines and free carnitine with a decreasing concentration profile. The second cluster revealed metabolites with a fluctuating but largely unchanged concentration profile. For clustering, the Ward method was used with euclidean distance measurement. Data were log-normalized and auto-scaled, but not clustered based on sampling time point.

Figure 24 shows the concentration time courses of the most strongly changed metabolites. Free carnitine, three acylcarnitines, namely C2, C5 and C16, as well as several amino acids showed strongly decreasing concentration time courses. In detail, Glu, Gly, Leu, Met, ornithine (Orn), Phe, Pro, and Tyr were those with the most marked changes over time.

Results

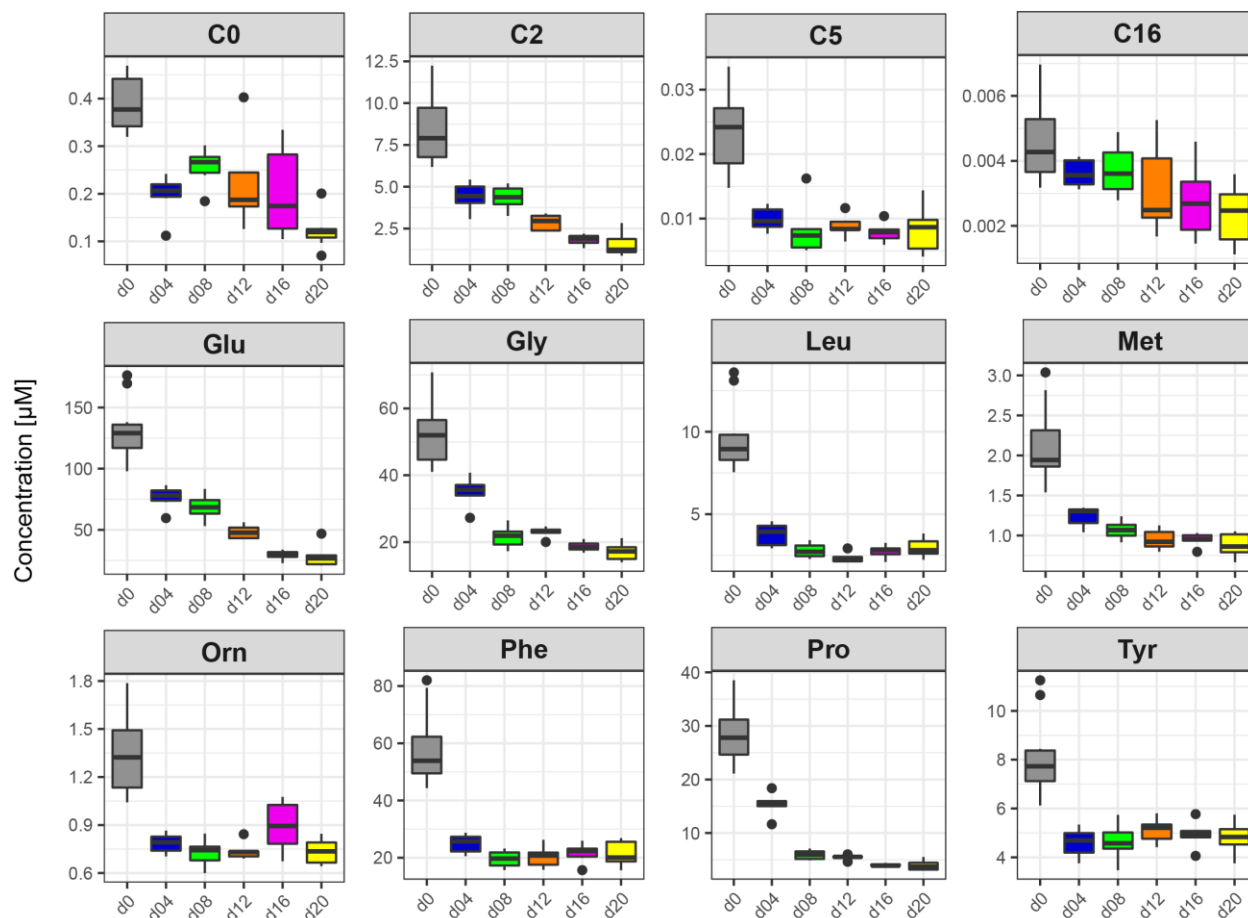


Figure 24: Newborn Screening assay quantified strongly decreasing concentration levels of most of the amino acids as well as free carnitine and three acylcarnitine.

To sum up, the Newborn Screening assay for the measurement of samples from another experiment could mostly confirm the results from the measurement with Biocrates Absolute/IDQ p180 kit. The different time points of human adipogenesis could be separated by PLS-DA. In addition, the method also quantified strongly decreasing concentration levels over time for most of the amino acids. In contrast to the Biocrates' method, the Newborn Screening assay could not quantify strongly changing levels of acylcarnitines as well as strongly decreasing concentration levels of Val during adipogenesis.

3.2.5. Non-targeted metabolomics using the technology by Metabolon Inc.

Besides amino acids and biogenic amines, polar metabolites from other pathways are also helpful to shed light on the human adipogenesis. Therefore, Metabolon's non-targeted approach was chosen, which enables the analysis of analytes from additional metabolic pathways. Metabolites such as amino acids, carbohydrates, cofactors and vitamins, lipids, nucleotides, peptides, and xenobiotics were measured in the same samples, that were used for the GC-MS based

Results

quantification assay. Quality assessment was done for the instrument variability as well as for the total process variability as described in section 2.9.6. For instrument variability, the precision [relative standard deviation (RSD)] was calculated of the internal standards in the QC samples that were added to the sample prior to injection into the mass spectrometry system. For measuring the total process variability, the RSD was calculated of all endogenous metabolites that were present in 100% of the matrix samples and which are technical replicates of pooled samples. Values for instrument and total process variability, were 4% and 11%, respectively, showing high data quality.

In total, 338 metabolites and lipid species could be measured in differentiating SGBS cells. To investigate putative differences between the signal intensity levels of all analytes at different time points, PCA (Figure 25 A) and PLS-DA (Figure 25 B) were performed. In general, a clear separation of the individual time points could be obtained in both analyses. The first (principal) component was nearly sufficient to separate all time points for both approaches, respectively. In the PCA, the first two principal components had 48.5 and 18.4% explained variances, whereas the components of the PLS-DA had 48.4 and 6.3% explained variances.

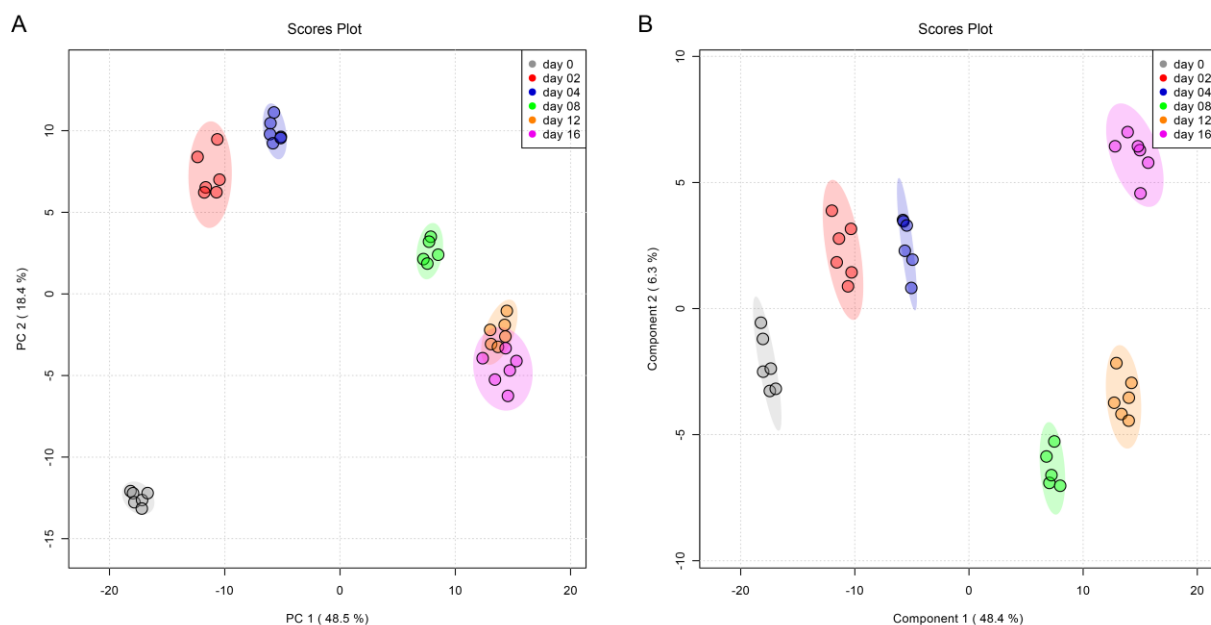


Figure 25: PCA and PLS-DA scores plot showed clear separation of the different time points.

Panel A illustrates PCA, whereas PLS-DA is shown in panel B. The box inside the figure illustrates the used color code for the different days of adipogenesis. Shown are also the 95 % confidence intervals for each group. The model was predictive and not overfitted as the results from cross-validation and permutation test showed (R^2 : 0.99, Q^2 : 0.99, $p < 5e-4$ [0/2000 permutation numbers], test statistics selected by separation distance (B/W)).

Additionally, a heatmap was generated to display the auto-scaled and normalized concentration changes of the analytes of the whole dataset during adipogenesis (Figure 26). Obviously, analyte clusters of distinct concentration profiles can be observed. The first cluster is characterized by analytes with increasing concentration levels over time. The second cluster summarizes metabolites which had decreasing concentration levels over time. Interestingly, the metabolites

Results

of this cluster showed small gradations in their concentration decrease. The third cluster revealed analytes with increasing concentrations from day 0 to day 2 followed by decreasing concentrations. The fourth cluster shows analytes which had a fluctuating concentration profile.

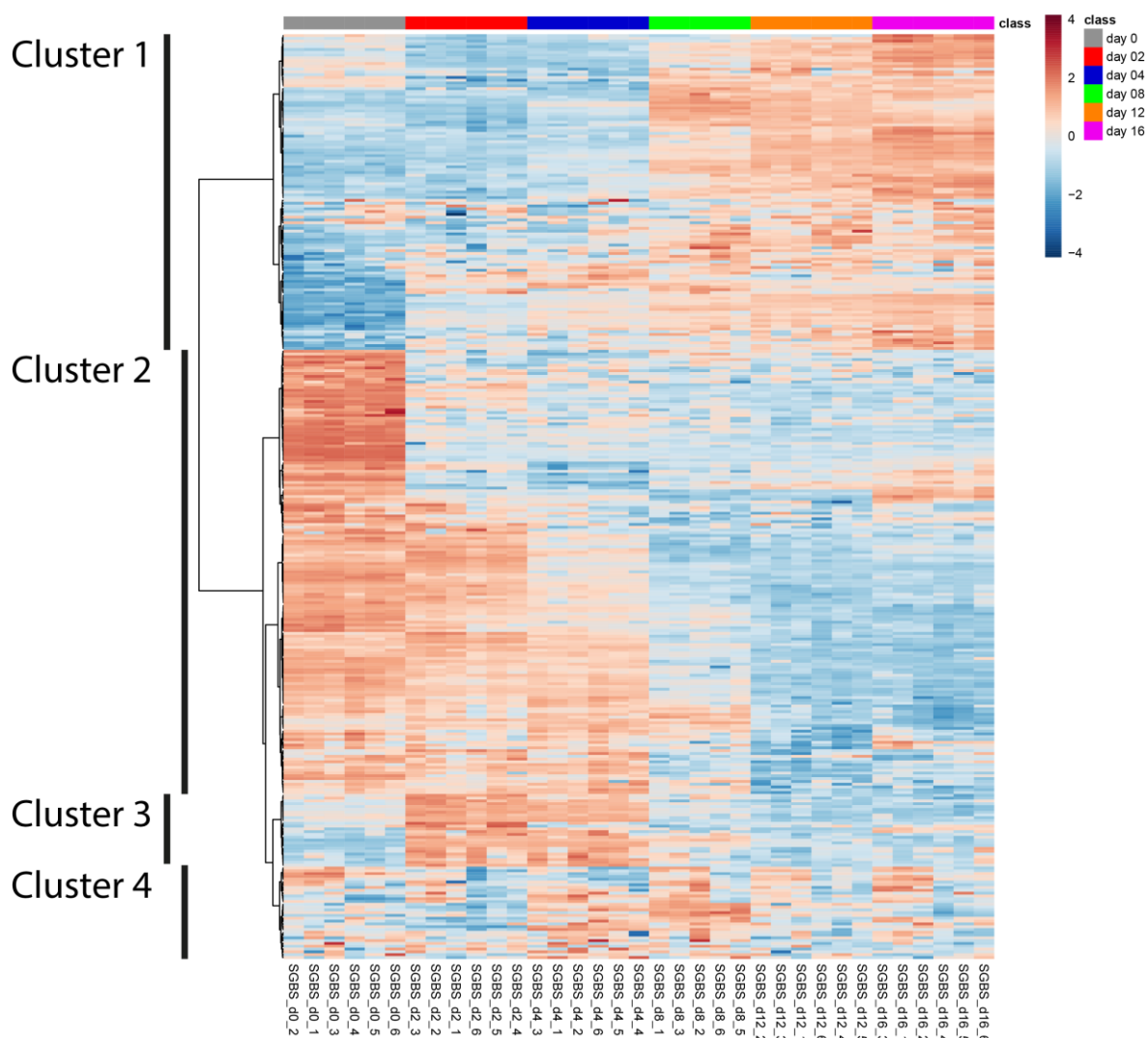


Figure 26: Heatmap of the non-targeted dataset revealed a strong clustering of the metabolites according to different stages of adipogenesis.

The metabolites could be assigned into four cluster based on their concentration time course. The first cluster contained metabolites with an increasing concentration pattern throughout the analyzed time. The second cluster summarizes metabolites, which had markedly decreasing concentration levels over time. The third cluster revealed analytes whose concentration increased from day 0 to day 2 followed by decreasing concentrations. The fourth cluster shows analytes which had a fluctuating concentration profile. For clustering, the Ward method was used with euclidean distance measurement. Data were log-normalized and auto-scaled, but not clustered based on sampling time points.

Additionally, a classification approach by Random Forest was performed to obtain information on the contribution of single metabolites to the separation. Figure 27 illustrates the top 15 analytes ranked by their contribution to classification accuracy. Fumarate, coenzyme A, mannonate, 1-ribosyl-imidazoleacetate, phosphoenolpyruvate (PEP), glycerophosphocholine (GPC) and -inositol (GPI), and several glycerophospholipids, especially PC, were the analytes with the greatest

Results

influence on this separation. All 15 metabolites had clearly changing concentration levels over time in common.

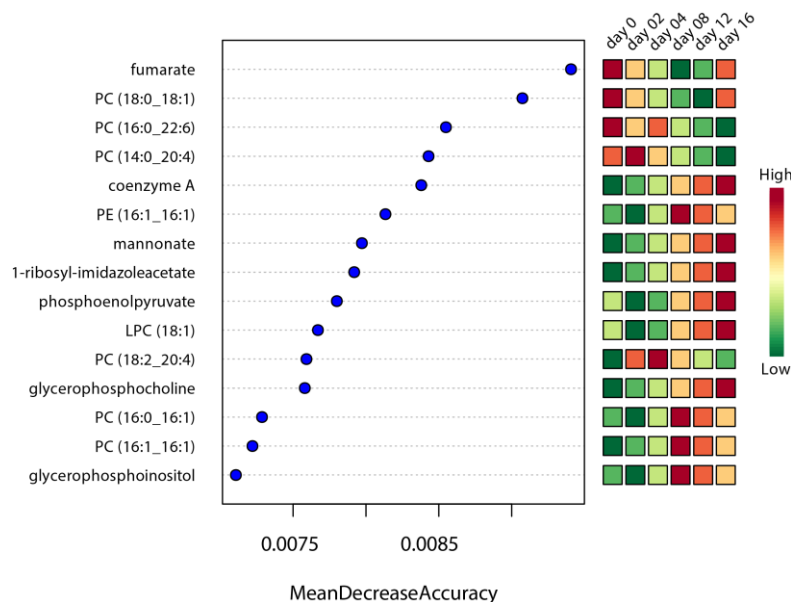


Figure 27: Random forest analysis revealed the top 15 analytes ranked by their contributions to the classification accuracy. Several polar metabolites like fumarate, coenzyme A, mannonate, as well as some glycerophospholipids had a strong influence on the separation of the different time points of adipogenesis.

Since glycerophospholipids were already quantified by the Lipidizer™ method, further data analysis was focused on lipid species that were not included in the Lipidizer™ method as well as other metabolites, which could not be measured by other assays. With Metabolon's approach, lipid species from six additional classes could be detected. They belong to the classes of phosphatidylglycerol (PG), phosphatidylinositol (PI), phosphatidylserine (PS), and their respective intermediates, namely lysophosphatidylglycerol (LPG), lysophosphatidylinositol (LPI), and lysophosphatidylserine (LPS). Figure 28 A illustrates their signal intensity time courses. The species from LPG, LPI, and LPS had distinct signal intensities time courses among themselves and their corresponding products with two bound fatty acids. However, species with one C20:4 fatty acid tended to decrease signal intensities levels during adipogenesis.

In Figure 28 B, metabolites from phospholipid metabolism are shown. These metabolites were amongst the most strongly changing signal intensity values of the whole data set. For example, GPC increased from $117.7 \pm 9.7 \times e6$ at day 0 to $2204.4 \pm 119.3 \times e6$ signal intensity at day 16, choline increased strongly from $74.3 \pm 8.2 \times e6$ to $116.4 \times e6 \pm 10.8 \times e6$ signal, and choline phosphate decreased from $592.0 \pm 25.8 \times e6$ to $152.4 \pm 7.4 \times e6$.

Figure 28 C shows the polar metabolites from Random Forest analysis (see Figure 27) which had a strong influence on the separation of the different time points. Coenzyme A (CoA), mannonate, 1-ribosyl-imidazoleacetate, and PEP had markedly increasing signal intensity profiles, whereas the

Results

A: Signal intensity courses of phosphatidylglycerols, -inositols, and -serines and their respective lysophospho-species showed distinct changes during adipogenesis.

B: Metabolites from phospholipid metabolism showed in parts the strongest signal intensity changes during adipogenesis.

C: Other polar metabolites selected by Random Forest analysis showed markedly changing signal intensities profiles.

Since there were strong opposing trends in the individual metabolite and lipid species concentrations, Spearman's rank correlations of the lipid species concentration trajectories were computed to analyze possible associations between the metabolites and lipids. Figure 29 illustrates the correlation coefficients of the top 25 compounds from this analysis. Overall, metabolites and lipids in four clusters showed high correlations. Panel A illustrates compounds with strongly increasing (red) as well as decreasing (blue) signal intensity time profiles during the whole observation time. For example, GPC, GPE, and GPG were positively correlated with increasing concentrations during adipogenesis whereas some PC species and choline phosphate were negatively correlated with increasing concentrations. Panel B shows the top 25 compounds with positive or negative correlation coefficients regarding an increasing (red) or decreasing (blue) signal intensity profile until day 12 of adipogenesis. Subsequently, the species had an opposed concentration profile. Positively correlated (red) compounds with a concentration maximum at day 12 were lipid species with at least one FA with 16 C-atoms, myo-inositol or GPI, whereas negatively correlated compounds (blue) were lipid species with higher C-atom numbers and metabolites from the TCA cycle (malate and fumarate) as well as amino acid pathways.

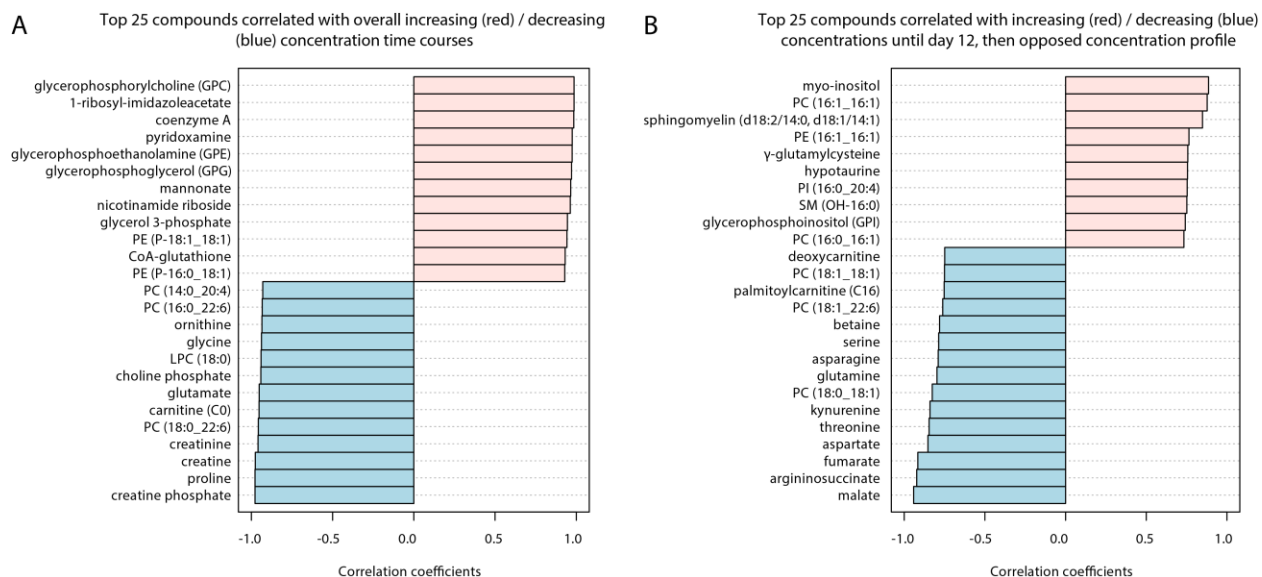


Figure 29: Spearman's rank correlation analysis showed strong correlations of metabolites and lipid species with distinct concentration profiles.

Positive correlations between the variables are shown in red, while negative correlations are shown in blue. Panel A illustrates the top 25 compounds, based on the correlation coefficients, with an overall increasing (red) concentration time course whereas the negatively correlated compounds (blue) had an overall decreasing concentration profile.

Panel B illustrates the top 25 compounds with increasing (red) concentrations until day 12 of adipogenesis. Subsequently, these species had a decreasing concentration profile. The negatively correlated compounds (blue) had an opposed concentration profile.

Results

To conclude, the analysis with Metabolon's non-targeted approach showed strongly changes in signal intensity levels for several metabolites during adipogenesis. These changes enabled a clear separation of the different time points of adipogenesis. Additionally, lipid species from six other lipid classes could be measured with this approach, thus extending the lipid panel that was measured with the Lipidizer™ method. The lipids had distinct intensity patterns during adipogenesis. However, lipid species with C20:4 showed mostly decreasing signal intensity values during adipogenesis. Moreover, several metabolites of the phospholipid metabolism were amongst the most changed ones during adipogenesis of all metabolites. All in all, these results implicate strongly regulated processes of phospholipids during adipogenesis.

3.2.6. Energy metabolism assay

The GC-MS based EM assay was successfully developed and validated for the measurement of EM metabolites in undifferentiated, differentiating, maturing, and mature adipocyte cell samples (3.1). For the measurements, the same cell samples as for Metabolon's non-targeted approach were used. The obtained concentration time courses reflect the concentration profiles that were observed with non-targeted metabolomics (Figure 30). Fumarate and malate decreased strongly from day 0 to day 8, stayed at low concentration levels, and increased from day 12 to day 16. Succinate, α -ketoglutarate, 2-hydroxyglutarate, and citrate markedly decreased over the whole observed time period to low concentration levels. Pyruvate and glucose showed similar concentration profiles. Concentrations of both peaked between day 2 and 4 (pyruvate: $19.5 \pm 6.3 \mu\text{M}$, day 2; glucose: $611.1 \pm 72.0 \mu\text{M}$, day 4), and decreased afterwards to starting levels. The concentration levels of lactate decreased on day 0 ($116.3 \pm 8.4 \mu\text{M}$) to day 12 ($44.7 \pm 8.0 \mu\text{M}$), then increased in the following four days to $74.3 \pm 11.9 \mu\text{M}$. 3-Hydroxybutyrate was the only metabolite with an increasing concentration time course. At day 0, the concentration fluctuated around Cal1 ($0.3 \pm 0.3 \mu\text{M}$), then increased during the next 16 days to $3.3 \pm 0.5 \mu\text{M}$.

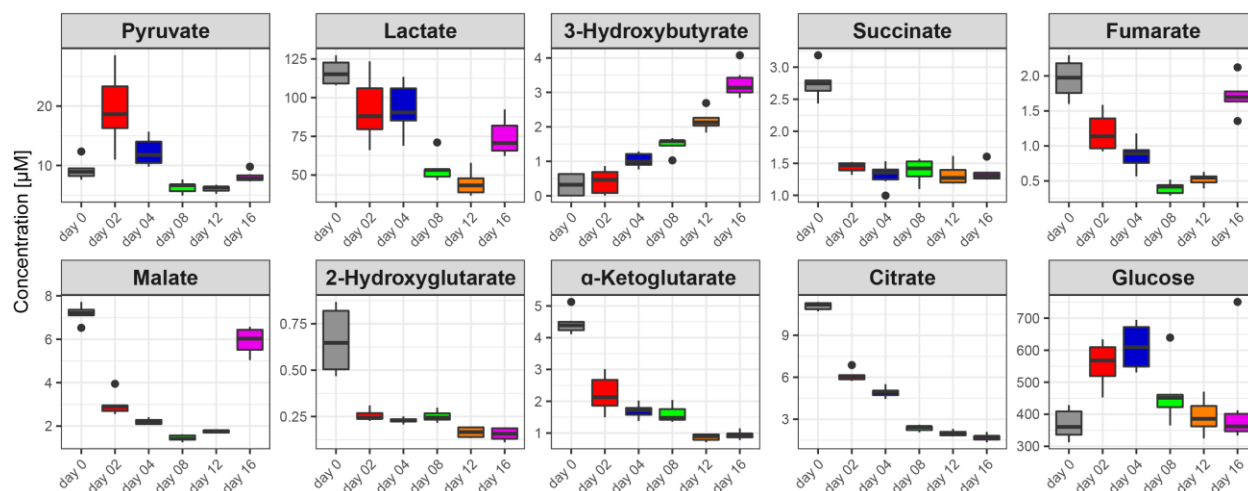


Figure 30: EM assay revealed strongly changed concentration levels of metabolites of the TCA cycle and cellular energy related pathways.

Results

Lactate, succinate, 2-hydroxyglutarate, α -ketoglutarate, and citrate had strongly decreased concentration levels, while 3-hydroxybutyrate had strongly increased levels throughout the observed time. The concentration levels of fumarate and malate also strongly decreased; however, increased from day 12 to day 16 to levels at day 0. Pyruvate and Glucose had a concentration maximum between day 2 and 4.

3.2.7. Comparison of mass spectrometry-based results

Due to the high number of applied metabolomics and lipidomics approaches, several metabolites were measured multiple times. This allows the comparison of the results for single analytes obtained with the different assays. However, for direct comparison studies, the different datasets had to be normalized, because the non-targeted approach did only deliver signal intensity values whereas the other approaches produced absolute concentration values. Therefore, the results were auto-scaled according to Equation 6. The comparisons of the most important auto-scaled concentration and signal intensity time courses are illustrated in Figure 31 – Figure 35. In general, all metabolomics approaches revealed similar profiles of metabolites over differentiation time. Especially the methods that used the same cell samples – Metabolon's non-targeted approach and EM assay – revealed almost identical profiles. Thus, the targeted and quantitative EM assay (3.2.6) could confirm the non-targeted results that were gained in a qualitative approach (3.2.5). Moreover, the overlapping dataset from the non-targeted approach could be mostly confirmed with the Lipidyzer™ technique although both methods used biologically independent samples. In addition, the measurement with the NBS assay could mostly confirm the results from the measurements with the Biocrates Absolute/DQ p180 kit. However, the NBS assay quantified strongly decreasing carnitine and acylcarnitine (C2, C5, and C16) concentrations while the Biocrates method quantified a concentration peak on day 4 followed by decreasing concentration levels of several acylcarnitines. It should be mentioned that these two measurements used different cell samples.

Results

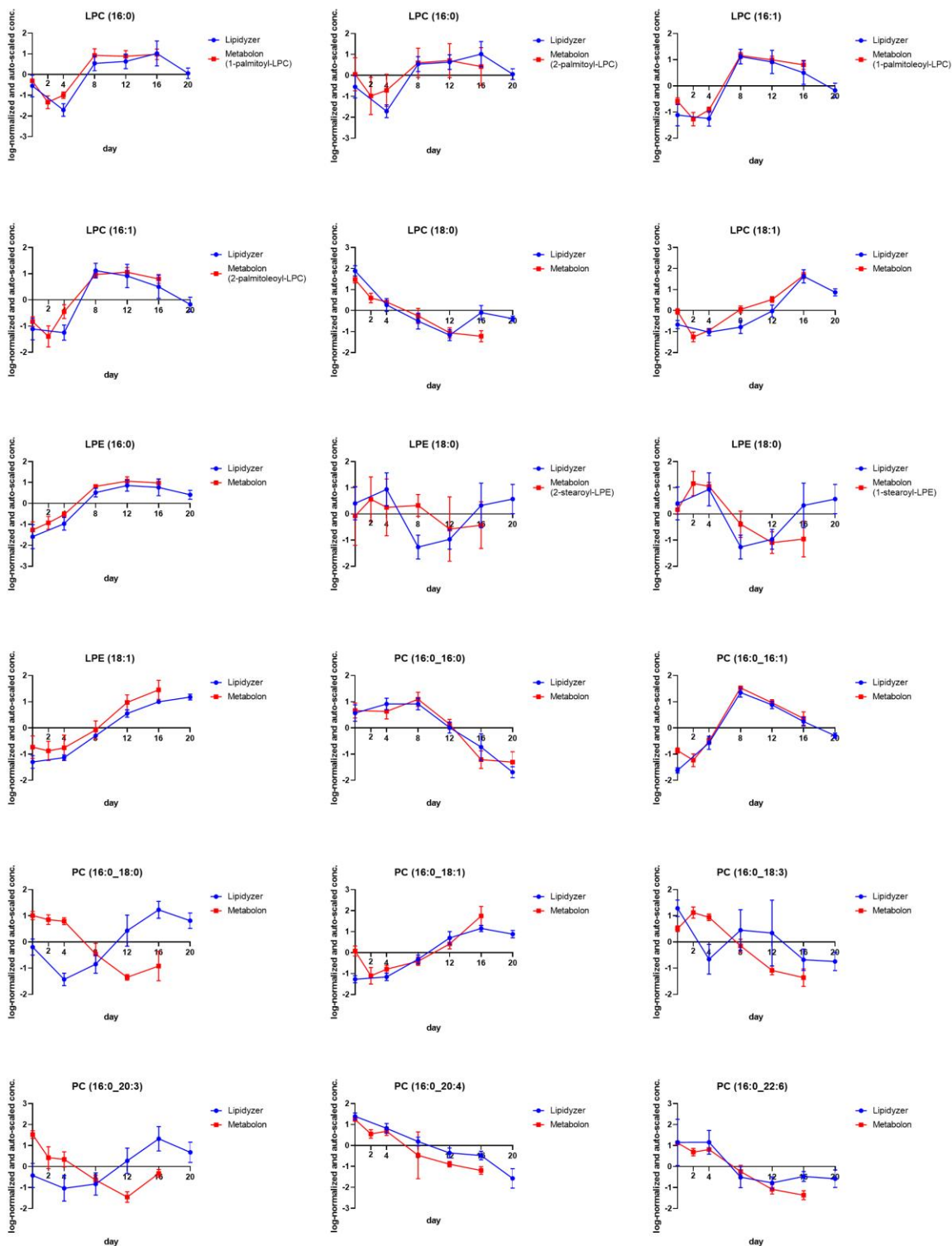


Figure 31: Comparison of the different metabolomics and lipidomics measurements revealed strong consistency. Measured metabolites in two or more assay were selected. For some of the assays, cells were collected on different time points as described in the previous sections (see sections 3.2.2 – 3.2.6). For the analysis, concentration and signal intensity values were auto-scaled to allow comparability.

Results

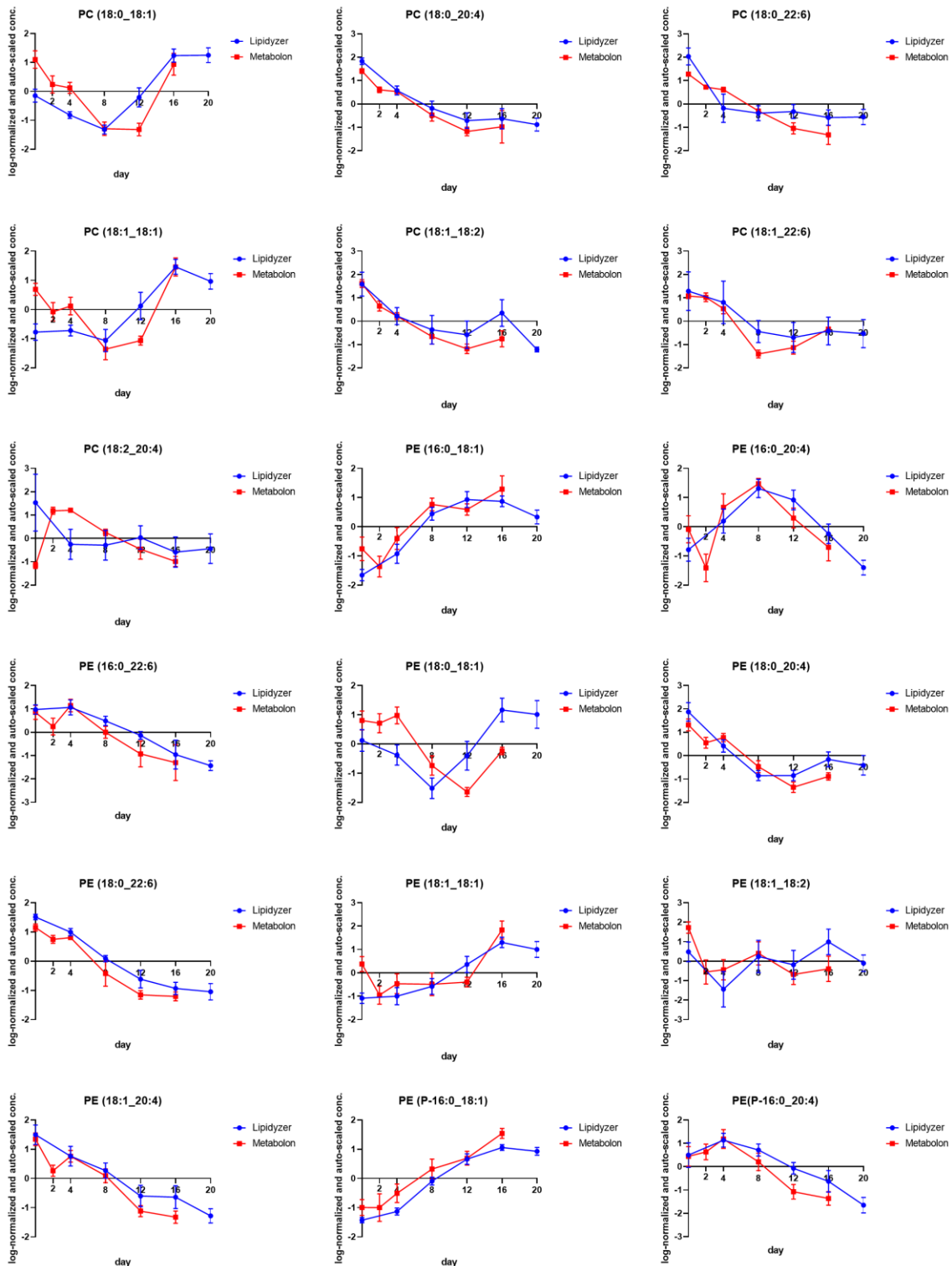


Figure 32: Comparison of the different metabolomics and lipidomics measurements revealed strong consistency. Measured metabolites in two or more assay were selected. For some of the assays, cells were collected on different time points as described in the previous sections (see sections 3.2.2 – 3.2.6). For the analysis, concentration and signal intensity values were auto-scaled to allow comparability.

Results

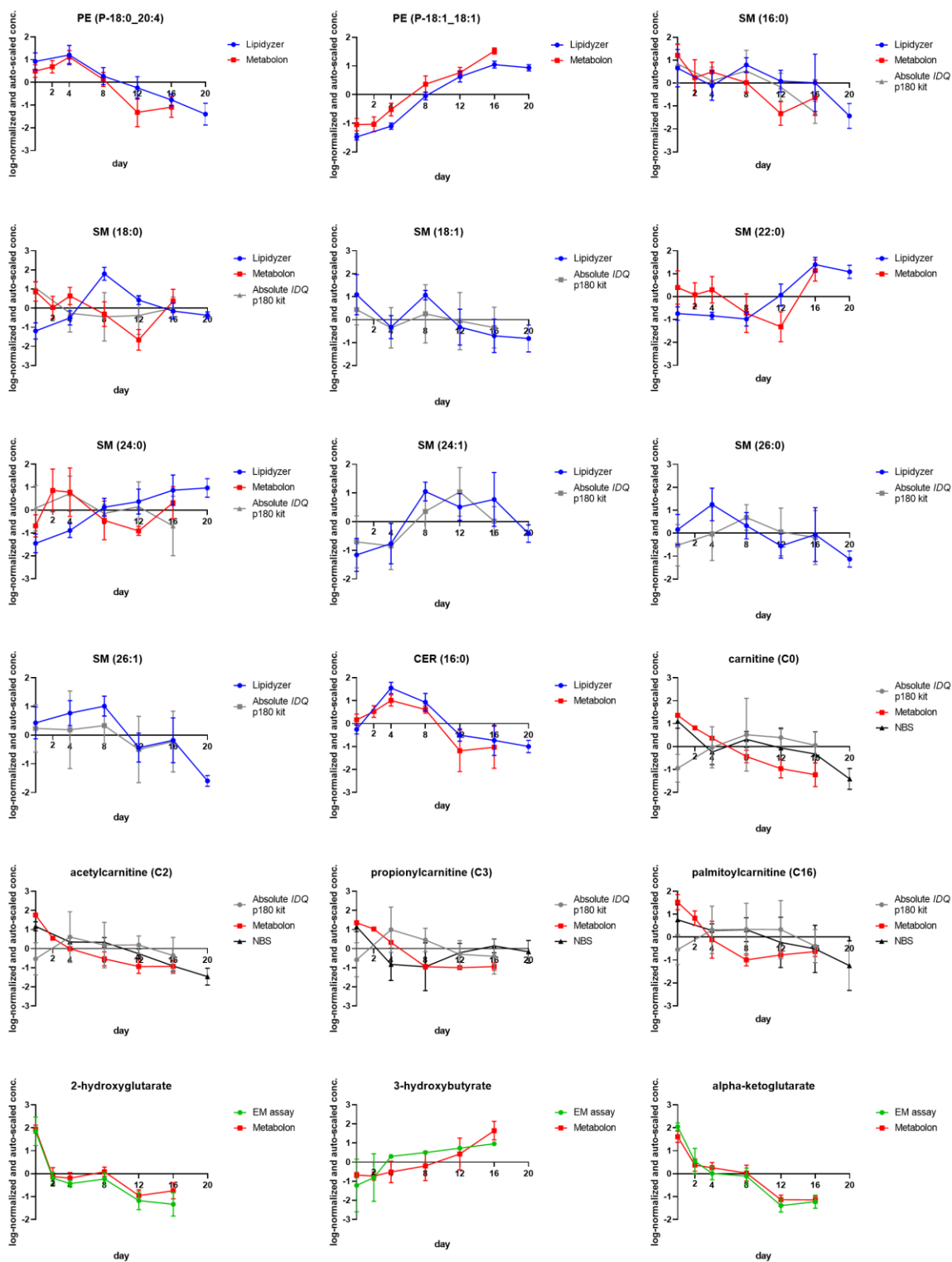


Figure 33: Comparison of the different metabolomics and lipidomics measurements revealed strong consistency. Measured metabolites in two or more assay were selected. For some of the assays, cells were collected on different time points as described in the previous sections (see sections 3.2.2 – 3.2.6). For the analysis, concentration and signal intensity values were auto-scaled to allow comparability.

Results

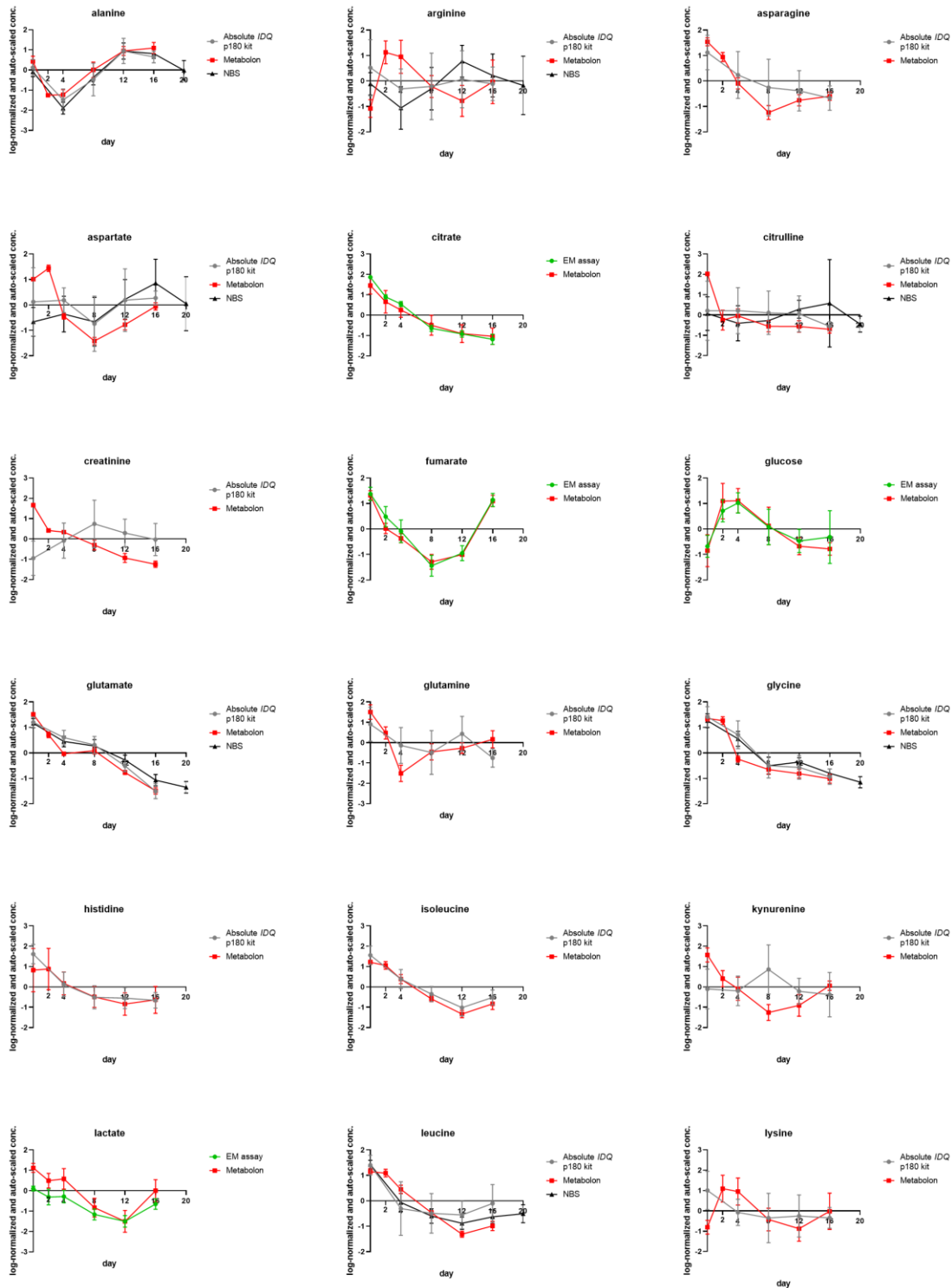


Figure 34: Comparison of the different metabolomics and lipidomics measurements revealed strong consistency. Measured metabolites in two or more assays were selected. For some of the assays, cells were collected on different time points as described in the previous sections (see sections 3.2.2 – 3.2.6). For the analysis, concentration and signal intensity values were auto-scaled to allow comparability.

Results

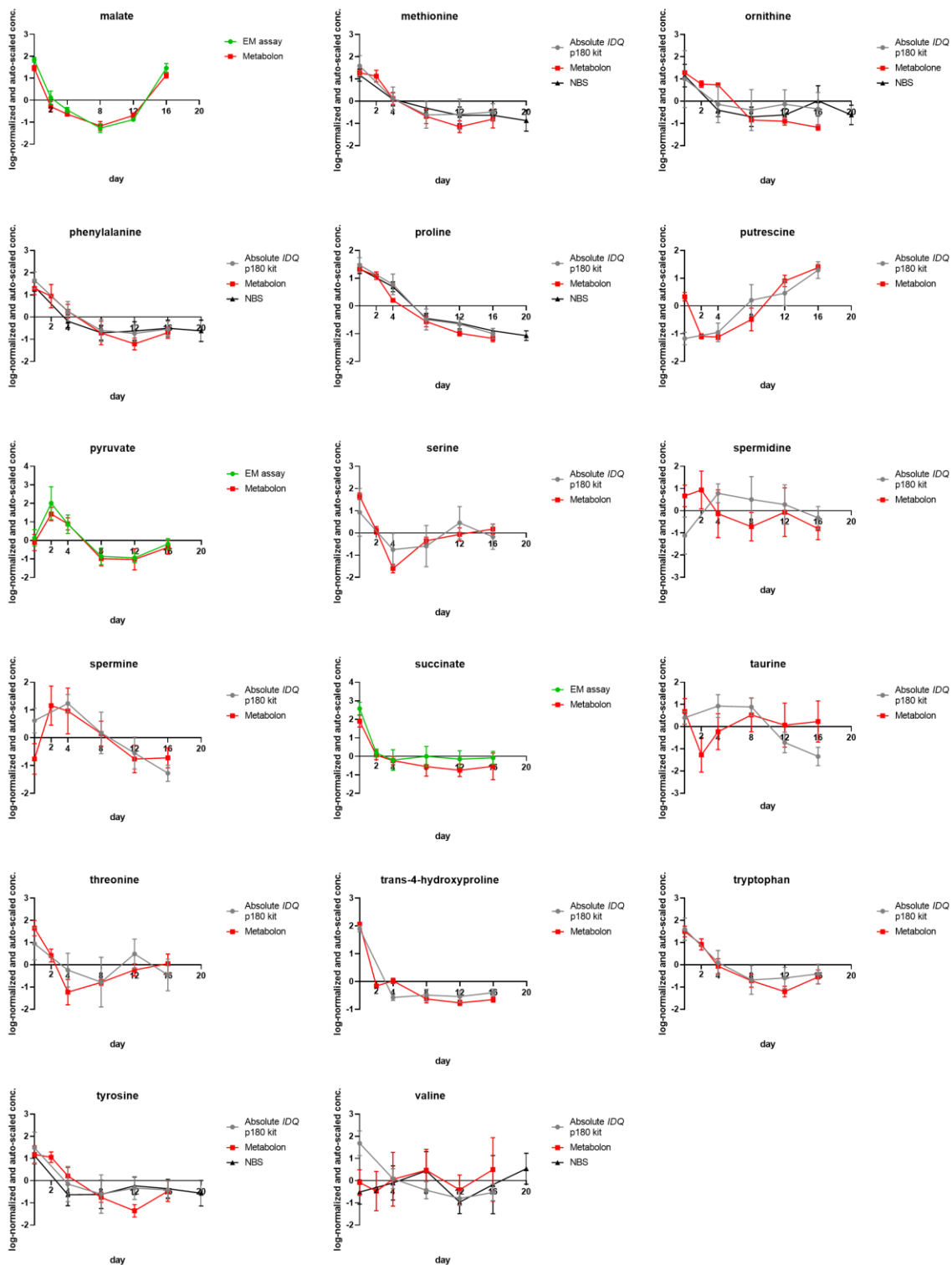


Figure 35: Comparison of the different metabolomics and lipidomics measurements revealed strong consistency. Measured metabolites in two or more assay were selected. For some of the assays, cells were collected on different time points as described in the previous sections (see sections 3.2.2 – 3.2.6). For the analysis, concentration and signal intensity values were auto-scaled to allow comparability.

3.2.8. Transcriptomics

Total RNA sequencing was performed to elucidate transcriptional processes during adipogenesis. The combination of sequencing results with results from metabolomics and lipidomics approaches are shown in the discussion section (see section 4.2). For transcriptomics, samples were collected as independent biological quadruplicates on day 0, 2, 4, 8, and 12. RNA isolation and quality assessment were performed by me. The sequencing unit (Head: Dr. Tim Strom) of the HMGU performed the library preparation and sequencing as described in the method section (see section 2.10). Differential expression analysis was kindly performed by Dr. Thomas Schwarzmayr from the sequencing unit using the R Bioconductor package DESeq2. All other downstream analyses were performed by me. To evaluate changes in transcription levels of up to 20973 detected transcripts, ratios were calculated in relation to the transcription level at day 0. Therefore, the single values of each transcript were summarized to four different comparisons, namely day 2 vs. day 0, abbreviated as "day 2", day 4 vs. day 0 (abbreviated. "day 4"), day 8 vs. day 0 (abbreviated. "day 8"), and day 12 vs. day 0 (abbreviated "day 12"). Other statistical and graphical analyses were performed by me.

Figure 36 illustrates the PCA of the four summarized ratios. In the following, "transcript" will be used synonymously for of "ratio". In general, a very good separation of the different time points was achieved. The first principal component separated the time points with 69.5% of explained variance, while PC2 explained 16.4% of the variance.

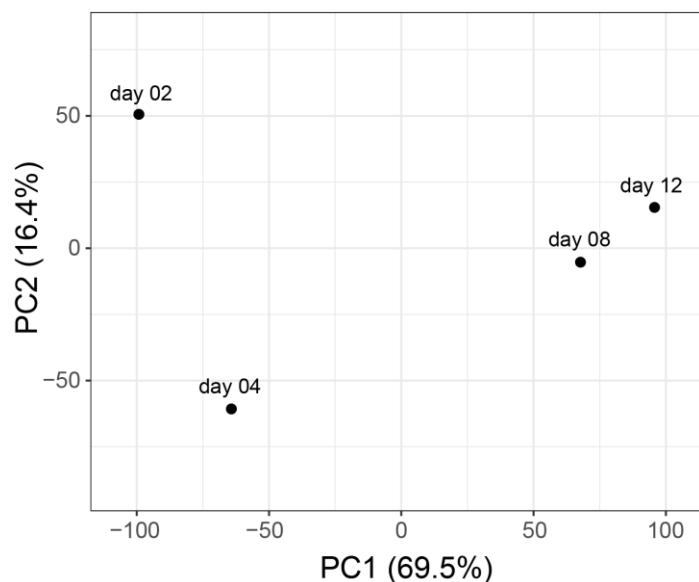


Figure 36: PCA scores plot showing clear separation of the different time points normalized to day 0. Principal component 1 separated the different phases with 69.5% variance, principal component 2 with 16.4%. Normalized transcripts were pareto-scaled.

Figure 37 shows the heatmap of the transcriptomics results and includes all detected transcripts. Overall, strongly changing transcript levels were detected throughout adipogenesis. All detected

Results

transcript levels were assigned into three clusters. Cluster 1 contained transcripts with increasing levels during adipogenesis whereas cluster 3 showed an opposed profile over time. Transcripts from cluster 2 were upregulated around day 4 and 8 and downregulated afterwards.

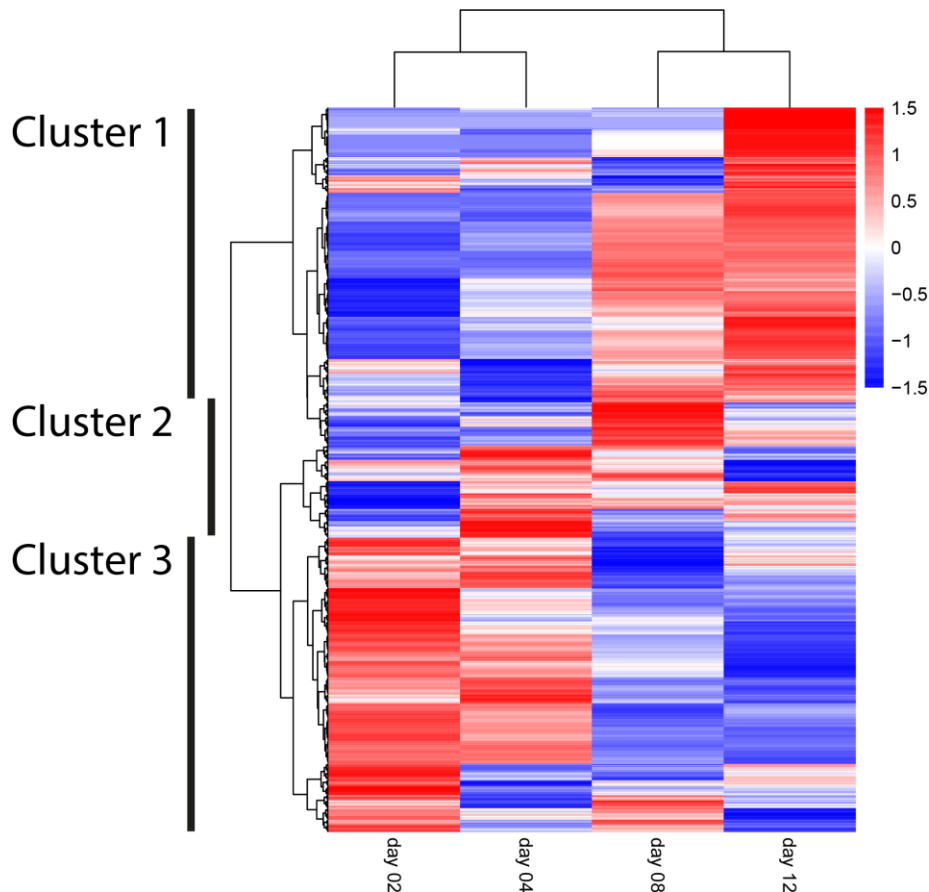


Figure 37: Heatmap of the whole data set of transcriptomics analysis revealed markedly changed transcript levels during adipogenesis.

The transcripts were assigned into three clusters based on their expression level time course. The first cluster contained transcripts with increasing levels throughout the analyzed time. The second cluster consisted of transcripts whose levels increased until day 4 – 8 followed by decreasing levels. The third cluster summarized transcripts with markedly decreasing concentration levels over time. Transcript levels were scaled with Euclidean distance measurements and the clustering method Ward2 algorithm was used. Each summarized group consisted of four individual samples that were normalized to day 0.

By mapping the transcriptomics data to KEGG pathways, 40 significantly changed pathways were identified (Table 14). As a whole, most of them were upregulated during adipogenesis, some had partly up- as well as partly downregulated transcripts, and the remaining pathways were downregulated. Many upregulated pathways can be assigned to the energy metabolism e.g. TCA cycle, fatty acid degradation, oxidative phosphorylation, BCAA degradation, fatty acid degradation, or butanoate metabolism. Additionally, pathways belonging to the metabolism of hormones, namely, steroid biosynthesis, steroid hormone biosynthesis pathways, terpenoid backbone biosynthesis, and insulin signaling were upregulated. Further upregulated pathways belonged to the metabolism of vitamins, such as vitamin digestion and absorption. The

Results

transcriptomics data also revealed strongly changed transcript levels in pathways involved in the metabolism of several amino acids (Ala; BCAA (Val, Leu, and Ile); Arg and Pro; Gly, Ser, and Thr; Tyr; Trp). These pathways were mostly characterized by mixed (up- and down) regulations. Lastly, strongly downregulated pathways belonged to the DNA or RNA machinery like RNA transport, DNA replication, homologous recombination, spliceosome or cell cycle.

Table 14: Significantly changed KEGG pathways.

Upregulated pathways are illustrated in red, downregulated in blue. KEGG pathways with both regulations are shown in grey. Time points of this pathway, which were not significantly regulated in comparison to day 0, are illustrated as white boxes.

KEGG pathways	day 2	day 4	day 8	day 12
hsa00010 Glycolysis/Gluconeogenesis				up / down
hsa00020 Citrate cycle (TCA cycle)			up	up
hsa00071 Fatty acid degradation		up	up	up
hsa00100 Steroid biosynthesis				up
hsa00140 Steroid hormone biosynthesis	up	up	up	up
hsa00190 Oxidative phosphorylation			up	
hsa00260 Gly, Ser, and Thr metabolism				up / down
hsa00280 Val, Leu, and Ile degradation			up	up
hsa00330 Arg and Pro metabolism			up / down	
hsa00350 Tyrosine metabolism		up / down		up
hsa00380 Tryptophan metabolism			up / down	up / down
hsa00410 β -Alanine metabolism			up / down	up / down
hsa00590 Arachidonic acid metabolism	up	up	up / down	up / down
hsa00591 Linoleic acid metabolism			up	up
hsa00620 Pyruvate metabolism			up	up
hsa00630 Glyoxylate and dicarboxylate metabolism			up	
hsa00640 Propanoate metabolism			up	up
hsa00650 Butanoate metabolism			up	up
hsa00830 Retinol metabolism	up	up	up	up
hsa00900 Terpenoid backbone biosynthesis			up	up
hsa00980 Metabolism of xenobiotics by cytochrome P450	up	up	up	up
hsa00982 Drug metabolism - cytochrome P450	up / down	up	up	up
hsa01040 Biosynthesis of unsaturated FA			up	up
hsa02010 ABC transporters	up	up	up / down	up / down
hsa03010 Ribosome	up	up		
hsa03013 RNA transport	down		down	down
hsa03030 DNA replication	down	down	down	down
hsa03040 Spliceosome	down		down	down

Results

hsa03050 Proteasome	down			
hsa03320 PPAR signaling pathway	up	up	up	up
hsa03440 Homologous recombination	down			
hsa04110 Cell cycle	down	down	down	down
hsa04114 Oocyte meiosis	down	down		
hsa04120 Ubiquitin mediated proteolysis	down			
hsa04146 Peroxisome		up	up	up
hsa04910 Insulin signaling pathway		up / down	up / down	up / down
hsa04920 Adipocytokine signaling pathway	up / down	up / down	up / down	up / down
hsa04975 Fat digestion and absorption		up	up	up
hsa04976 Bile secretion				up
hsa04977 Vitamin digestion and absorption			up	up

Since the adipogenic process requires large amounts of energy for the synthesis of lipids, four important pathways for cellular energy generation were analyzed in greater detail: glycolysis (Figure 38), TCA cycle (Figure 39) with oxidative phosphorylation (Figure 40), and fatty acid degradation (β -oxidation, Figure 41). The glycolysis and gluconeogenesis pathway showed a biphasic transcriptional regulation. The transcript levels of enzymes converting glucose into dihydroxyacetone phosphate (DHAP) and glyceraldehyde 3-phosphate (G3P) were mostly upregulated during adipogenesis whereas the subsequent steps generating pyruvate were mostly downregulated. As glycolysis can be also reversed, the figure also represents the gluconeogenesis and glyceroneogenesis. Members of the same enzyme family putatively catalyzing the same reactions showed opposed regulation patterns. For example, the transcript levels of *HK1* were strongly downregulated whereas the transcript levels of *HK2* and *GCK* were markedly upregulated. Similar findings were observed for the family of phosphofructokinases because *PFKL* (L = liver) was upregulated whereas *PFKP* (P = platelet) isoforms were downregulated during the whole observed time period. The transcript levels of *PFKM* (M = muscle) were only upregulated until day 4, but afterwards significantly downregulated. In addition, the transcript levels of phosphoenolpyruvate carboxykinase 1 (*PCK1*) were strongly upregulated while *PCK2* showed strongly decreased levels.

Results

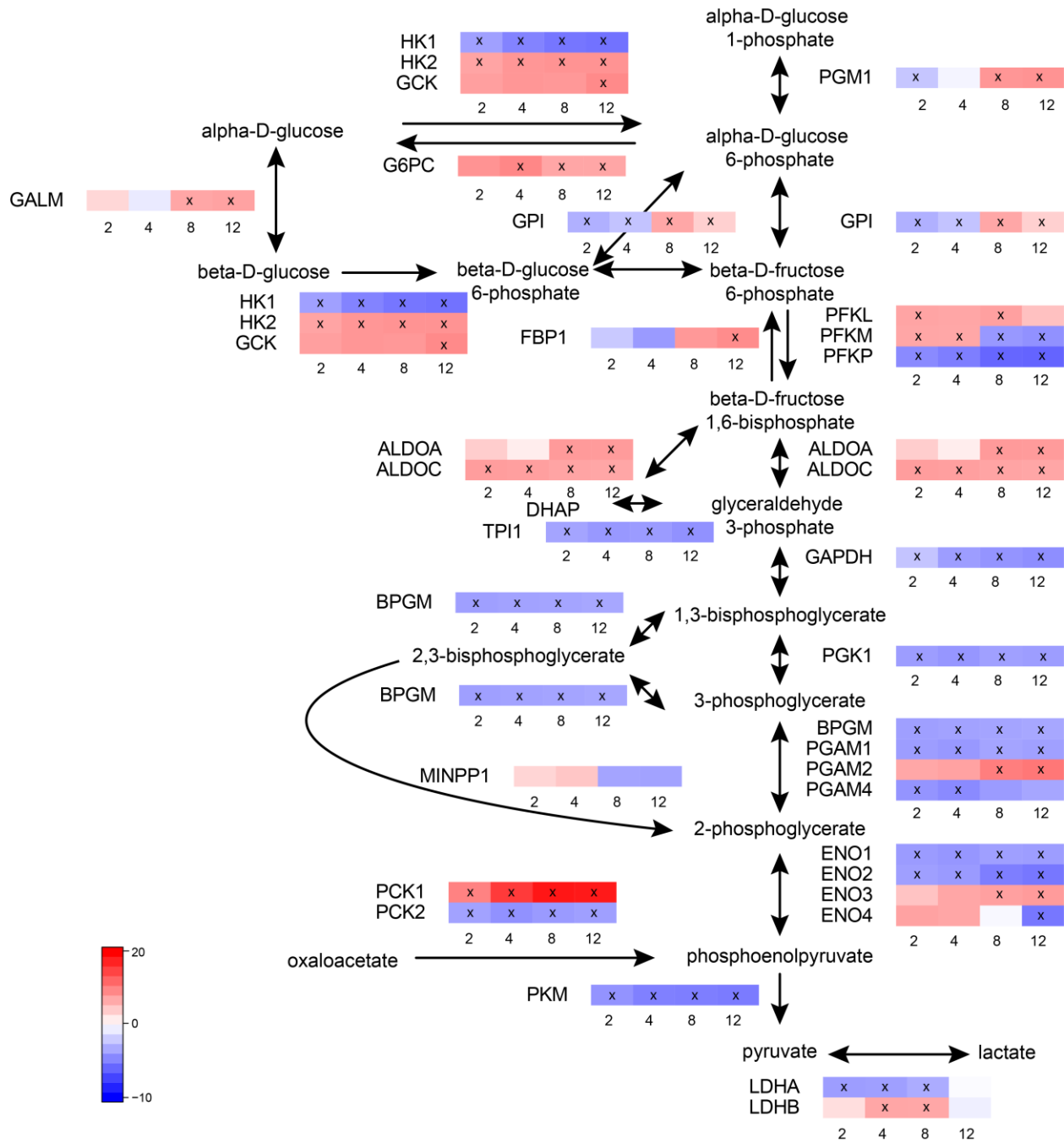


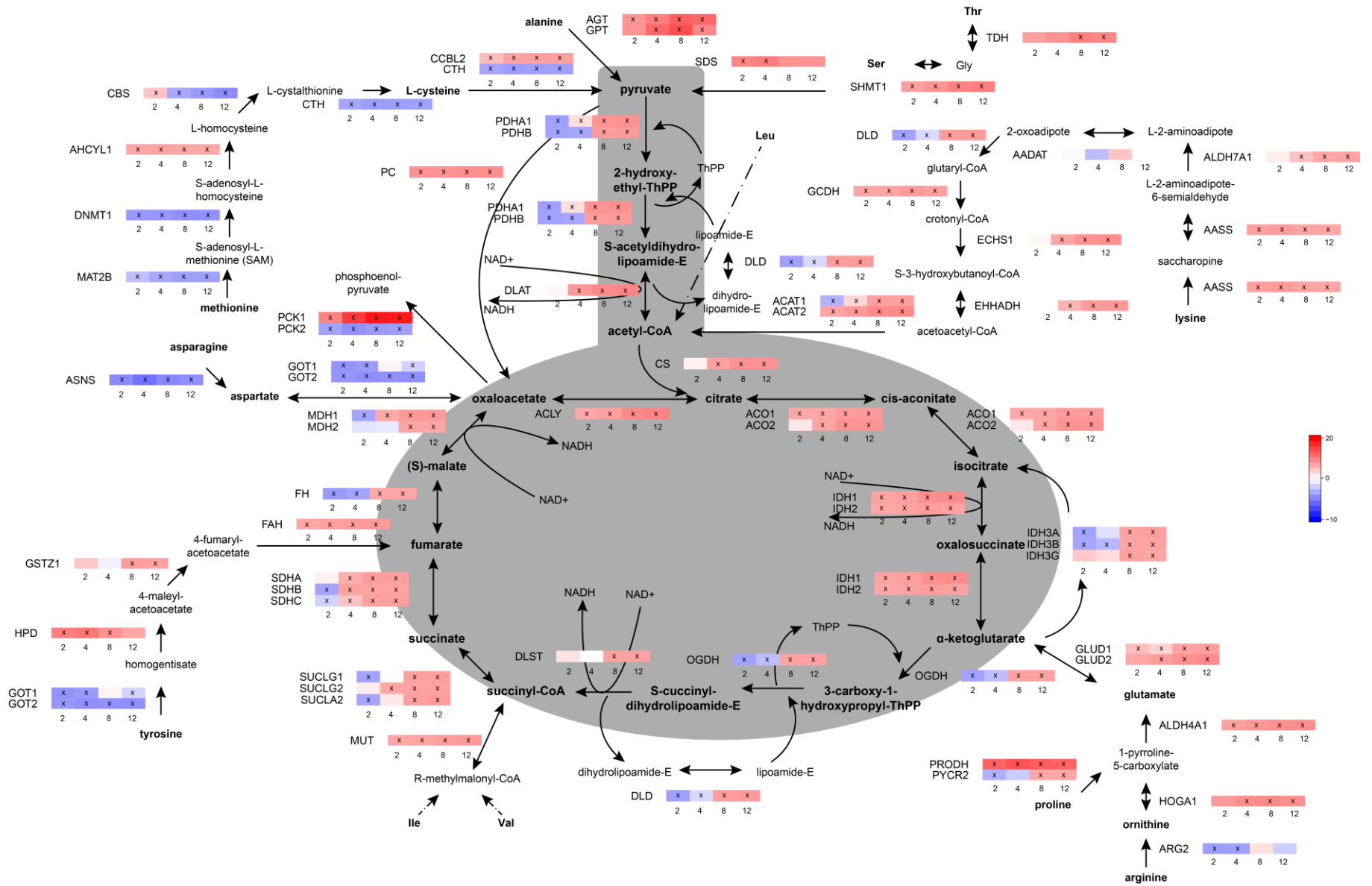
Figure 38: Transcripts of enzymes involved in glycolysis /gluconeogenesis / glyceroneogenesis were significantly regulated during adipogenesis.

The transcript levels of enzymes catalyzing glucose into dihydroxyacetone phosphate (DHAP) and glyceraldehyde 3-phosphate (G3P) were mostly upregulated during adipogenesis, whereas the following steps generating pyruvate were mostly downregulated. Transcript levels are indicated by small boxes. Every single box represents the averaged transcript level at the indicated day of adipogenesis. Red indicates upregulation, and blue indicates downregulation. Significantly changed transcript levels (p -adjusted < 0.05) are indicated by an "x" inside the box and log₂-fold changes and p -values are listed in appendix 5.3.

Results

Figure 39 shows the TCA cycle with selected amino acid degradation pathways whose metabolites are incorporated into the TCA cycle. The TCA cycle was highly and significantly upregulated during adipogenesis. The regulation of the transcription levels of enzymes catalyzing the same reactions were consistent. For example, *ACO1* and *ACO2* or *SDHA*, *SDHB*, and *SDHC* had similar transcription level time courses. Interestingly, the transcription levels of the enzymes catalyzing the degradation of amino acids showed differential regulation patterns. The degradation pathways of Ala, Thr, Gly, Ser, Lys, Orn, Pro, and Glu were completely upregulated. In contrast, the degradation pathways of Met, Cys, Asn, Asp, Arg, and Tyr had at least in part some downregulated transcript levels.

Results



Results

Figure 39: Transcripts of enzymes involved in the TCA cycle were highly upregulated during adipogenesis. The TCA cycle is shaded in gray. The degradation pathways of amino acids which lead to the TCA cycle showed mixed regulations. The transcript levels of these catabolic enzymes were upregulated for the majority of the amino acids. However, the enzymes for the degradation of Tyr, Asn, Asp, Met, Cys, and Arg were downregulated. Transcript levels are indicated by small boxes. Every single box represents the averaged transcript level at the indicated day of adipogenesis. Red indicates upregulation, and blue indicates downregulation. Significantly changed transcript levels (p -adjusted < 0.05) are indicated by an "x" inside the box and the log₂-fold changes and the p -values are listed in appendix 5.3.

The oxidative phosphorylation is coupled to the TCA cycle, because the energy precursors (NADH) are produced during the TCA cycle. In addition, complex II oxidizes the TCA metabolites succinate into fumarate. The electrons from NADH are transferred to ADP during oxidative phosphorylation thus forming ATP. The transcripts of proteins involved in the oxidative phosphorylation were also highly upregulated during adipogenesis (Figure 40). All five complexes showed significantly changed transcript levels until day 12. For illustration purposes, the transcripts forming each complex were summarized.

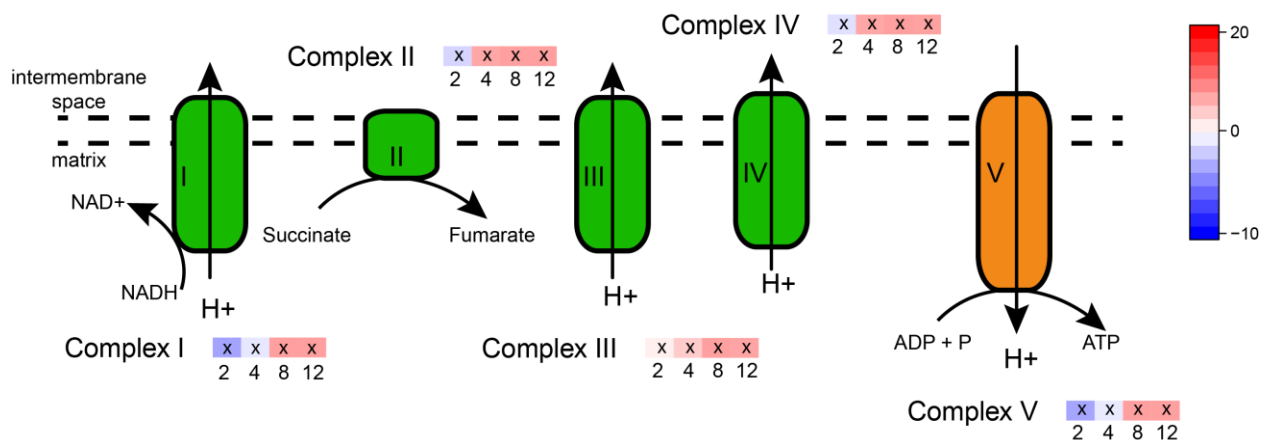
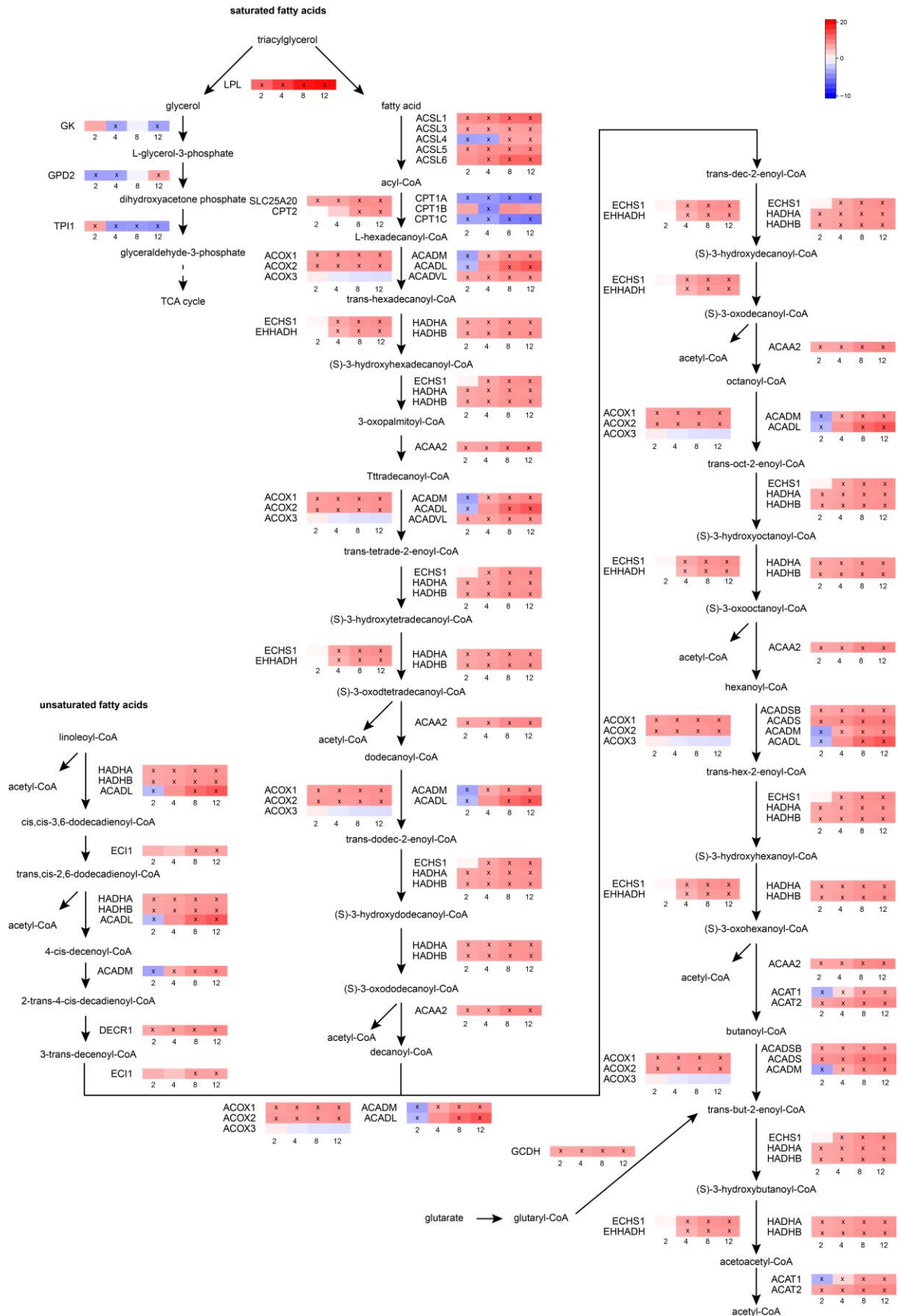


Figure 40: Transcripts of enzyme involved in the oxidative phosphorylation were significantly upregulated during adipogenesis.

For illustration purposes, the various transcripts of the subunits of each complex were summarized. Transcript levels are indicated by small boxes. Every single box represents the averaged transcript level at the indicated day of adipogenesis. Red indicates upregulation, and blue indicates downregulation. Significantly changed transcript levels (p -adjusted < 0.05) are indicated by an "x" inside the box and the log₂-fold changes and the p -values are listed in appendix 5.3.

Degradation of saturated and unsaturated fatty acids was highly upregulated during adipogenesis (Figure 41). This pathway is one of the most important ones for generating acetyl-CoA that will be used for NADH formation during TCA cycle and for the resynthesis of fatty acids. In general, the regulation of the transcription levels of enzymes catalyzing same degradation reactions were highly consistent. Interestingly, the transcript level of LPL was upregulated, which catalyze the degradation of TAG into fatty acids and glycerol. However, the downstream degradation of glycerol into G3P was not upregulated, because the responsible transcripts were on average downregulated.

Results



Results

Figure 41: Transcripts of enzymes involved into the degradation of saturated and unsaturated fatty acids were highly upregulated during adipogenesis.

All transcript regulations showed high similarity. The three transcript levels of the enzymes catalyzing the degradation of glycerol into glyceraldehyde-3-phosphate were mostly downregulated. Transcript levels are indicated by small boxes. Every single box represents the averaged transcript level at the indicated day of adipogenesis. Red indicates upregulation, and blue indicates downregulation. Significantly changed transcript levels (p -adjusted < 0.05) are indicated by an "x" inside the box and the log₂-fold changes and the p -values are listed in appendix 5.3.

The released acetyl-CoA molecules from the degradation of fatty acids can be directly used for the re-synthesis of new fatty acids for storing energy in TAG. In human cells, the fatty acid elongation is separated into three different locations: the majority of fatty acid elongation up to 16 C-atoms takes place in the cytoplasm. To a minor degree, the β -oxidation is reversed for the synthesis of fatty acids in the mitochondria. Fatty acids with more than 16 C-atoms are exclusively elongated in the endoplasmic reticulum. In general, the transcript levels of the three initial elongation steps in the cytoplasm and the mitochondria were highly upregulated (Figure 42). The levels of *MECR*, which forms in the last step an acyl-CoA (n+2), were significantly downregulated in the beginning of adipogenesis. However, its transcript was significantly upregulated at day 8 and 12. *PPT1*, which catalyzes the release of CoA and is thereby forming the free fatty acid, had during the whole observed time period markedly decreased transcript levels. The transcript levels of the enzymes catalyzing the elongation of fatty acids with chain lengths longer than C16 were mostly markedly and significantly upregulated. Interestingly, the levels of elongation of very long-chain fatty acids protein 2 (*ELOVL2*) and *ELOVL4* were strongly downregulated. Both enzymes are responsible for the elongation of mostly polyunsaturated fatty acids with a chain length longer than C20. In addition, *ELOVL4* also catalyzes the elongation of saturated very long-chain fatty acids with chain lengths longer than C26. Interestingly, *ELOVL1* and *ELOVL6* also had decreased transcript levels during the initial phase of differentiation (*ELOVL1* at day 2 and 4, and *ELOVL6* at day 2). In contrast, the transcript levels of *ELOVL3* and *ELOVL5* were strongly increased during the complete observed time period. *ELOVL3* catalyzes the elongation of fatty acids C18:0 and C18:1 to C24:0 and C24:1, while *ELOVL5* is responsible for the elongation of fatty acids C18:2, C18:3, C18:4 to C20:5 to C20:2, C20:3, C24:4, and C24:5. In addition, the transcript level of *ACOT2*, which catalyzes the release of CoA and thereby forming the free fatty acid, was significantly upregulated during the 12 observed days of adipogenesis.

Results

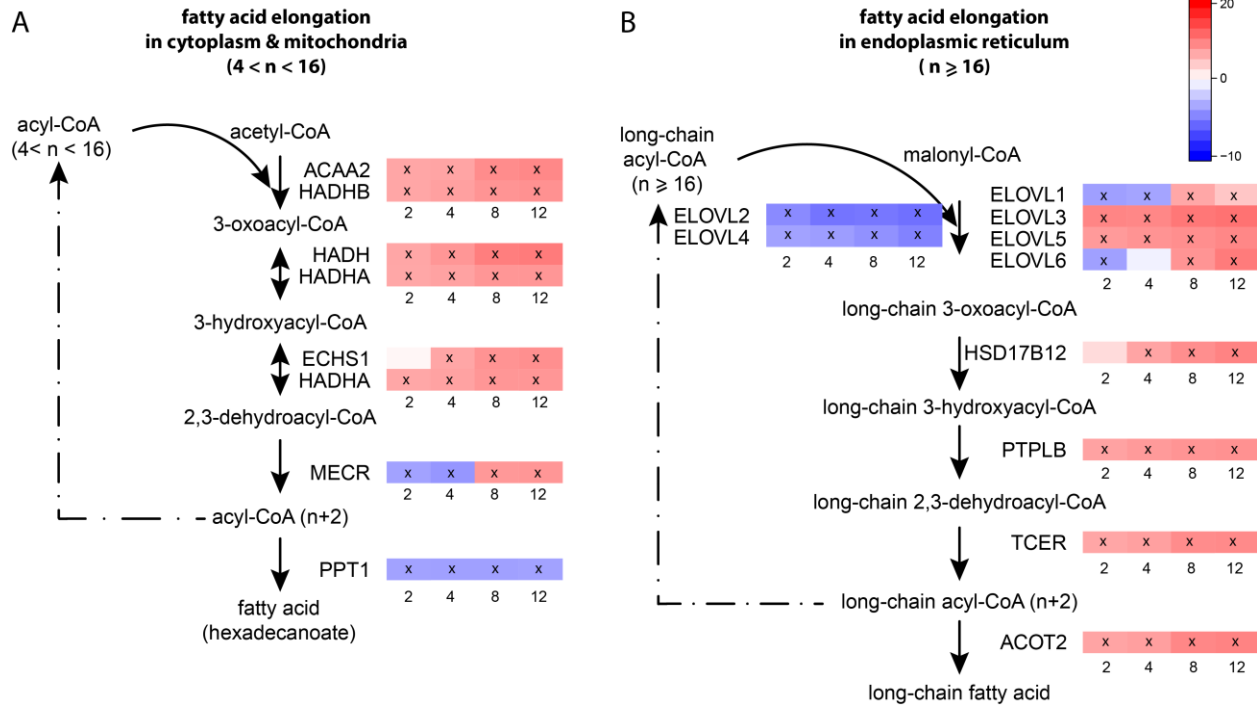


Figure 42: Transcript levels of enzymes involved in the elongation of fatty acids were highly and significantly regulated during adipogenesis.

Transcript levels of enzymes catalyzing the elongation of fatty acids were in the majority upregulated. Fatty acid elongation in cytoplasm and mitochondria, panel A: Only the two second last steps showed partly downregulated transcript levels. Fatty acid elongation in endoplasmic reticulum, panel B: ELOVL2 and ELOVL4 were period strongly downregulated during the whole observed time. ELOVL1 and ELOVL6 had downregulated transcript levels during the initial adipogenesis. Transcript levels are indicated by small boxes. Every single box represents the averaged transcript level at the indicated day of adipogenesis. Red indicates upregulation, and blue indicates downregulation. Significantly changed transcript levels (p -adjusted < 0.05) are indicated by an "x" inside the box and the \log_2 -fold changes and the p -values are listed in appendix 5.3.

The transcriptomic data included also transcripts of enzymes which are necessary for the head group remodeling of several glycerolipids: phosphatidic acid (PA), DAG, PC, PE, PS, cytidine diphosphate diacylglycerol (CDP-DAG), phosphatidylinositol (PI), phosphatidylglycerol phosphate (PGP), phosphatidylglycerol (PG), and cardiolipin. Their possible interconversion by head group substitutions together with the responsible transcript levels can be seen in Figure 43. In general, the head group remodeling between nearly all lipid classes was significantly upregulated during adipogenesis. Only the conversion of PC into PS (*PTDSS1*) was downregulated. In addition, the transcript levels of the members of the diacylglycerol kinase (DGK) family showed both upregulation and downregulation.

Results

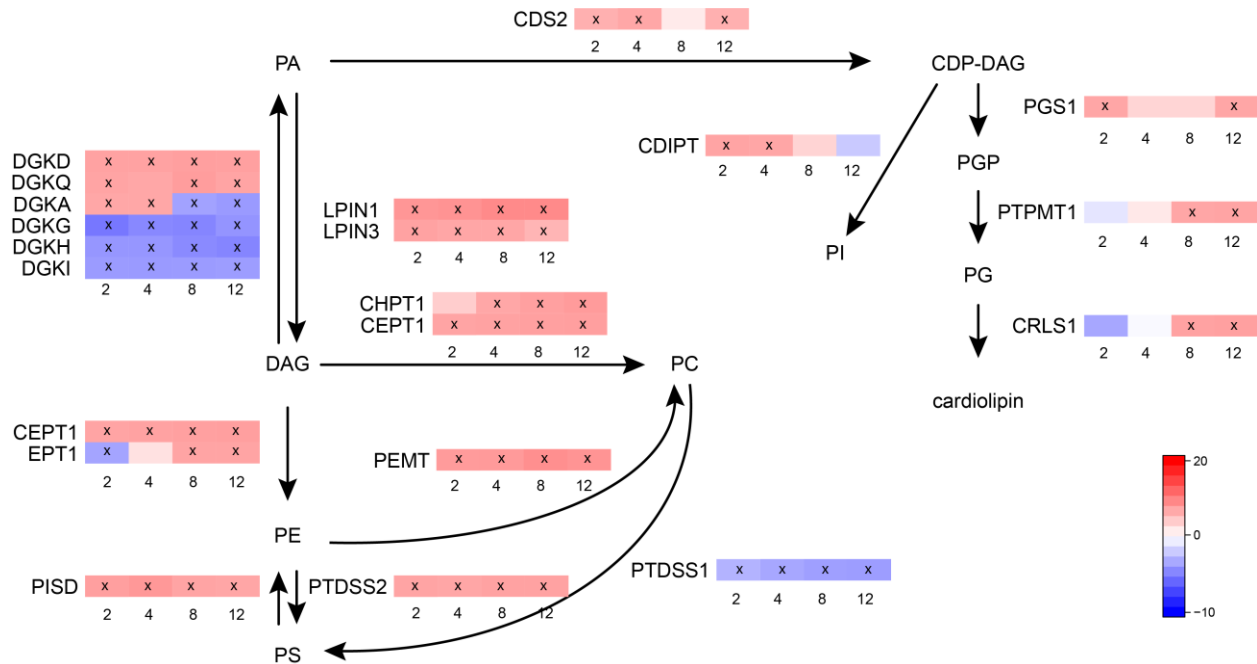


Figure 43: Transcript levels of enzymes involved in the head group remodeling of glycerophospholipids were highly regulated during adipogenesis.

Transcript levels are indicated by small boxes. Every single box represents the averaged transcript level at the indicated day of adipogenesis. Red indicates upregulation, and blue indicates downregulation. Significantly changed transcript levels (p -adjusted < 0.05) are indicated by an "x" inside the box and the \log_2 -fold changes and the p -values are listed in appendix 5.3.

In addition to the transcript levels of enzymes responsible for the remodeling of glycerophospholipids, also the transcript levels of enzymes catalyzing the remodeling of sphingolipids during adipogenesis were strongly regulated. Figure 44 illustrates the synthesis of ceramides from serine and their interconversion into other ceramides, glycosphingolipids as well as sphingomyelins. In general, the pathways were significantly regulated on the transcriptome level. However, the results were quite inconsistent for different members of an enzyme family putatively catalyzing the same reaction. For example, up to the half of the transcripts (*SPTLC3* and *SPTSSA*), whose enzyme products are responsible for the synthesis of 3-ketosphinganine from Ser, were upregulated. In contrast, the transcript levels of the involved enzymes of the forward and backward reactions of DCER and sphinganine were mostly and significantly upregulated. The level of *DEGS1*, which catalyzes the conversion of DCER into CER, was significantly downregulated during the whole observed time period. CER can be used for the synthesis of SM, for the formation of galactosylceramides (GalCER) and glucosylceramides (GlcCER), and ceramide 1-phosphate. GlcCer is then used for LCER and other glycosphingolipids like gangliosides. GalCER can be used as building block for other glycosphingolipids like sulfatides. The conversion of CER into galactosylceramides (GalCER) was upregulated (*GALC*), which can be used for other glycosphingolipids like sulfatides. However, the transcript levels for the degradation of GalCER into Cer was inconsistently regulated because levels of *GBA* were strongly downregulated whereas *GBA2* was upregulated. The transcript levels of the enzymes catalyzing the forward (*UGCG*) and

Results

backward (*GBA*) reactions of CER and GlcCER were significantly downregulated, and the forward (*B4GALT6*) and backward (*GLB1*) reactions of GlcCER into LCER was upregulated.

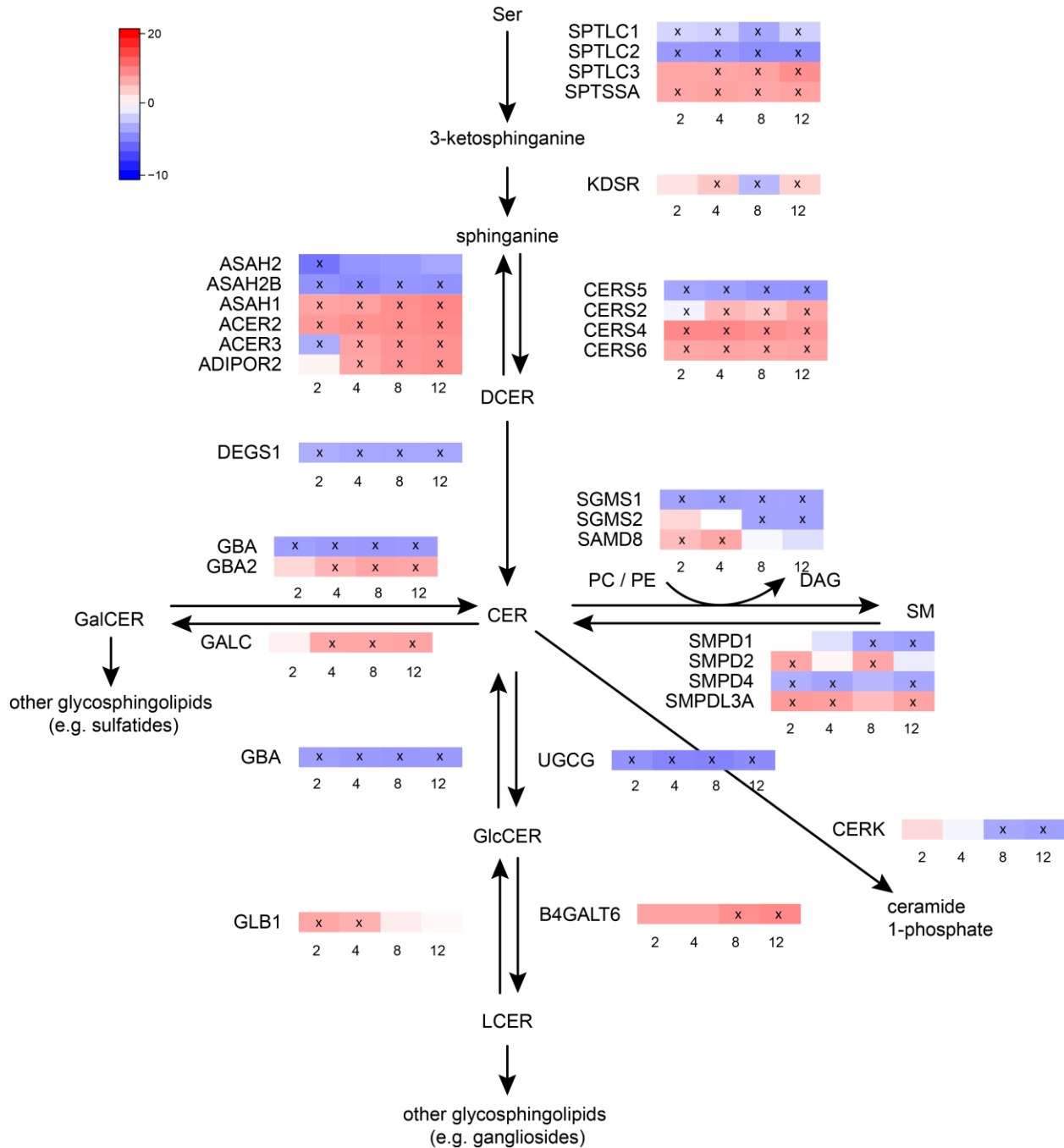


Figure 44: Transcripts of enzymes involved in the synthesis and degradation of sphingolipids were highly regulated during adipogenesis.

However, some members of enzyme families catalyzing the same reactions were regulated in opposed directions. Transcript levels are indicated by small boxes. Every single box represents the averaged transcript level at the indicated day of adipogenesis. Red indicates upregulation, and blue indicates downregulation. Significantly changed transcript levels (p -adjusted < 0.05) are indicated by an "x" inside the box and the log₂-fold changes and the p -values are listed in appendix 5.3.

In summary, the total RNA-sequencing could enormously shed light on the transcriptional processes during cell differentiation of human preadipocytes into adipocytes. The data analysis revealed markedly upregulated KEGG pathways of energy metabolism like TCA cycle with oxidative phosphorylation, fatty acid degradation, or the first steps of the glycolysis. In addition, some amino acid degradation pathways which fuel the TCA cycle were markedly upregulated. In contrast, several pathways required for the synthesis and processing of RNA and DNA were downregulated. The transcriptomics analysis could also reveal strongly change transcript levels of enzymes involved in lipid remodeling within the classes of glycerophospholipids as well as sphingolipids.

4. Discussion

The main aim of this PhD thesis was to characterize human adipogenesis with a combined multi-omics approach consisting of lipidomics, metabolomics, and transcriptomics. Such a global, multi-omics approach enables an accurate analysis of the cell differentiation process on different cellular levels. Especially the combination of lipidomics and transcriptomics is a novelty in the -omics field. The lipidomics approach was recently published (22). Nevertheless, -omics experiments can only build hypotheses, which have to be verified with more specific downstream experiments using, e.g., biochemical and molecular biology approaches.

Another important aim of this PhD thesis was the development and validation of a targeted method for the quantification of metabolites of energy metabolism that subsequently could be used for the characterization of adipogenesis.

4.1. Validation of the GC-MS based quantification assay for metabolites of energy metabolism

An important requirement for the analysis of adipogenesis was the development of a method for the quantification of analytes of energy metabolism, as there was no established quantitative method available in the lab.

The GC-MS was chosen due to availability of the instrument. However, a better analysis system for these polar, non-volatile metabolites would be a hydrophilic interaction chromatography coupled with mass spectrometry (HILIC-MS/MS) (175, 176), because a GC-MS system is best suited for unpolar analytes. Nonetheless, polar metabolites can be measured with a GC-MS system when derivatization of analytes is performed. Therefore, the samples were derivatized with two reagents to increase the analyte's volatility. In addition, the used derivatization steps silylation of hydroxy-groups and oxymation of carbonyl-groups increases the sensitivity of the mass spectrometry-

Discussion

based detection of the used single quadrupole. With such derivatization reactions, successful methods for chemically similar analytes were developed in the last years (177-180).

The sample preparation procedure was kept as simple as possible to allow high throughput. Besides the two derivatization reactions that took 60 min each, only an evaporation step of the cell homogenate, was necessary prior to the derivatizations. In total, the measurements could be initiated within 3 h after start of the sample preparation procedure. The measurement itself could be performed within 32 min including post-injection. Compared to other GC-MS methods with analysis times of up to one hour, this is a short analysis time (177, 179). Nevertheless, run times of a GC-MS system are in most cases longer than using LC-MS systems, because of long column lengths and the slow column flow.

The validation showed that the developed GC-MS based method allowed the quantification of up to 13 analytes of energy metabolism. However, when homogenates of SGBS cells were used, only 11 metabolites could be quantified, because two metabolites were below LOD in SGBS cells.

A major requirement of the GC-MS assay was the compatibility with other analytical methods to avoid additional cell cultivations and to increase the flexibility of cell culture experiments. For that, cells were harvested with 80% methanol so that the resulting cell homogenates could also be used for the DNA-based cell number normalization and the other metabolomics, as well as lipidomics measurements. Another important prerequisite was an acceptable sample volume, as low volumes enable the conduction of multiple analyses from the same cell samples. However, most of the analytes which were included in the energy metabolism assay had very low concentrations in SGBS cells, except for glucose and lactate. Therefore, a sample volume of 400 μ L was necessary to obtain sufficient signals for 9 of 11 analytes. To reach this volume, at least two wells of a six-well plate had to be pooled for measurements.

The developed and validated method mostly met the FDA and EMA criteria for bioanalytical methods as listed in the results section. In terms of LOD, LLOQ, inter-run and intra-day precision, 12 of 13 calibrators revealed ideal values. However, accuracy values were outside the acceptable range for 8 analytes at calibration level 1 and for succinate also at level 2. Nevertheless, six out of seven calibrator levels had good values for most analytes. In addition, the EMA and FDA guidelines recommend at least six calibrators per analyte. Thus, the minimal prerequisites were successfully fulfilled.

The long-term stability tests also showed good results for most of the analytes. However, lactate, 2-hydroxyglutarate, ribose, isocitrate, and glucose showed higher deviation values compared to freshly prepared calibrators. This might be explained by the expiry date, as most analytes were over the recommended storage duration. The analytes with higher deviations in the stability test might be more sensitive for long-term storage than the others. Nevertheless, the stability tests showed overall good results for the aspired experiments. However, it is highly recommended to use new ISTDs and analytes for future measurements.

As already mentioned in section 3.1, the cell differentiation process into lipid-laden adipocytes is accompanied with a markedly changing cellular composition. It was shown that this had an influence on the ISTDs and putatively also on the analytes. Ion suppression could be monitored at day 2 and 4 for $^{13}\text{C}_4$ -fumarate. The opposite effect could also be seen: the peak areas of $^{13}\text{C}_4$ -ribose, $^{13}\text{C}_3$ -lactate, and especially $^{13}\text{C}_6$ -glucose showed matrix effects, which resulted in increasing peak values. However, the influence of the matrix on the results can be diminished, because ISTD were included in this developed and validated method, correcting for these effects. It is assumed that matrix effects affect ISTD and analyte similarly (181, 182).

To sum up, this study showed that the developed and validated GC-MS based method allows the reliable quantification of up to 11 analytes of energy metabolism in cell homogenates of SGBS samples. Moreover, the quantification method can be easily combined with other metabolomics and lipidomics methods as well as the DNA based normalization assay.

4.2. Analyzing human adipogenesis with different -omics techniques

In the present study, human adipogenesis was characterized with a multi-omics approach consisting of lipidomics, metabolomics, and transcriptomics. This is a novelty in the field of adipogenesis research. However, the combination of different methods poses a major challenge in data analysis and illustration of the results. In detail, the Lipidizer™ method, Biocrates Absolute/DQ p180 kit, NBS, and EM assay quantify lipid and metabolite concentrations, whereas the non-targeted metabolomics method from Metabolon only determines signal intensity values. In addition, the data output unit of the transcriptomics approach was “log₂ fold-change” values. Therefore, the datasets cannot be directly combined for analysis and illustration. Because of that, all values, – concentrations, signal intensities, and transcript levels – were auto-scaled as it is routinely performed during heatmap calculation.

Prior to the characterization of human adipogenesis, the differentiation process of the SGBS cell model was confirmed using two different approaches. First, the expected morphological changes during cell differentiation of fibroblast-like preadipocytes into lipid-laden adipocytes could be observed by microscopy. Second, a strong transcriptional activation of *PPARG* and *CEBPA* already starting at day 2 was observed by RT-qPCR analysis. Therefore, the human SGBS cell model can be used as a valid model for the characterization of human adipogenesis.

In general, the tight clustering of the data in the PCA and PLS-DA plots showed high quality of the data obtained with each approach respectively. Moreover, the shift from differentiating (day 0–4) to maturing (day 4–12) human SGBS cells became clearly visible by the change of the (principal) component 1 to (principal) component 2 as the main contributor for clustering in the score plots. This shift can be explained by the change from differentiation to maturation medium at day 4 of differentiation. The shift is in line with findings from a former colleague who

Discussion

characterized murine cell differentiation of 3T3-L1 cells using a combined metabolomics (Biocrates Absolute/DQ p180 kit) and transcriptomics (Chip sequencing) approach (146).

The transcriptomics measurements (see section 3.2.8) identified strongly regulated transcripts during cell differentiation which were mapped to existing KEGG pathways. Most of them belong to the metabolism of hormones like steroid biosynthesis and insulin signaling, or to the metabolism of vitamins like vitamin digestion and absorption. The upregulation of these pathways during human adipogenesis might be explained with the cultivation medium and the cell differentiation cocktail. Pantothenate and biotin were supplemented to the DMEM/F12 medium, which was used for the cultivation before differentiation start (additionally with 10% FBS) as well as basal medium for the two distinct differentiation media. This might have caused the regulation of the metabolism of vitamins. Furthermore, insulin, dexamethasone, and cortisone were part of the differentiation medium. This might be also caused the regulation of pathways belonging to the metabolism of hormones. The most strongly downregulated pathways could be assigned to the DNA / RNA machinery like RNA transport, DNA replication, and cell cycle. This is in harmony with published results, as cell cycle arrest and the inhibition of cell proliferation are essential for the induction of the early cell differentiation stages of preadipocytes (183, 184).

The transcripts involved in the regulation of the metabolism of several amino acids as well as lipids will be discussed in detail in the following sections separately.

4.2.1. Strongly upregulated BCAA degradation during human adipogenesis

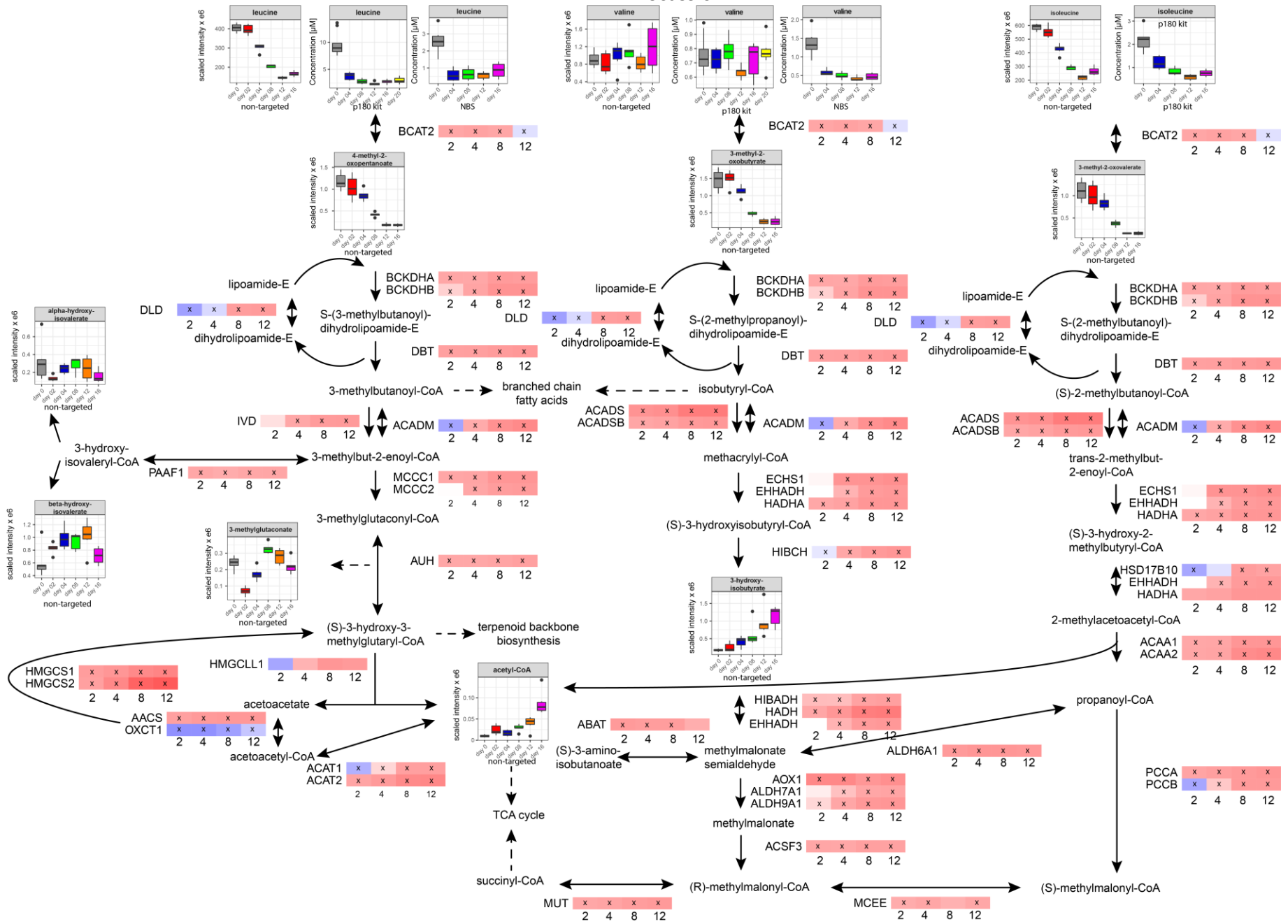
Elevated plasma levels of the branched-chain amino acids (BCAA), Leu, Ile, and Val, have been associated with obesity and insulin resistance (185-187). Recently published papers showed that the oxidative catabolism of BCAA is strongly induced during murine 3T3-L1 differentiation (146, 151). Moreover, Green and coworkers also found that the functional knockdown of the BCAA degradation pathway in 3T3-L1 preadipocytes impaired lipid accumulation and cell differentiation (151). Estrada-Alcalde and coworkers shed more light onto this interesting topic as they studied the fate of BCAA during murine 3T3-L1 adipogenesis in greater detail (188). They identified that all three BCAA are mostly incorporated into proteins and barely oxidized or used for lipid synthesis during the early stages of cell differentiation. However, this changed during the later stages of adipogenesis as both Leu and Ile oxidation as well as their incorporation into lipids strongly increased. At day 8, incorporation of both amino acids into proteins had the lowest priority. However, at day 12, Leu was mostly used for the incorporation into lipids whereas Ile's values decreased to the same level as oxidation and protein synthesis. In contrast, they also showed that Val was used differently than the other two amino acids as it was mostly incorporated in proteins throughout the observed time (188). Based on these results, it was expected to find the BCAA degradation pathway among the top regulated pathways in human adipogenesis. Therefore, the results from transcriptomics and metabolomics were combined to study the human BCAA degradation pathway on different levels. Figure 45 illustrates the highly upregulated catabolism

Discussion

reactions of Leu, Ile, and Val during SGBS differentiation. In detail, all transcripts levels were significantly upregulated. The concentrations of Leu and Ile strongly decreased whereas their catabolism products in the majority showed increased concentrations. However, Val showed only a decreasing concentration profile during measurements with the NBS assay whereas the results from the Biocrates Absolute/DQ p180 and the non-targeted approaches revealed fluctuating concentrations until day 20 of cell differentiation. The reason for that might be the use of different cell samples for all three measurements. Therefore, different concentration profiles might be explained by variations in cell cultivation. In addition, it is possible that the degradation of Val is not as important for cellular energy metabolism as Leu and Ile and therefore small variations among individual cultivations lead to this heterogeneity of Val's concentration profiles. During the degradation of these three BCAA species, different amounts of acetyl-CoA are synthesized which are used in adipocytes for FA elongation (Figure 42) and NADH synthesis in the TCA cycle (Figure 39 and Figure 46). In total three molecules of acetyl-CoA are produced from Leu, two acetyl-CoA and one propionyl-CoA are produced from Ile, and only one molecule propionyl-CoA is produced from Val (151). Propionyl-CoA is subsequently metabolized via methylmalonyl-CoA to succinyl-CoA under consumption of two ATP molecules whereas acetyl-CoA is directly incorporated into citrate pools of differentiated 3T3-L1 adipocytes without ATP consumption (151). Therefore, Leu and Ile might be the substrates of choice for acetyl-CoA generation, while Val is only used to a lesser extent, reflected in fluctuating to decreasing concentrations.

To sum up, the analysis of differentiating SGBS cells demonstrated a strong upregulation of BCAA degradation leading to a high supply of acetyl-CoA e.g. for energy synthesis in form of ATP via the TCA cycle and oxidative phosphorylation (see section 4.2.2) as well as energy storage by the fatty acid synthesis. Leu and Ile showed similarly strong decreasing concentration profiles, whereas Val 's profile varied between the used measurements pointing to disturbing cultivation influences or different utilization of this amino acid during human adipogenesis. In murine 3T3-L1 cells, Val is predominantly incorporated into proteins, whereas Ile and especially Leu are used to build-up lipids (188). These observations of the metabolite profiles and transcript levels hint to similar processes as described in murine cells.

Discussion



Discussion

Figure 45: Combination of metabolomics and transcriptomics revealed significantly upregulated BCAA degradation pathway in human adipogenesis.

Most transcript levels were strongly upregulated starting at day 2. The concentrations of Leu and Ile strongly decreased during adipogenesis, whereas Val showed fluctuating concentration profiles in two different measurements. Transcript levels are indicated by small boxes. Every single box represents the averaged transcript level at the indicated day of adipogenesis. Red indicates upregulation, and blue indicates downregulation. Significantly changed transcript levels (p -adjusted < 0.05) are indicated with an "x" inside the box and p -values are listed in appendix 5.3.

4.2.2. TCA cycle and oxidative phosphorylation are highly upregulated during human adipogenesis

The tricarboxylic acid (TCA) cycle, also known as the citric acid cycle, is the main biochemical pathway that oxidizes acetyl-CoA, derived from carbohydrates, fat, and proteins, into H₂O and CO₂ to generate reduction equivalents that provide energy in the oxidative phosphorylation. In greater detail, pyruvate from glycolysis (see section 4.2.3), acetyl-CoA from β -oxidation of fatty acids (see section 4.2.4), and acetyl-CoA from amino acid degradation like BCAA degradation (see section 4.2.1) are further metabolized during the TCA cycle. The TCA cycle also generates cofactors like nicotinamide adenine dinucleotide (NADH) and precursors for several amino acids. This pathway is closely linked to the oxidative phosphorylation that generates ATP under NADH oxidation. In addition, the TCA cycle is also connected with the glyceroneogenesis / gluconeogenesis / glycolysis pathway via oxaloacetate that can be metabolized into phosphoenolpyruvate (PEP). Phosphoenolpyruvate carboxykinases (PCK) catalyze this conversion under consumption of GTP. Proteomic studies of isolated mitochondria from differentiating murine 3T3-L1 cells revealed strong upregulation of TCA-enzymes, which indicates strong flux through the TCA cycle (189). Because of these results and generally high importance of the TCA cycle and oxidative phosphorylation for cellular metabolism, we hypothesized that these pathways are highly upregulated during adipogenesis of human SGBS cells.

In the analyzed transcriptome, most transcript levels of the genes involved in the oxidative phosphorylation and the TCA cycle were already upregulated starting at day 2. However, others like *OGDH* (Oxoglutarate Dehydrogenase), *DLD* (dihydrolipoamide dehydrogenase), *FH* (fumarate hydratase), and *SUCLG* (s) were significantly downregulated at this time point. Nevertheless, all transcript levels were upregulated at the latest at day 8. In contrast, the transcript levels of the enzymes catalyzing amino acid degradation, whose products feed into the TCA cycle, showed heterogeneous regulations. The majority of them had strongly upregulated degradation pathways, e.g., Lys, Thr, Glu, Ser, Ala as well as Ile, Leu, and Val. Only the transcripts of the degradation pathways of Asn, Asp, and Met were mostly downregulated. These results point to distinct utilization and regulation of amino acid degradation during human adipogenesis. However, this is incompletely understood and should therefore be analyzed in greater detail in the future. Bloor and coworkers analyzed the influence of different Lys concentration on bovine preadipocyte differentiation (190). They showed that low levels of Lys increase adipogenic potential (190). In contrast, slightly decreasing Asp concentrations might be explained by its fundamental role in the

Discussion

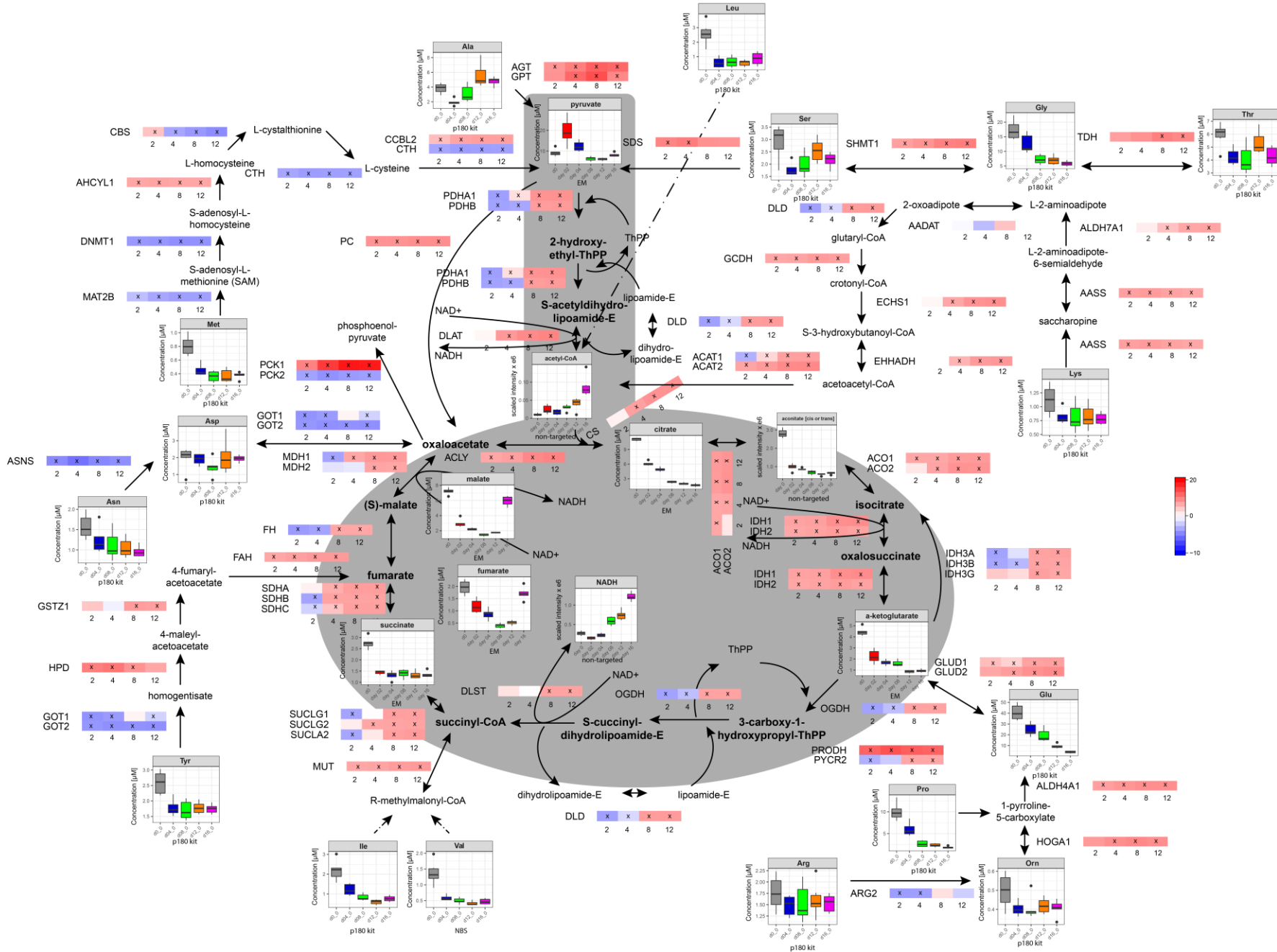
malate-aspartate-shuttle where it is used for the transport of NADH from the cytosol into the mitochondria. Increasing signal intensity values of NADH support this hypothesis.

In addition to the flux into the TCA cycle, the efflux was also highly regulated because the levels of *PCK1*, metabolizing oxaloacetate into PEP, were highly upregulated. It is known that *PCK1* protein is highly abundant in adipose tissue, liver, and kidney (191); however, its regulation during adipogenesis has not been analyzed so far. In contrast, the mitochondrial *PCK2* was markedly downregulated, indicating that this enzyme might not play an important role during human adipogenesis.

Transcriptome regulations are reflected in the metabolome, because the metabolites of the TCA cycle showed strongly decreased concentration levels during adipogenesis. Coenzyme A (CoA) and acetyl-CoA had strongly increasing signal intensity values indicating strongly upregulated oxidation processes for energy production. Interestingly, the concentration levels as well as signal intensity values of fumarate and malate decreased until day 12; however, subsequently, they increased nearly to starting values. The reason for this observation currently remains unclear. One can only speculate that complex negative feedback-loops or enzyme inhibitions due to metabolite accumulations lead to this increase at the later stages of adipogenesis. For example, a high supply of acetyl-CoA from BCAA (see results section 4.2.1) and FA degradation (see results section 4.2.4) lead to the upregulation of the TCA cycle which might result in increased metabolism of citrate in the TCA cycle. However, high citrate concentrations also facilitated the export of citrate with the tricarboxylate-carrier into the cytoplasm (192), where citrate is converted into oxaloacetate and acetyl-CoA using ATP. Acetyl-CoA accumulates in the cytoplasm, which is in harmony with the increasing signal intensity values of acetyl-CoA and CoA, and oxaloacetate is reduced using NADH to malate. However, malate is not further metabolized, leading to an accumulation at day 16. As malate and fumarate can be easily converted into each other, malate's accumulation also resulted in the accumulation of fumarate at day 16 of adipogenesis. Nevertheless, the experiment and analyses setup did not allow detection of any negative regulations and therefore this is highly speculative.

To sum up, the TCA cycle and oxidative phosphorylation were highly upregulated in the metabolome as well as in the transcriptome. Strongly increased transcript levels of TCA enzymes and strongly decreased concentration levels of TCA metabolites indicate a highly activated TCA metabolism. Thereby, immense amounts of ATP, NADH and precursors for distinct metabolites were generated. However, the increase of malate and fumarate at day 16 of adipogenesis cannot be really explained. Therefore, further experiments are necessary to elucidate this accumulation.

Discussion



Discussion

Figure 46: Results from transcriptomics and metabolomics show upregulation of TCA cycle during human SGBS cell differentiation.

Transcript levels are indicated by small boxes. Every single box represents the averaged transcript level at the indicated day of adipogenesis. Red indicates upregulation, and blue indicates downregulation. Significantly changed transcript levels (p -adjusted < 0.05) are indicated with an "x" inside the box and p -values are listed in appendix 5.3.

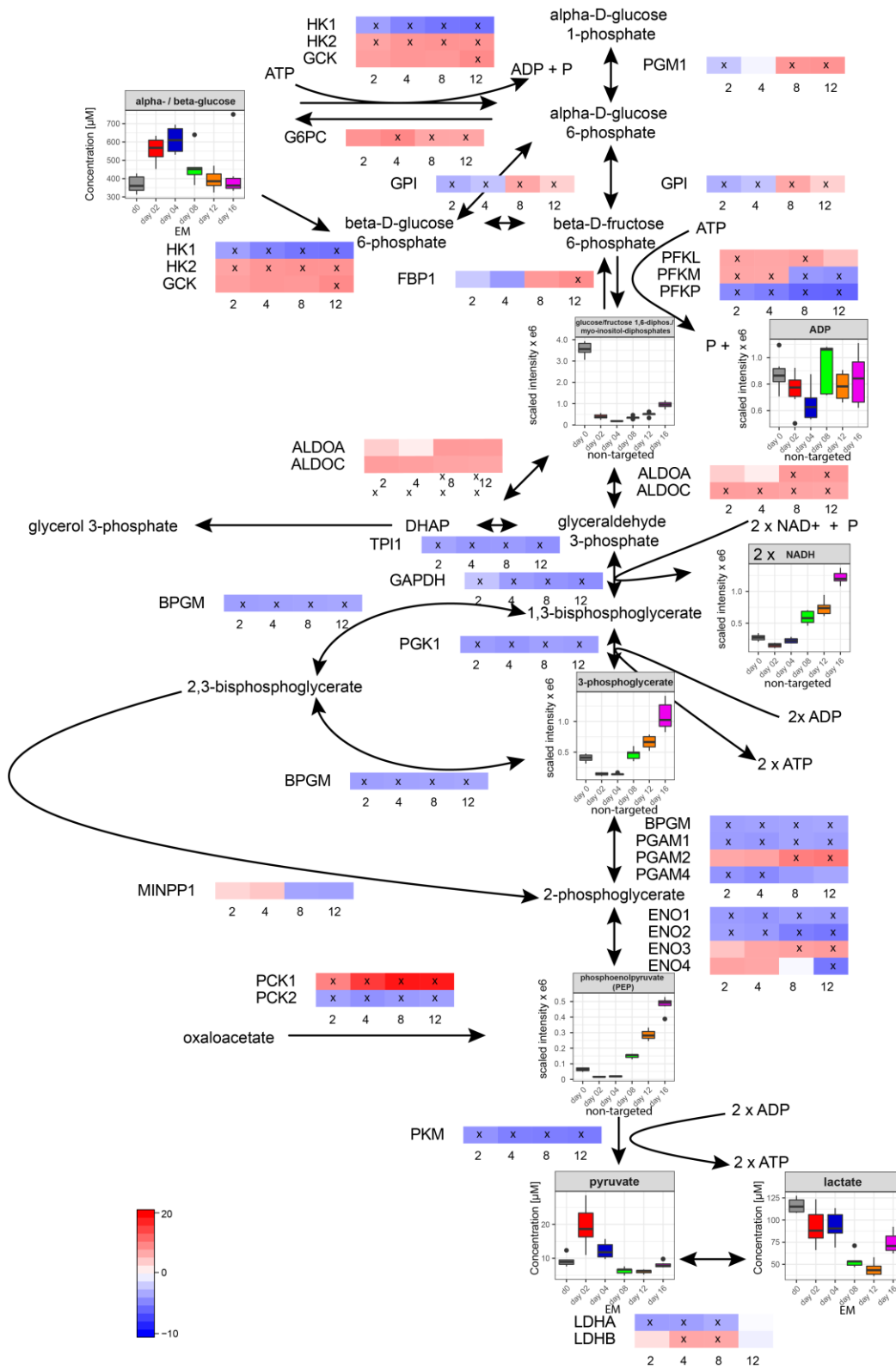
4.2.3. Glycolysis, gluconeogenesis, and glyceroneogenesis are highly upregulated during human adipogenesis

Human subcutaneous preadipocytes are highly dependent on glycolytic ATP production (193). Around 85% of the cellular ATP is produced by cytosolic glycolysis, whereas only 15% is produced by the mitochondrial oxidative phosphorylation (193). However, mitochondrial ATP production gets more important during adipogenesis as the mitochondria's relative contribution to ATP production increases up to 73% in mature adipocytes (193). To analyze the cellular glycolytic processes during this process, the transcriptomics and metabolomics results were combined. Figure 47 illustrates a highly regulated glycolysis on both transcriptome and metabolome levels. As the glycolysis can also be reversed, the figure additionally represents the gluconeogenesis. The initial steps of the gluconeogenesis are also used in the glyceroneogenesis, namely the build-up of glycerol 3-phosphate from pyruvate, lactate, glutamine, and other metabolites. Interestingly, the glycolytic ATP-consuming degradation of glucose into glyceraldehyde 3-phosphate (G3P) and dihydroxyacetone phosphate (DHAP) were mostly upregulated, whereas the following ATP-generating reactions mostly showed downregulated transcript levels. This downregulation, especially in the later stages of adipogenesis, is in accordance with the publication of Keuper and coworkers (193). However, others showed that the glyceroneogenesis pathway is almost exclusively used for glycerol synthesis in adipose tissue of rats (194). In detail, about 90% of all glycerol for triacylglycerol synthesis originates from glyceroneogenesis, whereas glucose as source was insignificant (194). However, most transcript levels of the glyceroneogenesis pathway of this PhD study cannot confirm their findings. The reason for that might be in the use of different cell models. However, two transcripts were upregulated, especially at day 8 and 12 of SGBS cell differentiation, namely phosphoglycerate mutase 2 (*PGAM2*) and enolase 4 (*ENO4*). *PGAM2* protein is known to be expressed in muscle tissue (195), although the observations in this work imply a role of the enzyme in adipocytes. In addition, phosphoenolpyruvate carboxykinase 1 (*PCK1*), which catalyzes the decarboxylation of oxaloacetate to phosphoenolpyruvate (PE) and is the main regulator of glyceroneogenesis, was highly upregulated. This reaction ensures the supply of TCA cycle metabolites and amino acids for the build-up of DHAP, which is reduced into glycerol 3-phosphate (194).

To sum up, glycolysis, gluconeogenesis, and glyceroneogenesis were highly regulated during adipogenesis. The initial steps of the gluconeogenesis synthesizing DHAP and G3P were strongly upregulated, whereas most transcript levels of the final steps were downregulated. However, the transcripts *PCK1*, *ENO4*, and *PGAM2*, which are important in glyceroneogenesis, were strongly

Discussion

upregulated. These regulations point towards a high production of glycerol, which might be used for lipid storage during adipogenesis.



Discussion

Figure 47: Results from transcriptomics and metabolomics show strong regulation of glycolysis, gluconeogenesis, and glyceroneogenesis during human SGBS cell differentiation.

The initial steps of glycolysis leading to dihydroxyacetone phosphate (DHAP) and glycerol 3-phosphate (G3P) were strongly upregulated. Further metabolism of DHAP and G3P was downregulated. In contrast, phosphoenolpyruvate carboxykinase 1 (PCK1), phosphoglycerate mutase 2 (PGAM2), and enolase 4 (ENO4) were highly upregulated, indicating activated glyceroneogenesis. Transcript levels are indicated by small boxes. Every single box represents the averaged transcript level at the indicated day of adipogenesis. Red indicates upregulation, and blue indicates downregulation. Significantly changed transcript levels (p -adjusted < 0.05) are indicated with an "x" inside the box and p -values are listed in appendix 5.3.

4.2.4. Lipid remodeling is highly activated during human adipogenesis

This PhD study also analyzed cellular processes on the lipidome and combined these results with the transcriptome. For lipid analysis, the novel Lipidyzer™ method was used which allowed the simultaneous quantification of 743 lipid species of 11 different lipid classes. This lipidomics study was recently published (22). Moreover, this technology enabled the identification of lipid species at the fatty acyl/alkyl level, except TAG. A comparable detection is not possible with the Biocrates Absolute/DQ p180 kit or Metabolon's non-targeted technology. Furthermore, non-targeted metabolomics using Metabolon's technology was applied for the identification of lipid species from other classes as well as precursor lipid molecules that could not be measured with the Lipidyzer™ method. This detailed, global lipid analysis enabled the identification of several correlations between lipid species over several classes. Together with transcriptomics, it opened the possibility to generate hypotheses on lipid remodeling during human adipogenesis.

The cell differentiation process on lipid level was accompanied by general markedly decreasing concentration levels of CE, CER, HCER, and LCER, whereas the lipid classes LPE, PC, PE, SM, and TAG showed strongly increasing levels. In addition to these lipid classes, their precursor molecules had distinct levels during adipogenesis. The phosphodiester glycerophosphocholine (GPC), glycerophosphoethanolamine (GPE), and glycerophosphoglycerol (GPG), as well as choline showed strong increases. In contrast, choline phosphate decreased markedly during adipogenesis. However, a closer look into the concentration profiles revealed slight differences among lipid classes. For example, CER showed increasing concentration levels until day 4, followed afterwards by the strongly decreasing concentrations of CE, HCER, and LCER. This concentration maximum at day 4 might reflect an involvement of CER in signaling for cell cycle arrest and for the inhibition of cell proliferation during early stages of adipogenesis (183). In line with this observation, Reichert and coworkers found that both processes are required for the initiation of cell differentiation of preadipocytes (184). Decreasing concentration levels of ceramides after day 4 were accompanied with simultaneously increasing concentration levels of SM. Spearman's rank correlation analysis revealed high negative correlation coefficients between several SM species and ceramides from the sphingolipid and PUFA cluster (cluster 2) pointing to correlations between the involved species. This lipid remodeling of sphingolipids could partly be seen using non-targeted metabolomics and transcriptomics as shown in Figure 48. In detail, the synthesis of CER via serine, 3-ketosphinganine, sphinganine, and dihydroceramides was highly regulated during

Discussion

adipogenesis. The signal intensity values of serine and sphinganine strongly decreased; however, serine showed an increase in its signal intensity values after day 8. Most transcript levels of the enzymes, which catalyze CER-related anabolism reactions, were highly upregulated. However, some transcript levels belonging to the same enzyme family showed a heterogeneous regulation profile. For example, the three members of the ceramide synthase (*CERS*) 2, 4, and 6 were upregulated, whereas *CERS5* was downregulated. This might indicate a tissue specific transcription and enzyme expression. In addition, delta 4-desaturase sphingolipid 1 (*DEGS1*) had downregulated transcript levels until day 12 of cell differentiation. Its corresponding enzyme catalyzes the last synthesis reaction of CER from DCER. Interestingly, the transcript levels of UDP-glucose ceramide glucosyltransferase (*UGCG*) and glycosylceramidase beta (*GBA*) were both strongly downregulated. These enzymes catalyze the forward (*UGCG*) and backward (*GBA*) reaction of CER into glucosylceramide (GlcCER). Yet, the transcript levels of galactosidase beta 1 (*GLB1*) and beta-1,4-galactosyltransferase 6 (*B4GALT6*) were both strongly upregulated. Their enzymes catalyzing the downstream forward and backward reactions of GlcCER into LCER. Taken together, the results from lipidomics, metabolomics, and transcriptomics point towards lipid remodeling between SM species and species from the classes CER, HCER, and LCER. After CER's contribution to signaling of cell cycle arrest and of the inhibition of cell proliferation, the ceramide species are no longer required in high amounts. Therefore, lipid remodeling of ceramides into SM is initiated, which are required for build-up of plasma membrane during lipid storage at the later stages of adipogenesis. However, future experiments are necessary to shed more light onto the details of these processes. Especially an analysis on protein level might clarify remodeling processes. In addition, other analytical methods are helpful to detect and quantify changes on related lipid classes like glycosphingolipids.

Discussion

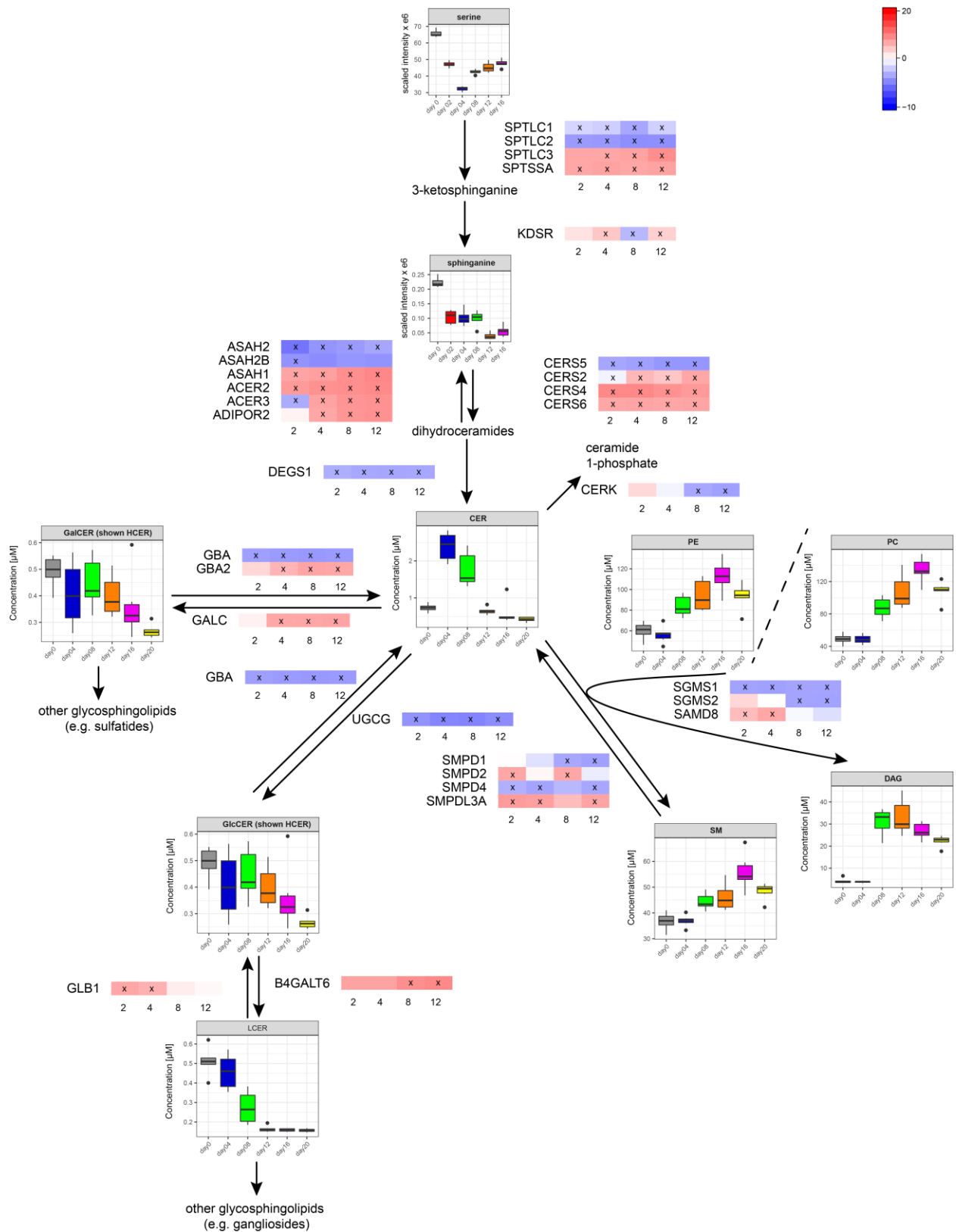


Figure 48: Results from transcriptomics, lipidomics, and metabolomics show strong regulation of synthesis, degradation, and remodeling of sphingolipids during adipogenesis.

Discussion

Lipidomics analysis showed decreasing levels of ceramides whereas SM, PC, and PE simultaneously increased during cell differentiation. Transcriptomics analysis showed regulated transcript levels of these cellular processes. Transcript levels are indicated by small boxes. Every single box represents the averaged transcript level at the indicated day of adipogenesis. Red indicates upregulation, and blue indicates downregulation. Significantly changed transcript levels (p -adjusted < 0.05) are indicated with an "x" inside the box and p -values are listed in appendix 5.3.

A possible explanation for the decreasing concentrations of CE during cell differentiation might be their role as cellular transport intermediate of cholesterol. The steroid is an important component of cell membranes and the decreasing concentrations might indicate marked release of cholesterol and insertion into cellular membranes (196-198). During the cell differentiation process, the morphology of the cells changes dramatically as shown in Figure 7. The incorporation of cholesterol changes the fluidity of membranes (199). In addition to membranes, cholesterol is an important constituent of the triglyceride lipid droplet surface where it serves as intracellular free cholesterol reservoir (197). The hypothesis is further supported by negative correlation coefficients down to -0.78 between CE species in clusters 1 and 2 and TAG species in clusters 4 and 5 (Figure 15).

After a lag-phase until day 4 of differentiation, the Lipidizer™ method quantified increasing TAG concentrations from micromolar to millimolar levels. This is not surprising as adipocytes are the main cells for storage and supply of fatty acids. Moreover, the cells start with lipid accumulation after successful cell differentiation from preadipocytes into adipocytes. Collins and coworkers showed by using ^{13}C -labeled substrates that the high generation of TAG species is based on *de novo* lipogenesis from glucose which is supplemented in the cell culture medium (152). However, the results from the Spearman's rank correlation analysis shows a possible contribution of VLCFA-carrying PE species as source for the TAG synthesis due to the very negative correlations between both classes. Possibly, the PE species have been catabolized by phospholipase C to DAG, then metabolized into TAG, and finally incorporated into lipid droplets (200, 201). The increasing lipid droplets during adipogenesis in size and number require also an expansion of cell surface and volume. For that, high amounts of membrane lipids (PC, PE, SM, and cholesterol) are required (202-204). In fact, the concentration of PC, PE, and SM species simultaneously increased after day 4. The metabolic intermediates of PC and PE, LPC and LPE, also increased during adipogenesis (205). The amounts of the head groups of these lipid species also increased strongly during adipogenesis. In addition, DAG levels also markedly increased after day 4. DAG species are the intermediate of TAG biosynthesis (206, 207) which is supported by high positive correlations between species of these two lipid classes. Using transcriptomics, clear head group remodeling could be detected between several glycerolipid classes. In detail, the transcript levels of the enzymes catalyzing the interconversion of cardiolipin, CDP-DAG, DAG, PA, PC, PE, PG, PGP, PI, and PS were mostly upregulated. Only PTDSS1, which catalyzes the conversion of PC into PS, had downregulated transcript levels.

Specific FA concentration profiles were detected during adipogenesis. With the exception of C20:4, all LCFA as well as the MCFA lauric acid (C12:0) showed increasing concentrations levels whereas most of the VLCFA had decreasing concentration levels. These specific profiles were

Discussion

verified with the transcriptomic analysis. The strong increase of the LCFA and MCFA can be explained by the upregulated transcripts *ELOVL3* and *ELOVL5* which are necessary for the elongation of FA in the cytoplasm and mitochondria for FA of up to 16 C-atoms (208). In contrast, *ELOVL2* and *ELOVL4* which are mostly responsible for the elongation of polyunsaturated fatty acids with a chain length longer than C20, were strongly downregulated (209-211). In addition, these VLCFA might be degraded into shorter FA as the transcriptomics measurements showed an upregulation of degradation of FA during adipogenesis. Since the involved enzymes (and their transcripts) catalyze the reactions unspecifically, it cannot be differentiated which specific FA were degraded. Nevertheless, the transcriptomics results support the results from lipidomics.

Besides even chain fatty acids, odd chain fatty acids were quantified. In detail, C15:0 and 17:0 showed increasing concentration time courses during human adipogenesis. These results are in line with Roberts and coworkers who also quantified odd chain fatty acid levels which increased during cell differentiation in murine 3T3-L1 adipocytes (149). A possible explanation for these increasing concentration levels could be the sequential peroxisomal fatty acid α -oxidation, which has been shown to occur in differentiating adipocytes (53).

However, these concentration changes on lipid as well as on fatty acid levels could be partly explained by the composition of the cell culture medium. The analysis of the FBS-containing medium for cell cultivation before induction of differentiation revealed high concentrations of all fatty acids. Especially the fatty acids C16:0, C18:0, and C18:1 were highly abundant. In addition, the lipids with very long-chain PUFAs were also highly concentrated in the FBS-containing medium compared to the medium used for cell differentiation. Since the concentrations of very long-chain PUFAs markedly decreased during adipogenesis, it could be speculated that this is an artifact from the cultivation with FBS-containing medium.

4.2.5. Polyamine metabolism is highly regulated during human adipogenesis

Polyamines like putrescine, spermidine, and spermine are involved in several fundamental cellular processes including proliferation, cell growth, cell survival, stabilization of chromatin structure, protection from oxidative damage, and maintenance of protein and nucleic acid synthesis (72-77). In addition, recent publications also showed that they are required in the early adipogenic processes (70, 71). In detail, Brenner and coworkers found that the depletion of polyamines inhibits the second division of the mitotic clonal expansion and the expression of the main adipogenic transcription factors PPAR γ and CEBP α resulting in inhibition of adipogenesis. Others identified a regulation of the metabolome during 3T3-L1 cell differentiation (146, 149, 150, 212, 213). Roberts and coworkers identified an altered polyamine metabolism during 3T3-L1 cell differentiation, because putrescine's concentrations increased during the first day of differentiation, followed by a decrease until day 9 (149). However, before-mentioned studies were

Discussion

only performed on murine adipocytes while levels of polyamines were not determined during humans adipogenesis so far. In addition, the individual concentration levels of polyamines were not combined with the levels of transcripts of the involved enzymes. Therefore, metabolomics and transcriptomics were applied on human SGBS cells during cell differentiation. Figure 49 illustrates the results of the combined metabolomics and transcriptomics analyses. In general, polyamine metabolism was regulated on metabolome and transcriptome level during human adipogenesis. All transcript levels that are directly involved in the biosynthesis of spermine from spermidine and putrescine were downregulated until day 12. In detail, these transcripts are ornithine decarboxylase 1 (*ODC1*), the first and rate-limiting enzyme of the biosynthetic pathway, spermidine synthase (*SRM*), and spermine synthase (*SMS*). In line, the transcript levels of the enzymes catalyzing the backwards reaction were upregulated. These are spermidine/spermine N1-acetyltransferase 1 and 2 (*SAT1* and *SAT2*) as well as polyamine oxidase (*PAOX*). It can be speculated that the regulated transcript levels also had an influence on the metabolome. Putrescine, which is synthesized from ornithine by *ODC1* had a triphasic signal intensity profile. The signal intensity values of putrescine decreased from day 0 to day 2 and stayed at this level until day 8. Then, the value markedly increased on day 12 and 16. In addition, this thesis confirmed putrescine's concentration levels during the first 48 h of 3T3-L1 differentiation (150). Interestingly, they identified increasing levels within the first 8-12 hours, then the levels declined until day 2 down to values as before differentiation start. During SGBS differentiation, ornithine's signal intensity values decreased to non-detectable values during the maturing phase. This points towards consumption of ornithine as the transcript levels of arginase 2 (*ARG2*) were not clearly downregulated during the whole observed time. N-acetylputrescine, which can be metabolized from putrescine, had a similar concentration profile to putrescine. It can be speculated that putrescine and N-acetylputrescine accumulate during adipogenesis as its metabolization into 4-acetamidobutanoate revealed non-detectable values after day 2. In contrast, spermidine's concentrations slightly decreased during the whole observed process. Its product, spermine, had a signal intensity peak at day 2 – 4 and then decreased to values as before differentiation. Additionally, Kirkwood and coworkers identified increased levels of spermidine and spermine between 12 and 48 hours during 3T3-L1 differentiation (150). The biosynthesis of spermidine and spermine each requires an aminopropyl group from decarboxylated S-adenosylmethionine (dcAdoMet) (214). This enzymatic reaction produces 5-methylthioadenosine (MTA) as side-product from dcAdoMet, which showed decreased signal intensity values during adipogenesis. Decarboxylation of S-adenosylmethionine (AdoMet) is catalyzed by S-adenosylmethionine decarboxylase (*AMD1*), the second rate-limiting enzyme of the biosynthetic polyamine pathway. The transcript levels of *AMD1* were significantly upregulated on day 4 and 12 of adipogenesis possibly due to increased consumption of AdoMet into dcAdoMet. However, AdoMet might also be metabolized into S-adenosylhomocystein (SAH) because this metabolite had a signal intensity peak at day 8. Furthermore, MTA is cleaved into adenine and 5-methylthioribose-1-phosphate by methylthioadenosine phosphorylase (*MTAP*) (215, 216). The transcript levels of *MTAP* were downregulated, whereas the levels of adenine phosphoribosyltransferase (*APRT*) were upregulated. *APRT* catalyzes the build-up of AMP from adenine and phosphoribosyl

Discussion

pyrophosphate. AMP, whose signal intensity values were markedly increased during adipogenesis, is then further processed to ATP. 5-methylthioribose-1-phosphate is metabolized into methionine, which showed decreased signal intensity values during adipogenesis.

To sum up, the polyamine metabolism of putrescine, spermidine, and spermine was strongly regulated during human adipogenesis. Spermine might be particularly required during the differentiation phase as its amount increased during this phase. Putrescine and its acetylated product accumulated during adipogenesis. Additionally, ATP production might be also upregulated as AMP build-up was upregulated on the metabolome and transcriptome. However, to understand these regulations in greater detail, the processes need to be studied more intensively in the future with biochemical and molecular biology approaches. In addition, the levels of polyamines should be also analyzed during the first hours of differentiation, because others showed an involvement in very early processes during cell differentiation (150).

Discussion

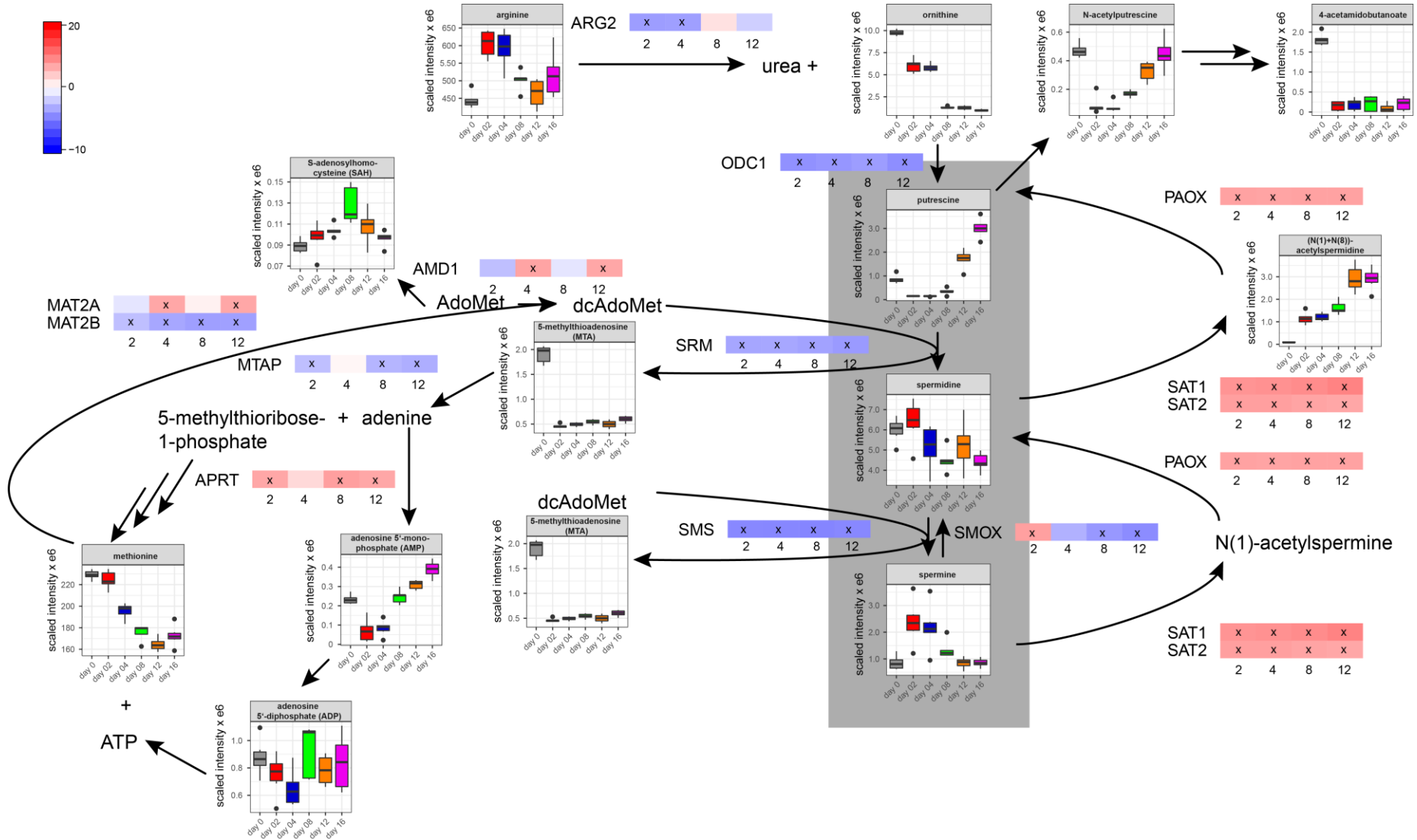


Figure 49: Polyamine and methionine metabolism was highly regulated on metabolome and transcriptome level. All levels of transcripts, whose enzymes are involved in the biosynthesis of putrescine, spermidine, and spermine, were downregulated. In contrast, transcript levels of the enzymes catalyzing the catabolism of spermine and spermidine were strongly upregulated. Putrescine accumulated during maturing; the amount of spermidine amount decreased during adipogenesis. Spermine increased until day 2, then decreased. Additionally, the synthesis of AMP, which is related to the polyamine metabolism, was upregulated during adipogenesis. Transcript levels are indicated by small boxes. Every single box represents the averaged transcript level at the indicated day of adipogenesis. Red indicates upregulation, and blue indicates downregulation. Significantly changed transcript levels (p -adjusted < 0.05) are indicated with an "x" inside the box and p -values are listed in appendix 5.3.

4.2.6. Limitations of the study

It is very important to keep in mind that cell culture experiments are only a model under artificial conditions, mostly requiring non-physiologically high concentrations of nutrients, hormones, growth factors, or stimulation factors (22). As an example, SGBS cell differentiation of preadipocytes into mature adipocytes requires the PPAR γ agonist rosiglitazone, the corticosteroid dexamethasone, and 17.5 mM glucose. Jeucken and Breuwens recently showed that rosiglitazone influences the lipidome of HeLa cells (60). Such media supplements might even lead to changes in the phenotype of the cells because Yeh and coworkers showed that rosiglitazone and the endogenous myokine irisin are able to induce browning in white adipocytes (61). Others detected a propensity of the SGBS cells towards a beige phenotype (111, 113, 114, 217). However, it seems that not only SGBS but also ADSCs cells have this tendency when the cells were differentiated with same cell culture medium (112). In addition, Halbgebauer and coworkers were able to show that SGBS and ADSCs cells have similar levels of key white adipogenic markers after using the same differentiation medium (112). Furthermore, SGBS show similar morphology and functionality compared to human primary adipocytes with such media supplements (103). Therefore, the postulated SGBS-specific browning propensity (111, 113, 114, 217) might not hold true after all. However, cell culture media always have an important influence on the outcome of each study. Therefore, media components should always be reduced to a minimum. Nevertheless, some endogenous as well as synthetic components like rosiglitazone are necessary, because the cells cannot fully differentiate *in vitro* without the initial four-day stimulation with rosiglitazone.

Moreover, some of the observed concentration patterns of the lipid species might be explained by influences of cell culture medium composition (22). In general, all measured lipids were highly concentrated in the FBS-containing medium, which is used for the cultivation before differentiation start. In contrast, the differentiation medium (day 0 – 4) and maturation medium (day 4 – 20) contain only one fatty acid source, which is linoleic acid (C18:2). In consequence, the detected concentration profiles of the FA and lipid species might have been artificially influenced using the FBS-containing medium before differentiation. As a result, the decreasing concentration levels of the lipid species carrying VLCFA might also be explained by a lack of these FA in the FBS-free differentiation and maturation media during cell differentiation. Thus, it is always important to analyze the medium used for cell culture lipidomics / metabolomics studies to prevent misinterpretation of the data (22).

Besides the presence and the non-physiologically high concentration levels of growth or differentiation factors, *in vitro*, the cells also do not act like the original cells *in vivo*. For example, lipid synthesis in adipose tissue *in vivo* is not solely based on *de novo* synthesis from mostly glucose but also on fatty acids derived from circulation (218). Nevertheless, cell culture experiments are helpful to elucidate cellular processes and specific molecular mechanisms separately. However, they cannot fully represent physiological *in vivo* conditions due to their simplicity and artificial nutrition.

Discussion

In addition to the limitations of the cell cultivation and the cell model itself, the used instrumentations and methods have some limitations. The Lipidyzer™ method, Biocrates Absolute/DQ p180 kit, and non-targeted metabolomics approach using Metabolon's technology were developed for the analysis of human plasma, not cell culture samples. Similarly, the NBS assay was developed for the analysis of whole blood on dried blood spots. These sample types have naturally different metabolite and lipid compositions than SGBS cell samples. The ISTD concentrations (except EM assay and non-targeted metabolomics) were also optimized for human plasma, which might lead to a potential mismatch of the metabolite concentrations in the used cell culture samples. In addition to the discrepancy of the ISTD concentration levels, the set of ISTDs also did not cover all analytes which were included in the distinct assays. For example, the Lipidyzer™ method contains only up to 10 ISTDs per lipid class, which might influence the results, because some ISTDs might differ slightly during analysis compared to their related analytes. However, up to now there is no ISTD available for every single lipid species. To avoid mis- and overinterpretation, the determined concentrations, especially the lipid concentrations, should be interpreted carefully. Moreover, the mass spectrometry instrumentation does not allow the measurement of several hundreds of analytes and internal standards with the same measurement time and sensitivity. Thus, a strong increase in the number of ISTDs would have a negative impact on sensitivity and throughput, which is important for metabolomics and lipidomics. Furthermore, the Lipidyzer™ method and the NBS assay were not developed for absolute quantification, because they do not use a calibration curve. Therefore, the absolute concentrations should be used carefully when interpreting biological processes. However, this can be avoided by the use of ratios and concentration time courses, as done in this thesis.

4.2.7. Proposed model of human adipogenesis using SGBS cells

This work analyzed the adipogenic process using human SGBS cells with approaches from metabolomics, lipidomics, and transcriptomics. Thereby, more than 20,000 transcript levels and about 1000 distinct metabolites and lipids from several classes were analyzed for up to 20 days in great detail. This experimental setup enables an exceptionally broad and deep analysis of the highly complex cell differentiation process. During the first four days, a switch in the cellular energy metabolism take place as indicated by strong concentration peaks of glucose and pyruvate. This energy switch is accompanied by a strong upregulation of BCAA degradation. Thereby, huge amounts of acetyl-CoA are synthesized, which are further metabolized into ATP via the TCA cycle and oxidative phosphorylation. These two pathways, which are the core of cellular energy synthesis, are clearly activated starting at day 4 of adipogenesis. High amounts of ATP are needed for all cellular processes, including the initial remodeling of metabolism and morphology of fibroblast-like preadipocytes as well as massive build-up and storage of TAG species later on. For the synthesis of only one molecule of palmitic acid, seven molecules of ATP are required (219). To be able to supply this amount of ATP, energy is not only obtained from the breakdown of BCAA, but also from fatty acid oxidation of unneeded (V)LCFA, which was upregulated significantly

Discussion

already at day 2. The oxidation of these fatty acids, which might be largely derived from the cultivation with FBS-containing medium before differentiation start, becomes increasingly important during the ongoing adipogenesis. Since most energy producing processes peaked upregulation after day 4, ATP might also be derived from a cellular ATP-pool for the very early processes of cell differentiation. This hypothesis is supported by the levels of AMP, which had their concentration minimum at day 2 and 4 indicating a high consumption of AMP for the build-up of ATP during this initial adipogenic phase.

During this early phase of adipogenesis, nearly all amino acids showed a strong concentration decrease, which mostly carried on over the whole observed time period. Since differentiating and fully differentiated adipocytes do not proliferate anymore, high amounts of amino acids for protein biosynthesis are no longer needed. Therefore, most of the amino acids are degraded and converted into ATP via the TCA cycle and oxidative phosphorylation. In addition, amino acids might be metabolized into oxaloacetate, which is used to build up glycerol for TAG species.

Besides the energetic switch, the initial phase is also characterized by CER-mediated cell cycle arrest and inhibition of cell proliferation (183, 184). The lipidomics findings showed that the concentration of CER species increased during this required process for adipogenesis. After finishing this first and very important phase of adipogenesis, CER-signaling less important during cellular homeostasis. Accordingly, ceramide concentrations strongly decreased whereas concentrations of the classical plasma membrane lipids, SM, PC, and PE, as well as their precursor species (LPC and LPE) markedly increased. The lipidomics data suggests that a remodeling of ceramide species into lipid species of the plasma membrane occurs.

TAG-synthesis and -storage, which are the main functions of white adipocytes, start after this initial morphological remodeling and continue throughout the complete observed time period. For these processes, immense amounts of acetyl-CoA are used for elongation of FA under ATP-consumption, which are then linked to the glycerol backbone (220). These acetyl-CoA molecules are derived from several degradation pathways like BCAA and other amino acids as well as the degradation of unneeded (V)LCFA (220).

In conclusion, the cell differentiation process of undifferentiated SGBS cells into fully matured, lipid-laden adipocytes is a highly complex and dynamic process. It involves the concerted action of several transcription factors, lipids, and metabolites, which coordinates the remodeling of metabolism and cellular morphology from undifferentiated, fibroblast-like cells to big, oval adipocytes containing lipid-droplets. During the first four days, the cellular metabolism is switched resulting in upregulated degradation of several amino acids as well as unneeded fatty acids fueling the adipogenic process. These cellular processes have an important influence on the development and the manifestation of obesity in humans. Diets with high amounts of saturated lipids fuels the adipogenic process (221). Therefore, lifestyle interventions that reduce the intake of saturated lipids, or medications, stopping stops the immense fatty acid degradation as well as incorporation into lipid droplets, are key strategies to overcome the pandemic disorder of overweight and obesity.

Index of figures

Figure 1: Prevalence of overweight (panel A) and obesity (panel B) strongly increased worldwide from 1980 until 2015.	1
Figure 2: Transcriptional activation of adipogenesis requires a large number of different factors with a precise timing.....	4
Figure 3: Transcriptional regulation of adipogenesis is highly dependent on PPAR γ and members of the C/EBP protein family.....	5
Figure 4: Matrix effects were similar in all matrices obtained during adipogenesis of SGBS cells with the EM assay.	38
Figure 5: Total ion chromatogram of Cal 5 revealed a good separation of the analytes.....	39
Figure 6: Total ion chromatogram of a maturing SGBS sample (day 8) revealed clear detection of eight analytes (panel A).....	40
Figure 7: SGBS cells were successfully differentiated based on the microscopic analysis.	42
Figure 8: Transcript levels of the key adipogenic transcription factors PPAR γ (PPARG) and C/EBP α (CEBPA) were highly upregulated during adipogenic cell differentiation.....	42
Figure 9: Analysis of the analytical performance of the Lipidyzer™ method revealed high linearity for most lipid classes using undifferentiated and differentiated cells.	44
Figure 10: Analysis of the analytical performance of the Lipidyzer™ method revealed high linearity for the lipid classes LPE, PC, PE, SM, and TAG using undifferentiated and differentiated cells.....	45
Figure 11: PCA (A) and PLS-DA (B) score plots showed clear separation of the different adipogenic time points and a clear clustering of individual samples of each time point.....	46
Figure 12: Lipid class compositions and concentrations were highly changed during adipogenesis.....	49
Figure 13: Individual concentration time courses of each FA side chains bound in the lipids were summarized and showed consistent patterns.	52
Figure 14: Analyses of concentrations and compositions of FA identified marked changes during adipogenesis.....	53
Figure 15: Spearman’s rank correlation analysis of lipid concentration trajectories identified marked correlations and clustering of the lipid species.	54
Figure 16: Clusters from Spearman’s rank correlation analysis differed markedly regarding lipid species and lipid class composition.....	57
Figure 17: Analysis of the cluster showed distinct relative lipid class compositions.....	58
Figure 18: All fatty acids in FBS-containing medium were highly concentrated.	59
Figure 19: PLS-DA scores plot (Panel A) showing very clear clustering of the analytes regarding the different time points of adipogenesis.	60
Figure 20: Heatmap of the top 80 metabolites revealed a strong clustering of metabolites and samples.....	61

Index of figures

Figure 21: Analysis of amino acids and biogenic amines revealed markedly changed concentration time courses (Biocrates AbsoluteIDQ p180 kit).....	62
Figure 22: PLS-DA analysis revealed clustering of the samples into separate time points based on the metabolites of the Newborn Screening assay.....	63
Figure 23: Heatmap of the metabolites from the analysis with the NBS assay revealed two clusters.	64
Figure 24: Newborn Screening assay quantified strongly decreasing concentration levels of most of the amino acids as well as free carnitine and three acylcarnitine.	65
Figure 25: PCA and PLS-DA scores plot showed clear separation of the different time points....	66
Figure 26: Heatmap of the non-targeted dataset revealed a strong clustering of the metabolites according to different stages of adipogenesis.	67
Figure 27: Random forest analysis revealed the top 15 analytes ranked by their contributions to the classification accuracy.....	68
Figure 28: Metabolon's non-targeted approach could detect strongly changing signal intensity time courses during adipogenesis.....	69
Figure 29: Spearman's rank correlation analysis showed strong correlations of metabolites and lipid species with distinct concentration profiles.....	70
Figure 30: EM assay revealed strongly changed concentration levels of metabolites of the TCA cycle and cellular energy related pathways.	71
Figure 31: Comparison of the different metabolomics and lipidomics measurements revealed strong consistency.....	73
Figure 32: Comparison of the different metabolomics and lipidomics measurements revealed strong consistency.....	74
Figure 33: Comparison of the different metabolomics and lipidomics measurements revealed strong consistency.....	75
Figure 34: Comparison of the different metabolomics and lipidomics measurements revealed strong consistency.....	76
Figure 35: Comparison of the different metabolomics and lipidomics measurements revealed strong consistency.....	77
Figure 36: PCA scores plot showing clear separation of the different time points normalized to day 0.....	78
Figure 37: Heatmap of the whole data set of transcriptomics analysis revealed markedly changed transcript levels during adipogenesis.....	79
Figure 38: Transcripts of enzymes involved in glycolysis /gluconeogenesis / glyceroneogenesis were significantly regulated during adipogenesis.....	82
Figure 39: Transcripts of enzymes involved in the TCA cycle were highly upregulated during adipogenesis.....	85
Figure 40: Transcripts of enzyme involved in the oxidative phosphorylation were significantly upregulated during adipogenesis.	85
Figure 41: Transcripts of enzymes involved into the degradation of saturated and unsaturated fatty acids were highly upregulated during adipogenesis.....	87

Index of figures

Figure 42: Transcript levels of enzymes involved in the elongation of fatty acids were highly and significantly regulated during adipogenesis.....	88
Figure 43: Transcript levels of enzymes involved in the head group remodeling of glycerophospholipids were highly regulated during adipogenesis.....	89
Figure 44: Transcripts of enzymes involved in the synthesis and degradation of sphingolipids were highly regulated during adipogenesis.	90
Figure 45: Combination of metabolomics and transcriptomics revealed significantly upregulated BCAA degradation pathway in human adipogenesis.....	97
Figure 46: Results from transcriptomics and metabolomics show upregulation of TCA cycle during human SGBS cell differentiation.	100
Figure 47: Results from transcriptomics and metabolomics show strong regulation of glycolysis, gluconeogenesis, and glyceroneogenesis during human SGBS cell differentiation.	102
Figure 48: Results from transcriptomics, lipidomics, and metabolomics show strong regulation of synthesis, degradation, and remodeling of sphingolipids during adipogenesis.....	104
Figure 49: Polyamine and methionine metabolism was highly regulated on metabolome and transcriptome level.....	109
Figure 50: Fatty acid compositions and concentrations were heterogenous in all lipid classes at day 0.....	117
Figure 51: Fatty acid compositions and concentrations were heterogenous in all lipid classes at day 4.....	118
Figure 52: Fatty acid compositions and concentrations were heterogenous in all lipid classes at day 8.....	119
Figure 53: Fatty acid concentrations were homogenous in all lipid classes at day 12 as C16:0, C16:1, C18:0, and C18:1 were highly abundant.	120
Figure 54: Fatty acid concentrations were homogenous in all lipid classes at day 16 as C16:0, C16:1, C18:0, and C18:1 were highly abundant.	121
Figure 55: Fatty acid concentrations were homogenous in all lipid classes at day 20 as C16:0, C16:1, C18:0, and C18:1 were highly abundant.	122

5. Appendix

5.1. Significances from analyzing adipogenesis with Lipidyzer™ method

Table 15: Illustrated are the p-values from significant testing of lipid class and summarized FA concentration changes over time with Kruskal-Wallis test and Dunn's post-hoc testing. Cell sample homogenates from in total six samples per time point were compared. The significance level was set at $p < 0.05$.

Lipid class	p-value		Fatty acid	p-value
CE	4.52E-04		FA12:0	1.15E-05
CER	1.51E-05		FA14:0	< 1E-15
DAG	3.40E-05		FA14:1	< 1E-15
HCER	5.23E-03		FA15:0	< 1E-15
LCER	2.80E-05		FA16:0	< 1E-15
LPC	1.50E-04		FA16:1	< 1E-15
LPE	6.00E-06		FA17:0	< 1E-15
PC	2.13E-05		FA18:0	< 1E-15
PE	4.90E-05		FA18:1	< 1E-15
SM	5.04E-05		FA18:2	< 1E-15
TAG	4.01E-06		FA18:3	< 1E-15
			FA20:0	< 1E-15
			FA20:1	< 1E-15
			FA20:2	< 1E-15
			FA20:3	< 1E-15
			FA20:4	< 1E-15
			FA20:5	< 1E-15
			FA22:0	3.60E-14
			FA22:1	< 1E-15
			FA22:2	1.91E-07
			FA22:4	< 1E-15
			FA22:5	< 1E-15
			FA22:6	< 1E-15
			FA24:0	5.71E-13
			FA24:1	8.18E-08
			FA26:0	3.83E-08
			FA26:1	6.00E-15

Appendix

5.2. Analysis of the fatty acid concentrations during adipogenesis with respect to the lipid classes

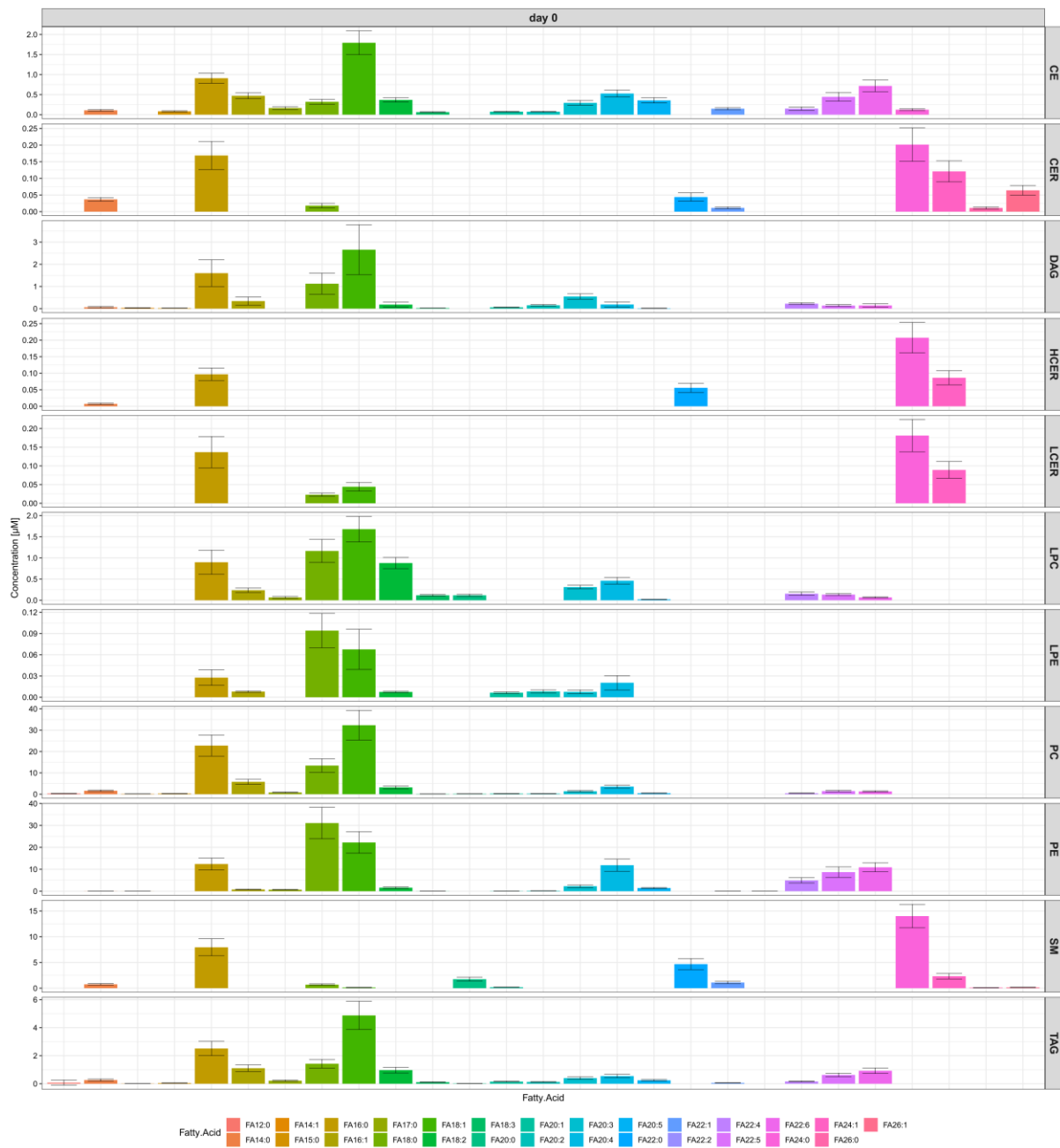


Figure 50: Fatty acid compositions and concentrations were heterogenous in all lipid classes at day 0.

Appendix

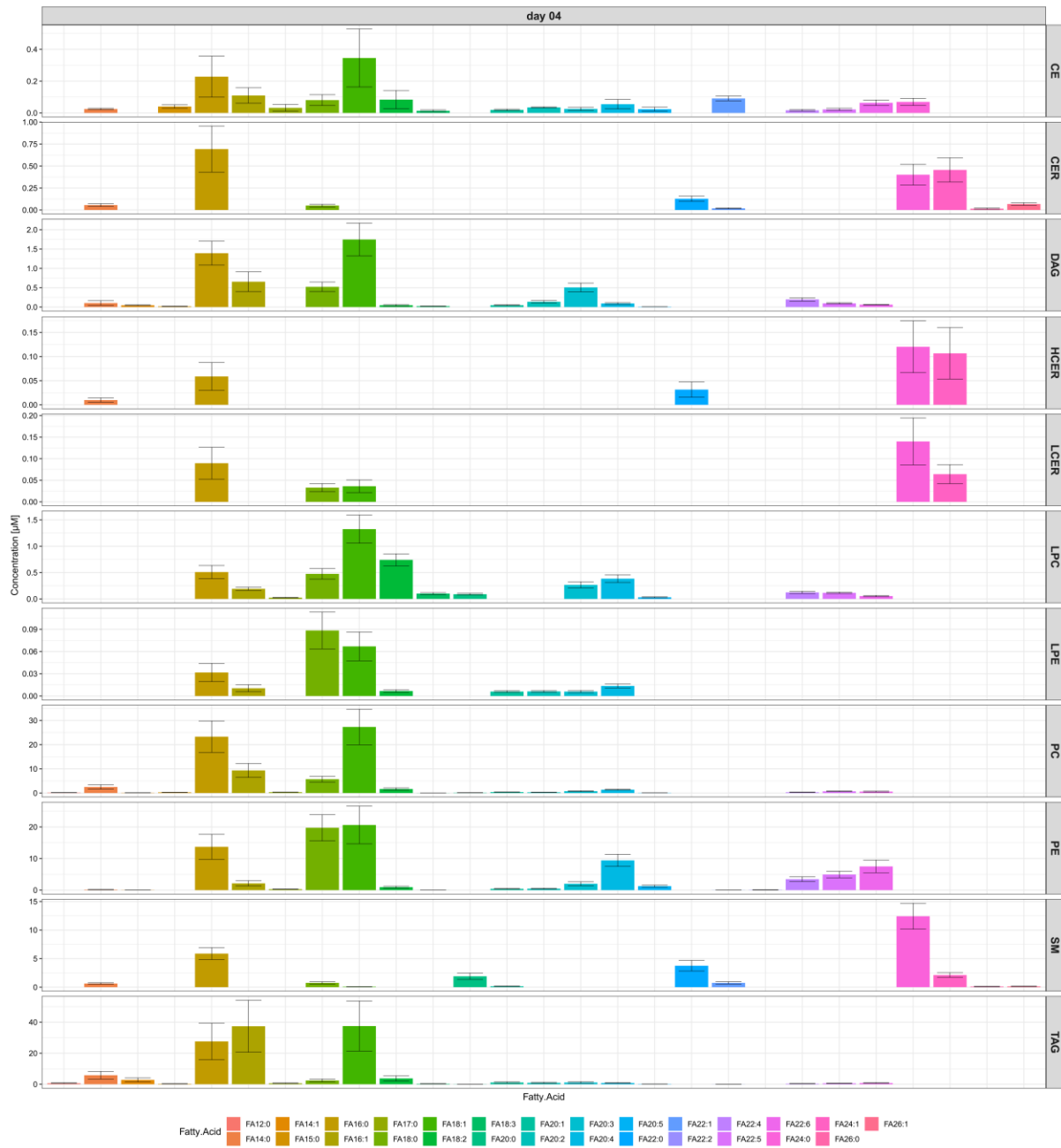


Figure 51: Fatty acid compositions and concentrations were heterogenous in all lipid classes at day 4.

Appendix

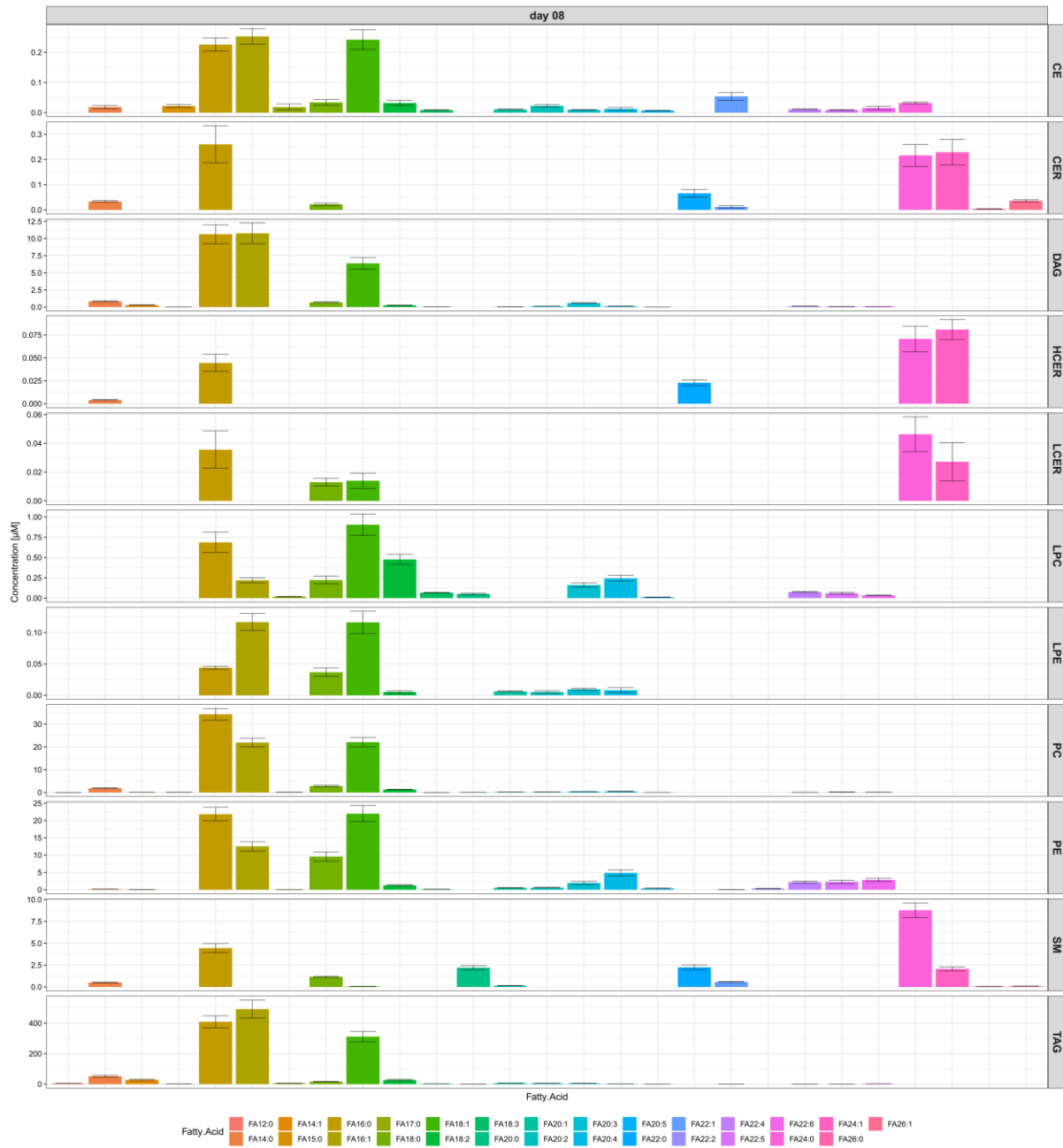


Figure 52: Fatty acid compositions and concentrations were heterogenous in all lipid classes at day 8. The fatty acid C16:0, C16:1, and C18:1 were the most abundant ones.

Appendix

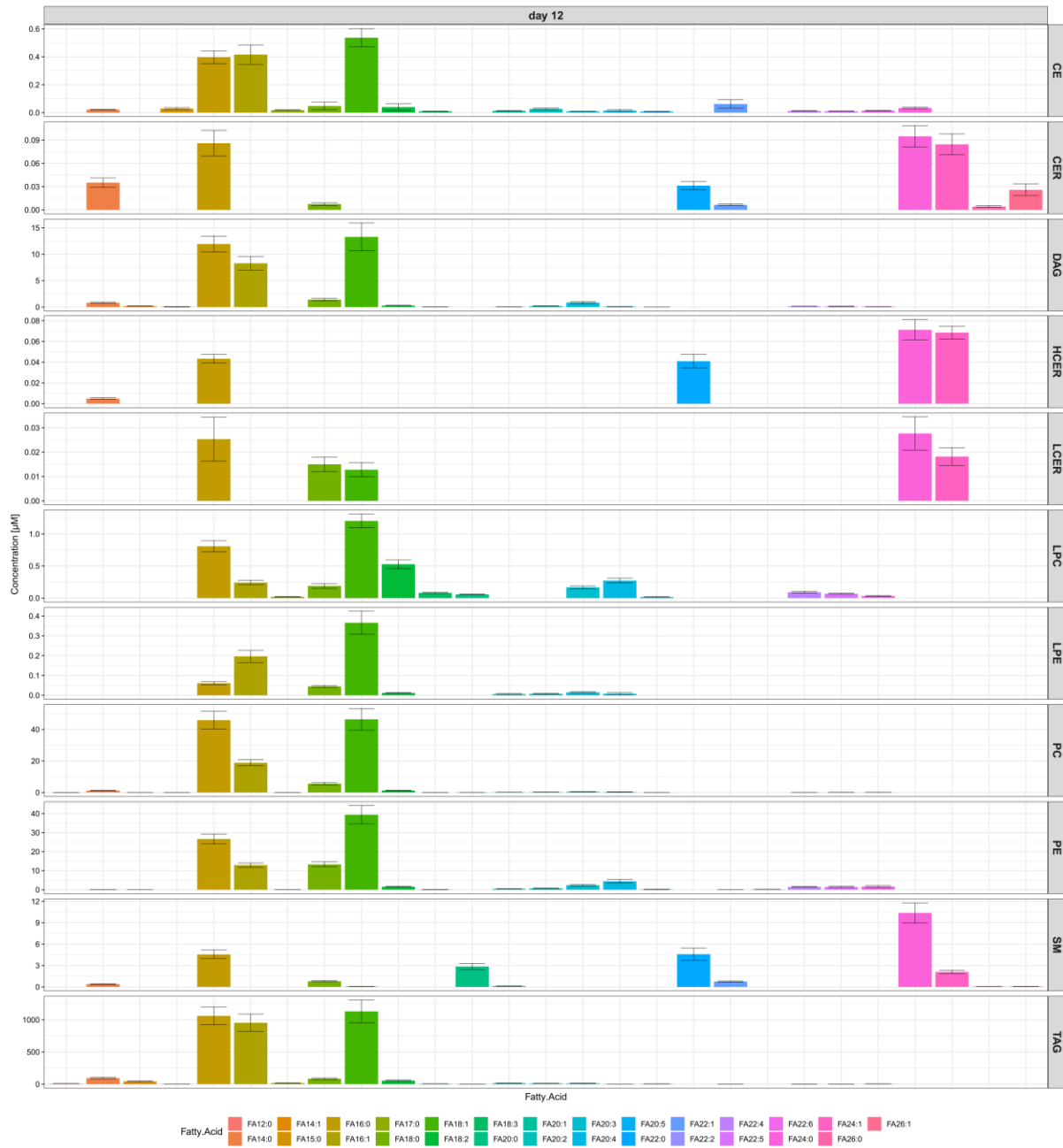


Figure 53: Fatty acid concentrations were homogenous in all lipid classes at day 12 as C16:0, C16:1, C18:0, and C18:1 were highly abundant.

Appendix

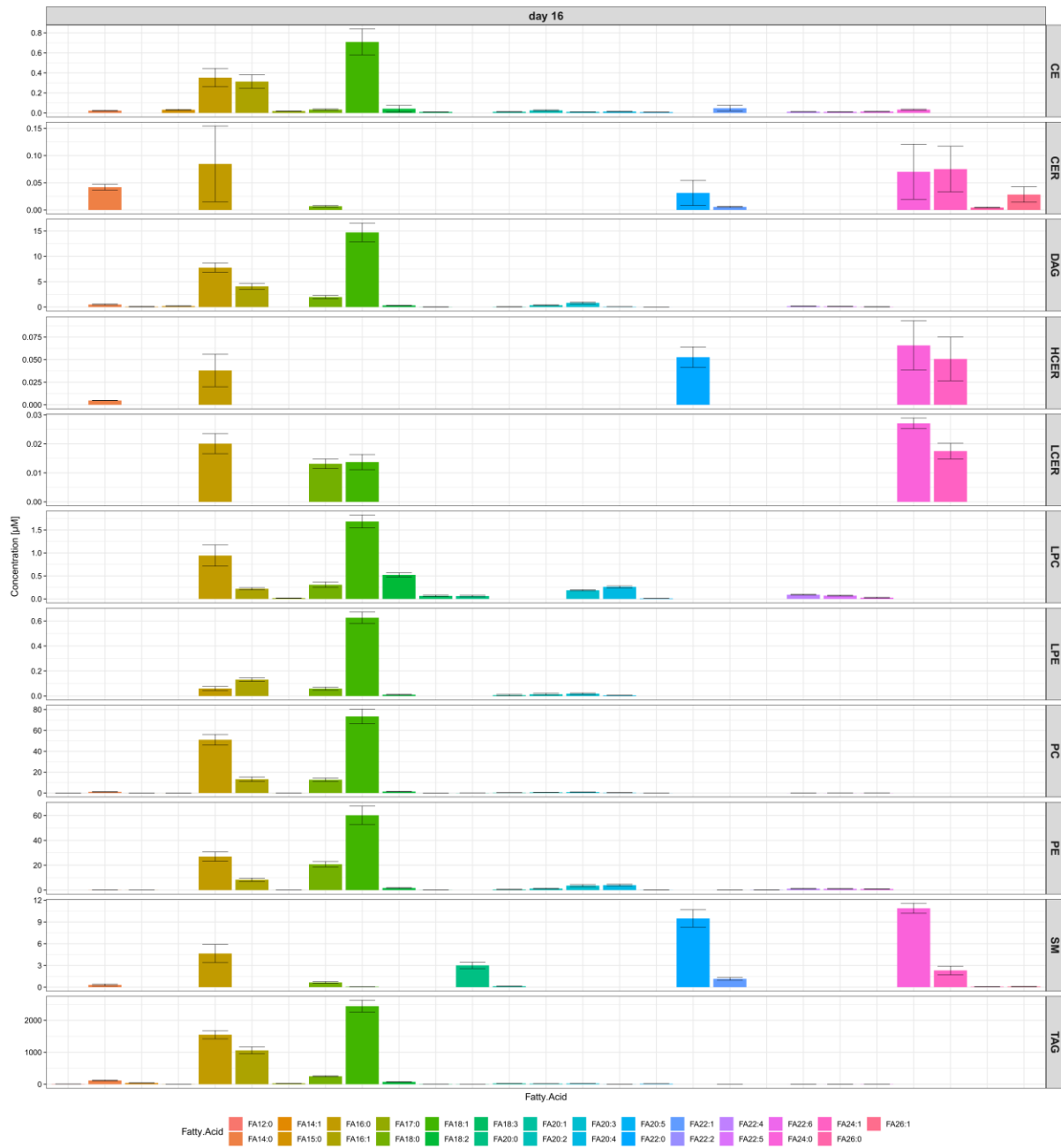


Figure 54: Fatty acid concentrations were homogenous in all lipid classes at day 16 as C16:0, C16:1, C18:0, and C18:1 were highly abundant.

Appendix

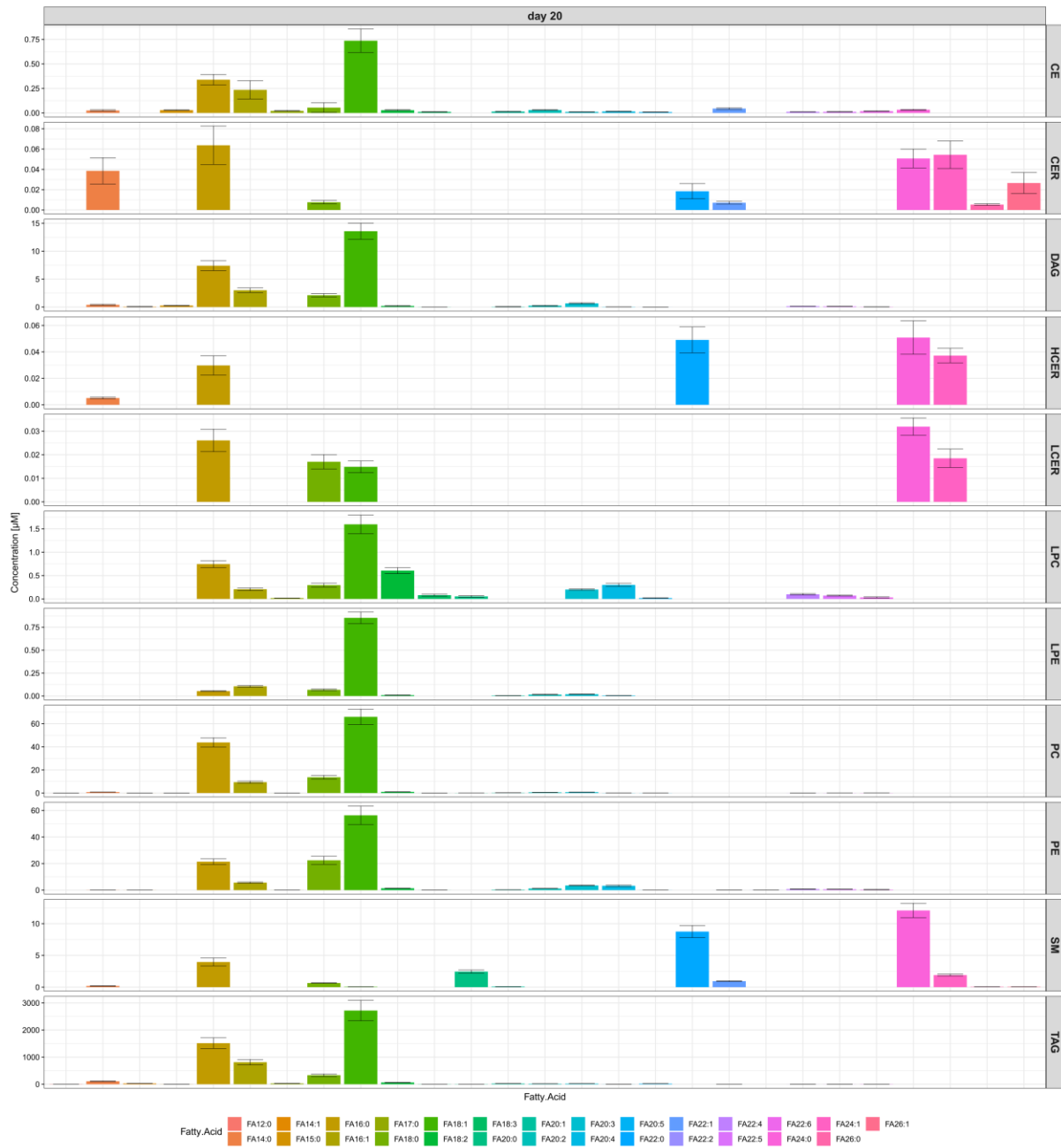


Figure 55: Fatty acid concentrations were homogenous in all lipid classes at day 20 as C16:0, C16:1, C18:0, and C18:1 were highly abundant.

Appendix

5.3. Significances of transcriptomics data

Table 16: P-adjusted values from RNA-sequencing. Transcripts are alphabetically sorted.

	day 2	day 4	day 8	day 12		day 2	day 4	day 8	day 12
AACS	1.47E-68	4.11E-187	4.71E-138	2.70E-206	GCDH	6.44E-05	7.24E-09	1.95E-32	3.20E-29
AADAT	9.34E-01	1.31E-01	1.77E-01	9.90E-01	GCK	7.13E-01	3.31E-01	5.18E-01	2.49E-02
AASS	7.07E-59	1.55E-162	1.25E-36	7.14E-24	GK	4.76E-01	3.86E-05	7.52E-01	6.84E-10
ABAT	6.58E-60	1.09E-51	4.66E-45	5.59E-02	GLB1	7.81E-08	2.96E-08	4.25E-01	7.57E-01
ACAA1	1.60E-06	9.25E-10	1.39E-168	3.95E-212	GLUD1	4.98E-05	7.04E-04	3.35E-65	2.48E-137
ACAA2	4.99E-15	7.79E-53	<1.00E-314	<1.00E-314	GLUD2	5.34E-02	5.57E-11	6.43E-39	1.04E-85
ACAD10	1.30E-11	4.24E-19	9.73E-99	1.08E-141	GOT1	4.49E-81	2.63E-64	7.52E-01	2.21E-02
ACAD11	1.30E-06	5.47E-30	2.15E-226	1.55E-261	GOT2	2.41E-41	9.12E-153	5.34E-103	8.18E-134
ACAD8	5.80E-05	6.05E-15	5.47E-169	2.88E-202	GPD2	2.17E-25	5.54E-21	7.48E-01	2.64E-08
ACAD9	7.31E-05	5.35E-02	4.03E-25	3.55E-39	GPI	5.19E-05	1.75E-04	2.19E-08	4.11E-03
ACADL	9.49E-01	1.66E-01	4.88E-12	5.06E-21	GPT	3.90E-01	1.76E-12	1.69E-20	1.37E-16
ACADM	7.79E-13	4.04E-05	<1.00E-314	<1.00E-314	GSTZ1	1.97E-01	7.91E-01	1.74E-44	3.23E-38
ACADS	8.58E-41	5.72E-58	1.05E-246	1.74E-115	HADH	1.68E-09	1.53E-213	<1.00E-314	<1.00E-314
ACADSB	1.44E-11	2.20E-36	3.75E-126	3.95E-222	HADHA	1.55E-20	3.92E-106	<1.00E-314	<1.00E-314
ACADVL	7.70E-25	1.61E-59	<1.00E-314	<1.00E-314	HADHB	1.17E-28	1.05E-127	<1.00E-314	<1.00E-314
ACAT1	7.80E-05	3.59E-02	2.29E-52	1.54E-101	HAL	7.09E-01	1.28E-01	6.40E-01	9.13E-01
ACAT2	2.96E-26	5.22E-260	<1.00E-314	<1.00E-314	HGD	1.37E-02	9.89E-04	2.32E-01	5.44E-02
ACER2	8.29E-15	2.16E-62	3.86E-62	1.05E-103	HIBADH	3.48E-03	1.23E-03	1.25E-23	6.93E-78
ACER3	4.70E-03	1.20E-56	9.21E-248	<1.00E-314	HIBCH	4.68E-01	4.95E-06	1.35E-106	9.51E-236
ACLY	1.85E-26	2.78E-220	<1.00E-314	<1.00E-314	HK1	5.19E-32	3.27E-20	8.33E-33	5.77E-73
ACO1	7.20E-05	8.00E-30	5.09E-192	<1.00E-314	HK2	9.93E-23	<1.00E-314	<1.00E-314	<1.00E-314
ACO2	4.84E-01	2.47E-16	2.87E-178	2.56E-292	HMGCLL1	9.34E-01	9.51E-01	4.51E-01	5.60E-01
ACOT2	2.71E-09	3.00E-40	<1.00E-314	<1.00E-314	HMGCS1	1.93E-52	<1.00E-314	<1.00E-314	<1.00E-314
ACOX1	5.57E-50	<1.00E-314	<1.00E-314	<1.00E-314	HMGCS2	8.40E-01	2.01E-02	1.46E-13	8.55E-19
ACOX2	4.60E-35	1.62E-62	1.42E-74	6.87E-70	HOGA1	8.54E-02	1.71E-04	7.71E-07	2.39E-05
ACOX3	7.31E-01	5.91E-01	4.88E-01	3.81E-01	HPD	5.22E-31	3.40E-51	3.55E-05	5.89E-01
ACSF3	4.06E-05	1.70E-02	2.43E-15	2.61E-11	HSD17B10	4.74E-05	3.33E-01	1.42E-87	2.84E-48
ACSL1	<1.00E-314	<1.00E-314	<1.00E-314	<1.00E-314	HSD17B12	2.31E-01	1.25E-71	<1.00E-314	<1.00E-314
ACSL3	5.82E-09	1.33E-08	1.60E-83	3.28E-255	IDH1	1.04E-71	7.02E-166	<1.00E-314	<1.00E-314
ACSL4	1.39E-08	3.94E-13	5.35E-28	1.22E-72	IDH2	4.10E-07	1.42E-33	2.51E-67	7.16E-44
ACSL5	2.04E-56	<1.00E-314	<1.00E-314	<1.00E-314	IDH3A	1.68E-15	1.47E-01	1.41E-47	8.04E-83
ACSL6	3.90E-01	3.72E-03	3.60E-12	7.59E-24	IDH3B	5.18E-06	4.92E-04	1.23E-38	1.04E-52
ACSS2	7.51E-206	<1.00E-314	<1.00E-314	<1.00E-314	IDH3G	1.47E-01	3.16E-01	9.87E-23	1.12E-06
ADH1B	<1.00E-314	<1.00E-314	<1.00E-314	<1.00E-314	IVD	2.79E-01	1.31E-09	1.31E-115	2.06E-230
ADIPOR2	7.01E-01	7.18E-15	<1.00E-314	<1.00E-314	KDSR	2.37E-01	7.52E-03	7.94E-03	2.27E-02
AGT	3.04E-03	1.06E-24	3.25E-77	6.03E-66	LDHA	1.39E-32	7.86E-51	1.27E-04	9.26E-01
AHCYL1	2.60E-22	2.03E-60	1.14E-19	6.67E-44	LDHB	6.77E-02	1.31E-26	4.30E-08	4.14E-01

Appendix

ALDH2	4.86E-32	4.24E-56	5.47E-170	3.40E-290	LPIN1	<1.00E-314	<1.00E-314	<1.00E-314	<1.00E-314
ALDH3B2	9.34E-01	1.98E-02	7.30E-26	5.21E-32	LPIN3	6.23E-19	1.85E-07	8.96E-06	4.41E-02
ALDH4A1	2.95E-20	3.24E-116	1.21E-184	2.62E-183	LPL	2.06E-31	2.28E-88	8.40E-160	4.49E-172
ALDH6A1	9.61E-70	1.56E-245	3.20E-155	4.17E-171	MAT2A	3.51E-01	2.14E-10	6.82E-01	5.57E-09
ALDH7A1	5.46E-01	2.77E-03	1.85E-21	5.67E-29	MAT2B	6.57E-04	1.64E-08	1.44E-29	1.11E-23
ALDH9A1	4.16E-02	1.12E-29	6.81E-280	<1.00E-314	MCCC1	2.40E-17	8.68E-47	1.09E-283	9.50E-265
ALDOA	1.13E-01	8.18E-01	7.76E-34	4.74E-26	MCCC2	9.34E-01	1.26E-23	3.86E-147	4.12E-178
ALDOC	1.54E-37	2.66E-69	2.27E-11	5.80E-10	MCEE	4.29E-02	1.19E-09	6.23E-02	9.47E-05
AMDHD1	7.51E-01	4.73E-01	6.47E-01	6.32E-01	MDH1	4.07E-25	3.76E-11	6.75E-275	2.56E-296
AOX1	<1.00E-314	<1.00E-314	7.24E-185	<1.00E-314	MDH2	3.23E-01	3.93E-01	1.51E-25	3.16E-08
APRT	2.20E-03	6.63E-01	8.79E-10	2.20E-02	MECR	1.96E-02	4.74E-08	2.06E-124	8.26E-167
ARG2	2.20E-06	2.18E-06	6.91E-01	4.49E-01	MINPP1	9.67E-02	5.51E-03	1.28E-08	2.21E-13
ASAH1	1.06E-45	2.99E-151	<1.00E-314	<1.00E-314	MTAP	3.51E-03	6.86E-01	3.69E-03	2.52E-05
ASAH2	1.42E-02	1.19E-01	2.54E-01	6.66E-01	MUT	1.38E-05	4.39E-29	7.70E-87	5.18E-166
ASAH2B	1.27E-04	4.26E-06	1.33E-03	2.62E-04	OAT	3.08E-21	3.46E-27	1.33E-31	1.17E-54
ASNS	6.06E-122	<1.00E-314	7.30E-127	1.99E-246	ODC1	8.13E-58	5.76E-155	3.73E-69	0.00E+00
AUH	9.17E-04	3.17E-03	9.27E-14	3.32E-35	OGDH	6.96E-15	3.80E-03	3.37E-35	2.86E-58
B4GALT6	8.71E-02	5.24E-02	2.30E-20	2.90E-42	OXCT1	3.28E-94	2.65E-139	1.64E-16	7.69E-04
BCAT2	1.52E-06	1.64E-14	3.35E-04	5.47E-01	P4HA3	1.66E-07	3.20E-11	7.71E-37	5.89E-52
BCKDHA	2.17E-06	1.16E-02	1.62E-33	4.39E-45	PAAF1	8.86E-03	4.13E-03	7.58E-03	5.71E-07
BCKDHB	5.96E-02	2.60E-30	8.11E-239	<1.00E-314	PAOX	2.13E-03	2.12E-03	2.49E-03	5.37E-04
BPGM	1.04E-20	6.94E-19	4.33E-09	6.91E-06	PC	9.71E-32	1.15E-43	3.05E-60	4.99E-83
CBS	6.42E-02	6.55E-03	1.11E-28	2.76E-81	PCCA	2.70E-21	1.21E-68	1.71E-160	3.46E-241
CCBL2	1.78E-03	5.23E-33	2.04E-76	8.78E-99	PCCB	1.50E-08	2.60E-03	2.24E-216	3.21E-250
CDIPT	2.63E-12	8.77E-09	2.69E-01	6.15E-02	PCK1	7.82E-04	7.88E-37	8.70E-64	7.28E-60
CDS2	2.90E-05	2.94E-11	3.99E-01	4.24E-06	PCK1	7.82E-04	7.88E-37	8.70E-64	7.28E-60
CEBPA	8.87E-22	3.72E-32	9.78E-44	4.99E-44	PCK2	2.55E-10	8.41E-56	3.71E-24	4.27E-17
CEPT1	1.31E-28	5.27E-53	4.41E-45	3.37E-95	PDHA1	7.89E-32	3.63E-02	<1.00E-314	<1.00E-314
CERK	7.88E-02	6.69E-01	4.36E-05	3.67E-25	PDHA1	7.89E-32	3.63E-02	<1.00E-314	<1.00E-314
CERS2	5.90E-01	7.04E-08	1.59E-03	1.54E-15	PDHB	2.94E-23	1.44E-10	2.74E-132	<1.00E-314
CERS4	NA	NA	8.04E-01	7.60E-01	PEMT	4.46E-23	7.21E-36	1.95E-36	2.48E-58
CERS5	3.65E-08	1.65E-08	2.30E-03	4.25E-02	PFKL	3.39E-04	7.68E-02	6.02E-05	5.30E-01
CERS6	7.69E-07	5.56E-21	4.83E-38	3.56E-51	PFKM	9.48E-24	1.53E-24	1.16E-73	8.77E-130
CHPT1	8.32E-02	4.31E-07	3.17E-31	3.83E-134	PFKP	9.18E-69	3.58E-247	<1.00E-314	<1.00E-314
CPT1A	8.48E-05	5.33E-73	2.53E-138	1.73E-225	PGAM1	1.89E-32	3.97E-164	1.83E-26	3.64E-68
CPT1B	9.18E-01	5.29E-01	3.74E-02	5.54E-01	PGAM2	9.34E-01	8.27E-01	1.16E-04	6.80E-07
CPT1C	1.17E-04	3.15E-04	5.69E-38	6.89E-48	PGAM4	6.53E-03	7.12E-05	9.17E-02	4.64E-01
CPT2	9.79E-01	5.07E-02	2.15E-212	<1.00E-314	PGK1	8.93E-18	6.20E-188	2.05E-40	2.35E-82
CRLS1	9.88E-05	8.95E-01	4.24E-49	1.58E-72	PGM1	3.24E-03	6.03E-01	<1.00E-314	<1.00E-314
CS	5.98E-01	1.13E-178	<1.00E-314	<1.00E-314	PGS1	1.49E-09	1.99E-01	2.66E-01	4.60E-08
CTH	8.77E-06	3.74E-21	3.95E-14	4.55E-13	PISD	3.93E-62	3.17E-159	3.05E-22	7.92E-12

Appendix

DBT	9.66E-59	1.25E-100	2.28E-106	6.74E-207	PKM	3.12E-97	<1.00E-314	<1.00E-314	<1.00E-314
DECR1	7.29E-29	1.65E-97	<1.00E-314	<1.00E-314	PPARG	2.08E-102	<1.00E-314	<1.00E-314	<1.00E-314
DEGS1	7.14E-04	2.42E-07	2.20E-07	2.40E-09	PPT1	1.00E-20	4.01E-40	5.88E-20	6.73E-28
DGKA	8.37E-08	2.98E-10	1.65E-14	7.58E-44	PRODH	4.39E-08	3.43E-22	2.02E-16	1.77E-14
DGKD	3.99E-18	1.37E-22	2.28E-28	4.91E-23	PTDSS1	4.85E-05	4.34E-12	1.24E-32	2.01E-69
DGKG	9.29E-10	2.12E-08	7.08E-07	8.71E-05	PTDSS2	7.16E-13	2.69E-07	6.21E-16	2.19E-17
DGKH	3.12E-26	1.84E-37	7.17E-37	1.14E-65	PTPLAD1	7.72E-01	2.83E-06	3.13E-01	7.12E-27
DGKI	1.59E-17	3.65E-25	4.43E-15	4.65E-14	PTPLAD2	6.04E-03	6.23E-01	5.21E-26	4.50E-28
DGKQ	2.47E-05	9.83E-02	1.33E-16	1.36E-05	PTPLB	5.57E-26	4.65E-186	2.65E-208	2.42E-278
DLAT	7.38E-01	<1.00E-314	<1.00E-314	<1.00E-314	PTPMT1	5.12E-01	5.07E-01	1.51E-07	5.42E-20
DLD	4.55E-27	2.80E-02	1.29E-133	4.85E-227	PYCR2	5.28E-03	6.15E-02	9.05E-04	3.04E-04
DLST	1.38E-01	9.24E-01	1.74E-73	4.87E-131	SAMD8	4.83E-05	1.08E-17	7.86E-01	5.04E-02
DNMT1	3.30E-66	4.90E-82	4.11E-76	1.68E-116	SAT1	2.15E-134	<1.00E-314	<1.00E-314	<1.00E-314
ECHDC1	4.85E-06	8.48E-17	<1.00E-314	<1.00E-314	SAT2	1.95E-44	3.50E-89	1.56E-14	3.80E-05
ECHDC2	7.09E-05	2.76E-12	1.24E-56	4.54E-109	SDHA	6.73E-01	2.93E-05	2.05E-99	9.15E-115
ECHDC3	1.01E-19	5.81E-106	2.92E-224	<1.00E-314	SDHB	2.52E-14	5.72E-03	2.30E-60	7.86E-78
ECHS1	8.40E-01	1.56E-17	<1.00E-314	<1.00E-314	SDHC	2.87E-02	1.01E-03	5.76E-52	1.46E-92
ECI1	2.01E-01	3.09E-01	9.32E-11	8.54E-10	SDS	2.74E-02	4.69E-05	3.63E-01	3.87E-01
EHHADH	1.00E+00	8.41E-03	3.22E-70	2.84E-123	SDSL	1.07E-05	1.64E-06	9.40E-01	5.18E-02
ELOVL1	2.40E-34	3.16E-20	8.08E-07	6.33E-04	SGMS1	2.31E-16	3.12E-28	4.42E-12	7.47E-13
ELOVL2	4.57E-24	2.19E-43	1.51E-30	7.00E-36	SGMS2	7.75E-02	9.83E-01	4.20E-09	2.78E-28
ELOVL3	4.96E-38	2.26E-37	5.39E-88	9.67E-121	SHMT1	4.31E-23	6.64E-211	<1.00E-314	<1.00E-314
ELOVL4	3.61E-07	2.65E-15	3.43E-22	7.90E-45	SLC25A20	1.46E-03	7.24E-30	<1.00E-314	<1.00E-314
ELOVL5	<1.00E-314	<1.00E-314	<1.00E-314	<1.00E-314	SMOX	1.63E-20	7.84E-02	1.03E-10	9.02E-22
ELOVL6	1.16E-28	5.23E-01	6.40E-284	<1.00E-314	SMPD1	9.51E-01	2.41E-01	1.16E-03	9.17E-17
ELOVL7	9.74E-01	4.47E-01	5.36E-01	1.09E-01	SMPD2	1.92E-02	8.85E-01	2.91E-02	7.66E-01
ENO1	3.89E-36	3.98E-186	1.44E-46	4.33E-76	SMPD4	1.79E-02	1.71E-06	7.93E-02	2.39E-03
ENO2	4.28E-06	4.87E-23	2.81E-81	2.00E-103	SMPDL3A	9.47E-47	5.49E-52	1.67E-01	5.54E-15
ENO3	6.48E-01	1.17E-01	6.27E-04	1.77E-11	SMS	3.65E-164	3.19E-282	8.01E-240	<1.00E-314
ENO4	4.97E-01	6.19E-01	9.89E-01	9.28E-01	SPTLC1	3.54E-02	6.35E-03	3.71E-05	3.74E-03
EPT1	1.93E-09	1.80E-01	1.97E-18	5.24E-19	SPTLC2	6.06E-63	9.47E-113	3.13E-130	6.71E-161
FAH	2.49E-14	1.20E-72	5.51E-121	5.32E-166	SPTLC3	2.48E-01	2.45E-02	8.26E-05	7.54E-70
FBP1	9.60E-01	8.48E-01	3.57E-01	1.10E-02	SPTSSA	4.62E-12	3.26E-42	2.44E-04	1.66E-34
FH	2.71E-65	7.82E-24	1.41E-10	3.80E-20	SRM	6.76E-05	1.92E-03	9.82E-06	2.32E-24
FTCD	1.45E-02	4.28E-01	4.42E-01	4.20E-01	SUCLA2	2.93E-09	3.16E-01	3.79E-90	5.82E-151
G6PC	4.98E-01	1.56E-02	3.78E-05	1.94E-06	SUCLG1	4.74E-13	9.42E-01	2.14E-96	1.72E-99
GALC	7.33E-01	2.27E-04	1.49E-09	3.78E-19	SUCLG2	4.61E-01	2.09E-11	6.21E-34	1.20E-66
GALM	3.22E-01	6.31E-01	6.20E-06	3.78E-26	TCER	1.40E-06	4.90E-03	5.99E-12	7.57E-11
GAPDH	5.63E-03	2.47E-56	2.22E-94	1.35E-197	TP11	4.36E-11	9.06E-144	4.91E-77	1.35E-201
GBA	1.50E-22	1.70E-46	7.40E-39	1.71E-49	UGCG	1.29E-32	3.22E-261	3.92E-177	6.86E-155
GBA2	1.53E-01	1.42E-03	9.09E-28	4.58E-10					

5.4. Publication and presentations

5.4.1. Publication

Miehle F, Möller G, Cecil A, Lintelmann J, Wabitsch M, Tokarz J, Adamski J, Haid M. Lipidomic Phenotyping Reveals Extensive Lipid Remodeling during Adipogenesis in Human Adipocytes. *Metabolites*. 2020;10(6).

5.4.2. Poster presentations

Symposium on Metabolomics and Circadian Rhythm

November 25-26, 2019, Singapore, Singapore

Florian Miehle, Mark Haid, Jerzy Adamski: *"Lipidomic Phenotyping of Human Adipogenesis with Targeted Lipidomics"*

Metabolomics 2018

June 24-28, 2018, Seattle, United States of America

Florian Miehle, Janina Tokarz, Cornelia Prehn, Gabriele Möller, Jerzy Adamski: *"Metabolic phenotyping of adipogenesis in a human cell strain"*

International Symposium on Insulin Receptor and Insulin Action (IR2017) & 5th DZD Diabetes Research School

April 19-22, 2017

Florian Miehle, Janina Tokarz, Gabriele Zieglmeier, Maria Kugler, Cornelia Prehn, Gabriele Möller, Jerzy Adamski: *"Impact of Metformin on Metabolism of Human Adipocytes during Differentiation"*

6. Reference list

1. Meldrum DR, Morris MA, Gambone JC. Obesity pandemic: causes, consequences, and solutions-but do we have the will? *Fertil Steril*. 2017;107(4):833-9.
2. Chooi YC, Ding C, Magkos F. The epidemiology of obesity. *Metabolism*. 2019;92:6-10.
3. Organization. WH. Fact sheets: Obesity and overweight 2020 [updated 1 April 2020; cited 2020 5 May]. Available from: <https://www.who.int/news-room/fact-sheets/detail/obesity-and-overweight>.
4. Global Burden of Disease Study 2015 (GBD 2015) Obesity and Overweight Prevalence 1980-2015 [Internet]. Institute for Health Metrics and Evaluation (IHME). 2015.
5. Singh GM, Danaei G, Farzadfar F, Stevens GA, Woodward M, Wormser D, et al. The age-specific quantitative effects of metabolic risk factors on cardiovascular diseases and diabetes: a pooled analysis. *PLoS One*. 2013;8(7):e65174-e.
6. Czernichow S, Kengne AP, Stamatakis E, Hamer M, Batty GD. Body mass index, waist circumference and waist-hip ratio: which is the better discriminator of cardiovascular disease mortality risk?: evidence from an individual-participant meta-analysis of 82 864 participants from nine cohort studies. *Obes Rev*. 2011;12(9):680-7.
7. Ackerman SE, Blackburn OA, Marchildon F, Cohen P. Insights into the Link Between Obesity and Cancer. *Current Obesity Reports*. 2017;6(2):195-203.
8. Calle EE, Thun MJ. Obesity and cancer. *Oncogene*. 2004;23(38):6365-78.
9. Anandacoomarasamy A, Caterson I, Sambrook P, Fransen M, March L. The impact of obesity on the musculoskeletal system. *Int J Obes (Lond)*. 2008;32(2):211-22.
10. Anstey KJ, Cherbuin N, Budge M, Young J. Body mass index in midlife and late-life as a risk factor for dementia: a meta-analysis of prospective studies. *Obes Rev*. 2011;12(5):e426-37.
11. Fontaine KR, Redden DT, Wang C, Westfall AO, Allison DB. Years of life lost due to obesity. *JAMA*. 2003;289(2):187-93.
12. Prospective Studies C. Body-mass index and cause-specific mortality in 900 000 adults: collaborative analyses of 57 prospective studies. *The Lancet*. 2009;373(9669):1083-96.
13. Berrington de Gonzalez A, Hartge P, Cerhan JR, Flint AJ, Hannan L, MacInnis RJ, et al. Body-Mass Index and Mortality among 1.46 Million White Adults. *N Engl J Med*. 2010;363(23):2211-9.
14. von Lengerke T, Krauth C. Economic costs of adult obesity: A review of recent European studies with a focus on subgroup-specific costs. *Maturitas*. 2011;69(3):220-9.
15. Kim DD, Basu A. Estimating the Medical Care Costs of Obesity in the United States: Systematic Review, Meta-Analysis, and Empirical Analysis. *Value Health*. 2016;19(5):602-13.
16. (CDC) CfDCaP. Adult Obesity Causes & Consequences 2020 [27.06.2020]. Available from: <https://www.cdc.gov/obesity/adult/causes.html>.
17. Swinburn BA, Sacks G, Hall KD, McPherson K, Finegood DT, Moodie ML, et al. The global obesity pandemic: shaped by global drivers and local environments. *The Lancet*. 2011;378(9793):804-14.
18. Joslin's Diabetes Mellitus 2004.
19. Kwok KHM, Lam KSL, Xu A. Heterogeneity of white adipose tissue: molecular basis and clinical implications. *Exp Mol Med*. 2016;48(3):e215-e.
20. Ruiz-Ojeda FJ, Ruperez AI, Gomez-Llorente C, Gil A, Aguilera CM. Cell Models and Their Application for Studying Adipogenic Differentiation in Relation to Obesity: A Review. *Int J Mol Sci*. 2016;17(7).
21. Gregoire FM, Smas CM, Sul HS. Understanding adipocyte differentiation. *Physiol Rev*. 1998;78(3):783-809.
22. Miehle F, Möller G, Cecil A, Lintelmann J, Wabitsch M, Tokarz J, et al. Lipidomic Phenotyping Reveals Extensive Lipid Remodeling during Adipogenesis in Human Adipocytes. *Metabolites*. 2020;10(6).
23. Ali AT, Hochfeld WE, Myburgh R, Pepper MS. Adipocyte and adipogenesis. *Eur J Cell Biol*. 2013;92(6-7):229-36.
24. Lefterova MI, Lazar MA. New developments in adipogenesis. *Trends Endocrinol Metab*. 2009;20(3):107-14.
25. Trayhurn P. Endocrine and signalling role of adipose tissue: new perspectives on fat. *Acta Physiol Scand*. 2005;184(4):285-93.
26. Farmer SR. Molecular determinants of brown adipocyte formation and function. *Genes Dev*. 2008;22(10):1269-75.
27. Cohade C, Osman M, Pannu HK, Wahl RL. Uptake in supraclavicular area fat ("USA-Fat"): description on 18F-FDG PET/CT. *J Nucl Med*. 2003;44(2):170-6.

Reference list

28. Yeung HW, Grewal RK, Gonen M, Schöder H, Larson SM. Patterns of (18)F-FDG uptake in adipose tissue and muscle: a potential source of false-positives for PET. *J Nucl Med.* 2003;44(11):1789-96.
29. van Marken Lichtenbelt WD, Vanhommerig JW, Smulders NM, Drossaerts JM, Kemerink GJ, Bouvy ND, et al. Cold-activated brown adipose tissue in healthy men. *N Engl J Med.* 2009;360(15):1500-8.
30. Leitner BP, Huang S, Brychta RJ, Duckworth CJ, Baskin AS, McGehee S, et al. Mapping of human brown adipose tissue in lean and obese young men. *Proc Natl Acad Sci U S A.* 2017;114(32):8649-54.
31. Harms M, Seale P. Brown and beige fat: development, function and therapeutic potential. *Nat Med.* 2013;19(10):1252-63.
32. Luong Q, Huang J, Lee KY. Deciphering White Adipose Tissue Heterogeneity. *Biology (Basel).* 2019;8(2):23.
33. Mulya A, Kirwan JP. Brown and Beige Adipose Tissue: Therapy for Obesity and Its Comorbidities? *Endocrinol Metab Clin North Am.* 2016;45(3):605-21.
34. Rosen ED, Sarraf P, Troy AE, Bradwin G, Moore K, Milstone DS, et al. PPAR gamma is required for the differentiation of adipose tissue in vivo and in vitro. *Mol Cell.* 1999;4(4):611-7.
35. Farmer SR. Transcriptional control of adipocyte formation. *Cell Metab.* 2006;4(4):263-73.
36. Fajas L, Auboeuf D, Raspé E, Schoonjans K, Lefebvre A-M, Saladin R, et al. The Organization, Promoter Analysis, and Expression of the Human PPAR γ Gene. *J Biol Chem.* 1997;272(30):18779-89.
37. Tontonoz P, Hu E, Graves RA, Budavari AI, Spiegelman BM. mPPAR gamma 2: tissue-specific regulator of an adipocyte enhancer. *Genes Dev.* 1994;8(10):1224-34.
38. Hu E, Tontonoz P, Spiegelman BM. Transdifferentiation of myoblasts by the adipogenic transcription factors PPAR gamma and C/EBP alpha. *Proc Natl Acad Sci U S A.* 1995;92(21):9856-60.
39. Tontonoz P, Spiegelman BM. Fat and Beyond: The Diverse Biology of PPAR γ . *Annu Rev Biochem.* 2008;77(1):289-312.
40. Zhu Y, Qi C, Korenberg JR, Chen XN, Noya D, Rao MS, et al. Structural organization of mouse peroxisome proliferator-activated receptor gamma (mPPAR gamma) gene: alternative promoter use and different splicing yield two mPPAR gamma isoforms. *Proc Natl Acad Sci U S A.* 1995;92(17):7921-5.
41. Tontonoz P, Spiegelman BM. Fat and beyond: the diverse biology of PPARgamma. *Annu Rev Biochem.* 2008;77:289-312.
42. Barak Y, Nelson MC, Ong ES, Jones YZ, Ruiz-Lozano P, Chien KR, et al. PPAR gamma is required for placental, cardiac, and adipose tissue development. *Mol Cell.* 1999;4(4):585-95.
43. Shekelle RB, Missell L, Paul O, Shryock AM, Stamler J, Vollset SE, et al. Fish consumption and mortality from coronary heart disease. *N Engl J Med.* 1985;313(13):820-4.
44. Neschen S, Morino K, Dong J, Wang-Fischer Y, Cline GW, Romanelli AJ, et al. n-3 Fatty acids preserve insulin sensitivity in vivo in a peroxisome proliferator-activated receptor-alpha-dependent manner. *Diabetes.* 2007;56(4):1034-41.
45. Krey G, Braissant O, L'Horsset F, Kalkhoven E, Perroud M, Parker MG, et al. Fatty acids, eicosanoids, and hypolipidemic agents identified as ligands of peroxisome proliferator-activated receptors by coactivator-dependent receptor ligand assay. *Mol Endocrinol.* 1997;11(6):779-91.
46. Taniguchi A, Fukushima M, Sakai M, Tokuyama K, Nagata I, Fukunaga A, et al. Effects of bezafibrate on insulin sensitivity and insulin secretion in non-obese Japanese type 2 diabetic patients. *Metabolism - Clinical and Experimental.* 2001;50(4):477-80.
47. BAKRIS GL, DOLE JF, PORTER LE, HUANG C, FREED MI. Rosiglitazone improves blood pressure in patients with type 2 diabetes mellitus. *Diabetes.* 2000;49(5):A96-A.
48. Nakamura T, Ushiyama C, Shimada N, Hayashi K, Ebihara I, Koide H. Comparative effects of pioglitazone, glibenclamide, and voglibose on urinary endothelin-1 and albumin excretion in diabetes patients. *J Diabetes Complications.* 2000;14(5):250-4.
49. Willson TM, Brown PJ, Sternbach DD, Henke BR. The PPARs: from orphan receptors to drug discovery. *J Med Chem.* 2000;43(4):527-50.
50. Adams M, Reginato MJ, Shao D, Lazar MA, Chatterjee VK. Transcriptional activation by peroxisome proliferator-activated receptor gamma is inhibited by phosphorylation at a consensus mitogen-activated protein kinase site. *J Biol Chem.* 1997;272(8):5128-32.
51. Floyd ZE, Stephens JM. Interferon-gamma-mediated activation and ubiquitin-proteasome-dependent degradation of PPARgamma in adipocytes. *J Biol Chem.* 2002;277(6):4062-8.
52. Floyd ZE, Stephens JM. Control of peroxisome proliferator-activated receptor gamma2 stability and activity by SUMOylation. *Obes Res.* 2004;12(6):921-8.

Reference list

53. Qiang L, Wang L, Kon N, Zhao W, Lee S, Zhang Y, et al. Brown remodeling of white adipose tissue by SirT1-dependent deacetylation of Ppar γ . *Cell*. 2012;150(3):620-32.
54. Mota de Sá P, Richard AJ, Hang H, Stephens JM. Transcriptional Regulation of Adipogenesis. *Compr Physiol*. 2017;7(2):635-74.
55. Otto TC, Lane MD. Adipose Development: From Stem Cell to Adipocyte. *Crit Rev Biochem Mol Biol*. 2005;40(4):229-42.
56. Vinson CR, Sigler PB, McKnight SL. Scissors-grip model for DNA recognition by a family of leucine zipper proteins. *Science*. 1989;246(4932):911-6.
57. Yu H, He K, Wang L, Hu J, Gu J, Zhou C, et al. Stk40 represses adipogenesis through translational control of CCAAT/enhancer-binding proteins. *J Cell Sci*. 2015;128(15):2881.
58. Wang ND, Finegold MJ, Bradley A, Ou CN, Abdelsayed SV, Wilde MD, et al. Impaired energy homeostasis in C/EBP alpha knockout mice. *Science*. 1995;269(5227):1108-12.
59. Linhart HG, Ishimura-Oka K, DeMayo F, Kibe T, Repka D, Poindexter B, et al. C/EBPalpha is required for differentiation of white, but not brown, adipose tissue. *Proc Natl Acad Sci U S A*. 2001;98(22):12532-7.
60. Yang J, Croniger CM, Lekstrom-Himes J, Zhang P, Fenyus M, Tenen DG, et al. Metabolic Response of Mice to a Postnatal Ablation of CCAAT/Enhancer-binding Protein α . *J Biol Chem*. 2005;280(46):38689-99.
61. Tanaka T, Yoshida N, Kishimoto T, Akira S. Defective adipocyte differentiation in mice lacking the C/EBPbeta and/or C/EBPdelta gene. *The EMBO journal*. 1997;16(24):7432-43.
62. Cao Z, Umek RM, McKnight SL. Regulated expression of three C/EBP isoforms during adipose conversion of 3T3-L1 cells. *Genes Dev*. 1991;5(9):1538-52.
63. Yeh WC, Cao Z, Classon M, McKnight SL. Cascade regulation of terminal adipocyte differentiation by three members of the C/EBP family of leucine zipper proteins. *Genes Dev*. 1995;9(2):168-81.
64. Rosen ED, Hsu CH, Wang X, Sakai S, Freeman MW, Gonzalez FJ, et al. C/EBPalpha induces adipogenesis through PPARgamma: a unified pathway. *Genes Dev*. 2002;16(1):22-6.
65. Wu Z, Rosen ED, Brun R, Hauser S, Adelmant G, Troy AE, et al. Cross-regulation of C/EBP alpha and PPAR gamma controls the transcriptional pathway of adipogenesis and insulin sensitivity. *Mol Cell*. 1999;3(2):151-8.
66. Price TM, O'Brien SN. Determination of estrogen receptor messenger ribonucleic acid (mRNA) and cytochrome P450 aromatase mRNA levels in adipocytes and adipose stromal cells by competitive polymerase chain reaction amplification. *J Clin Endocrinol Metab*. 1993;77(4):1041-5.
67. Crandall DL, Busler DE, Novak TJ, Weber RV, Kral JG. Identification of estrogen receptor beta RNA in human breast and abdominal subcutaneous adipose tissue. *Biochem Biophys Res Commun*. 1998;248(3):523-6.
68. Jeong S, Yoon M. 17 β -Estradiol inhibition of PPAR γ -induced adipogenesis and adipocyte-specific gene expression. *Acta Pharmacol Sin*. 2011;32(2):230-8.
69. Okazaki R, Inoue D, Shibata M, Saika M, Kido S, Ooka H, et al. Estrogen promotes early osteoblast differentiation and inhibits adipocyte differentiation in mouse bone marrow stromal cell lines that express estrogen receptor (ER) alpha or beta. *Endocrinology*. 2002;143(6):2349-56.
70. Brenner S, Bercovich Z, Feiler Y, Keshet R, Kahana C. Dual Regulatory Role of Polyamines in Adipogenesis. *J Biol Chem*. 2015;290(45):27384-92.
71. Ishii I, Ikeguchi Y, Mano H, Wada M, Pegg AE, Shirahata A. Polyamine metabolism is involved in adipogenesis of 3T3-L1 cells. *Amino Acids*. 2012;42(2-3):619-26.
72. Pegg AE. Mammalian polyamine metabolism and function. *IUBMB Life*. 2009;61(9):880-94.
73. Pegg AE, Casero RA, Jr. Current status of the polyamine research field. *Methods Mol Biol*. 2011;720:3-35.
74. Terui Y, Yoshida T, Sakamoto A, Saito D, Oshima T, Kawazoe M, et al. Polyamines protect nucleic acids against depurination. *Int J Biochem Cell Biol*. 2018;99:147-53.
75. Kurata HT, Akrouh A, Li JB, Marton LJ, Nichols CG. Scanning the topography of polyamine blocker binding in an inwardly rectifying potassium channel. *J Biol Chem*. 2013;288(9):6591-601.
76. Rao JN, Rathor N, Zhuang R, Zou T, Liu L, Xiao L, et al. Polyamines regulate intestinal epithelial restitution through TRPC1-mediated Ca(2)+ signaling by differentially modulating STIM1 and STIM2. *Am J Physiol Cell Physiol*. 2012;303(3):C308-17.
77. Casero RA, Murray Stewart T, Pegg AE. Polyamine metabolism and cancer: treatments, challenges and opportunities. *Nature Reviews Cancer*. 2018;18(11):681-95.
78. Rodbell M. METABOLISM OF ISOLATED FAT CELLS. I. EFFECTS OF HORMONES ON GLUCOSE METABOLISM AND LIPOLYSIS. *J Biol Chem*. 1964;239:375-80.

Reference list

79. Green H, Meuth M. An established pre-adipose cell line and its differentiation in culture. *Cell*. 1974;3(2):127-33.
80. Green H, Kehinde O. An established preadipose cell line and its differentiation in culture. II. Factors affecting the adipose conversion. *Cell*. 1975;5(1):19-27.
81. Kuri-Harcuch W, Green H. Increasing activity of enzymes on pathway of triacylglycerol synthesis during adipose conversion of 3T3 cells. *J Biol Chem*. 1977;252(6):2158-60.
82. Kaur G, Dufour JM. Cell lines: Valuable tools or useless artifacts. *Spermatogenesis*. 2012;2(1):1-5.
83. Todaro GJ, Green H. Quantitative studies of the growth of mouse embryo cells in culture and their development into established lines. *J Cell Biol*. 1963;17(2):299-313.
84. Soukas A, Socci ND, Saatkamp BD, Novelli S, Friedman JM. Distinct transcriptional profiles of adipogenesis in vivo and in vitro. *J Biol Chem*. 2001;276(36):34167-74.
85. GREGOIRE FM, SMAS CM, SUL HS. Understanding Adipocyte Differentiation. *Physiol Rev*. 1998;78(3):783-809.
86. Rentsch J, Chiesi M. Regulation of ob gene mRNA levels in cultured adipocytes. *FEBS Lett*. 1996;379(1):55-9.
87. Reznikoff CA, Brankow DW, Heidelberger C. Establishment and characterization of a cloned line of C3H mouse embryo cells sensitive to postconfluence inhibition of division. *Cancer Res*. 1973;33(12):3231-8.
88. Yamaguchi A, Komori T, Suda T. Regulation of osteoblast differentiation mediated by bone morphogenetic proteins, hedgehogs, and Cbfa1. *Endocr Rev*. 2000;21(4):393-411.
89. Wolins NE, Quaynor BK, Skinner JR, Tzekov A, Park C, Choi K, et al. OP9 mouse stromal cells rapidly differentiate into adipocytes: characterization of a useful new model of adipogenesis. *J Lipid Res*. 2006;47(2):450-60.
90. Pang W, Wang Y, Wei N, Xu R, Xiong Y, Wang P, et al. Sirt1 inhibits akt2-mediated porcine adipogenesis potentially by direct protein-protein interaction. *PLoS One*. 2013;8(8):e71576.
91. Cheng J, Song ZY, Pu L, Yang H, Zheng JM, Zhang ZY, et al. Retinol binding protein 4 affects the adipogenesis of porcine preadipocytes through insulin signaling pathways. *Biochem Cell Biol*. 2013;91(4):236-43.
92. Pang WJ, Wei N, Wang Y, Xiong Y, Chen FF, Wu WJ, et al. Obese and lean porcine difference of FoxO1 and its regulation through C/EBP β and PI3K/GSK3 β signaling pathway. *J Anim Sci*. 2014;92(5):1968-79.
93. Ji HL, Song CC, Li YF, He JJ, Li YL, Zheng XL, et al. miR-125a inhibits porcine preadipocytes differentiation by targeting ERR α . *Mol Cell Biochem*. 2014;395(1-2):155-65.
94. Shi XE, Li YF, Jia L, Ji HL, Song ZY, Cheng J, et al. MicroRNA-199a-5p affects porcine preadipocyte proliferation and differentiation. *Int J Mol Sci*. 2014;15(5):8526-38.
95. Esteve Ràfols M. Adipose tissue: cell heterogeneity and functional diversity. *Endocrinol Nutr*. 2014;61(2):100-12.
96. Clark ER, Clark EL. Microscopic studies of the new formation of fat in living adult rabbits. *Am J Anat*. 1940;67(2):255-85.
97. Cawthorn WP, Scheller EL, MacDougald OA. Adipose tissue stem cells meet preadipocyte commitment: going back to the future. *J Lipid Res*. 2012;53(2):227-46.
98. Lee MJ, Fried SK. Optimal protocol for the differentiation and metabolic analysis of human adipose stromal cells. *Methods Enzymol*. 2014;538:49-65.
99. Bunnell BA, Flaatt M, Gagliardi C, Patel B, Ripoll C. Adipose-derived stem cells: isolation, expansion and differentiation. *Methods*. 2008;45(2):115-20.
100. Lessard J, Laforest S, Pelletier M, Leboeuf M, Blackburn L, Tchernof A. Low abdominal subcutaneous preadipocyte adipogenesis is associated with visceral obesity, visceral adipocyte hypertrophy, and a dysmetabolic state. *Adipocyte*. 2014;3(3):197-205.
101. Michaud A, Lacroix-Pépin N, Pelletier M, Daris M, Biertho L, Fortier MA, et al. Expression of genes related to prostaglandin synthesis or signaling in human subcutaneous and omental adipose tissue: depot differences and modulation by adipogenesis. *Mediators Inflamm*. 2014;2014:451620.
102. Wabitsch M, Brüderlein S, Melzner I, Braun M, Mechttersheimer G, Möller P. LiSa-2, a novel human liposarcoma cell line with a high capacity for terminal adipose differentiation. *Int J Cancer*. 2000;88(6):889-94.
103. Wabitsch M, Brenner RE, Melzner I, Braun M, Möller P, Heinze E, et al. Characterization of a human preadipocyte cell strain with high capacity for adipose differentiation. *Int J Obes*. 2001;25(1):8-15.
104. van Beek EA, Bakker AH, Kruyt PM, Vink C, Saris WH, Franssen-van Hal NL, et al. Comparative expression analysis of isolated human adipocytes and the human adipose cell lines LiSa-2 and PAZ6. *Int J Obes (Lond)*. 2008;32(6):912-21.
105. Zhang K, Chu K, Wu X, Gao H, Wang J, Yuan YC, et al. Amplification of FRS2 and activation of FGFR/FRS2 signaling pathway in high-grade liposarcoma. *Cancer Res*. 2013;73(4):1298-307.

Reference list

106. Straub BK, Witzel HR, Pawella LM, Renner M, Eiteneuer E, Hashani M, et al. Perilipin 1 Expression Differentiates Liposarcoma from Other Types of Soft Tissue Sarcoma. *Am J Pathol.* 2019;189(8):1547-58.
107. Simpson JL, Landey S, New M, German J. A previously unrecognized X-linked syndrome of dysmorphia. *Birth Defects Orig Artic Ser.* 1975;11(2):18-24.
108. Golabi M, Rosen L. A new X-linked mental retardation-overgrowth syndrome. *Am J Med Genet.* 1984;17(1):345-58.
109. Behmel A, Plöchl E, Rosenkranz W. A new X-linked dysplasia gigantism syndrome: identical with the Simpson dysplasia syndrome? *Hum Genet.* 1984;67(4):409-13.
110. DeBaun MR, Ess J, Saunders S. Simpson Golabi Behmel syndrome: progress toward understanding the molecular basis for overgrowth, malformation, and cancer predisposition. *Mol Genet Metab.* 2001;72(4):279-86.
111. Klusóczyki Á, Veréb Z, Vámos A, Fischer-Posovszky P, Wabitsch M, Bacso Z, et al. Differentiating SGBS adipocytes respond to PPAR γ stimulation, irisin and BMP7 by functional browning and beige characteristics. *Sci Rep.* 2019;9(1):5823.
112. Halbgebauer D, Dahlhaus M, Wabitsch M, Fischer-Posovszky P, Tews D. Browning capabilities of human primary adipose-derived stromal cells compared to SGBS cells. *Sci Rep.* 2020;10(1):9632.
113. Yeo CR, Agrawal M, Hoon S, Shabbir A, Shrivastava MK, Huang S, et al. SGBS cells as a model of human adipocyte browning: A comprehensive comparative study with primary human white subcutaneous adipocytes. *Sci Rep.* 2017;7(1):4031.
114. Tews D, Fromme T, Keuper M, Hofmann SM, Debatin KM, Klingenspor M, et al. Teneurin-2 (TENM2) deficiency induces UCP1 expression in differentiating human fat cells. *Mol Cell Endocrinol.* 2017;443:106-13.
115. Venes D. *Taber's Cyclopedic Medical Dictionary.* 23 ed: F.A. Davis Company; 2017.
116. Williams. *Individual metabolic patterns and human disease : an exploratory study utilizing predominantly paper chromatographic methods:* The University of Texas Publication; 1951.
117. Horning EC, Horning MG. *Metabolic profiles: gas-phase methods for analysis of metabolites.* *Clin Chem.* 1971;17(8):802-9.
118. Mamer OA, Crawhall JC, Tjoa SS. The identification of urinary acids by coupled gas chromatography-mass spectrometry. *Clin Chim Acta.* 1971;32(2):171-84.
119. Kimble BJ, Cox RE, McPherron RV, Olsen RW, Roitman E, Walls FC, et al. Real-time gas chromatography/high resolution mass spectrometry and its application to the analysis of physiological fluids. *J Chromatogr Sci.* 1974;12(11):647-55.
120. Jellum E. Profiling of human body fluids in healthy and diseased states using gas chromatography and mass spectrometry, with special reference to organic acids. *J Chromatogr.* 1977;143(5):427-62.
121. Gates SC, Sweeley CC. Quantitative metabolic profiling based on gas chromatography. *Clin Chem.* 1978;24(10):1663-73.
122. Makarov A. Electrostatic Axially Harmonic Orbital Trapping: A High-Performance Technique of Mass Analysis. *Anal Chem.* 2000;72(6):1156-62.
123. Hu Q, Noll RJ, Li H, Makarov A, Hardman M, Graham Cooks R. The Orbitrap: a new mass spectrometer. *J Mass Spectrom.* 2005;40(4):430-43.
124. Vestal ML, Campbell JM. *Tandem Time-of-Flight Mass Spectrometry.* *Methods Enzymol.* 402: Academic Press; 2005. p. 79-108.
125. Wenk MR. The emerging field of lipidomics. *Nat Rev Drug Discov.* 2005;4(7):594-610.
126. Adamski J. Genome-wide association studies with metabolomics. *Genome Med.* 2012;4(4):34.
127. Gertsman I, Barshop BA. Promises and pitfalls of untargeted metabolomics. *J Inherit Metab Dis.* 2018;41(3):355-66.
128. Roberts LD, Souza AL, Gerszten RE, Clish CB. Targeted metabolomics. *Curr Protoc Mol Biol.* 2012;Chapter 30:Unit30.2-.2.24.
129. US FDA D. *Bioanalytical method validation guidance for industry.* 2018.
130. Agency E. *Guideline on bioanalytical method validation.* Committee for Medicinal Products for Human Use (EMA/CHMP/EWP/192217/2009). 2011.
131. Fiehn O, Robertson D, Griffin J, van der Werf M, Nikolau B, Morrison N, et al. The metabolomics standards initiative (MSI). *Metabolomics.* 2007;3(3):175-8.
132. Liebisch G, Vizcaíno JA, Köfeler H, Trötz Müller M, Griffiths WJ, Schmitz G, et al. Shorthand notation for lipid structures derived from mass spectrometry. *J Lipid Res.* 2013;54(6):1523-30.

Reference list

133. Liebisch G, Ekroos K, Hermansson M, Ejsing CS. Reporting of lipidomics data should be standardized. *Biochim Biophys Acta Mol Cell Biol Lipids*. 2017;1862(8):747-51.
134. Cuperlovic-Culf M, Barnett DA, Culf AS, Chute I. Cell culture metabolomics: applications and future directions. *Drug Discov Today*. 2010;15(15-16):610-21.
135. Muschet C, Moller G, Prehn C, de Angelis MH, Adamski J, Tokarz J. Removing the bottlenecks of cell culture metabolomics: fast normalization procedure, correlation of metabolites to cell number, and impact of the cell harvesting method. *Metabolomics*. 2016;12(10):151.
136. Bordag N, Janakiraman V, Nachtigall J, González Maldonado S, Bethan B, Laine J-P, et al. Fast Filtration of Bacterial or Mammalian Suspension Cell Cultures for Optimal Metabolomics Results. *PLoS One*. 2016;11(7):e0159389-e.
137. Silva LP, Lorenzi PL, Purwaha P, Yong V, Hawke DH, Weinstein JN. Measurement of DNA concentration as a normalization strategy for metabolomic data from adherent cell lines. *Anal Chem*. 2013;85(20):9536-42.
138. Teng Q, Huang W, Collette TW, Ekman DR, Tan C. A direct cell quenching method for cell-culture based metabolomics. *Metabolomics*. 2008;5(2):199.
139. Cao B, Aa J, Wang G, Wu X, Liu L, Li M, et al. GC-TOFMS analysis of metabolites in adherent MDCK cells and a novel strategy for identifying intracellular metabolic markers for use as cell amount indicators in data normalization. *Anal Bioanal Chem*. 2011;400(9):2983-93.
140. Haid M, Muschet C, Wahl S, Römisch-Margl W, Prehn C, Möller G, et al. Long-Term Stability of Human Plasma Metabolites during Storage at -80 ° C. *J Proteome Res*. 2018;17(1):203-11.
141. Piétu G, Mariage-Samson R, Fayein NA, Matingou C, Eveno E, Houlgatte R, et al. The Genexpress IMAGE knowledge base of the human brain transcriptome: a prototype integrated resource for functional and computational genomics. *Genome Res*. 1999;9(2):195-209.
142. Velculescu VE, Zhang L, Zhou W, Vogelstein J, Basrai MA, Bassett DE, Jr., et al. Characterization of the Yeast Transcriptome. *Cell*. 1997;88(2):243-51.
143. Velculescu VE, Zhang L, Vogelstein B, Kinzler KW. Serial Analysis of Gene Expression. *Science*. 1995;270(5235):484.
144. Galhardo M, Sinkkonen L, Berninger P, Lin J, Sauter T, Heinaniemi M. Integrated analysis of transcript-level regulation of metabolism reveals disease-relevant nodes of the human metabolic network. *Nucleic Acids Res*. 2014;42(3):1474-96.
145. Galhardo M, Sinkkonen L, Berninger P, Lin J, Sauter T, Heinaniemi M. Transcriptomics profiling of human SGBS adipogenesis. *Genom Data*. 2014;2:246-8.
146. Halama A, Horsch M, Kastenmuller G, Moller G, Kumar P, Prehn C, et al. Metabolic switch during adipogenesis: From branched chain amino acid catabolism to lipid synthesis. *Arch Biochem Biophys*. 2016;589:93-107.
147. Kiss T. Small nucleolar RNA-guided post-transcriptional modification of cellular RNAs. *The EMBO Journal*. 2001;20(14):3617-22.
148. Marzluff WF, Wagner EJ, Duronio RJ. Metabolism and regulation of canonical histone mRNAs: life without a poly(A) tail. *Nat Rev Genet*. 2008;9(11):843-54.
149. Roberts LD, Virtue S, Vidal-Puig A, Nicholls AW, Griffin JL. Metabolic phenotyping of a model of adipocyte differentiation. *Physiol Genomics*. 2009;39(2):109-19.
150. Kirkwood JS, Miranda CL, Bobe G, Maier CS, Stevens JF. 18O-Tracer Metabolomics Reveals Protein Turnover and CDP-Choline Cycle Activity in Differentiating 3T3-L1 Pre-Adipocytes. *PLoS One*. 2016;11(6):e0157118.
151. Green CR, Wallace M, Divakaruni AS, Phillips SA, Murphy AN, Ciaraldi TP, et al. Branched-chain amino acid catabolism fuels adipocyte differentiation and lipogenesis. *Nat Chem Biol*. 2016;12(1):15-21.
152. Collins JM, Neville MJ, Pinnick KE, Hodson L, Ruyter B, van Dijk TH, et al. De novo lipogenesis in the differentiating human adipocyte can provide all fatty acids necessary for maturation. *J Lipid Res*. 2011;52(9):1683-92.
153. Wu J, Boström P, Sparks Lauren M, Ye L, Choi Jang H, Giang A-H, et al. Beige Adipocytes Are a Distinct Type of Thermogenic Fat Cell in Mouse and Human. *Cell*. 2012;150(2):366-76.
154. Liaw L, Prudovsky I, Koza RA, Anunciado-Koza RV, Siviski ME, Lindner V, et al. Lipid Profiling of In Vitro Cell Models of Adipogenic Differentiation: Relationships With Mouse Adipose Tissues. *J Cell Biochem*. 2016;117(9):2182-93.
155. Moreno-Navarrete JM, Jove M, Ortega F, Xifra G, Ricart W, Obis E, et al. Metabolomics uncovers the role of adipose tissue PDXK in adipogenesis and systemic insulin sensitivity. *Diabetologia*. 2016;59(4):822-32.
156. Chong J, Soufan O, Li C, Caraus I, Li S, Bourque G, et al. MetaboAnalyst 4.0: towards more transparent and integrative metabolomics analysis. *Nucleic Acids Res*. 2018;46(W1):W486-W94.

Reference list

157. R Core Team. R: A language and environment for statistical computing. R Foundation for Statistical Computing; 2014.
158. Ye J, Coulouris G, Zaretskaya I, Cutcutache I, Rozen S, Madden TL. Primer-BLAST: a tool to design target-specific primers for polymerase chain reaction. *BMC Bioinformatics*. 2012;13:134.
159. Fischer-Posovszky P, Newell FS, Wabitsch M, Tornqvist HE. Human SGBS cells - a unique tool for studies of human fat cell biology. *Obes Facts*. 2008;1(4):184-9.
160. Muschet C. Molecular impact of metformin on hepatocellular metabolism: Technische Universität München; 2016.
161. Untergasser A, Cutcutache I, Koressaar T, Ye J, Faircloth BC, Remm M, et al. Primer3--new capabilities and interfaces. *Nucleic Acids Res*. 2012;40(15):e115-e.
162. Pfaffl MW. A new mathematical model for relative quantification in real-time RT-PCR. *Nucleic Acids Res*. 2001;29(9):e45.
163. Matyash V, Liebisch G, Kurzchalia TV, Shevchenko A, Schwudke D. Lipid extraction by methyl-tert-butyl ether for high-throughput lipidomics. *J Lipid Res*. 2008;49(5):1137-46.
164. Franko A, Merkel D, Kovarova M, Hoene M, Jaghutriz BA, Heni M, et al. Dissociation of Fatty Liver and Insulin Resistance in I148M PNPLA3 Carriers: Differences in Diacylglycerol (DAG) FA18:1 Lipid Species as a Possible Explanation. *Nutrients*. 2018;10(9).
165. Vitello DJ, Ripper RM, Fettiplace MR, Weinberg GL, Vitello JM. Blood Density Is Nearly Equal to Water Density: A Validation Study of the Gravimetric Method of Measuring Intraoperative Blood Loss. *J Vet Med*. 2015;2015:152730.
166. Zukunft S, Sorgenfrei M, Prehn C, Möller G, Adamski J. Targeted Metabolomics of Dried Blood Spot Extracts. *Chromatographia*. 2013;76(19):1295-305.
167. Zukunft S, Prehn C, Rohring C, Moller G, Hrabe de Angelis M, Adamski J, et al. High-throughput extraction and quantification method for targeted metabolomics in murine tissues. *Metabolomics*. 2018;14(1):18.
168. Halama A, Möller G, Adamski J. Metabolic Signatures in Apoptotic Human Cancer Cell Lines. *OMICS*. 2011;15(5):325-35.
169. Haimerl P, Bernhardt U, Schindela S, Henkel F, Lechner A, Zissler UM, et al. Inflammatory macrophage memory in nonsteroidal anti-inflammatory drug-exacerbated respiratory disease. *J Allergy Clin Immunol*. 2020.
170. Breuninger TA, Wawro N, Meisinger C, Artati A, Adamski J, Peters A, et al. Associations between fecal bile acids, neutral sterols, and serum lipids in the KORA FF4 study. *Atherosclerosis*. 2019;288:1-8.
171. Dobin A, Davis CA, Schlesinger F, Drenkow J, Zaleski C, Jha S, et al. STAR: ultrafast universal RNA-seq aligner. *Bioinformatics*. 2013;29(1):15-21.
172. Anders S, Pyl PT, Huber W. HTSeq--a Python framework to work with high-throughput sequencing data. *Bioinformatics*. 2015;31(2):166-9.
173. Love MI, Huber W, Anders S. Moderated estimation of fold change and dispersion for RNA-seq data with DESeq2. *Genome Biol*. 2014;15(12):550.
174. Lintonen TP, Baker PR, Suoniemi M, Ubhi BK, Koistinen KM, Duchoslav E, et al. Differential mobility spectrometry-driven shotgun lipidomics. *Anal Chem*. 2014;86(19):9662-9.
175. West JA, Beqqali A, Ament Z, Elliott P, Pinto YM, Arbustini E, et al. A targeted metabolomics assay for cardiac metabolism and demonstration using a mouse model of dilated cardiomyopathy. *Metabolomics*. 2016;12:59-.
176. Liu Q, Cai J, Nichols RG, Tian Y, Zhang J, Smith PB, et al. A Quantitative HILIC-MS/MS Assay of the Metabolic Response of Huh-7 Cells Exposed to 2,3,7,8-Tetrachlorodibenzo-p-Dioxin. *Metabolites*. 2019;9(6):118.
177. Ooi M, Nishiumi S, Yoshie T, Shiomi Y, Kohashi M, Fukunaga K, et al. GC/MS-based profiling of amino acids and TCA cycle-related molecules in ulcerative colitis. *Inflamm Res*. 2011;60(9):831-40.
178. Boudonck KJ, Mitchell MW, Nemet L, Keresztes L, Nyska A, Shinar D, et al. Discovery of metabolomics biomarkers for early detection of nephrotoxicity. *Toxicol Pathol*. 2009;37(3):280-92.
179. Chen M, Rao RSP, Zhang Y, Zhong CX, Thelen JJ. A modified data normalization method for GC-MS-based metabolomics to minimize batch variation. *SpringerPlus*. 2014;3(1):439.
180. Hofmann U, Maier K, Niebel A, Vacun G, Reuss M, Mauch K. Identification of metabolic fluxes in hepatic cells from transient ¹³C-labeling experiments: Part I. Experimental observations. *Biotechnol Bioeng*. 2008;100(2):344-54.
181. Colby BN, McCaman MW. A comparison of calculation procedures for isotope dilution determinations using gas chromatography mass spectrometry. *Biomed Mass Spectrom*. 1979;6(6):225-30.

Reference list

182. Berg T, Strand DH. ¹³C labelled internal standards--a solution to minimize ion suppression effects in liquid chromatography-tandem mass spectrometry analyses of drugs in biological samples? *J Chromatogr A*. 2011;1218(52):9366-74.
183. Bourbon NA, Yun J, Kester M. Ceramide Directly Activates Protein Kinase C ζ to Regulate a Stress-activated Protein Kinase Signaling Complex. *J Biol Chem*. 2000;275(45):35617-23.
184. Reichert M, Eick D. Analysis of cell cycle arrest in adipocyte differentiation. *Oncogene*. 1999;18(2):459-66.
185. Adams SH. Emerging perspectives on essential amino acid metabolism in obesity and the insulin-resistant state. *Adv Nutr*. 2011;2(6):445-56.
186. Newgard CB. Interplay between lipids and branched-chain amino acids in development of insulin resistance. *Cell Metab*. 2012;15(5):606-14.
187. Caballero B, Finer N, Wurtman RJ. Plasma amino acids and insulin levels in obesity: response to carbohydrate intake and tryptophan supplements. *Metabolism*. 1988;37(7):672-6.
188. Estrada-Alcalde I, Tenorio-Guzman MR, Tovar AR, Salinas-Rubio D, Torre-Villalvazo I, Torres N, et al. Metabolic Fate of Branched-Chain Amino Acids During Adipogenesis, in Adipocytes From Obese Mice and C2C12 Myotubes. *J Cell Biochem*. 2017;118(4):808-18.
189. Newton BW, Cologna SM, Moya C, Russell DH, Russell WK, Jayaraman A. Proteomic analysis of 3T3-L1 adipocyte mitochondria during differentiation and enlargement. *J Proteome Res*. 2011;10(10):4692-702.
190. Beloor J, Kang HK, Yun C-H, Kim SH, Moon YS. Low Lysine Treatment Increases Adipogenic Potential of Bovine Intramuscular Preadipocytes. *Asian-Australas J Anim Sci*. 2009;22(5):721-6.
191. Mendez-Lucas A, Duarte JA, Sunny NE, Satapati S, He T, Fu X, et al. PEPCK-M expression in mouse liver potentiates, not replaces, PEPCK-C mediated gluconeogenesis. *J Hepatol*. 2013;59(1):105-13.
192. Palmieri F, Stipani I, Quagliariello E, Klingenberg M. Kinetic Study of the Tricarboxylate Carrier in Rat Liver Mitochondria. *Eur J Biochem*. 1972;26(4):587-94.
193. Keuper M, Jastroch M, Yi CX, Fischer-Posovszky P, Wabitsch M, Tschop MH, et al. Spare mitochondrial respiratory capacity permits human adipocytes to maintain ATP homeostasis under hypoglycemic conditions. *FASEB J*. 2014;28(2):761-70.
194. Nye CK, Hanson RW, Kalhan SC. Glyceroneogenesis is the dominant pathway for triglyceride glycerol synthesis in vivo in the rat. *The Journal of biological chemistry*. 2008;283(41):27565-74.
195. Tsujino S, Shanske S, Sakoda S, Fenichel G, DiMauro S. The molecular genetic basis of muscle phosphoglycerate mutase (PGAM) deficiency. *Am J Hum Genet*. 1993;52(3):472-7.
196. Ikonen E. Cellular cholesterol trafficking and compartmentalization. *Nat Rev Mol Cell Biol*. 2008;9(2):125-38.
197. Prattes S, Horl G, Hammer A, Blaschitz A, Graier WF, Sattler W, et al. Intracellular distribution and mobilization of unesterified cholesterol in adipocytes: triglyceride droplets are surrounded by cholesterol-rich ER-like surface layer structures. *J Cell Sci*. 2000;113(17):2977.
198. Wang Y, Castoreno AB, Stockinger W, Nohturfft A. Modulation of endosomal cholesterol ester metabolism by membrane cholesterol. *J Biol Chem*. 2005;280(12):11876-86.
199. Cooper RA. Influence of increased membrane cholesterol on membrane fluidity and cell function in human red blood cells. *J Supramol Struct*. 1978;8(4):413-30.
200. Fukami K. Structure, Regulation, and Function of Phospholipase C Isozymes. *The Journal of Biochemistry*. 2002;131(3):293-9.
201. Fong W-K, Sánchez-Ferrer A, Rappolt M, Boyd BJ, Mezzenga R. Structural Transformation in Vesicles upon Hydrolysis of Phosphatidylethanolamine and Phosphatidylcholine with Phospholipase C. *Langmuir*. 2019;35(46):14949-58.
202. Casares D, Escriba PV, Rossello CA. Membrane Lipid Composition: Effect on Membrane and Organelle Structure, Function and Compartmentalization and Therapeutic Avenues. *Int J Mol Sci*. 2019;20(9).
203. Haczeyni F, Bell-Anderson KS, Farrell GC. Causes and mechanisms of adipocyte enlargement and adipose expansion. *Obes Rev*. 2018;19(3):406-20.
204. Kasturi R, Wakil SJ. Increased synthesis and accumulation of phospholipids during differentiation of 3T3-L1 cells into adipocytes. *J Biol Chem*. 1983;258(6):3559-64.
205. Gauster M, Rechberger G, Sovic A, Horl G, Steyrer E, Sattler W, et al. Endothelial lipase releases saturated and unsaturated fatty acids of high density lipoprotein phosphatidylcholine. *J Lipid Res*. 2005;46(7):1517-25.
206. Weiss SB, Kennedy EP, Kiyasu JY. The Enzymatic Synthesis of Triglycerides. *J Biol Chem*. 1960;235(1):40-4.
207. Coleman RA, Mashek DG. Mammalian triacylglycerol metabolism: synthesis, lipolysis, and signaling. *Chem Rev*. 2011;111(10):6359-86.

Reference list

208. Tvrdik P, Westerberg R, Silve S, Asadi A, Jakobsson A, Cannon B, et al. Role of a new mammalian gene family in the biosynthesis of very long chain fatty acids and sphingolipids. *J Cell Biol.* 2000;149(3):707-18.
209. Leonard AE, Kelder B, Bobik EG, Chuang LT, Lewis CJ, Kopchick JJ, et al. Identification and expression of mammalian long-chain PUFA elongation enzymes. *Lipids.* 2002;37(8):733-40.
210. Wang Y, Torres-Gonzalez M, Tripathy S, Botolin D, Christian B, Jump D. Elevated hepatic fatty acid elongase-5 activity affects multiple pathways controlling hepatic lipid and carbohydrate composition. *J Lipid Res.* 2008;49:1538-52.
211. Agbaga MP, Brush RS, Mandal MN, Henry K, Elliott MH, Anderson RE. Role of Stargardt-3 macular dystrophy protein (ELOVL4) in the biosynthesis of very long chain fatty acids. *Proc Natl Acad Sci U S A.* 2008;105(35):12843-8.
212. Hyvönen Mervi T, Koponen T, Weisell J, Pietilä M, Khomutov Alex R, Vepsäläinen J, et al. Spermidine promotes adipogenesis of 3T3-L1 cells by preventing interaction of ANP32 with HuR and PP2A. *Biochem J.* 2013;453(3):467-74.
213. Vuohelainen S, Pirinen E, Cerrada-Gimenez M, Keinänen TA, Uimari A, Pietilä M, et al. Spermidine is indispensable in differentiation of 3T3-L1 fibroblasts to adipocytes. *J Cell Mol Med.* 2010;14(6b):1683-92.
214. Ikeguchi Y, Bewley MC, Pegg AE. Aminopropyltransferases: function, structure and genetics. *J Biochem.* 2006;139(1):1-9.
215. Albers E. Metabolic characteristics and importance of the universal methionine salvage pathway recycling methionine from 5'-methylthioadenosine. *IUBMB Life.* 2009;61(12):1132-42.
216. Bertino JR, Waud WR, Parker WB, Lubin M. Targeting tumors that lack methylthioadenosine phosphorylase (MTAP) activity: current strategies. *Cancer Biol Ther.* 2011;11(7):627-32.
217. Tews D, Fischer-Posovszky P, Fromme T, Klingenspor M, Fischer J, Rütther U, et al. FTO Deficiency Induces UCP-1 Expression and Mitochondrial Uncoupling in Adipocytes. *Endocrinology.* 2013;154(9):3141-51.
218. Shadid S, Koutsari C, Jensen MD. Direct Free Fatty Acid Uptake Into Human Adipocytes In Vivo Relation to Body Fat Distribution. *Diabetes.* 2007;56(5):1369-75.
219. Berg JM TJ, Stryer L. *Biochemistry: Palgrave Macmillan; 2002.*
220. Jakobsson A, Westerberg R, Jacobsson A. Fatty acid elongases in mammals: their regulation and roles in metabolism. *Prog Lipid Res.* 2006;45(3):237-49.
221. Hafidi ME, Buelna-Chontal M, Sánchez-Muñoz F, Carbó R. Adipogenesis: A Necessary but Harmful Strategy. *Int J Mol Sci.* 2019;20(15):3657.

Acknowledgements

Zum Schluss dieser Arbeit möchte ich DANKE sagen.

Eine Vielzahl verschiedener Menschen haben zum Gelingen dieser Dissertation beigetragen.

Zunächst danke ich meinem Doktorvater Prof. Jerzy Adamski für die Bereitstellung dieses Themas und das Vertrauen, das er mir zukommen ließ. Dank seiner ideellen und finanziellen Unterstützung konnte ich erst dieses interessante Themengebiet erforschen. Des Weiteren danke ich herzlich meinen Mentorinnen und Mentoren, allen voran Jutta Lintelmann, Gabriele Möller, Cornelia Prehn, Janina Tokarz und Mark Haid. Euer stets offenes Ohr, eure große Hilfsbereitschaft und euer Korrekturlesen haben mir sehr geholfen während der vergangenen Jahre. Ein sehr herzliches Dankeschön sage ich Gabriele Zieglmeier, Maria Kugler und Silke Becker für Ihre große Unterstützung im Labor und den vielen netten Gesprächen. Anna Artati, Simone Huber, Dalia Goldhaber-Padillas und Elisabeth Schindler danke ich für die non-targeted Messungen. Fabian Riols danke ich für die gemeinsame Zeit und die große Unterstützung bei analytischen Problemen. Merci beaucoup! Auch Alexander Cecil möchte ich Danke sagen für die vielen R-Skripte und die Unterstützung in der statistischen Datenauswertung. Ebenso bedanke ich mich bei Marion Schieweg, Julia Scarpa und Patrick Pann für die gemeinsame Zeit und eure Hilfe.

Meinen Kooperationspartner danke ich auch sehr herzlich. Hier sind vor allem Thomas Schwarzmayer, Elisabeth Graf und Sandy Löseke zu nennen für ihre Hilfe bei den Transcriptomics-Messungen und -Auswertungen.

Danke sage ich auch allen anderen, die ich womöglich vergessen habe. Vielen lieben Dank.

Zum Schluss sage ich von Herzen DANKE bei meiner Familie und meinen Freunden. Ohne die Unterstützung meiner Eltern wäre diese Arbeit nie entstanden. Ebenso danke ich von Herzen meiner Freundin Selina für ihre Unterstützung, dem Rückhalt und das Korrekturlesen dieser Dissertation. Vielen, vielen Dank!